DOI:10.14753/SE.2014.1976

The importance of electrophysiological and imaging methods in the diagnostics of inherited retinal degenerations: Genotype-phenotype correlations

PhD thesis

Annamária Ditta Zobor MD

Doctoral School of Clinical Medicine
Semmelweis University

Consultant: Dr. Eberhart Zrenner MD, D.Sc

Official reviewers:
Dr. János Hargitai MD, Ph.D
Dr. Illés Kovács MD, Ph.D

Head of the Final Examination Committee:
Dr. János Németh MD, D.Sc

Members of the Final Examination Committee:
Dr. Miklós Resch MD, Ph.D
Dr. Mária Ferencz MD, Ph.D

Tübingen, 2014

DOI:10.14753/SE.2014.1976

Table of content

DOI:10.14753/SE.2014.1976

DOI:10.14753/SE.2014.1976

1. Abbreviations

ABCA4	ATP-binding cassette, subfamily A, member 4 (gene)
ACHM	achromatopsia
AD	autosomal dominant
AR	autosomal recessive
CD	cone dystrophy
CDSRR	cone dystrophy with supernormal rod responses
CNNM4	cyclin M4, metal transporter (gene)
CRD	cone-rod dystrophy
CRT	cathode ray tube
CRX	cone-rod homeobox
cSLO	confocal scanning laser ophthalmoscope
CSNB	congenital stationary night blindness
DTL	Dawson-Trick-Litzkow electrode
ELM	external limiting membrane
EOG	electrooculography or electrooculogram
ERG	electroretinography or electroretinogram
ETDRS	early treatment diabetic retinopathy study
FAF	fundus autofluorescence
FD-OCT	Fourier Domain optical coherence tomography
FOK	first order kernel
GCAP1	guanylyl cyclase activating protein 1
GCAP2	guanylyl cyclase activating protein 2
GCL	ganglion cell layer
GCP	good clinical practice
GUCA1A	guanylate cyclase activator 1A (gene)
GUCY2D	guanylate cyclase 2D (gene)
HCN	hyperpolarization-activated cyclic nucleotide-gated channel
ILM	internal limiting membrane
INL	inner nuclear layer

IPL	inner plexiform layer
ISCEV	International Society for Clinical Electrophysiology of Vision
IS/OS	inner segment/outer segment
LCA	Leber congenital amaurosis
LED	light emitting diode
KCNV2	potassium channel, subfamily V, member 2 (gene)
MRI	magnetic resonance imaging
NF1	neurofibromatosis type 1
NFL	nerve fibre layer
OCT	optical coherence tomography
ONL	outer nuclear layer
OPs	oscillatory potentials
OPG	optic pathway glioma
OPL	outer plexiform layer
PTC	premature termination codon
SD-OCT	spectral domain optical coherence tomography
RP	retinitis pigmentosa
RPE	retinal pigment epithelium
STGD	Stargardt disease
TCDS	total colour discrimination score
VEP	visually evoked potential
VERIS	visual evoked response imaging system

DOI:10.14753/SE.2014.1976

2. Introduction

Inherited retinal dystrophies are a heterogeneous group of rare diseases affecting the posterior segment of the eye, including photoreceptors and retinal pigment epithelium (RPE). They all belong to the group of „rare dieases“ or „orphan diseases“, however, their prevalence is highly variable[1,2]. The most common form of retinal degenerations, retinitis pigmentosa (RP) is reported in 1 case for each 3000-5000 individuals[2,3], while some rare conditions are described only in very few cases in the literature (i.e. Jalili syndrome)[4]. The diseases can be classified based on whether they predominantly affect the rods (i.e. RP) or the cones (i.e. cone- dystrophies), cause a rather localized defect (i.e. macular dystrophies) or even a more generalized retinal degeneration[2,5,6]. The clinical patterns are also variable: some conditions are progressive, while others are rather stationary; they can become manifest at birth or show first symptoms only in later decades of life; and the course of disease is highly individual[1-3,5]. The distinction between retinal dystrophies can further become challenging, as the clinical features of some diseases can be overlapping in early or late stages (**Figure 1**)[1,2]. Most retinal dystrophies are associated with a progressive deterioration over time and – in some cases – can lead to blindness[1-3,5].

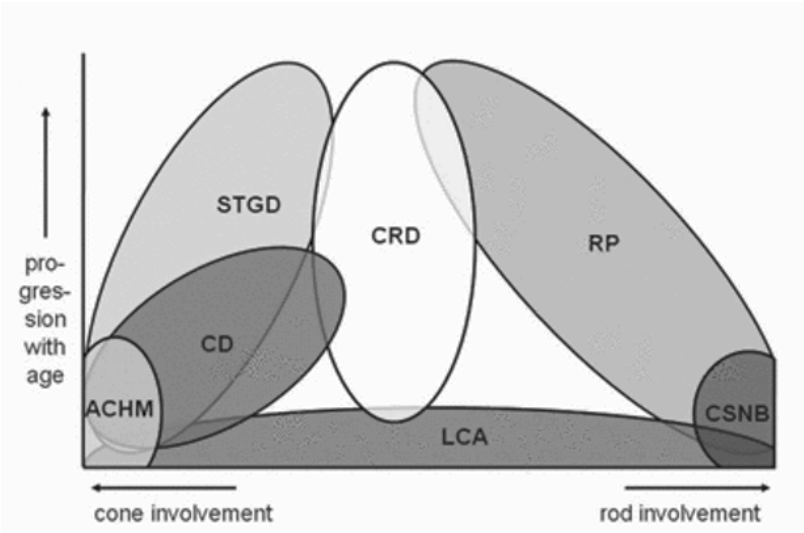

Figure 1: Phenotypic overlap between autosomal recessive retinal diseases. ACHM: achromatopsia; CD: cone-dystrophy; CRD: cone-rod dystrophy; CSNB: congenital stationary noght blindness; LCA: Leber`s congenital amaurosis; RP: retinitis pigmentosa; STGD: Stargardt`s disease. (illustration from Neveling et al. [1])

DOI:10.14753/SE.2014.1976

A particular hallmark of retinal dystrophies is the impressing genetic heterogeneity. More than 200 genes have been associated with inherited retinal degenerations so far, whose defects cause a stationary or progressive loss of photoreceptors or affect the RPE (**Figure 2**)[7]. Consequently, the underlying pathomechanisms are manifold and can affect phototransduction, synaptic signal transduction, specific metabolic features of photoreceptors or structural elements required in the visual cycle or in intracellular ion balance[1-3]. Some genetic mutations lead to different clinical phenotypes (i.e. mutations in the *ABCA4* gene), on the other hand, certain forms of retinal degenerations (i.e. retinitis pigmentosa) can be associated with various genotypes[2,3,7,8]. This high degree of clinical an genetic heterogeneity poses challenges in making the correct clinical diagnosis and in identifying the underlying defects in known genes or detecting novel retinal disease genes.

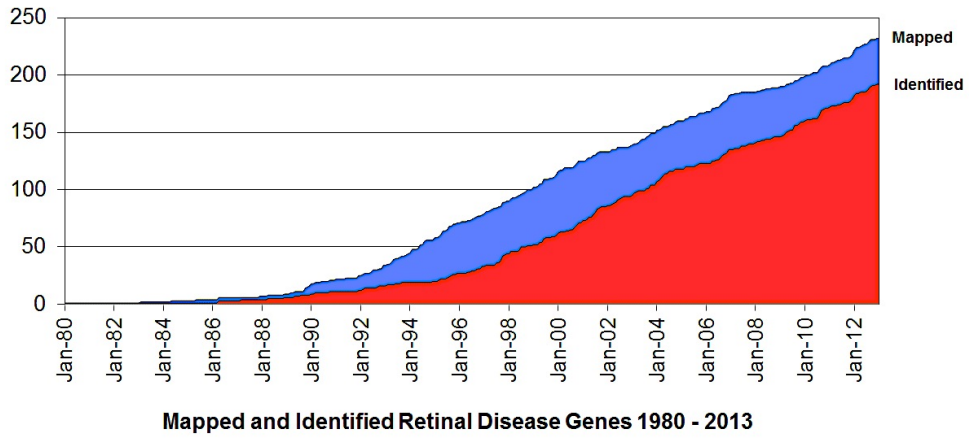

Figure 2: The growing number of identified genes and loci causing inherited retinal diseases (current status at https://sph.uth.edu/retnet/ [7]).

Up to date no established therapy is available for inherited retinal disorders, therefore, social and professional consequences are essential tasks to deal with. Inherited retinal disorders a major cause of visual disability and legal blindness in the working population and thus have a considerable socioeconomic impact[1-3].

In recent years, enormous efforts have been made in research and the new therapeutic approaches are promising[9-11]. Furthermore, with the help of improved molecular genetic and functional diagnostic tools an early recognition and differentiation has become possible.

DOI:10.14753/SE.2014.1976

3. Aims

In my research studies, I was focusing on two essential diagnostic tools:

1. on electrophysiological measurements, especially on the usefulness of the Ganzfeld and multifocal electroretinography
2. on retinal imaging techniques, especially on fundus autofluorescence (FAF) and optical coherence tomography (OCT) imaging.

The aim was to achieve a better clinical characterization of retinal dystrophies and to provide a better understanding of the nature of these disorders. The modern ophthalmological functional diagnostic tools enable a precise characterisation and early recognition of inherited retinal diseases. The detailed results can help to extend our understanding of the pathological mechanisms involved in these diseases.

This work summarises novel clinical findings, the usefulness of functional and morphological diagnostic tools and also describes some very unique retinal conditions. The results provide valuable information for clinicians and can help to improve early and correct recognition and proper follow-up of various inherited retinal disorders. The better understanding of genotype-phenotype correlations reveals important information with respect to the likelihood of disease development and choices of therapy.

DOI:10.14753/SE.2014.1976

4. Methods: Good clinical practice (GCP) or how to manage clinical phenotyping

Despite the relatively high rate of occurrence of this heterogeneous pathologic category, the various forms of inherited retinal degenerations belong to the group of rare diseases[2]. Such uncommon, chronically debilitating diseases are of such low prevalence that special combined efforts and expert knowledge are needed to address them[1,2].

The phenotyping of isolated or syndromic forms of retinal disorders can be a very challenging task, that should be preferentially carried out in a specialized center, where possibilities of extensive clinical examination and interdisciplinary collaboration are present[1,12]. „A good patient history is a half of a diagnosis“, therefore, detailed interviewing of the patient is essential, including following aspects of the disease:

- age of onset, that considers four possibilities for the beginning of specific symptoms and/or signs, detectable in children (or even at birth), adolescents, young adults or adults;
- course of disease, whether it is a stationary condition or progression can be noticed
- symptoms regarding central visual acuity, visual field defects, color vision disturbances, night vision, daily vision, adaptation time and photophobia
- information on pedigree, mode of inheritance that includes autosomal dominant (AD), autosomal recessive (AR), X-linked or in some very rare conditions digenic and mitochondrial inheritance patterns.

Furthermore, affection of other organs (i.e. central nervous system, hearing, metabolic disorders, etc.) and careful medical/toxicological history can provide useful information for the differential diagnosis[1-3,5,6]. This clinical starting point is necessary to obtain an effectual interdisciplinary collaboration among ophthalmologists, geneticists and other specialties[12].

During the routine clinical practice of each specialized center, a standardized patient’s phenotyping and monitoring should be realized to maximize the chance of

successful characterization of inherited retinal degenerations[1,12]. Considering the extraordinary variability of retinal phenotypes, an extensive and standardized functional and morphological diagnostic protocol is required. These protocols for patients with ascertained or suspected retinal dystrophies can be schematized in[12]:

1) *Functional characterization*
   a) *Psychophysical measurements*
      i) central visual acuity (mainly ETDRS chart, in low vision patients special tests like grating acuity might be desirable[9])
      ii) visual field testing (kinetic and/or static perimetry depending on symptoms)
      iii) microperimetry
      iv) color vision tests (Panel D-15, Roth 28 Hue test, anomaloscopy)
      v) measurement of dark adaptation thresholds
   b) *Objective measurements - electrophysiology*
      i) Ganzfeld electroretinography (ERG)
      ii) multifocal ERG (mfERG)
      iii) electrooculography (EOG)
      iv) visually evoked potentials (VEP)
   c) *Objective measurements - pupillography*

2) *Morphological characterization*
   a) biomicroscopy of the ocular anterior segment and ophthalmoscopy of the posterior segment
   b) fundus color photography
   c) **optical coherence tomography (OCT)** of the macular area and peri-papillary retinal nerve fiber layer
   d) **fundus autofluorescence imaging (FAF)**
   e) retino-choroidal angiography

3) *Genetic counseling*

Considering the extraordinary variability of clinical phenotypes, genes responsible

for retinal degenerations, as well as of their modifiers, the applicability of these approaches will likely require the planning of several local, nationally or internationally coordinated clinico-genetic studies[1,2,12].

4.1. Methods of Electrophysiology

4.1.1. Ganzfeld Electroretinogram (ERG)

The Ganzfeld electroretinogram (ERG) is the record of diffuse electrical response to light stimuli generated by neural and nonneural cells in the retina[6,13]. The response occurs as the result of light-induced changes in the transretinal movements of ions, principally sodium and potassium, in the extracellular space. The two components, that are most often measured are the *a*- and *b-waves*. The first negative deflection, designated as the *a-wave*, is the result of the light-induced hyperpolarization of photoreceptor outer segments, therefore provides valuable information on the phototransduction cascade. This is followed by a subsequent positive component, the *b-wave*, mainly a consequence of ON-bipolar cell depolarization. The superimposed wavelets on the the ascending limb of the b-wave were termed *oscillatory potentials (OPs)*. Their cellular origin is somewhat uncertain, although it is likely they are generated by the amacrine or possibly interplexiform cells in the inner retina. The change in ion concentration (i.e. decrease in extracellular potassium) around photoreceptor outer segments following light absorption also alters the standing electrical potential that exists between the basal and apical surfaces of the RPE cells. This transient hyperpolarization of the RPE and the hyperpolarization of the Müller cells combine to form a monophasic positive deflection following the b-wave and is desginated as the *c-wave*. The traditionally very brief flash stimuli used for ERG recordings preclude isolation of the response of OFF-bopolar cells. However, with prolonged flashes photopic b-wave can be demonstrated to contain substantial OFF-response, the *d-wave* indicates activity of the OFF bipolar cells.

Depending on recording conditions (i.e. scotopic or photopic), stimulus intensity, wavelenght, frequency or stimulus duration, the function of various retinal

DOI:10.14753/SE.2014.1976

cells can be isolated[6,13].

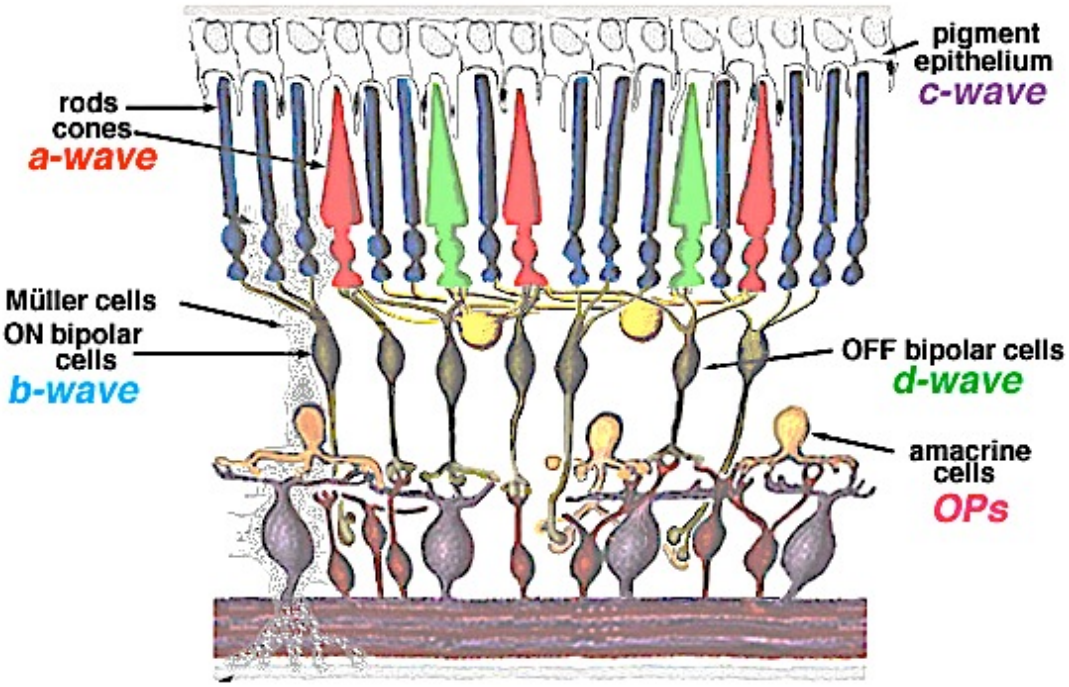

Figure 3: Schematic drawing of the retinal showing the origin of ERG components. (illustration from Webvision: The Organization of the Retina and Visual System)

In 1989 a basic protocol was standardized by the International Society for Clinical Electrophysiology of Vision (ISCEV) and is being regulary updated (last update 2008)[14], so that comparable ERGs can be recorded throughout the world. An ISCEV standard ERG should include the following responses (**Figure 4**), named according to conditions of adaptation and the stimulus (flash strength in $cd*s*m^{-2}$):

(1) Dark-adapted 0.01 ERG (formerly ‘‘rod response’’)
(2) Dark-adapted 3.0 ERG (formerly ‘‘maximal or standard combined rod–cone response’’)
(3) Dark-adapted 3.0 oscillatory potentials (formerly ‘‘oscillatory potentials’’)
(4) Light-adapted 3.0 ERG (formerly ‘‘single-flash cone response’’)
(5) Light-adapted 3.0 flicker ERG (formerly ‘‘30 Hz flicker’’).

DOI:10.14753/SE.2014.1976

Recommended additional response: either Dark-adapted 10.0 ERG or Dark-adapted 30.0 ERG.

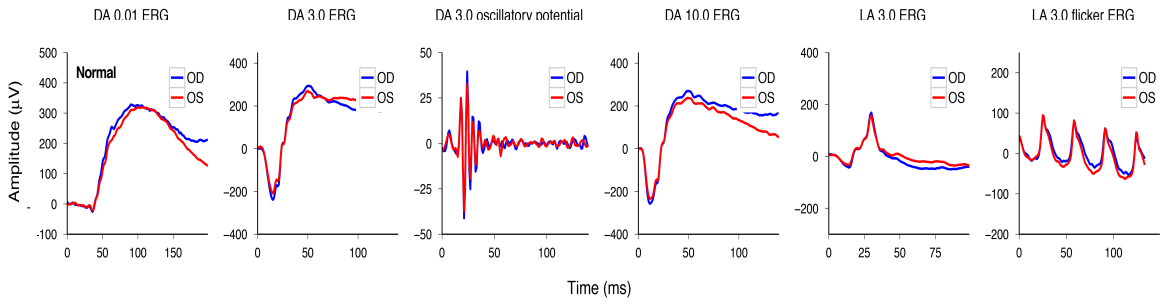

Figure 4: ISCEV Standard ERG recording in a normal subject. The blue colour indicated the results of the right eye, the red colour the left eye.

The five basic ERGs represent the minimum ERG evaluation for clinical diagnosis. It is intended that ISCEV Standard ERG protocols be used widely, but not to the exclusion of other tests or protocols that are not covered by this standard. Thus electrophysiologists are encouraged to extend test protocols to maximize the diagnostic value of the ERG for their patients and for clinical trials[14].

4.1.2. Multifocal Electroretinogram (mfERG)

The conventional Ganzfeld ERG is a mass response to diffuse illumination of the retina and shows alterations only, when large areas of the retina are functionally impaired. Although the retinal cone system in humans is spatially heterogenous and the density of cone photoreceptors is highest in the fovea, their total number in the retina represents only less than 10% oft he total cone population. Therefore, diseases limited to the macular area typically do not produce Ganzfeld ERG abnormalities[6,13-17].

The innovative technique of the multifocal ERG (mfERG) allows determining a topographic measure of electrical activity of the central retina based on a technique introduced by Sutter (1992)[16,17]. Although electrical responses from the retina are recorded with a similar corneal electrode as the Ganzfeld ERG, the nature of the

stimulus and the form of the analysis differ. These differences allow a topographic map of local ERG activity to be measured. For the basic mfERG described here, the retina is stimulated with an array of hexagonal elements, each of which has a 50% chance of being illuminated every time the frame changes. Although the pattern appears to flicker randomly, each element follows the same pseudo-random sequence of illumination with the starting point displaced in time relative to other elements. By correlating the continuous ERG signal with the sequence of on- and off-phases of each element, each local ERG signal is calculated. Although these local ERG signals are referred to as mfERG responses, it is important to keep in mind that they are not direct electrical potentials from local regions of retina, but rather they are a mathematical extraction of the signal (**Figure 5**)[6,13-17].

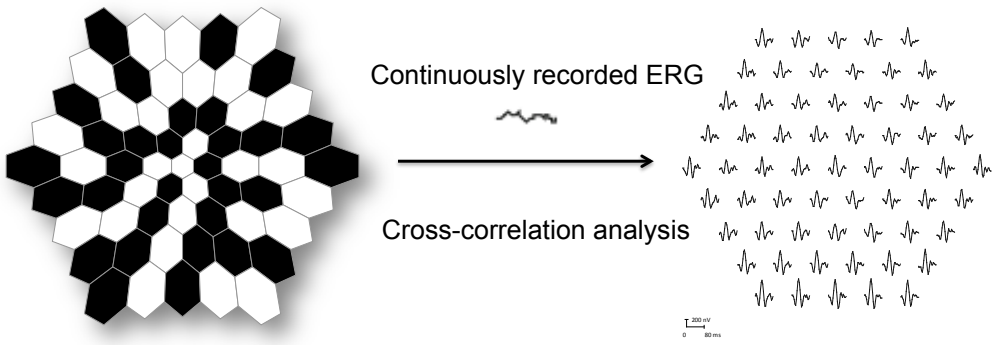

Figure 5: The mERGs are elicited by an array of black and white hexagons (left). The hexagons go through a pseudo-random sequence of black and white as the frame changes. Then a cross-correlation technique produces multiple ERGs (right).

The typical waveform of the basic mfERG response (also called the first-order response or first-order kernel) is a biphasic wave with an initial negative deflection followed by a positive peak. There is usually a second negative deflection after the positive peak. These three peaks are called N1, P1, and N2, respectively. There is evidence that N1 includes contributions from the same cells that contribute to the a-wave of the light-adapted Ganzfeld ERG and that P1 and N2 include contributions from the cells contributing to the light-adapted b-wave and oscillatory potentials. Although there are homologies between the mfERG waveform and the conventional ERG, the stimulation rates are higher for the mfERG and, as noted above, the mfERG responses are mathematical extractions[15].

Although evaluations of the macula of the retina by electrophysiological methods have been available for less than a quarter-of-a-century, their uses in clinical and research studies have been expanding with great enthusiasm. MfERG has become a standard and essential electrophysiological tool[18-22]. The technique continues to advance for the diagnosis of macular diseases, and in determining the underlying pathology of macular diseases. Coupled with the development of imaging technology mfERG will certainly produce much more advances in ophthalmology[23].

4.2. Methods of Retinal Imaging

4.2.1. Fundus Autofluorescence (FAF)

Fundus autofluorescence (FAF) imaging is a novel imaging method that allows topographic mapping of lipofuscin distribution in the RPE cells as well as of other fluorophores that may occur with disease in the outer retina and the subneurosensory space[24,25]. Lipofuscin is an autofluorescent pigment that accumulates in the lysosomes of most aging eukaryotic cells. Excessive accumulation of lipofuscin granules in the lysosomal compartment of RPE represents a common downstream pathogenetic pathway in various hereditary and complex retinal diseases. Therefore, it can be used as a „visible“ biomarker for cellular aging and oxidative damage[24-26].

The autofluoresence signal from RPE cells is very much correlated with lipofuscin content and accumulation[27]. FAF is increased with RPE dysfunction due to impaired processing and clearing of lipofuscin. Conversely, the FAF signal may be decreased in the setting of RPE or photoreceptor loss — if there are no photoreceptor outer segments, the source for lipofuscin formation may be lost[25,26].

Lipofuscin is not a single compound but is actually composed of a number of molecules, not all of which have been fully characterized. The best-described component of lipofuscin is A2E, a bis-retinoid composed of two vitamin A molecules bound together. A2E is not recognized by lysosomal enzymes, so it may accumulate in lysosomes, and it possesses toxic properties that could result in RPE cell apoptosis.

There are many other components of lipofuscin, however, including peroxidation products of proteins and lipids and possibly over 10 different fluorophores[28,29]. Because of its diverse composition, lipofuscin has a broad spectrum of excitation (300-600 nm) and emission (480-800). Thus it can be excited by many wavelengths of visible light in the blue and green portion of spectrum. The intensity of the FAF emission signal returning from the RPE, however, is quite weak[27-29].

Only with the advent of confocal scanning laser ophthalmoscopic technology could FAF approaches become clinically relevant. Confocal SLO (cSLO) uses a focused, low-power laser that is swept across the fundus in a raster pattern[30]. The confocal nature ensures that reflectance and fluoresence are from same optical plane and allows suppression and rejection of FAF originating from sources anterior to the retina, eg, the crystalline lens. Another advantage of cSLO imaging is that multiple frames may be acquired rapidly. This permits several single FAF images to be averaged to reduce background noise and increase image contrast. This allows FAF imaging to be performed at relatively low intensities, which is critical given that high-intensity blue light is uncomfortable and potentially harmful. With further development of the software, a semi-automated atrophy detection and quantification has become possible enabling an accurate identification and measurement of atrophic areas[30].

FAF imaging has been shown to be useful with regard to understanding of pathophysiologic mechanisms, diagnostics, genotype-phenotype correlation, identification of predictive markers for disease progression, and monitoring of novel therapies. FAF imaging gives information above and beyond that obtained by conventional imaging methods, such as fundus photography, fluorescein angiography, and optical coherence tomography. Its clinical value coupled with its simple, efficient, and noninvasive nature is increasingly appreciated[31-37].

4.2.2. Optical Coherence Tomography (OCT)

Optical Coherence Tomography (OCT) is one of the most valuable advances in retinal diagnostic imaging since the introduction of fluorescein angiography in 1959.

DOI:10.14753/SE.2014.1976

OCT is a non-invasive imaging technique relying on low coherence interferometry to generate in vivo, cross-sectional images of ocular tissues[38-40]. Originally developed in 1991 as a tool for imaging the retina[41], OCT technology has continually evolved and expanded within ophthalmology as well as other medical specialties. With the introduction of Spectral (Fourier) Domain OCT (SD-OCT, FD-OCT) technology, it now provides greater tissue resolving power, significantly higher scan density, and faster data acquisition than original Time Domain OCT[42-44].

Cross-sectional visualization is an extremely powerful tool in the identification and assessment of retina abnormalities. The high resolving power (10um - Time Domain, 5um – Spectral Domain) provides excellent details for evaluating the vitreo-retinal interface, neurosensory retinal morphology, and the RPE-choroid complex in the macular area (**Figure 6**). The ability to perform volumetric and retinal thickness analysis also provides a quantitative and repeatable methods to evaluate retinal abnormalities, surgical and pharmacological interventions[40-44].

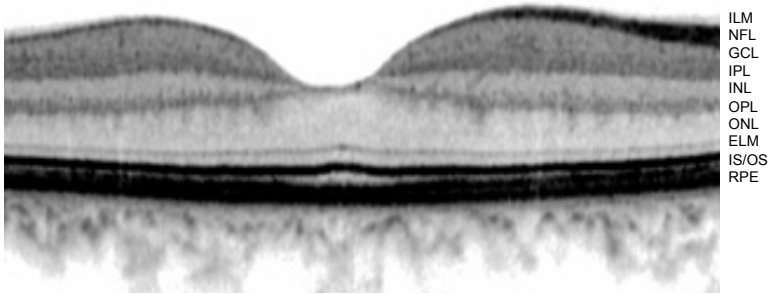

Figure 6: Retinal layers observed with SD-OCT (ILM: internal limiting membrane, NFL: nerve fiber layer, GCL: ganglion cell layer, IPL: inner plexiform layer, INL: inner nuclear layer, OPL: outer plexiform layer, ONL: outer nuclear layer, ELM: external limiting membrane, IS/OS: photoreceptor inner- and outer segments, RPE: retinal pigment epithelium)

Inherited retinal disorders exhibit a huge variability of retinal changes, mainly affecting the outer retina and RPE cells. With the help of high resolution imaging, the integrity or abnormality of RPE cells, photoreceptor inner/outer segments and external limiting membrane can be analyzed even during early stages of disease, when the fundus appears normal. Furthermore, OCT has become one of the most important tools in clinical testing of experimental therapeutic strategies (surgical procedures, gene therapy trials)[45-50].

DOI:10.14753/SE.2014.1976

5. Results

5.1. Electrophysiological Methods and Their Clinical Relevance

5.1.1. Methodology of the multifocal ERG

D. Nagy, E. Zrenner, H. Jägle (2007). Direct fundus-controlled multifocal ERG: first evaluation of a novel technique. ARVO Abstract

H. Jägle, **D. Nagy**, E. Zrenner (2007). ERG with a fundus imaging system: technique and a comparison with other stimulation methods. Meeting abstract Zhengzhou, China

D. Nagy, E. Zrenner, H. Jägle (2008). Three types of multifocal ERG: classical CRT, LED, and a CRT fundus imaging system ARVO Abstract

The multifocal electroretinogram (mfERG) was introduced into clinical application about 20 years ago and has been established as a useful diagnostic tool in retinal diseases[15-17]. Still, there are limitations of its use due to - among others - technical problems like incorrect electrode placement, low stimulation luminance, eye movement artefacts, opacity of ocular media, refractive errors, unstable or eccentric fixation. Furthermore, the available mfERG systems differ from each other in several aspects including both hardware and software[51-53].

In our first study, we introduced a novel technique, which combined a fundus camera with a stimulation display allowing for compensation of eccentric fixation and direct fundus control. The purpose of this study was to evaluate the new method of fixation-controlled measurements in healthy subjects and to compare the reliability of the mfERG response amplitudes and implicit times of stimulation patterns with different number of hexagons. In a second study, we described the similarities and differences and the clinical relevance between three multifocal ERG systems – including the fundus-controlled mfERG system. Therefore, measurements in healthy subjects have been carried out using three different stimulation and recording systems.

First order kernel (FOK) responses were measured in ten healthy subjects (5 female and 5 male, mean age: 30, range: 14 to 46 years) using the direct fundus-controlled multifocal ERG (Roland Consult GmbH, Germany). The stimulating monitor (VM225, Lucius & Baer GmbH) was integrated into a fundus camera (VISUCAM Pro

NM, Carl Zeiss Meditec AG) and connected to a RetiPort system (**Figure 7**)[54]. Stimuli were presented at a resolution of 800x600 pixels with a maximum luminance of approx. 500 cd/m2. MfERGs were recorded twice from the right eye of every subject using a scaled stimulus array consisting of 7, 19, 37 hexagons and were recorded once with a stimulus consisting of 61 hexagons covering a visual field of approx. 40x40 deg. Responses were amplified (low pass: 10 Hz, high pass: 100 Hz) and analyzed according to ring averages of the first order kernel responses. Amplitude and implicit time were analyzed for each setting. Finally, fundus photographs were taken from each subject for direct overlay with the response topography.

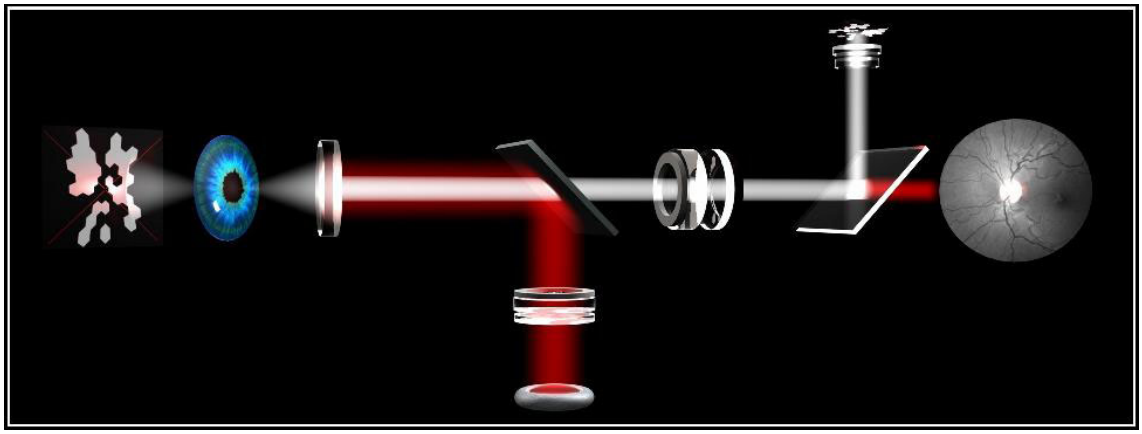

Figure 7: Direct fundus-controlled mfERG measurement. The fundus camera allows the correction of spherical refractive errors, which helps to provide a focused stimulus to the subject's retina during measurement. Furthermore, the infrared fundus camera provides a real-time fundus image for accurate fixation monitoring during testing.

For comparison, the same healthy volunteers were measured by using a RETIscan system with LED-stimulation (Roland Consult GmbH, Germany)[54] and the VERIS system (Electro-Diagnostic Imaging, Inc.)[55]. MfERGs were carried out twice with each device using DTL fibre electrodes, and a scaled stimulus array consisting of 61 hexagons according to ISCEV Standards[15]. Responses were amplified (200 000x) and band pass filtered (10-100 Hz) using a Grass amplifier (model 12, Quincy, USA) for the VERIS system (sampling rate 1024 Hz), and a built-in amplifier for the RETIscan systems (band pass: 5-100 Hz, sampling rate 1020 Hz). Parameters of the

DOI:10.14753/SE.2014.1976

different multifocal systems are listed in **Table 1**. Additionally, recordings with a light-triggered waveform generator were performed to compare response waveforms and timing differences.

Table 1: Parameters of the three multifocal ERG devices.

	VISUCAM-RETIscan fundus-controlled multifocal ERG (Roland Consult GmbH, Germany)	**RETIscan system with LED-stimulator (Roland Consult GmbH, Germany):**	**VERIS system (Electro-Diagnostic Imaging, Inc.):**
Monitor	CRT monitor (VM225, Lucius&Baer GmbH, luminance up to 500 cd/m^2)	LED (light emitting diodes) stimulating device (luminance up to 700 cd/m^2)	19" color CRT-monitor (luminance approx. 100 cd/m^2)
Field diameter	40x40°	60x60°	55x55°
Amplifier	built-in amplifier of the RETIscan systems	built-in amplifier of the RETIscan systems	2 channel model 12 Grass amplifier (Quincy, USA)
Filter	band pass filter (5-100 Hz)	band pass filter (5-100 Hz)	band pass filter (10-100 Hz)
Sampling rate	1020 Hz	1020 Hz	1024 Hz

In the fundus-controlled mfERG measurements, typical mfERG response topographies were obtained for all conditions. The P1 amplitude varied between 42.1 and 165.0nV/deg2 in the central hexagon depending on the total number of hexagons in the stimulus and between 15.0 and 32.5 nV/deg2 in the outermost ring. The P1 implicit time changed from ca. 43.0 ms in the center to 37.4 ms in the outer ring and was similar for all recording conditions. We found significant variability in the response amplitude of the central hexagon between consecutive runs (difference between runs up to 64% of mean amplitude) but a good reproducibility for the outer rings. Smallest variability between subjects was found for 61 hexagons (**Figure 8**).

DOI:10.14753/SE.2014.1976

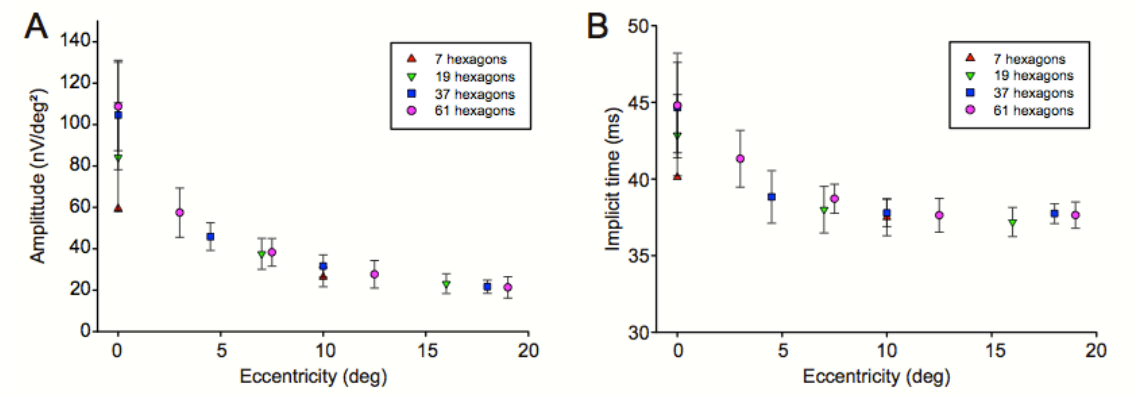

Figure 8: Mean amplitude and standard deviation of the mfERG analysis of all recordings according to concentric rings for stimuli consisting of 7, 19, 37 or 61 hexagons (A). The higher variability of the central hexagon is consistent with fixation instability during the recordings. The lower amplitude for recordings with 7 and 19 hexagons is due to the lower average cone density within the larger central hexagons. The implicit time also decreases with eccentricity (B).

Our study showed that the fundus-controlled multifocal ERG is a convenient and precise technique for monitoring fixation during measurement. Although we found a great variability of response amplitudes in the central hexagon, this may be improved in the future by head stabilization and automatic fixation detection. One major advantage of the system is the continuous fundus imaging while mfERGs are recorded and fundus controlled compensation for eccentric fixation, which makes it an ideal device for mfERGs in patients with macular disease. Additionally, it allows for accurate overlay of functional data on fundus images. However, to achieve best results the head has to be kept in precise position relative to the device's ocular lense. Further, an automatic analysis of fixation combined with ERG response waveform rejection may significantly improve recording quality.

When compared to other mfERG devices, response amplitudes showed a strong correlation between all three systems, being the largest with LED stimulation, due to the highest stimulus luminance (700 cd/m^2). Response amplitude and implicit time of the central hexagon strongly depends on stimulus scaling and varies by 25 to 50% even though the stimulated field size is similar; we found significant variability in the P1 implicit times between the different techniques, even between the two RETIscan systems (**Figure 9**). Variability was greatest for the central hexagon (38 ms to 49.5 ms).

DOI:10.14753/SE.2014.1976

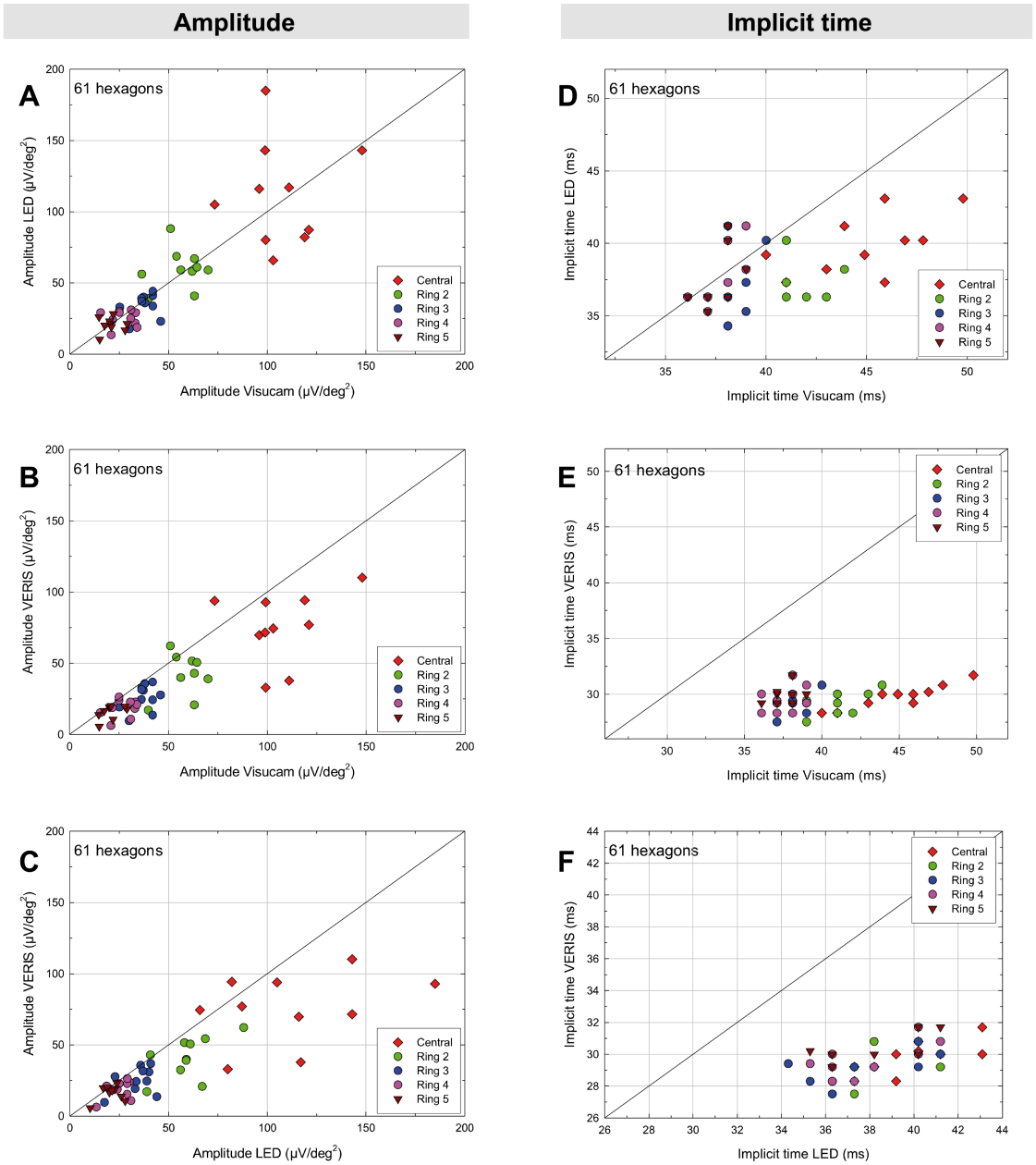

Figure 9: Comparison of response amplitudes between the RETIscan system with LED-stimulator and the VERIS System (A), the VISUCAM-RETIscan and the VERIS System (B) and between the VISUCAM-RETIscan and the RETIscan system with LED-stimulator (C). Response amplitudes show a good correlation between the systems. The largest amplitudes were obtained with LED stimulation due to highest luminance (700 cd/m^2). For all systems, we found high variability for the central hexagon. In contrast, implicit time varied signficantly, beeing much shorter for the VERIS system (D-F).

The test recordings showed different waveforms for each system, same latency for response onset (10 ms), but a peak implicit time difference of approx. 2 ms between the LED and the fundus ERG system (**Figure 10**). Compared to the variability estimated from repeat measurements aliasing effects on implicit time determination are negligible.

DOI:10.14753/SE.2014.1976

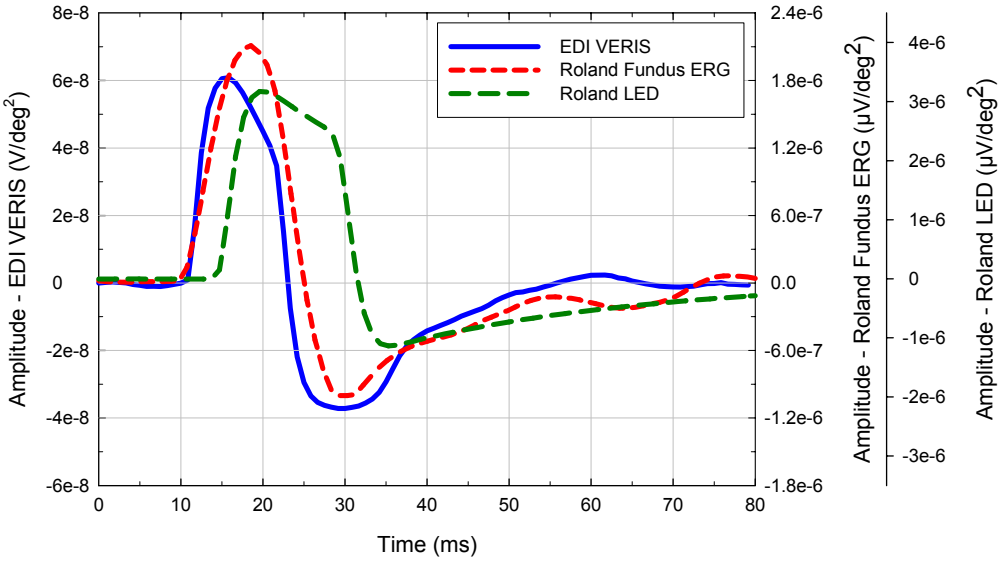

Figure 10: Test recordings performed with all three systems using a human subject simulation device (Roland Consult, Germany). The response waveform depends on the actual amplifier input characteristics. We found simliar latencies (time to response onset) for the VERIS and Fundus ERG system, but longer latency for the LED system. Due to differences in response waveform, the peak implicit time is similar for the two Roland RetiScan systems but shorter for the VERIS system.

Even though the stimulation, response recording and filtering follows ISCEV recommendations[15], hardware differences (especially those of the amplifiers and stimulating monitor) lead to significant waveform and response parameter variability. Therefore, a comparison of clinical data obtained with either system is restricted to larger effects with the central hexagon showing the largest variations[51-53].

DOI:10.14753/SE.2014.1976

5.1.2. Multifocal ERG in Retinitis Pigmentosa

Nagy D, Schönfisch B, Zrenner E, Jägle H (2008). Long-term follow-up in retinitis pigmentosa using the multifocal ERG. IOVS 49(10): 4664-71

Zobor D, Zrenner E (2012). [Retinitis pigmentosa - a review. Pathogenesis, guidelines for diagnostics and perspectives]. Ophthalmologe. 109(5):501-14;quiz 515.

Retinitis pigmentosa (RP) is a heterogenous group of degenerative retinal diseases, which is associated with night-blindness, progressive loss of the peripheral visual field and a slow reduction in central vision and Ganzfeld-ERG abnormalities. RP diffusely and primarily affects the photoreceptors, predominantly the rod system, and as the disease progresses, the function of the cone system also declines. The age of onset, rate of progression, and the presence or absence of associated ocular features are frequently related to the mode of inheritance, but the clinical appearance may vary even among family members with the disease[2,5,6].

Characterization and understanding of the visual loss is important for monitoring patients with RP. A detailed differential diagnosis and long-term follow-up are advisable for adequate patient counselling, for predicting visual outcome and for monitoring the efficacy and safety of new therapeutic options[18,56,57].

Clinical psychophysical and electrophysiological measurements have been used to provide objective information regarding changes of the retinal function. While examinations, like visual acuity testing, perimetry, etc., rely on subjective criteria, electrophysiological methods are used to quantify retinal function in a more objective way. The Ganzfeld-ERG allows recording of electrical responses originating from the entire retina when stimulating with a Ganzfeld globe[6,13,14]. In contrast, the multifocal ERG (mfERG) allows assessment of a "map" of electrical activity[15-18]. With disease progression in the Ganzfeld-ERG the waveforms may no longer be detected while still some residual visual field could be measured. In such cases localized responses may still be obtained using the mfERG[6,13].

The aim of our study therefore was to investigate the usefulness of the mfERG among other clinical psychophysical and electrophysiological techniques. Furthermore, we also provided a review of the characteristics and natural course of retinitis

pigmentosa. Emphasis was placed on determining the yearly progression of the mfERG responses. Our study also aimed at comparing multifocal ERGs and other parameters of disease development.

Twenty-three patients (9 male and 14 female, age between 12 and 66 years, mean: 36 years) with clinically defined RP were included in the study. Disease progression was monitored during a period of up to 10 years using psychophysical techniques, Ganzfeld ERG and multifocal ERGs recordings. Data were analyzed using the programs JMP 5.0.1 (SAS Institute Inc., Cary, NC, USA) and R 2.2.1 (R foundation for statistical computing, Vienna, Austria).

To describe disease progression we formulated linear regression models of the response variables visual field and mfERG values. The response variables were transformed by taking the logarithm to describe exponential decay of retinal function. In these models disease duration was included as fixed factor. Hence we fit the following equation:

$$\text{response} = e^{(\alpha+\beta\cdot\text{Disease\_duration})}$$

where *response* is visual field or one of the multifocal ERG values and α and β are intercept and slope.

For modelling repeated measurements, individuals were included as random factors on slope and intercept. The latter was included since disease onset data seemed not to be reliable (some patients could not remember correctly, when they first noticed changes in their visual function). Including the factor ‘eye’ (left/right) as a random effect nested in the factor ‘individual’ did not increase model fit significantly (ANOVA of the two model versions for all responses with p-value > 0.99). Therefore we omitted this factor, modelling for every individual the mean value of both eyes. In the plots data of both eyes are shown separately. Residuals' normality and homoscedasticity were assessed by quantile-quantile plots (QQ plot) and residuals by predicted plots, respectively. To identify outliers with high leverage Cook`s distance was calculated and the distribution of random parameters estimates was inspected by histograms. Quality of fits is recorded as adjusted coefficient of determination (adj R^2).

To estimate correlations between the different examination methods describing macular function (multifocal ERG, visual acuity and color vision) Spearman`s r_S was calculated and also scatterplots are shown. Correlations and scatterplots were also

produced for mid peripheral retinal function variables (perimetry, dark adaptation thresholds, Ganzfeld- and multifocal ERG).

In our results, the progression of visual field loss is fairly described by an exponential decay, which is similar to the description by Iannaccone et al.[58], a yearly progression of approximately 14.5 % can be calculated in patients affected with RP every year (**Table 2**). We were using the same type of regression model to define the natural progression of rod and cone functional loss measured by electrophysiological methods. We calculated the yearly progression according to the multifocal ERG values. Approximately 6-10 % of the amplitude is lost every year in the outer three rings (**Figure 11**).

Table 2: Parameter estimates and statistics (fixed effects) for disease duration according to visual field changes from the literature and in the present study.

Study	Target	R^2				95% confidence intervals		
				Estimate	SE	lower	upper	p
Iannaccone et al.[58] (n=19)	I4e		Intercept (α)	7.765	0.508	6.768	8.761	<0.0001
			Slope (β)	-0.172	0.023	-0.216	-0.127	<0.0001
	V4e		Intercept (α)	10.296	0.193	9.917	10.675	<0.0001
			Slope (β)	-0.136	0.010	-0.155	-0.117	<0.0001
Berson et al. [61] (n=90)	V4e		Slope (β)	-0.046	N/A	N/A	N/A	N/A
Massof et al.[59] (n=172)	II4e		Slope (β)	-0.170	N/A	N/A	N/A	N/A
	V4e		Slope (β)	-0.145	N/A	N/A	N/A	N/A
Holopigian et al.[60] (n=23)	V4e		Slope (β)	-0.112	N/A	-0.032	-0.192	N/A
Grover et al.[62] (n=71)	II4e		Slope (β)	-0.102	N/A	-0.078	-0.116	N/A
	V4e		Slope (β)	-0.095	N/A	-0.073	-0.144	N/A
Present study (n=23)	**III4e**	**0.95**	**Intercept (α)**	**10.100**	**0.679**	**8.752**	**11.447**	**0.214**
			Slope (β)	**-0.156**	**0.030**	**-0.216**	**-0.096**	**<0.0001**

DOI:10.14753/SE.2014.1976

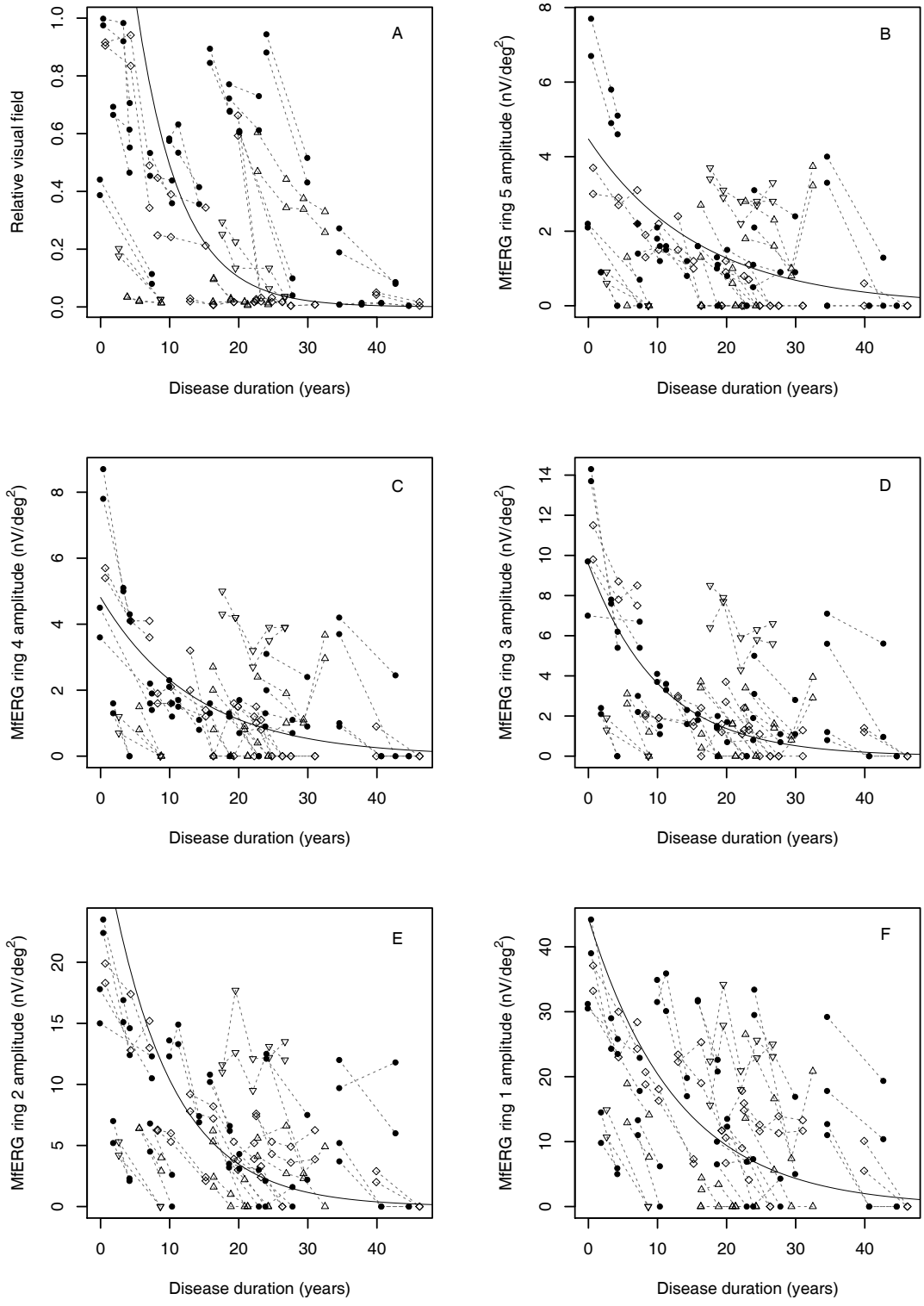

Figure 11: Changes of residual visual field (A) and multifocal ERG of the outermost ring 5 (B), rings 4 to 2 (C – E) and the centre hexagon (F) during disease progression. The progression of visual field loss and changes of the mfERG amplitudes are fairly described by an exponential decay Symbols indicate heredity of the disease (ad = filled circles, ar = triangles, simplex = diamond and Usher syndrome = upside down triangle).

We further compared parameters of disease development with the multifocal ERG values. We categorized the different examination methods according to macular and mid peripheral retinal function. We found a strong correlation between central visual acuity and multifocal ERG response amplitude of the central hexagon ($r_S = 0.75$). In contrast, there was no correlation between the multifocal ERG response amplitude of the central hexagon ($r_S = -0.40$) and color vision performance (TCDS value). Regarding mid peripheral retinal function, mfERG ring 5 amplitude correlated strongly with the maximum response amplitude ($r_S = 0.87$) and with the cone response amplitude ($r_S = 0.85$) of the Ganzfeld ERG.

In advanced cases no reproducible Ganzfeld-ERG scotopic response was recorded, but with the multifocal ERG significant responses could still be recorded and dark adaptation thresholds could be measured.

In conclusion, the progression of visual field loss followed an exponential decay, which was similar to the changes described by other authors[58,60]. Other studies where more patients were included found either a somewhat higher[59] or lower[61,62] loss of visual field per year. On the other hand, he multifocal ERG provides a useful measure of the retinal function; it does not replace, but complement psychophysical methods including visual field and color vision testing. The response amplitude follows a similar exponential decay as the visual field and may provide reproducible responses even if the Ganzfeld-ERG is diminished. This issue is becoming more important, now that essential steps towards possible therapies for retinal degenerations are made and reliable and objective testing methods are required. The mfERG is well-suited for observation and long-term follow-up in disease development and – besides other psychophysical methods - it could be used as an objective outcome measure in upcoming treatment studies involving patients with advanced retinal diseases.

DOI:10.14753/SE.2014.1976

5.2. Autosomal Dominant Cone- and Cone-Rod Dystrophies

5.2.1. *GUCY2D*- or *GUCA1A*-related Autosomal Dominant Cone-Rod Dystrophy: Is There a Phenotypic Difference?

Zobor D, Zrenner E, Wissinger B, Kohl S, Jägle H (2014). *GUCY2D*- or *GUCA1A*-related autosomal dominant cone-rod dystrophy: is there a phenotypic difference? Retina. [Epub ahead of print]

Inherited cone and cone–rod dystrophies (CD and CRD) are characterized by progressive loss of photoreceptor function accompanied by retinal degeneration. All modes of inheritance have been observed, and the extensive genetic heterogeneity is typical for these dystrophies. Heterozygous mutations of the *GUCY2D* and *GUCA1A* genes have been shown to cause autosomal dominant CD and CRD[63-71].Both genes are expressed in cone and rod photoreceptors and are essential for their functional integrity[72-74].*GUCY2D* encodes the retinal guanylate cyclase (retGC-1), which is responsible for the cyclic guanosine monophosphate synthesis in the recovery of the dark state after light activation within these cells[75]. *GUCA1A* encodes the activating protein guanylyl cyclase activating protein (GCAP1), which regulates GC1 function in a Ca^{2+}–sensitive manner (Figure 1)[72,75,76]. Mutations in *GUCA1A* or *GUCY2D*, in conclusion, result in an altered activity of retGC-1 in the dark. The thereby increased cyclic guanosine monophosphate levels keep cyclic nucleotide–gated channels open, allowing an increased Ca^{2+} influx into the photoreceptors causing cell death, which explains the progressive dysfunction in the phenotype. Indeed, this is one of the best-explained disease mechanisms for CRD or CD known in the literature[65,76].

We conducted a study to investigate whether the 2 different genotypes—mutations either in retGC-1 or its activating protein, GCAP1—make a difference in the phenotype, although they both act at the same step of the visual signal transduction cascade. Our aim was to compare the retinal function and morphology in patients affected by autosomal dominant CD or CRD carrying either a mutation in *GUCY2D* or *GUCA1A* using the same psychophysical, electrophysiological, and morphologic methods.

Five patients from a large family with known *GUCA1A* mutation (3 women and

2 men; mean age, 44 years; range, 32–57 years) and 9 patients from 4 families with *GUCY2D* mutation (6 women and 3 men; mean age, 49 years; range, 26–79 years) were included in this study. Psychophysical and electrophysiological examinations were performed to study retinal function. Fundus autofluorescence imaging and spectral domain optical coherence tomography were performed for morphologic characterization.

The typical phenotype in both of our patient groups was an autosomal dominant cone-dominated retinal dystrophy with disease onset in early adolescence, characterized by increased glare sensitivity, severe color vision disturbances, central defects in the visual field, but nearly normal outer boundaries. Retinal morphologic changes were relatively limited to the macular region, however, a great variability - from RPE mottling to large RPE defects - was detected even among families. The fundus autofluorescence (FAF) and optical coherence tomography (OCT) images also demonstrated the diversity of macular changes. In comparison, patients with *GUCY2D* mutations seemed to show more severe morphologic changes. Clinical findings of the *GUCA1A* patients are shown in **Figure 12**, findings of the *GUCY2D* group are presented in **Figure 13**.

Functional results also suggested a cone-dominated dystrophy in both groups with a rather more severe phenotype in *GUCY2D*. In patients with *GUCA1A* mutation, the diagnosis of CD was more likely, although a slight alteration of rod function in the extended scotopic ERG protocol did show up. Patients with *GUCY2D* mutation revealed even more pronounced scotopic changes, so the final diagnosis was mainly CRD—with a negative ERG in three cases, suggesting an early involvement of inner retinal neurons (**Figure 14**)[66]. This difference also showed up in the dark adaptation thresholds. Patients with *GUCA1A* mutations retained more preserved rod function, whereas patients of the *GUCY2D* groups showed elevated dark adaptation thresholds, especially in the elder generation. The more preserved central visual acuity and visual field findings further suggested milder disease characteristics in *GUCA1A* cases.

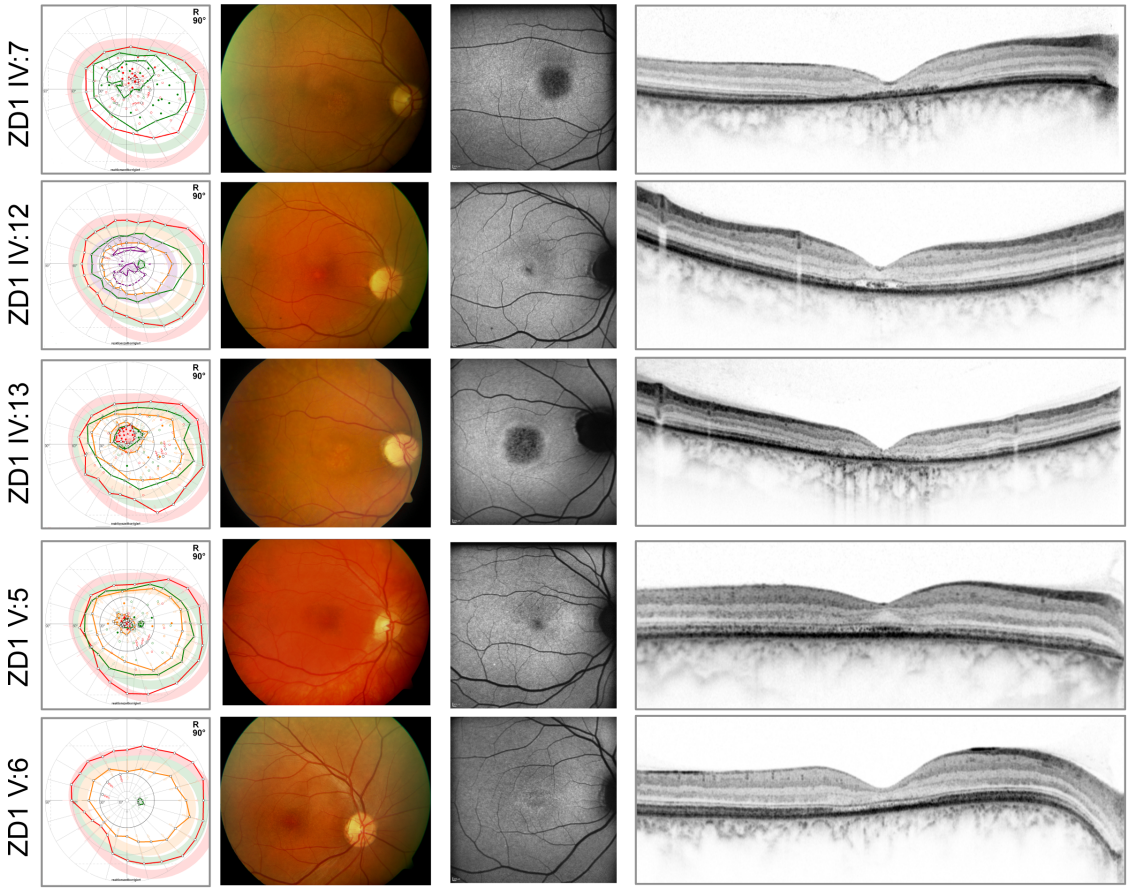

Figure 12: From left to right: Kinetic perimetry results, fundus photography, fundus autofluorescence, and optical coherence tomography images of the patients of the family with *GUCA1A* mutations. In the perimetric results, central defects were detected, whereas outer boundaries with target III4e (red) were nearly normal.

Our results suggest that the defects in GCAP1 (*GUCA1A*) signaling result in a less severe retinal dystrophy. What could be the explanation? GCAP1 and GCAP2 are both essential for normal phototransduction, but their expression in rods and cones shows differences with GCAP1 being predominantly expressed in cones[77,78]. The presence of GCAP1 and GCAP2 in mammalian rods is suggested to be almost equimolar; furthermore, their contribution to the biochemical pathway behind the GC regulation seems to differ. By participating in the activation of retGC-1 even at Ca^{2+} levels at which GCAP1 regulation is expected to predominate, GCAP2 quickens the recovery of the single-photon response and the responses to brighter flashes in rods. This suggests an equally important role for GCAP2 and GCAP1 in rods. Furthermore, GCAP2 has been shown to act with lower activity on retGC-1 (*GUCY2D*), which might explain the more preserved rod function in altered GCAP1 signaling[78,79].

DOI:10.14753/SE.2014.1976

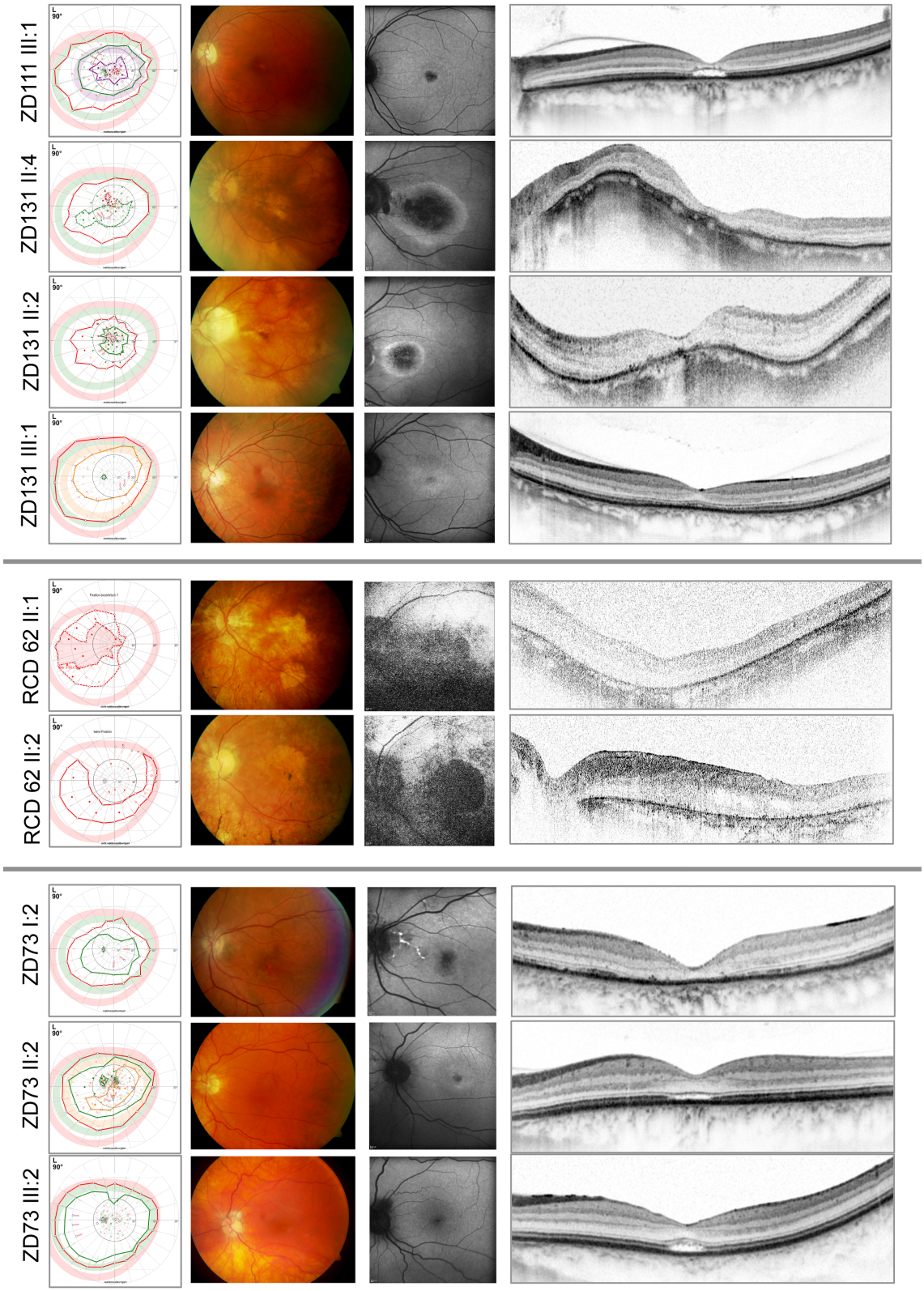

Figure 13: From left to right: Kinetic perimetry results, fundus photography, fundus autofluorescence, and optical coherence tomography images of the patients of the family with *GUCY2D* mutations. The upper 4 patients are from 2 nonrelated families carrying the same p.R838C mutations in the *GUCY2D* gene. The members of the RCD62 family carrying the p.R838G mutation show a more severe phenotype (fifth and sixth panels). The lower 3 patients are from family ZD73 with p.R838H mutation in the *GUCY2D* gene. The perimetric results show central defects and variable attenuation of the outer boundaries with target III4e (red).

DOI:10.14753/SE.2014.1976

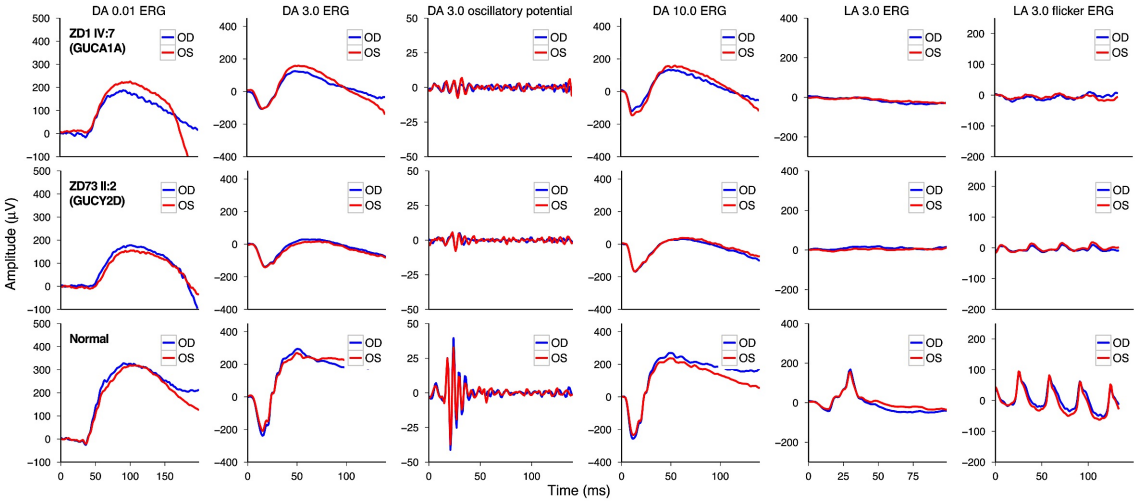

Figure 14: Ganzfeld ERG responses of a representative patient of each group (upper panel: *GUCA1A*, middle panel: *GUCY2D*) compared with a normal subject (lower panel). Color coding in each panel: blue curves show results of the right eye (OD) and red curves show results of the left eye (OS).

In contrast, retGC-1 is more predominant in cones but is present in both photoreceptor types, affecting both rod and cone function[75,80]. This clearly matches with the clinical findings, that an autosomal dominant mutation of *GUCY2D* causes CRD, as demonstrated in our cases as well. However, a difference in the severity of phenotype because of various mutation forms could not be further defined. The large variety of functional and morphologic appearance suggests a possible role of other modifying factors. Two siblings of the family RCD62 with a heterozygous *GUCY2D* mutation showed a strikingly more severe phenotype with markedly reduced visual acuity, only residual islands in the visual field and markedly reduced scotopic and photopic ERG responses. They were the only patients who showed bone spicule–like pigmentary changes and RPE atrophy in the peripheral retina. The genetic analysis detected an R838G substitution[62]. Whether this mutation or other additional yet unknown modifying factors could be responsible for the more severe phenotype in this family is still unknown.

Taken together, we suggest that mutations in the *GUCA1A* gene in autosomal dominant retinal dystrophies cause a less severe phenotype and less involvement of rod photoreceptors than *GUCY2D* mutations.

DOI:10.14753/SE.2014.1976

5.2.2. Cone and Cone-Rod Dystrophy Segregating in the Same Pedigree Due to the Same Novel *CRX* Gene Mutation

Kitiratschky VB, **Nagy D**, Zabel T, Zrenner E, Wissinger B, Kohl S, Jägle H (2008). Cone and cone-rod dystrophy segregating in the same pedigree due to the same novel CRX gene mutation. Br J Ophthalmol. 92(8):1086-91.

Here, we report the identification of a new *CRX* gene mutation in a family affected by autosomal dominant retinal dystrophy characterised by a highly variable disease expression, including cone dystrophy in some subjects and cone–rod dystrophy with a negative ERG in others (**Figure 15**).

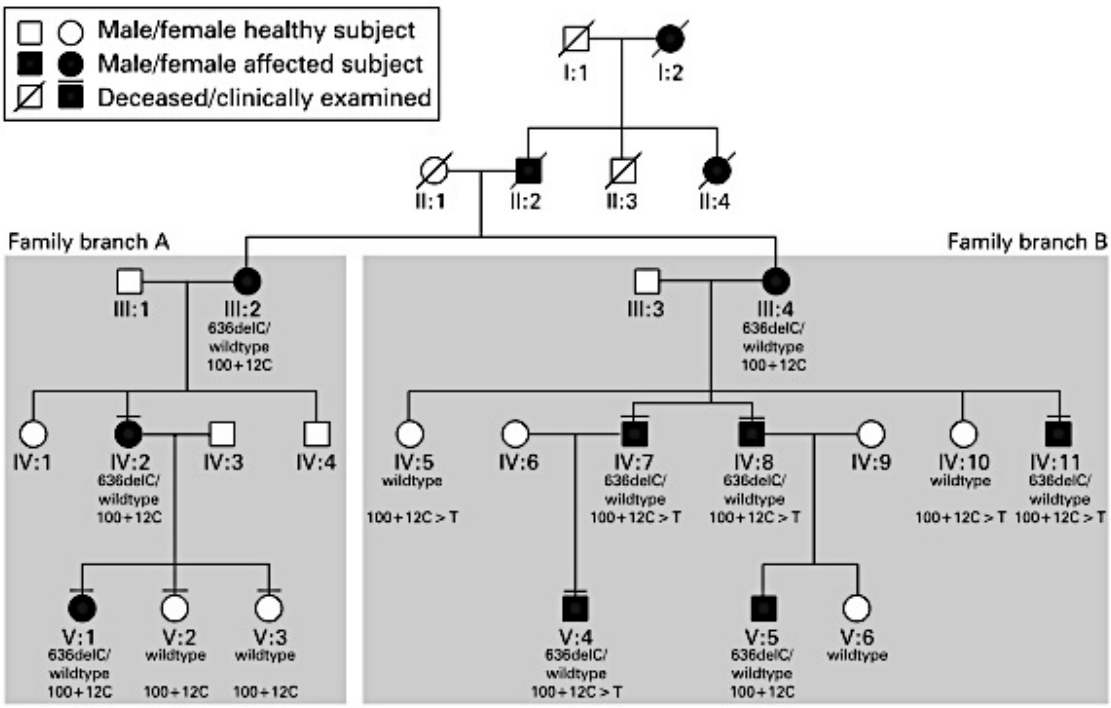

Figure 15: Pedigree of a five-generation family affected by autosomal dominant cone–rod dystrophy. Mutation screening of the *CRX* gene identified a clearly disease-causing mutation in the *CRX* gene, c.636delC, which segregated concordantly with the disease phenotype (the genetic status for the mutation is shown in bold letters). Segregating with the more severe phenotype and an additional rod involvement (family branch B, descendants of patient III:2) we identified the intronic sequence variant of the *CRX* gene c.100+12C.T (the genetic status for the variant is shown in italics under the respective pedigree symbol, c.100+12C for homozygotes, c.100+12C.T for heterozygotes).

The cone–rod homeobox (*CRX*) gene is one of the associated genes which, if mutated, causes non- syndromic autosomal dominant CRD (adCRD), retinitis pigmentosa (adRP) or Leber congenital amaurosis (LCA)[81,82]. The transcription factor CRX is important for transactivation of many retina-specific expressed genes, including rhodopsin and recoverin. It is expressed in rod and cone photoreceptors, and cells of the inner nuclear layer[83-85] from 10.5 weeks after conception[85] and maintained throughout life[83-85]. The transactivation domain of CRX has been localised to the C-terminus of the protein[86-88]. Furthermore, CRX has been proposed to form the centre of an interaction network of synergistically working common and retina-specific transcription factors[89,90] which comprises among others the retina-specific transcription factors Nrl and Nr2E3[89,90] and the transcriptional co-activators and histone acetyl transferases p300/CBP[86]. CRX and Nrl interact with each other via their respective DNA binding domains[90], whereas interaction between CRX and p300/CBP is mediated via their respective C-termini.

Taken together, there are several conclusive reasons which argue in favour of the pathogenicity of the novel 1 bp deletion in the *CRX* gene, c.636delC, present in this family. First, the mutation perfectly segregates with the disease phenotype. All affected family members carry the mutation, whereas all healthy subjects do not. Second, the frameshift mutation introduces a premature termination codon (PTC). Since this PTC is located in the ultimate exon of *CRX*, mutant transcripts may escape nonsense mediated mRNA decay[91]. Then, if translated, the mutation results in a severely truncated protein that is expected to have reduced transactivation activity[86-88]. However, via its intact homeodomain, the mutant protein may still be able to bind to cis-regulatory promoter elements or other transcription factors, such as Nrl, thereby blocking binding sites and sequestering normal transcription factors[90]. Thus, as described above the deleterious effects of the *CRX* mutant c.636delC may be manifold.

Phenotypically, all affected family members show signs of cone dystrophy with severe reduction of macular function in members of the fourth generation (**Figure 16**). However, in family members of branch B also the rod system is strongly affected. Moreover, patients present with a so-called negative ERG: while the a-wave of the Ganzfeld maximum response waveform, which originates in the photoreceptor outer

segments[92], is well maintained, the b-wave is largely reduced, which originates from retinal cells that are postsynaptic to the photoreceptors[93]. Moreover, maximum b-wave amplitudes and semisaturation intensities estimated from the Naka–Rushton function indicate a reduced number of rods but an almost normal function of the remaining rod photoreceptors[94].

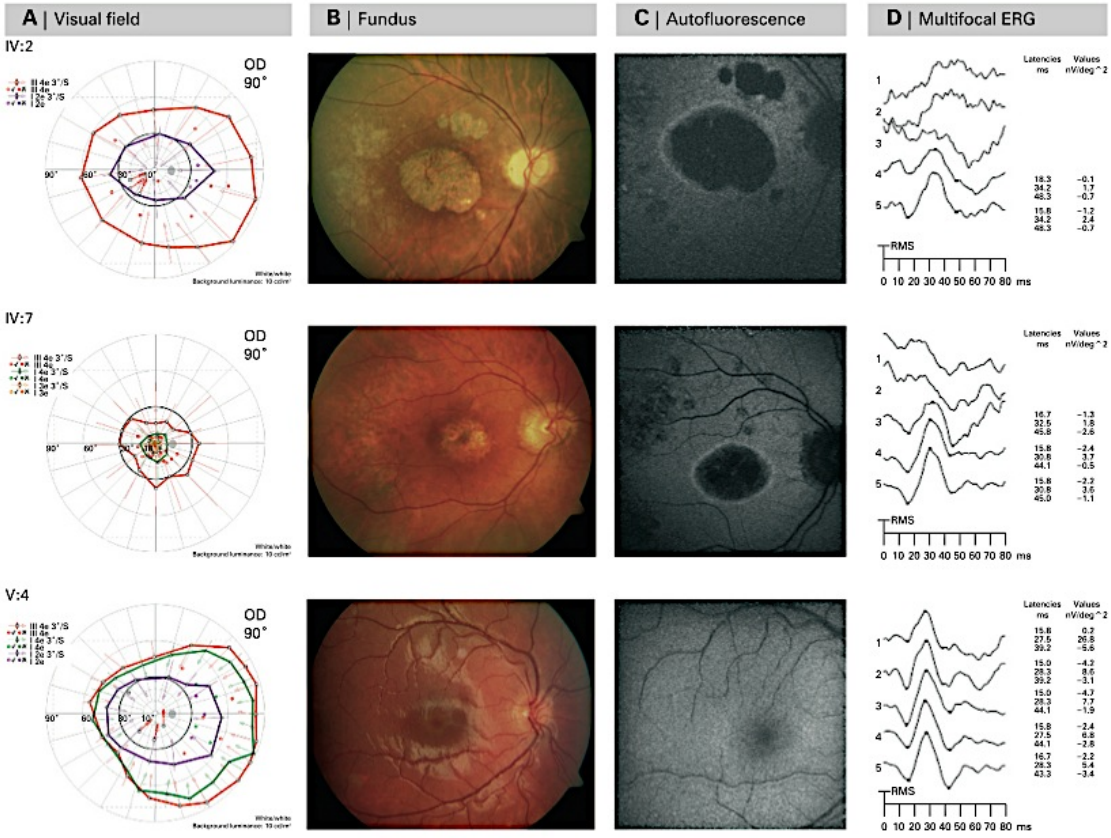

Figure 16: Examples of morphological changes and functional deficits found in three representative patients of two generations. At the age of 45 years, IV:2 had severely reduced visual acuity (0.1/0.1) and severe colour vision defects in the Panel D-15 saturated test. While static perimetry revealed a central scotoma, kinetic perimetry showed normal peripheral fields (A). Patchy atrophy of central RPE was seen in ophthalmoscopy (B) corresponding to the central hypofluorescent areas surrounded by a hyper-fluorescent rim in fundus autofluorescence (FA) (C). Multifocal electroretinogram (mfERG) in IV:2 shows central responses not discernible from noise and preserved peripheral responses with reduced amplitude and prolonged implicit time (D). Her cousin IV:7 also had reduced visual acuity (0.3/0.3), a colour vision disorder, but additionally he suffers from night blindness. Fundus appearance, FA and mfERG are similar in both cousins, but IV:7 had a largely restricted visual field. His son V:4 has normal visual acuity, colour and night vision, a normal fundus and FA appearance, unremarkable visual fields and mfERG (A–D) but a negative electroretinogram (ERG) response in fullfield ERG (see fig 3). Patient consent has been obtained for publication of this figure. OD, right eye.

The observed clinical variability among affected members in this family might have a genetic basis. Potential modifiers might be mutations in the *CRX* gene itself, such as sequence variants in regulatory regions or intronic variants. Noteworthy is that we found that the presence of intronic variant c.100+12T on the wildtype allele was always associated with the rod dysfunction in this family. Yet we cannot rule out mere coincidence without further genetic or functional data. Besides mutation in the *CRX* gene itself, sequence variants in interacting transcription factors, such as Nrl, Nr2E3, p300/CBP[86,89,90], or genes which are transactivated by CRX, such as rhodopsin[90] might be strong candidates for modulatory effects.

In conclusion, we described the phenotype of a multi-generation family affected by adCRD with marked intrafamilial variability. Whereas all patients presented a reduced cone ERG, those from only one branch also show a reduced rod ERG, with some even displaying a negative combined rod–cone response. We identified a novel disease-associated mutation in the *CRX* gene, c.636delC, which segregates with disease in all affected family members, and a sequence variant, c.100+12 C.T, which is only present in the more severely affected family members. We suggest that this polymorphism might have a modifying effect of the disease phenotype. In addition, we propose that a negative ERG in adCRD might be an indicator of *CRX* gene mutations.

DOI:10.14753/SE.2014.1976

5.3. „Some Very Rare Conditions“

5.3.1. KCNV2-Retinopathy

Zobor D, Kohl S, Wissinger B, Zrenner E, Jägle H (2012). Rod and cone function in patients with KCNV2 retinopathy. PLoS One. 7(10):e46762.

Wissinger B, Schaich S, Baumann B, Bonin M, Jägle H, Friedburg C, Varsányi B, Hoyng CB, Dollfus H, Heckenlively JR, Rosenberg T, Rudolph G, Kellner U, Salati R, Plomp A,De Baere E, Andrassi-Darida M, Sauer A, Wolf C, **Zobor D**, Bernd A, Leroy BP, Enyedi P, Cremers FP, Lorenz B, Zrenner E, Kohl S (2011). Large deletions of the KCNV2 gene are common in patients with cone dystrophy with supernormal rod response. Hum Mutat. 32:(12) pp. 1398-406.

In 1983 Gouras et al.[95] reported an unusual type of retinal dystrophy, which was associated with characteristic alterations in the rod electroretinogram (ERG). This rare, autosomal recessive condition has been reported in several further studies[96-103] and was named "cone dystrophy with supernormal rod responses (CDSRR)". CDSRR is characterized by an early markedly reduced central visual acuity with central scotoma, photophobia, severe color disturbances, and occasionally nystagmus. In contrast to other cone dystrophies, a disease-typical alteration of the rod system could be observed: while rod sensitivity to weak flashes was reduced, an augmented responsiveness to higher levels of flash stimuli could be detected, and implicit times were considerably prolonged[95-103]. These characteristics were unique for CDSRR, however, the underlying disease mechanism could not be elucidated at that time.

In 2006 Wu et al[104] successfully linked the disorder to chromosome 9p24 and the *KCNV2* gene, which is predominantly expressed in retinal rod and cone photoreceptors[105]. It encodes a member of voltage gated potassium channels (Kv channels), representing a silent subunit (Kv8.2) that is able to assemble with Kv2.1 to form functional heteromeric channels. This results in a shift in the steady-state activation curve of the Kv2.1 channel towards more negative potentials due to a permanent outward K^+ current, a lower threshold potential for activation, a shortened activation time and slower inactivation kinetics[105-107]. A mutation in *KCNV2* may thus alter important characteristics of the I_{kx} current that influences the photoreceptor membrane potential. However, the dysfunction and mechanisms that link *KCNV2* mutations with the clinical picture still remain to be elucidated.

Over 50 different mutations in *KCNV2* have been reported so far, mainly small indel mutations or point mutations that constitute protein truncation mutations and amino acid substitutions [104,108-110]. Recently, several large deletions within or of the *KCNV2* gene of up to 237 kb in size have been described[110]. Although the genetically detected patients did show altered rod responsiveness, the term „supernormal rod response“ was in many cases deceptive, as previously shown[111]. The term "supernormal rod ERG" is a misnomer and most recently, the disorder has been referred to as "KCNV2 retinopathy“[112].

We present detailed psychophysical and electrophysiological testing as well as spectral domain optical coherence tomography (OCT) and fundus autofluorescence (FAF) to reveal novel insights into disease-specific functional changes in KCNV2 retinopathy. Additionally, we explore differences of disease specific functional aspects in the phenotype that correlate with the underlying *KCNV2* gene alterations. The genotype of three patients has already been published[113], the remaining three patients´ genetic findings are presented here for the first time. In three patients the mutations resulted in a complete absence of Kv8.2 encoded by the *KCNV2* gene (NOP group). In the other three patients heterozygous mutations of the first allele resulted in a lack of protein product, mutations of the second allele led to mutant subunits with presumably remaining pore function (ALP group). The genetic and clinical characteristics of patients are presented in **Table 3**.

On the morphological level, macular pathology varied from mild RPE disturbances to large atrophic areas, while the periphery was normal in every case. It is interesting to see that the changes are strictly limited to the central macular area in every case, while the specific functional changes of this retinal disorder affect rod-rich mid periphery as well. The question of why cones degenerate and rods keep at least their morphological integrity still remains to be unraveled, but the distribution of Müller cells in the retina (i.e. absence in the fovea) could be one important factor, since their regulatory and buffering effect on the extracellular K^+ is missing in the cone-rich area, making cones more vulnerable. Although there was a tendency for a more pronounced

Table 3: Clinical and genetic findings of the six patients. The upper three patients (with grey-shaded background) show a complete absence of Kv8.2 due to large deletions or protein truncating mutations of *KCNV2* and so represent the NOP group. The lower three patients (with white background) represent the ALP group with altered Kv8.2 subunits due to *KCNV2* mutations. The BD27/I. and BD27/II. are brother and sister of one family, so are CHRO8/I. and CHRO/II. of another family. Each case shows an autosomal recessive inheritance. A considerable difference between the NOP and ALP group cannot be observed. However, there is a tendency for a slightly better visual acuity (VA) and higher myopia in the ALP group. Interestingly, night blindness, subjective disease progression and a severe protanomaly are present in the only homozygous patient (RCD307), while other patients reveal unchanged visual function over disease duration, no night blindness and color disturbances consistent with a rod dominated function. (Patients marked with * are published in Wissinger et al.[110])

Patient ID	Age / Gender	VA RE LE	Night blindness	Color vision	Nystagmus	Alteration nucleotide sequence	Alteration polypeptide	Allele status
BD27.I	36 / M	0.125 0.1	no	achromat	No	c.339C>A c.442G>T	p.Cys113X p.Glu148X	heterozygous
BD27.II	40 / F	0.04 0.05	no	achromat	Yes	c.339C>A c.442G>T	p.Cys113X p.Glu148X	heterozygous
RCD307*	60 / M	0.16 0.1	yes	protanomalous	No	c.19_1356+9571 delinsCATTTG	Arg7fs	homozygous
CHRO8.I*	37 / M	0.1 0.1	no	achromat	Yes	g.2657638_2737340del c.1211T>C	Deletion p.Leu404Pro	heterozygous
CHRO8.II*	35 / F	0.1 0.2	no	achromat	No	g.2657638_2737340del c.1211T>C	Deletion p.Leu404Pro	heterozygous
BCM5	28 / F	0.16 0.16	no	achromat	No	c.8_11del4 c.447_449del3	p.Lys3ArgfsX29 p.Phe150del	heterozygous

DOI:10.14753/SE.2014.1976

macular lesion (seen in the OCT and FAF imaging), higher myopia and more elevated dark adaptation thresholds in the NOP group, no clear-cut line can be drawn between the two groups. However, the investigated cohort is small, further large studies are necessary to better highlight the correlations between genotype and phenotype (**Figure 17**).

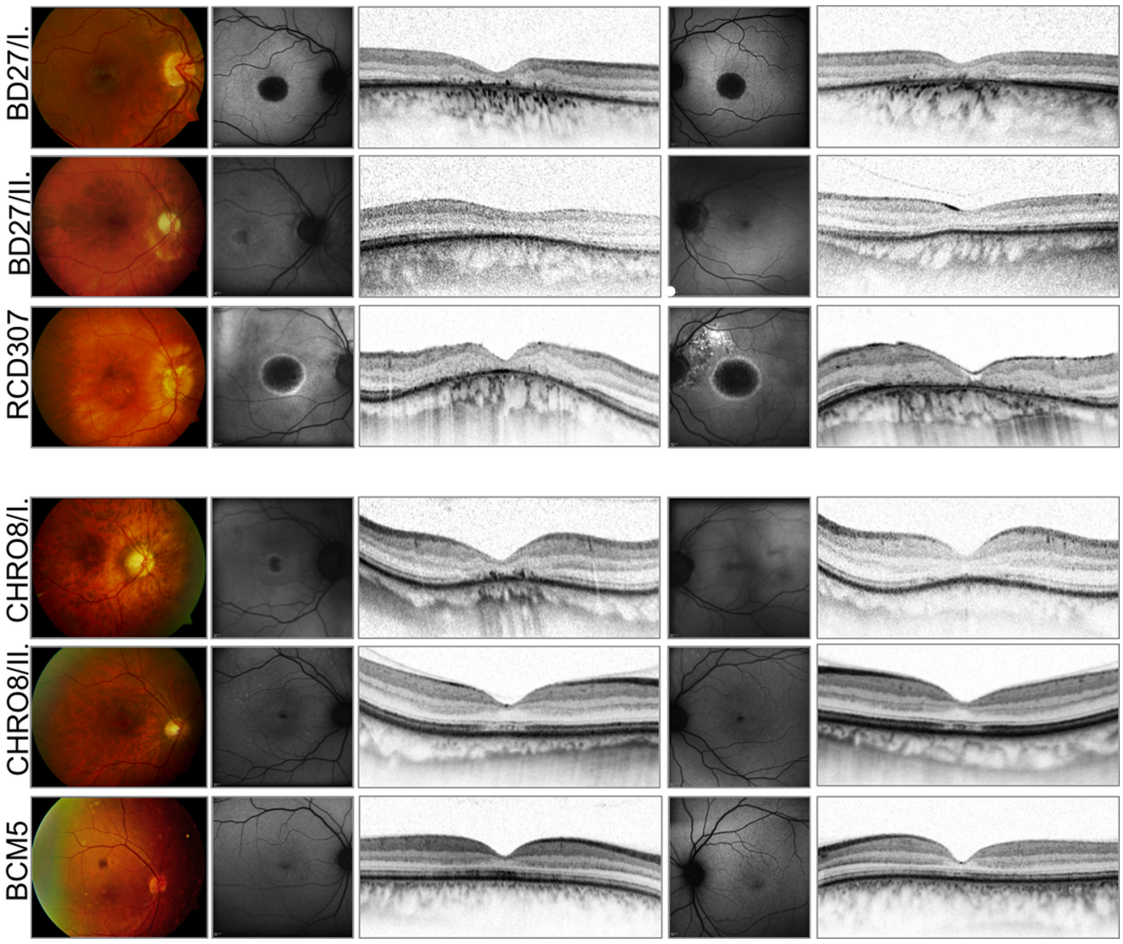

Figure 17. Fundus photographs of the right eye, FAF and spectral domain OCT images of both eyes of six patients illustrating the variability and extent of foveal changes (NOP group: upper three patients, ALP group: lower three patients). Notice the age-related changes, epiretinal gliosis and macular hole formation on the left eye of the RCD307 patient.

Several studies exist on the electrophysiological characteristics of KCNV2 retinopathy[95,98,100,111,114]. Nevertheless, there are still several aspects of this special retinal disorder, for which an explanation is needed. Our results are in accordance with previous reports and also confirm that ”supernormal rod responses” in the ERG - believed to be characteristic for this rare condition - often seem to be missing, as responses, even to high intensity flashes, stay within normal limits in many cases [110,111].

DOI:10.14753/SE.2014.1976

The dynamics of the b-wave intensity-response function is a more constant feature (**Figure 18**).

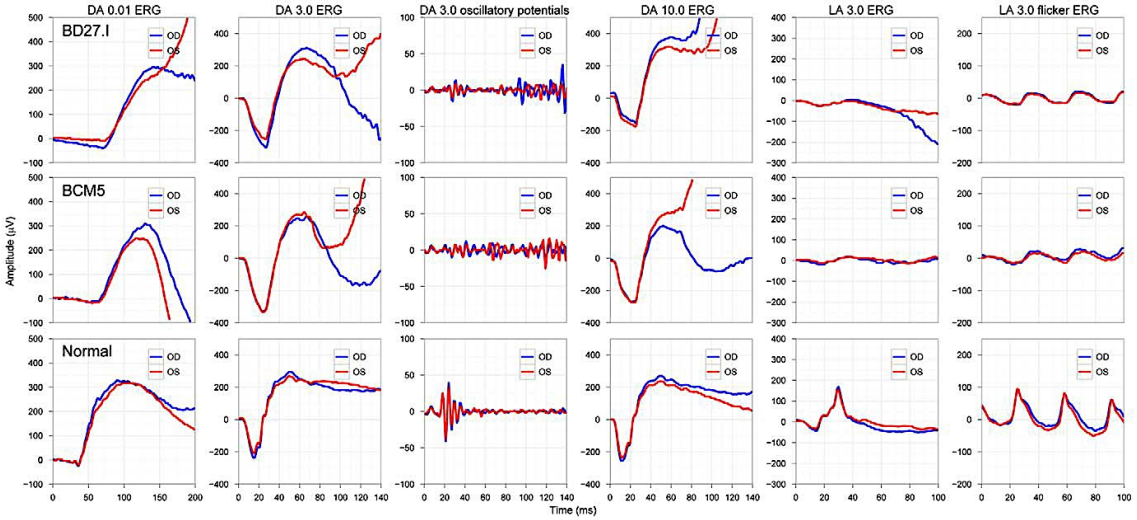

Figure 18: Ganzfeld ERG responses of a representative patient of each group (patient BD27.I in the upper panels represents the NOP group, while the result of patient BCM5 in the middle panels is an example for the ALP group) compared to a normal subject (bottom panels). The patients` findings show the characteristic features of the scotopic ERG (dark-adapted (DA)) and the small photopic responses (light adapted (LA). Notice the missing oscillatory potentials on the rising b-wave in patients. (Color coding in each panel: red curves show results of the right eye (OD), blue curves show results of the left eye (OS)).

In addition, our detailed electrophysiological data show other specific features. Based on the model fits to our electrophysiological data we conclude that phototransduction activation in this retinal dystrophy is normal, since the onset of the deflection from baseline appears with normal delay. While the maximum amplitude Rm_{PIII} was within normal limits, the sensitivity parameter S was significantly lower. There is also a delayed postreceptoral response, which seems independent from flicker frequency. The delay of the emerging b-wave may have two different origins. Firstly, voltage dependent transmitter release may be delayed due to a small prolongation in reaching hyperpolarization. Secondly, a delayed HCN channel activation and depolarization of the photoreceptor might result in an overshoot of the response of the downstream neuron. Such overshoot would not be associated with changes in the G-protein activation cascade of the bipolar cell, which can be assessed with the P_{II} response analysis. In our *KCNV2* patients the kinetics of the ON-bipolar cell G-protein cascade seems to be normal, however, the cascade is activated with a clear delay. A

further interesting finding was the marked reduction or even absence of the oscillatory potentials, either suggesting an altered function of the inner retina (i.e. amacrine or interplexiform cells) or more likely a significantly reduced cone function[115].

Moreover, we studied the temporal characteristics of the retina for the first time in this specific retinal disorder. Altered Kv2.1/Kv8.2 heteromers lose their ability to function as a high-pass amplifier, which explains the altered temporal characteristics observed in our patients (i.e. there is a constant prolongation of photoreceptor recovery time). Interestingly, even at the highest frequency of 45 Hz the response waveform was still significant with an almost normal phase, which indicates that even though we find clearly reduced amplitudes and a phase shift due to cone dystrophy, the temporal dynamics seem to be almost normal.

In summary, KCNV2 retinopathy is considered a very rare retinal disorder associated with high but often normal mixed rod-cone response amplitudes, a marked prolongation of b-wave implicit times and a delayed, almost sudden, steep amplitude-versus-intensity relationship under scotopic conditions. Furthermore, while rod phototransduction is intact, there is a constant delay of the responses, which suggests changes in the synapse or in postreceptoral signaling pathway. Inner retinal involvement is also probable, since oscillatory potentials are almost absent. These findings are diagnostic and are exclusively linked to *KCNV2* mutations.

DOI:10.14753/SE.2014.1976

5.3.2. Jalili Syndrome

Zobor D, Kaufmann DH, Weckerle P, Sauer A, Wissinger B, Wilhelm H, Kohl S (2012). Cone-rod dystrophy associated with amelogenesis imperfecta in a child with neurofibromatosis type 1. Ophthalmic Genet. 33:(1) pp. 34-38

If a diagnosis of a "common" disease has been decided, physicians often forget to pay enough attention to further details. Even if an unusual or rare clinical feature is observed, it is in many cases considered as a part of the already known medical condition. Here we report an unusual case of a girl with neurofibromatosis type 1, who unfortunately also suffers from a rare disease, Jalili syndrome, which is a combination of cone-rod dystrophy and amelogenesis imperfecta[4,116-119].

A 9-year-old girl from a Kosovan family was referred to our clinic with reduced visual acuity in both eyes. Previous pediatric examinations suggested the diagnosis of neurofibromatosis type 1 (NF1). Our patient underwent a detailed ophthalmological examination. Furthermore, magnetic resonance imaging (MRI) was carried out to investigate the optic pathway. During our examination, conspicuous dental changes were noticed, which initiated an additional dental consultation.

Our patient met at least four of the diagnostic criteria for NF1, according to the NIH Consensus Conference in 1987[120-123], however, NF1 with optic pathway glioma (OPG) was not the only disorder found. The symmetrical macular lesions, revealing a bull's eye pattern, suggested a retinal dystrophy, which could be confirmed by electrophysiological examinations. Scotopic responses were subnormal and no photopic responses could be detected. This constellation is typical for a cone-rod dystrophy. An association between NF1 and retinal dystrophies has not been reported yet. Furthermore, the severe dental anomalies are characteristic for NF1 either (**Figure 19**).

DOI:10.14753/SE.2014.1976

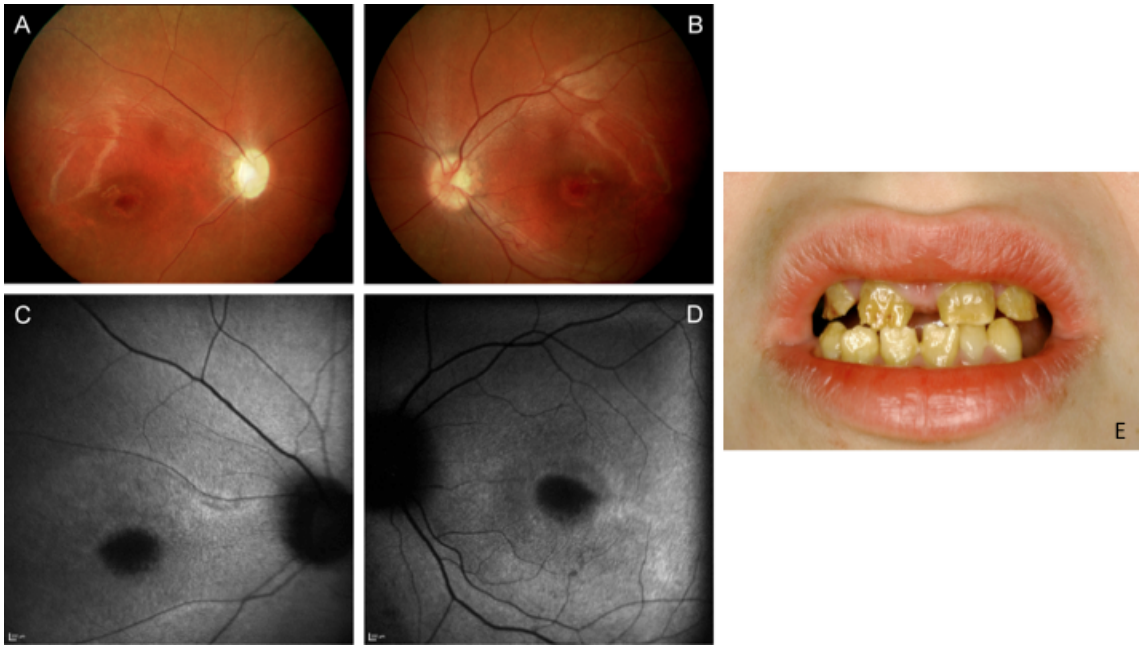

Figure 19: Clinical findings of Jalili syndrome. Fundus (A, B) and autofluorescence images (C, D) showing bilateral optic atrophy (R>L), additional macular retinal pigment epithelial mottling and atrophy similar to bull's eye maculopathy. (E) Amelogenesis imperfecta in the mixed dentitial phase observed in our patient.

The association of cone-rod dystrophy and amelogenesis imperfecta is a known, but very rare autosomal recessive condition, recently acknowledged as Jalili syndrome[4,116-119]. The first family was described by Jalili and Smith in 1988[4]. Twenty-nine members of a large consanguineous Arabian family were found to be affected with cone-rod dystrophy and amelogenesis imperfecta. In 2004, Michaelides[118] described another Kosovan family with two affected siblings showing very similar dental and retinal changes. Since then, only a few additional families of diverse ethnic origin have been reported with Jalili syndrome[118,119].

A locus for Jalili syndrome was mapped on chromosome 2q11 in the original Arabian family[116] and recently, mutations in the *CNNM4* gene were identified in this as well as other Jalili syndrome patients including families from Kosovo[124,125]. *CNNM4* encodes a putative metal transporter, which is implicated in ion transport, possibly of magnesium. Immunohistochemical localization of *CNNM4* showed its presence not only in the enamel organ, particularly in the ameloblasts, but also in the eye. In the cornea, *CNNM4* localization was mainly observed in the epithelium, keratocytes and in

the endoderm. More interestingly, *CNNM4* was also detected in the retina, most abundantly in the ganglion cell layers, the IPL (inner plexiform layer) and OPL (outer plexiform layer). The prime physiological function of the CNNM4 metal transporter still remains to be determined. It has been proposed that it may participate in the mineralization of the teeth and may play a supportive role for the trans- duction processes in the retina, since magnesium ions are an important cofactor of many enzymes involved in phototransduction, adaptation and other vision processes[124,125]. Based on these novel findings, we performed molecular genetic testing of the gene *CNNM4*. In fact, a homozygous mutation c.1312dupC p.Leu438ProfsX9 could be detected in our patient (**Table 4**). This mutation had already been described before in two independent families with Jalili syndrome originating from Kosovo and always in homozygous state[124,125]. Consequently it is justified to believe that this mutation is due to a founder mutation within this rather closed community most probably due to a higher allele frequency of this mutation within the Kosovan population.

Table 4: Genetic findings in our patient.

Gene	**Alteration on Nucleotide level**	**Alteration on Protein level**
NF1	c.2033insC heterozygous	p.Ile679AsnfsX21
CNNM4	c.1312dupC homozygous	p.Leu438ProfsX9

The various clinical findings in our case are now explained with the coincidence of two independent diseases, neurofibromatosis type 1 and Jalili syndrome. NF1 is a common and well-described genetic disorder with an estimated prevalence of 1 in 2000 to 1 in 5000. Almost half of all affected individuals have a de novo mutation, the cause of the unusually high mutation rate is unknown[120-123]. In contrast, Jalili syndrome is a very rare condition, only few cases are known worldwide[115-119]. The random association of two diseases is unusual and deserves attention. Cone dystrophies in children with NF1 might be overlooked because visual loss is attributed to OPGs. In our case, the

additional retinal dystrophy complicates the follow-up of tumor-growth by ophthalmological examinations. In this case, the progression of the OPGs can be determined mainly by MRI examinations. However, retinal dystrophies are usually more or less symmetric and do not show a relative afferent pupillary defect as was the case in our patient. To follow pupillary function is therefore especially helpful, and even the remission of the relative afferent pupillary defect would have to be considered as a sign of tumor progression because it would indicate tumor growth on the other eye.

It is therefore important even in “clinically clear” cases to watch out for unsual additional symptoms not compatible with the initial diagnosis. Our case points to the importance not only of thorough clinical examination, but also of interdisciplinary teamwork.

DOI:10.14753/SE.2014.1976

6. Discussion and Conclusions

This thesis aimed to show the importance of the previously discussed electrophysiological and imaging methods in the diagnostics and follow-up of inherited retinal degenerations. With the help of standard and extended protocols of electrophysiology and with the innovative imaging techniques of retinal morphology, a much more detailed characterisation of clinical phenotypes has become possible[1-3,6,12,23,31-35,82].

The results of this thesis are divided into three chapters, each of them dedicated to either a dianostic method or a special group of retinal disorders.

The first chapter dealed with the technical details and usefulness of multifocal ERG measurements. Our first study showed that a special setup, the fundus-controlled multifocal ERG is a convenient and precise technique for monitoring fixation during measurement. Even though the stimulation, response recording and filtering follows ISCEV recommendations, hardware differences (especially those of the amplifiers and stimulating monitor) lead to significant waveform and response parameter variability. Therefore, a comparison of clinical data obtained with either system is restricted to larger effects with the central hexagon showing the largest variations. Furthermore, we focused on the usefulness of the metohodology in inherited retinal disorders, especially in retinitis pigmentosa. This issue is becoming more important, now that essential steps towards possible therapies for retinal degenerations are made and reliable and objective testing methods are required[9-11]. The mfERG is well-suited for observation and long-term follow-up in disease development and – besides other psychophysical methods - it could be used as an objective outcome measure in upcoming treatment studies involving patients with advanced retinal diseases.

The second chapter dealed with the clinical characterization of the most common genotypes of autosomal dominant cone- and cone-rod dystrophies[63-66,80]. First, we presented a study, which was conducted in order to investigate, whether two different genotypes - mutations either in retGC-1 or its activating protein, GCAP1 –

make a difference in the phenotype, although they both act at the same step of the visual signal transduction cascade. Our aim was to compare the retinal function and morphology in patients affected by autosomal dominant CD or CRD carrying either a mutation in *GUCY2D* or *GUCA1A* by using the same psychophysical, electrophysiological and morphological methods. Taken together, we suggested that mutations in the *GUCA1A* gene in autosomal dominant retinal dystrophies cause a less severe phenotype and less involvement of rod photoreceptors than *GUCY2D* mutations. Furthermore, we presented detailed phenotypes of a multi-generation family suffering from adCRD with marked intrafamilial variability as well. We identified a novel disease-associated mutation in the *CRX* gene[83-88], c.636delC, which segregated with disease in all affected family members, and a sequence variant, c.100+12 C.T, which was only present in the more severely affected family members. We suggested that this polymorphism might have a modifying effect of the disease phenotype. In addition, we proposed that a negative ERG in adCRD might be an indicator of *CRX* gene mutations.

The third and last chapter showed two very rare conditions, both of them being described in the literature in very few cases[95-99]. Due to one-of-a-kind electrophysiological findings and strict association to mutations in the *KCNV2* gene, the first presented retinal disorder is considered a new entity called KCNV2-retinopathy[112]. In summary, KCNV2 retinopathy is considered a very rare retinal disorder associated with high but often normal mixed rod-cone response amplitudes, a marked prolongation of b-wave implicit times and a delayed, almost sudden, steep amplitude-versus-intensity relationship under scotopic conditions. Furthermore, while rod phototransduction is intact, there is a constant delay of the responses, which suggests changes in the synapse or in postreceptoral signaling pathway. Inner retinal involvement is also probable, since oscillatory potentials are almost absent. These findings are diagnostic and are exclusively linked to *KCNV2* mutations. Finally, as a highlight, an extremely rare condition was presented, only a handful of patients have been diagnosed with this syndromic disorder so far. Jalili syndrome[4] is the association cone-rod dystrophy and amelogenesis imperfecta and is caused by mutations in the *CNNM4* gene[124-125]. We reported a very unusual case of a girl with neurofibromatosis type 1, who unfortunately also suffers from Jalili syndrome. The random association of two genetic diseases is

very exceptional and deserves attention. Our case pointed out not only the importance of thorough clinical examination, but also of interdisciplinary teamwork.

In summary, we can conclude, that with the help of improved molecular genetic and functional diagnostic tools an early recognition and differentiation of inherited retinal disorders has become possible. The detailed results and information can help to extend our understanding of the pathological mechanisms involved in these diseases. Up to date, no established therapies are available, however, enormous efforts have been made in research in recent years and the new therapeutic approaches are underway and look very promising[9-11]. Therefore, precise clinical and genetic characterization plays a crucial role in not only managing diseases, but also in patients´ counselling regarding future therapeutic options.

DOI:10.14753/SE.2014.1976

7. Summary

This thesis aimed to show the importance of electrophysiological and imaging methods in the diagnostics and follow-up of inherited retinal degenerations. We conclude, that with the help of improved molecular genetic and functional diagnostic tools an early recognition and differentiation of inherited retinal disorders has become possible. Up to date, no established therapies are available, however, enormous efforts have been made in research in recent years and the new therapeutic approaches are underway and look very promising. Therefore, precise clinical and genetic characterization plays a crucial role in not only managing diseases, but also in patients´ counselling regarding future therapeutic options. Most important publications:

- We demonstrated the usefulness of mfERG in retinitis pigmentosa. The mfERG is well-suited for observation and long-term follow-up in disease development and could be used as an objective outcome measure in upcoming treatment studies (Nagy D, Schönfisch B, Zrenner E, Jägle H. Long-term follow-up in retinitis pigmentosa using the multifocal ERG. IOVS 2008 Oct;49(10):4664-71).
- Based on genotype-phenotype correlations, we suggested that mutations in the *GUCA1A* gene in autosomal dominant retinal dystrophies cause a less severe phenotype and less involvement of rod photoreceptors than *GUCY2D* mutations (Zobor D, Zrenner E, Wissinger B, Kohl S, Jägle H. *GUCY2D*- or *GUCA1A*-related autosomal dominant cone-rod dystrophy: is there a phenotypic difference? Retina. 2014 May 28. [Epub ahead of print] PubMed PMID: 24875811.).
- We studied the KCNV2-retinopathy, which is known for its one-of-a-kind electrophysiological findings and strict association to mutations in the *KCNV2* gene. Beyond identifying novel mutations, we presented a very detailed clinical characterization of the disease, which can help to better understand the underlying pathomechanisms (Zobor D, Kohl S, Wissinger B, Zrenner E, Jägle H: Rod and cone function in patients with KCNV2 retinopathy. PLoS One. 2012;7(10):e46762. doi: 10.1371/journal.pone.0046762. Epub 2012 Oct 15. PubMed PMID: 23077521; PubMed Central PMCID: PMC3471896).

DOI:10.14753/SE.2014.1976

Összefoglaló

A doktori értekezés mélyrehatóan foglalkozik az öröklődő retinabetegségekkel, valamint bemutatja az elektrofiziológiai és képalkotó eljárások jelentőségét a diagnosztikában és a betegségek nyomonkövetésében. Ezen információk segítségével érthetőbbé válik bizonyos kórképek patomechanizmusa, a klinikai vizsgálatok alkalmazhatósága és külön hangsúlyt kapnak a genetikai vizsgálatok, melyek együttesen eredményezik a megfelelő diagnózis felállítását. A világszerte folyó, intenzív kutatások eredményeként mára már megteremtődtek a jövőbeli terápiás lehetőségek feltételei, ezért a diagnózis korai klinikai felismerése és a genetikai háttér tisztázása a betegek számára lehetővé teheti a ma még csak klinikai tanulmányok kereteiben elérhető új terápiás módszerek kipróbálását. Legjelentősebb közlemények:

- Munkacsoportunk elsőként mutatott be retinitis pigmentosa esetében multifokális ERG-vel mért hosszútávú (10 éves) eredményeket. Ez a módszer igen jelentős szereppel bír nemcsak a betegség előrehaladott stádiumának követésében, de a közeljövőben rendelkezésre álló terápiák eredményességének monitorozásában is (Nagy D, Schönfisch B, Zrenner E, Jägle H (2008). Long-term follow-up in retinitis pigmentosa using the multifocal ERG. IOVS 49(10):4664-71).
- Egy klinikai tanulmányban ismert *GUCY2D* és *GUCA1A* mutációval rendelkező csap-pálcika disztrófiában szenvedő családokat hasonlítottunk össze. Eredményeink arra engednek következtetni, hogy *GUCA1A* mutációk esetében a pálcikák érintettsége enyhébb, így enyhébb klinikai manifesztációval számolhatunk (Zobor D, Zrenner E, Wissinger B, Kohl S, Jägle H (2014). *GUCY2D*- or *GUCA1A*-related autosomal dominant cone-rod dystrophy: is there a phenotypic difference? Retina. [Epub ahead of print] PubMed PMID: 24875811.).
- A KCNV2-retinopátiával nemcsak genetikai jelentősége, de klinikai egyedi megjelenése miatt intezíven foglalkoztunk. Új mutációk ismertetésén túl elsőként és a legalaposabban tanulmányoztuk a betegséget klinikailag, mely hasznos információival segíti a diagnózis egyszerű felállítását (Zobor D, Kohl S, Wissinger B, Zrenner E, Jägle H (2012). Rod and cone function in patients with KCNV2 retinopathy. PLoS One 7(10):e46762).

8. References

1. Neveling K, den Hollander AI, Cremers FP, Collin RW (2013). Identification and analysis of inherited retinal disease genes. Methods Mol Biol. 935:3-23.
2. www.orpha.net
3. Zobor D, Zrenner E (2012). [Retinitis pigmentosa - a review. Pathogenesis, guidelines for diagnostics and perspectives]. Ophthalmologe 109(5):501-14;quiz 515.
4. Jalili IK, Smith NJD (1988). A progressive cone-rod dystrophy and amelogenesis imperfecta: a new syndrome. J Med Genet 25:738–740.
5. Duane JF. Clinical Ophthalmology. Diseases of the Retina (Volume 3) Chapter 9. Lippincott Williams & Wilkins. 2006
6. Heckenlively JR, Arden GB (eds). Principles and Practice of Clinical Electrophysiology of Vision. Second Edition. The MIT Press Cambridge, Massachusetts, London, England 2006
7. https://sph.uth.edu/retnet/
8. Glöckle N, Kohl S, Mohr J, Scheurenbrand T, Sprecher A, Weisschuh N, Bernd A, Rudolph G, Schubach M, Poloschek C, Zrenner E, Biskup S, Berger W, Wissinger B, Neidhardt J (2014). Panel-based next generation sequencing as a reliable and efficient technique to detect mutations in unselected patients with retinal dystrophies. Eur J Hum Genet 22(1):99-104.
9. Zrenner E, Bartz-Schmidt KU, Benav H, Besch D, Bruckmann A, Gabel VP, Gekeler F, Greppmaier U, Harscher A, Kibbel S, Koch J, Kusnyerik A, Peters T, Stingl K, Sachs H, Stett A, Szurman P, Wilhelm B, Wilke R (2011). Subretinal electronic chips allow blind patients to read letters and combine them to words. Proc Biol Sci 278(1711):1489-97.
10. Ali RR (2012). Gene therapy for retinal dystrophies: twenty years in the making. Hum Gene Ther 23(4):337-9.
11. Busskamp V, Picaud S, Sahel JA, Roska B (2011). Optogenetic therapy for retinitis pigmentosa. Gene Ther 19(2):169-75.

12. Chizzolini M, Galan A, Milan E, Sebastiani A, Costagliola C, Parmeggiani F (2011). Good epidemiologic practice in retinitis pigmentosa: from phenotyping to biobanking. Curr Genomics; 12(4):260-6.
13. Fishman GA, Birch DG, Holder GE, Brigell MG. Electrophysiologic testing in disorders of the retina, optic nerve and visual pathway. 2nd edition 2001. Oxford University Press, Oxford
14. Marmor MF, Fulton AB, Holder GE, Miyake Y, Brigell M, Bach M (2009). ISCEV Standard for full-field clinical electroretinography (2008 update). Doc Ophthalmol 118: 69-77.
15. Hood DC, Bach M, Brigell M, Keating D, Kondo M, Lyons JS, Marmor MF, McCulloch DL, Palmowski-Wolfe AM (2012). ISCEV guidelines for clinical multifocal electroretinography (2011 edition). Doc Ophthalmol 124(1):1-13.
16. Sutter E. E. (1991). The fast m-transform: A fast computation of cross-correlations with binary m-sequences. SIAM Journal on Computing, 20(4), 686–694.
17. Sutter E. E., Tran D. (1992). The field topography of ERG components in man—I. The photopic luminance response. Vision Research, 32, 433–446.
18. Seeliger MW, Jurklies B, Kellner U, Palmowski A, Bach M, Kretschmann U (2001). Multifokale Elektroretinographie (mfERG). Ophthalmologe 98: 1112-1129
19. Seeliger MW, Narfström K, Reinhard J, Zrenner E, Sutter E (2000). Continuous monitoring of the stimulated area in multifocal ERG. Doc Ophthalmol 100: 167-184
20. Seeliger MW, Zrenner E, Apfelstedt-Sylla E, Jaissle GB (2001). Identification of Usher syndrome subtypes by ERG implicit time. IOVS 42(12): 3066-71
21. Granse L, Ponjavic V, Andreasson S (2004). Full-field ERG, multifocal ERG and multifocal VEP in patients with retinitis pigmentosa and residual central visual fields. Acta Ophthalmol Scand. 82(6): 701-6.
22. Bock M, Andrassi M, Belitsky L, Lorenz B (1998-1999). A comparison of two multifocal ERG systems. Doc Ophthalmol. 97(2):157-78.
23. Bernardes R, Lobo C, Cunha-Vaz JG (2002). Multimodal macula mapping: a new approach to study diseases of the macula. Surv Ophthalmol 47(6):580-9.

Review.

24. Jung T, Bader N, Grune T (2007). Lipofuscin: formation, distribution, and metabolic consequences. Ann N Y Acad Sci 1119:97-111. Review.
25. Delori FC, Fleckner MR, Goger DG, Weiter JJ, Dorey CK (2000). Autofluorescence distribution associated with drusen in age-related macular degeneration. Invest Ophthalmol Vis Sci. 41(2):496-504.
26. Delori FC, Goger DG, Dorey CK (2001). Age-related accumulation and spatial distribution of lipofuscin in RPE of normal subjects. Invest Ophthalmol Vis Sci. 42(8):1855-66.
27. Delori FC, Dorey CK, Staurenghi G, Arend O, Goger DG, Weiter JJ (1995). In vivo fluorescence of the ocular fundus exhibits retinal pigment epithelium lipofuscin characteristics. Invest Ophthalmol Vis Sci. 36(3):718-29.
28. Eldred GE, Katz ML (1988). Fluorophores of the human retinal pigment epithelium: separation and spectral characterization. Exp Eye Res 47(1):71-86.
29. Feeney-Burns L, Hilderbrand ES, Eldridge S (1984). Aging human RPE: morphometric analysis of macular, equatorial, and peripheral cells. Invest Ophthalmol Vis Sci. 25(2):195-200. PubMed PMID: 6698741.
30. von Rückmann A, Fitzke FW, Bird AC (1995). Distribution of fundus autofluorescence with a scanning laser ophthalmoscope. Br J Ophthalmol. 79(5):407-12. (2011)
31. Robson AG, Tufail A, Fitzke F, Bird AC, Moore AT, Holder GE, Webster AR. Serial imaging and structure-function correlates of high-density rings of fundus autofluorescence in retinitis pigmentosa. Retina. 31(8):1670-9.
32. Robson AG, Michaelides M, Saihan Z, Bird AC, Webster AR, Moore AT, Fitzke FW, Holder GE (2008). Functional characteristics of patients with retinal dystrophy that manifest abnormal parafoveal annuli of high density fundus autofluorescence; a review and update. Doc Ophthalmol. 116(2):79-89.
33. Robson AG, Michaelides M, Luong VA, Holder GE, Bird AC, Webster AR, Moore AT, Fitzke FW (2008). Functional correlates of fundus autofluorescence abnormalities in patients with RPGR or RIMS1 mutations causing cone or cone rod dystrophy. Br J Ophthalmol. 92(1):95-102.
34. Vaclavik V, Ooi KG, Bird AC, Robson AG, Holder GE, Webster AR (2007).

Autofluorescence findings in acute exudative polymorphous vitelliform maculopathy. Arch Ophthalmol. 125(2):274-7.

35. Robson AG, Saihan Z, Jenkins SA, Fitzke FW, Bird AC, Webster AR, Holder GE (2006). Functional characterisation and serial imaging of abnormal fundus autofluorescence in patients with retinitis pigmentosa and normal visual acuity. Br J Ophthalmol. 90(4):472-9.
36. Robson AG, Harding G, van Kuijk FJ, Pauleikhoff D, Holder GE, Bird AC, Fitzke FW, Moreland JD (2005). Comparison of fundus autofluorescence and minimum-motion measurements of macular pigment distribution profiles derived from identical retinal areas. Perception. 34(8):1029-34.
37. Scholl HP, Chong NH, Robson AG, Holder GE, Moore AT, Bird AC (2004). Fundus autofluorescence in patients with leber congenital amaurosis. Invest Ophthalmol Vis Sci. 45(8):2747-52.
38. Drexler W, Morgner U, Kärtner FX, Pitris C, Boppart SA, Li XD, Ippen EP, Fujimoto JG (1999). In vivo ultrahigh-resolution optical coherence tomography. Opt Lett. 24(17):1221-3.
39. Morgner U, Drexler W, Kärtner FX, Li XD, Pitris C, Ippen EP, Fujimoto JG (2000). Spectroscopic optical coherence tomography. Opt Lett. 15;25(2):111-3.
40. Drexler W, Morgner U, Ghanta RK, Kärtner FX, Schuman JS, Fujimoto JG (2001). Ultrahigh-resolution ophthalmic optical coherence tomography. Nat Med. 7(4):502-7. Erratum in: Nat Med 2001 May;7(5):636.
41. Huang D, Swanson EA, Lin CP, Schuman JS, Stinson WG, Chang W, Hee MR, Flotte T, Gregory K, Puliafito CA, et al (1991). Optical coherence tomography. Science. 22;254(5035):1178-81.
42. Nassif N, Cense B, Park B, Pierce M, Yun S, Bouma B, Tearney G, Chen T, de Boer J (2004). In vivo high-resolution video-rate spectral-domain optical coherence tomography of the human retina and optic nerve. Opt Express. 12(3):367-76.
43. Nassif N, Cense B, Park BH, Yun SH, Chen TC, Bouma BE, Tearney GJ, de Boer JF (2004). In vivo human retinal imaging by ultrahigh-speed spectral domain optical coherence tomography. Opt Lett. 1;29(5):480-2.
44. Wojtkowski M, Srinivasan V, Ko T, Fujimoto J, Kowalczyk A, Duker J (2004).

Ultrahigh-resolution, high-speed, Fourier domain optical coherence tomography and methods for dispersion compensation. Opt Express. 12(11):2404-22.

45. Adhi M, Regatieri CV, Branchini LA, Zhang JY, Alwassia AA, Duker JS (2013). Analysis of the morphology and vascular layers of the choroid in retinitis pigmentosa using spectral-domain OCT. Ophthalmic Surg Lasers Imaging Retina. 44(3):252-9.
46. Huynh N, Jeffrey BG, Turriff A, Sieving PA, Cukras CA (2014). Sorting out co-occurrence of rare monogenic retinopathies: Stargardt disease co-existing with congenital stationary night blindness. Ophthalmic Genet. 35(1):51-6.
47. Yeoh J, Rahman W, Chen F, Hooper C, Patel P, Tufail A, Webster AR, Moore AT, Dacruz L (2010). Choroidal imaging in inherited retinal disease using the technique of enhanced depth imaging optical coherence tomography. Graefes Arch Clin Exp Ophthalmol. 248(12):1719-28.
48. Chen Y, Roorda A, Duncan JL (2010). Advances in imaging of Stargardt disease. Adv Exp Med Biol. 664:333-40.
49. McAllister JT, Dubis AM, Tait DM, Ostler S, Rha J, Stepien KE, Summers CG, Carroll J (2010). Arrested development: high-resolution imaging of foveal morphology in albinism. Vision Res. 50(8):810-7.
50. Leitritz MA, Ziemssen F, Voykov B, Dimopoulos S, Zobor D, Bartz-Schmidt KU, Gelisken F (2014). Early postoperative changes of the foveal surface in epiretinal membranes: comparison of 23-gauge macular surgery with air vs. balanced salt solution. Graefes Arch Clin Exp Ophthalmol. 2014 Feb 4. [Epub ahead of print]
51. Bock M, Andrassi M, Belitsky L, Lorenz B (1998-1999). A comparison of two multifocal ERG systems. Doc Ophthalmol. 97(2):157-78.
52. Marmor FM (2002). Do you, doctor, take the mfERG…for better or for worse? Graefe's Arch Clin Exp Ophthalmol, Editorial 240. 241-243.
53. Rudolph G, Kalpadakis P (2002). The role of fixation for reliable mfERG results. Graefe's Arch Clin Exp Ophthalmol, Letter to the editor 240. 874-875.
54. www.roland-consult.de
55. www.veris-edi.com
56. Herse P (2005). Retinitis pigmentosa: visual function and multidisciplinary

management. Clin Exp Optom. 88(5): 335-50

57. Pagon RA (1988). Retinitis Pigmentosa. Major review. Surv Ophthalmol Vol. 33 No. 3: 137-177.
58. Iannaccone A, Kritchevsky SB, Ciccarelli ML, Tedesco SA, Macaluso C, Kimberling WJ, Somes GW (2004). Kinetics of visual field loss in Usher Syndrome type II. IOVS 45(3): 784-92
59. Massof RW, Dagnelie G, Benzschawel T, Palmer RW, Finkelstein D (1990). First-order dynamics of visual field loss in retinitis pigmentosa. Clin Vis Sci. 5:1–26. 77. 30.
60. Holopigian K, Greenstein V, Seiple W, Carr R (1996). Rates of change differ among measures of visual function in patients with retinitis pigmentosa. Ophthalmology. 103:398–405.
61. Berson EL, Sandberg MA, Rosner B, Birch DG, Hanson AH (1985). Natural course of retinitis pigmentosa over a three-year interval. Am J Ophthalmol. 99: 240-251
62. Grover S, Fishman GA, Anderson RJ, Alexander KR, Derlacki DJ (1997). Rate of visual field loss in retinitis pigmentosa. Ophthalmology. 104: 460-465.
63. Kitiratschky VB, Wilke R, Renner AB, Kellner U, Kellner U, Vadalà M, Birch DG, Wissinger B, Zrenner E, Kohl S (2008). Mutation analysis identifies GUCY2D as the major gene responsible for autosomal dominant progressive cone degeneration. Invest Ophthalmol Vis Sci. 49:5015–5023.
64. Kitiratschky VB, Behnen P, Kellner U, Heckenlively JR, Zrenner E, Jägle H, Kohl S, Wissinger B, Koch KW (2009). Mutations in the GUCA1A gene involved in hereditary cone dystrophies impair calcium-mediated regulation of guanylate cyclase. Hum Mutat 30:E782–E796.
65. Hunt DM, Wilkie SE, Newbold R (2004). Dominant cone and cone- rod dystrophies: functional analysis of mutations in retGC1 and GCAP1. Novartis Found Symp 255:37–49; discussion 49–50, 177–178.
66. Hunt DM, Buch P, Michaelides M (2010). Guanylate cyclases and associated activator proteins in retinal disease. Mol Cell Bio- chem 334:157–168.
67. Small KW, Silva-Garcia R, Udar N, Nguyen EV, Heckenlively JR (2008). New mutation, P575L, in the GUCY2D gene in a family with autosomal dominant

progressive cone degeneration. Arch Ophthalmol 126:397–403.

68. Sokal I, Dupps WJ, Grassi MA, Brown J Jr, Affatigato LM, Roychowdhury N, Yang L, Filipek S, Palczewski K, Stone EM, Baehr W (2005). A novel GCAP1 mis- sense mutation (L151F) in a large family with autosomal dominant cone-rod dystrophy (adCORD). Invest Ophthalmol Vis Sci. 46:1124–1132.
69. Jiang L, Katz BJ, Yang Z, Zhao Y, Faulkner N, Hu J, Baird J, Baehr W, Creel DJ, Zhang K (2005). Autosomal dominant cone dystrophy caused by a novel mutation in the GCAP1 gene (GUCA1A). Mol Vis 11:143–151.
70. Xiao X, Guo X, Jia X, Li S, Wang P, Zhang Q (2011). A recurrent mutation in GUCY2D associated with autosomal dominant cone dystrophy in a Chinese family. Mol Vis 17:3271–3278.
71. Zhao X, Ren Y, Zhang X, Chen C, Dong B, Li Y (2013). A novel GUCY2D mutation in a Chinese family with dominant cone dystrophy. Mol Vis 19:1039–1046.
72. Kachi S, Nishizawa Y, Olshevskaya E, Yamazaki A, Miyake Y, Wakabayashi T, Dizhoor A, Usukura J (1999). Detailed localization of photoreceptor guanylate cyclase activating protein-1 and -2 in mammalian retinas using light and electron microscopy. Exp Eye Res 68:465–473.
73. Larhammar D, Nordström K, Larsson TA (2009). Evolution of vertebrate rod and cone phototransduction genes. Philos Trans R Soc Lond B Biol Sci 364:2867–2880.
74. Olshevskaya EV, Ermilov AN, Dizhoor AM (1999). Dimerization of guanylyl cyclase-activating protein and a mechanism of pho toreceptor guanylyl cyclase activation. J Biol Chem 274:25583–25587.
75. Olshevskaya EV, Ermilov AN, Dizhoor AM (2002). Factors that affect regulation of cGMP synthesis in vertebrate photoreceptors and their genetic link to human retinal degeneration. Mol Cell Biochem 230:139–147. Review.
76. Duda T, Pertzev A, Sharma RK (2012). Differential Ca(2+) sensor guanylate cyclase activating protein modes of photoreceptor rod outer segment membrane guanylate cyclase signaling. Bio- chemistry 51:4650–4657.
77. Peshenko IV, Olshevskaya EV, Dizhoor AM. Binding of gua- nylyl cyclase activating protein 1 (GCAP1) to retinal guanylyl cyclase (RetGC1). The role of

individual EF-hands. J Biol Chem 2008;283:21747–21757.

78. Makino CL, Peshenko IV, Wen XH, Olshevskaya EV, Barrett R, Dizhoor AM (2008). A role for GCAP2 in regulating the photoresponse. Guanylyl cyclase activation and rod electrophysiology in GUCA1B knock-out mice. J Biol Chem 283:29135–29143
79. Kitiratschky VB, Glöckner CJ, Kohl S (2011). Mutation screening of the GUCA1B gene in patients with autosomal dominant cone and cone rod dystrophy. Ophthalmic Genet 32:151–155.
80. Wilkie SE, Newbold RJ, Deery E, Walker CE, Stinton I, Ramamurthy V, Hurley JB, Bhattacharya SS, Warren MJ, Hunt DM (2000). Functional characterization of missense mutations at codon 838 in retinal guanylate cyclase correlates with disease severity in patients with auto- somal dominant cone-rod dystrophy. Hum Mol Genet 9: 3065–3073.
81. Berson EL, Gouras P, Gunkel RD (1968). Progressive cone degeneration, dominantly inherited. Arch Ophthalmol 80:77–83.
82. Hamel C (2007). Cone rod dystrophies. Orphanet J Rare Dis 2:7.
83. Furukawa T, Morrow EM, Cepko CL (1997). Crx, a novel otx-like homeobox gene, shows photoreceptor-specific expression and regulates photoreceptor differentiation. Cell 91:531–41.
84. Chen S, Wang QL, Nie Z, Sun H, Lennon G, Copeland NG, Gilbert DJ, Jenkins NA, Zack DJ (1997). Crx, a novel Otx-like paired-homeodomain protein, binds to and transactivates photoreceptor cell-specific genes. Neuron 19:1017–30.
85. Bibb LC, Holt JK, Tarttelin EE, Hodges MD, Gregory-Evans K, Rutherford A, Lucas RJ, Sowden JC, Gregory-Evans CY (2001). Temporal and spatial expression patterns of the CRX transcription factor and its downstream targets. Critical differences during human and mouse eye development. Hum Mol Genet 10:1571–9.
86. Yanagi Y, Masuhiro Y, Mori M, Yanagisawa J, Kato S (2000). p300/CBP acts as a coactivator of the cone–rod homeobox transcription factor. Biochem Biophys Res Commun 269:410–14.
87. Chen S, Wang Q-L, Xu S, Liu I, Li LY, Wang Y, Zack DJ (2002). Functional analysis of cone–rod homeobox (CRX) mutations associated with retinal

dystrophy. Hum Mol Genet 11:873–84.

88. Chau KY, Chen S, Zack DJ, Ono SJ (2000). Functional domains of the cone–rod homeobox (CRX) transcription factor. J Biol Chem 275:37264–70.
89. Peng GH, Chen S (2005). Chromatin immunoprecipitation identifies photoreceptor transcription factor targets in mouse models of retinal degeneration: new findings and challenges. Vis Neurosci 22:575–86.
90. Mitton KP, Swain PK, Chen S, Xu S, Zack DJ, Swaroop A (2000). The leucine zipper of NRL interacts with the CRX homeodomain. A possible mechanism of transcriptional synergy in rhodopsin regulation. J Biol Chem 275:29794–9.
91. Holbrook JA, Neu-Yilik G, Hentze MW, Kulozik AE (2004). Nonsense-mediated decay approaches the clinic. Nat Genet 36:801–8.
92. Brown KT (1968). The electroretinogram: its components and their origins. Vision Res 8:633–77.
93. Miller RF, Dowling JE (1970). Intracellular responses of the Muller (glial) cells of mudpuppy retina: their relation to b-wave of the electroretinogram. J Neurophysiol 33:323–41.
94. Evans LS, Peachey NS, Marchese AL (1993). Comparison of three methods of estimating the parameters of the Naka–Rushton equation. Doc Ophthalmol 84:19–30.
95. Gouras P, Eggers HM, MacKay CJ (1983). Cone dystrophy, nyctalopia, and supernormal rod responses. A new retinal degeneration. Arch Ophthalmol 101:718-724.
96. Alexander KR, Fishman GA (1984). Supernormal scotopic ERG in cone dystrophy. Br J Ophthalmol 68:69-78.
97. Foerster MH, Kellner U, Wessing A (1990). Cone dystrophy and supernormal dark-adapted b-waves in the electroretinogram. Graefe's archive for clinical and experimental ophthalmology = Albrecht von Graefes Archiv fur klinische und experimentelle Ophthalmologie 228:116-119.
98. Hood DC, Cideciyan AV, Halevy DA, Jacobson SG (1996). Sites of disease action in a retinal dystrophy with supernormal and delayed rod electroretinogram b-waves. Vision research 36:889-901.

99. Kato M, Kobayashi R, Watanabe I (1993). Cone dysfunction and supernormal scotopic electroretinogram with a high-intensity stimulus. A report of three cases. Documenta ophthalmologica 84:71-81

100. Michaelides M, Holder GE, Webster AR, Hunt DM, Bird AC, Fitzke FW, Mollon JD, Moore AT (2005). A detailed phenotypic study of "cone dystrophy with supernormal rod ERG". Br J Ophthalmol 89:332-339.

101. Rosenberg T, Simonsen SE (1993). Retinal cone dysfunction of supernormal rod ERG type. Five new cases. Acta ophthalmologica 71:246-255.

102. Sandberg MA, Miller S, Berson EL (1990). Rod electroretinograms in an elevated cyclic guanosine monophosphate-type human retinal degeneration. Comparison with retinitis pigmentosa. Investigative ophthalmology & visual science 31:2283-2287.

103. Yagasaki K, Miyake Y, Litao RE, Ichikawa K (1986). Two cases of retinal degeneration with an unusual form of electroretinogram. Documenta ophthalmologica 63:73-82.

104. Wu H, Cowing JA, Michaelides M, Wilkie SE, Jeffery G, Jenkins SA, Mester V, Bird AC, Robson AG, Holder GE, Moore AT, Hunt DM, Webster AR (2006). Mutations in the gene KCNV2 encoding a voltage-gated potassium channel subunit cause "cone dystrophy with supernormal rod electroretinogram" in humans. American journal of human genetics 79:574-579.

105. Czirjak G, Toth ZE, Enyedi P (2007). Characterization of the heteromeric potassium channel formed by kv2.1 and the retinal subunit kv8.2 in Xenopus oocytes. Journal of neurophysiology 98:1213-1222.

106. Beech DJ, Barnes S (1989). Characterization of a voltage-gated K+ channel that accelerates the rod response to dim light. Neuron 3:573-581.

107. Mohapatra DP, Park KS, Trimmer JS (2007). Dynamic regulation of the voltage-gated Kv2.1 potassium channel by multisite phosphorylation. Biochemical Society transactions 35:1064-1068.

108. Ben Salah S, Kamei S, Senechal A, Lopez S, Bazalgette C, Bazalgette C, Eliaou CM, Zanlonghi X, Hamel CP (2008). Novel KCNV2 mutations in cone dystrophy

with supernormal rod electroretinogram. American journal of ophthalmology 145:1099-1106.

109. Thiagalingam S, McGee TL, Weleber RG, Sandberg MA, Trzupek KM, Berson EL, Dryja TP (2007). Novel mutations in the KCNV2 gene in patients with cone dystrophy and a supernormal rod electroretinogram. Ophthalmic genetics 28:135-142.

110. Wissinger B, Dangel S, Jagle H, ansen L, Baumann B, Rudolph G, Wolf C, Bonin M, Koeppen K, Ladewig T, Kohl S, Zrenner E, Rosenberg T (2008). Cone dystrophy with supernormal rod response is strictly associated with mutations in KCNV2. Investigative ophthalmology & visual science 49:751-757.

111. Robson AG, Webster AR, Michaelides M, Downes SM, Cowing JA, Hunt DM, Moore AT, Holder GE (2010). "Cone dystrophy with supernormal rod electroretinogram": acomprehensive genotype/phenotype study including fundus autofluorescence andextensive electrophysiology. Retina. 30(1):51-62.

112. Sergouniotis PI, Holder GE, Robson AG, Michaelides M, Webster AR, Moore AT (2012). High-resolution optical coherence tomography imaging in KCNV2 retinopathy. Br J Ophthalmol. 96(2):213-7.

113. Wissinger B, Schaich S, Baumann B, Bonin M, Jägle H, Friedburg C, Varsányi B, Hoyng CB, Dollfus H, Heckenlively JR, Rosenberg T, Rudolph G, Kellner U, Salati R, Plomp A, De Baere E, Andrassi-Darida M, Sauer A, Wolf C, Zobor D, Bernd A, Leroy BP, Enyedi P, Cremers FP, Lorenz B, Zrenner E, Kohl S (2011). Large deletions of the KCNV2 gene are common in patients with cone dystrophy with supernormal rod response. Hum Mutat. 32(12):1398-406.

114. Friedburg C, Wissinger B, Schambeck M, Bonin M, Kohl S, Lorenz B (2011). Long-term follow-up of the human phenotype in three siblings with cone dystrophy associated with a homozygous p.G461R mutation of KCNV2. Invest Ophthalmol Vis Sci. 52(12):8621-9. doi: 10.1167/iovs.11-8187. PubMed PMID: 21911584.

115. Barnes S (1994). After Transduction: Response Shaping and Control of Transmission by Ion Channels of the Photoreceptor Inner Segment. Neurosci 58: 447-459.

116. Downey LM, Keen TJ, Jalili IK, McHale J, Aldred MJ, Robertson SP, Mighell A, Fayle S, Wissinger B, Inglehearn CF (2002). Identification of a locus on chromosome 2q11 at which recessive amelogenesis imper- fecta and cone-rod dystrophy cosegregate. Eur J Hum Genet 2002 10(12):865–869.

117. Michaelides M, Bloch-Zupan A, Holder GE, Hunt DM, Moore AT (2004). An autosomal recessive cone-rod dystrophy associated with amelogenesis imperfecta. J Med Genet 41;468–473

118. Inglehearn CF, El-Sayed W, Shore RC, Jalili IK, Dollfus H, Carlos R, Blain KM, Mansfield DC, Moore AT, Mighell AJ (2008). Jalili syndrome- cone-rod dystrophy (CRD) and amelogenesis imperfecta (AI); six families and consistent linkage to 2q11. ARVO E-Abstract 457.

119. Mighell AJ, El-Sayed W, Shore RC, Jalili IK, Dollfus H, Bloch-Zupan A, Carlos R, Blain K, Mansfield D, Moore AT, Inglehearn CF (2008). Amelogenesis imperfecta and central blindness: an inherited syndrome. IADR 86th General Session & Exhibition, Abstract 1536.

120. Friedman JM. Neurofibromatosis 1. Gene Reviews: www. genetests.org

121. Listernick R, Ferner RE, Liu GT, Gutmann DH (2007). Optic path- way gliomas in neurofibromatosis-1: Controversies and recommendations. Ann Neurol 61:189–198.

122. Chang BC, Mirabella G, Yagev R, Banh M, Mezer E, Parkin PC, Westall CA, Buncic JR (2007). Screening and diagnosis of optic pathway gliomas in children with neurofibromatosis type 1 by using sweep visual evoked potentials. IOVS 48(6):2895–2902.

123. Opocher E, Kremer LCM, Da Dalt L, van de Wetering MD, Viscardi E, Caron HN, Perilongo G (2006). Prognostic factors for progression of childhood optic pathway glioma: a systematic review. Eur J Cancer 42(12):1807–1816.

124. Polok B, Escher P, Ambresin A, Chouery E, Bolay S, Meunier I, Nan F, Hamel C, Munier FL, Thilo B, Mégarbané A, Schorderet DF (2009). Mutations in CNNM4 cause recessive cone-rod dystrophy with amelogenesis imperfecta. Am J Hum Genet 2009;84:259–265

125. Parry DA, Mighell AJ, El-Sayed W, Shore RC, Jalili IK, Dollfus H, Bloch-Zupan A, Carlos R, Carr IM, Downey LM, Blain KM, Mansfield DC, Shahrabi M, Heidari M, Aref P, Abbasi M, Michaelides M, Moore AT, Kirkham J, Inglehearn CF(2009). Mutations in CNNM4 cause Jalili syndrome, consisting of autosomal- recessive cone-rod dystrophy and amelogenesis imperfecta. Am J Hum Genet 84:266–273.

DOI:10.14753/SE.2014.1976

9. Own publications

9.1. Publications relevant to the PhD thesis

Nagy D, Schönfisch B, Zrenner E, Jägle H (2008). Long-term follow-up in retinitis pigmentosa using the multifocal ERG. IOVS 49(10):4664-71.

Zobor D, Zrenner E (2012). [Retinitis pigmentosa - a review. Pathogenesis, guidelines for diagnostics and perspectives]. Ophthalmologe. 109(5):501-14;quiz 515. German. PubMed PMID: 22581051.

Zobor D, Zrenner E, Wissinger B, Kohl S, Jägle H (2014). *GUCY2D*- or *GUCA1A*-related autosomal dominant cone-rod dystrophy: is there a phenotypic difference? Retina. 2014 May 28. [Epub ahead of print]

Kitiratschky VB, **Nagy D**, Zabel T, Zrenner E, Wissinger B, Kohl S, Jägle H (2008). Cone and cone-rod dystrophy segregating in the same pedigree due to the same novel CRX gene mutation. Br J Ophthalmol. 92(8):1086-91.

Zobor D, Kohl S, Wissinger B, Zrenner E, Jägle H (2012). Rod and cone function in patients with KCNV2 retinopathy. PLoS One. 7(10):e46762.

Wissinger B, Schaich S, Baumann B, Bonin M, Jägle H, Friedburg C, Varsányi B, Hoyng CB, Dollfus H, Heckenlively JR, Rosenberg T, Rudolph G, Kellner U, Salati R, Plomp A,De Baere E, Andrassi-Darida M, Sauer A, Wolf C, **Zobor D**, Bernd A, Leroy BP, Enyedi P, Cremers FP, Lorenz B, Zrenner E, Kohl S (2011). Large deletions of the KCNV2 gene are common in patients with cone dystrophy with supernormal rod response. Hum Mutat. 32:(12) pp. 1398-406.

Zobor D, Kaufmann DH, Weckerle P, Sauer A, Wissinger B, Wilhelm H, Kohl S. Cone-rod dystrophy associated with amelogenesis imperfecta in a child with neurofibromatosis type 1. Ophthalmic Genet. 33:(1) pp. 34-38

9.2. Other publications

Zobor D, Balousha G, Baumann B, Wissinger B (2014). Homozygosity mapping reveals new nonsense mutation in the FAM161A gene causing autosomal recessive retinitis pigmentosa in a Palestinian family. Mol Vis. 20:178-82.

Leitritz MA, Ziemssen F, Voykov B, Dimopoulos S, **Zobor D**, Bartz-Schmidt KU, Gelisken F (2014). Early postoperative changes of the foveal surface in epiretinal membranes: comparison of 23-gauge macular surgery with air vs. balanced salt solution. Graefes Arch Clin Exp Ophthalmol. 2014 Feb 4. [Epub ahead of print]

Shao Y, Keliris GA, Papanikolaou A, Fischer MD, **Zobor D**, Jägle H, Logothetis NK, Smirnakis SM (2013). Visual cortex organisation in a macaque monkey with macular degeneration. Eur J Neurosci. 38(10):3456-64.

Perrault, A. Estrada-Cuzcano, I. Lopez, S. Kohl, S. Li, F. Testa, R. Zekveld, X. Wang, E. Pomares, J. Andorf, N. Aboussair, S. Banfi, N. Delphin, A. den Hollander, C. Edelson, R. Florijn, M. JeanPierre, C. Leowski, A. Megarbane, C. Villanueva, B. Flores, A. Munnich, H. Ren, **D. Zobor**, A. Bergen, R. Chen, F. Cremers, R. Gonzales-Duarte, R. K. Koenekoop, F. Simonelli, E. Stone, B. Wissinger, Q. Zhang, J. Kaplan, JM. Rozet (2013) Union Makes Strength: A worldwide collaborative genetic and clinical study to provide a comprehensive survey of RD3 mutations and delineate the associated phenotype. PLoS One. 8(1):e51622.

Pach J, Kohl S, Gekeler F, **Zobor D** (2013). Identification of a novel mutation in the PRCD gene causing autosomal recessive retinitis pigmentosa in a Turkish family. MolVis 19:1350-5. Print 2013.

Fischer MD*, **Zobor D***, Keliris GA, Shao Y, Jägle H, Logothetis NK, Smirnakis SS (2012). Juvenile macular degeneration in a rhesus macaque: structural and functional description. Doc Ophthalmol 125:(3): 179-194.

Jägle H, **Zobor D**, Brauns T (2010). Accomodation limits induced optical defocus in

defocus experiments. Doc Ophthalmol 121(2):103-9.

Becirovic E, Ebermann I, **Nagy D**, Zrenner E, Seeliger MW, Bolz HJ (2008). Usher syndrome type 1 due to missense mutations on both CDH23 alleles: investigation of mRNA splicing. Hum Mutat. 29(3):452.

Horsch, Wanka: Das Usher-Syndrom – eine erworbene Hörsehbehinderung. Kapitel: Das subretinale elektronische Implantat zur Wiederherstellung von Seheindrücken: künftig Einsatz auch beim Usher Syndrom möglich? Ernst Reinhardt Verlag München Basel, 2012 (Book chapter) pp.70-81.

10. Reprints of relevant publications

1. **Nagy D**, Schönfisch B, Zrenner E, Jägle H (2008). Long-term follow-up in retinitis pigmentosa using the multifocal ERG. IOVS 49(10):4664-71.
2. **Zobor D**, Zrenner E (2012). [Retinitis pigmentosa - a review. Pathogenesis, guidelines for diagnostics and perspectives]. Ophthalmologe. 109(5):501-14;quiz 515. German. PubMed PMID: 22581051.
3. **Zobor D**, Zrenner E, Wissinger B, Kohl S, Jägle H (2014). *GUCY2D*- or *GUCA1A*-related autosomal dominant cone-rod dystrophy: is there a phenotypic difference? Retina. 2014 May 28. [Epub ahead of print]
4. Kitiratschky VB, **Nagy D**, Zabel T, Zrenner E, Wissinger B, Kohl S, Jägle H (2008). Cone and cone-rod dystrophy segregating in the same pedigree due to the same novel CRX gene mutation. Br J Ophthalmol. 92(8):1086-91.
5. **Zobor D**, Kohl S, Wissinger B, Zrenner E, Jägle H (2012). Rod and cone function in patients with KCNV2 retinopathy. PLoS One. 7(10):e46762.
6. Wissinger B, Schaich S, Baumann B, Bonin M, Jägle H, Friedburg C, Varsányi B, Hoyng CB, Dollfus H, Heckenlively JR, Rosenberg T, Rudolph G, Kellner U, Salati R, Plomp A,De Baere E, Andrassi-Darida M, Sauer A, Wolf C, **Zobor D**, Bernd A, Leroy BP, Enyedi P, Cremers FP, Lorenz B, Zrenner E, Kohl S (2011). Large deletions of the KCNV2 gene are common in patients with cone dystrophy with supernormal rod response. Hum Mutat. 32:(12) pp. 1398-406.
7. **Zobor D**, Kaufmann DH, Weckerle P, Sauer A, Wissinger B, Wilhelm H, Kohl S. Cone-rod dystrophy associated with amelogenesis imperfecta in a child with neurofibromatosis type 1. Ophthalmic Genet. 33:(1) pp. 34-38

DOI: 10.1167/iovs.07-1360

Long-Term Follow-up of Retinitis Pigmentosa Patients with Multifocal Electroretinography

Ditta Nagy,[*,1] *Birgitt Schönfisch,*[2] *Eberhart Zrenner,*[1] *and Herbert Jägle*[*,1,3]

Purpose. To study the rate of multifocal electroretinographic (mfERG) response amplitude changes and their relation to other parameters of disease development in retinitis pigmentosa (RP).

Methods. Twenty-three patients (9 men and 14 women) with clinically defined RP were included in the study. Disease progression was monitored during a period of up to 10 years by psychophysical techniques and Ganzfeld electroretinography. In addition, ERGs were recorded with a mfERG imaging system (VERIS; Electro-Diagnostic Imaging, Inc., Redwood City, CA). The black and white stimulus consisted of 61 hexagons covering a visual field of approximately 60° × 55°. Responses were analyzed according to concentric ring averages.

Results. The progression of visual field loss for target III4e was approximately 14.5%. Using the same type of regression model, the yearly progression according to the mfERG values was found to be approximately 6% to 10% in the outer three rings. Visual acuity (median 0.8) correlated well with the amplitude of the central segment of the mfERGs, ring 5 amplitudes of the mfERG strongly correlated with the scotopic Ganzfeld ERG mixed cone–rod response amplitude. However, in advanced cases, reliable mfERG responses could still be recorded, even if the ISCEV scotopic Ganzfeld ERG was not reproducible. MfERG ring 5 amplitudes as well as the Ganzfeld ERG mixed cone–rod response amplitude showed only a mild correlation with visual field area.

Conclusions. The mfERG allows long-term follow-up of disease progression in retinitis pigmentosa. It does not replace, but complements psychophysical methods and could be used as an objective outcome measure in upcoming treatment studies involving patients with advanced retinal diseases. (*Invest Ophthalmol Vis Sci.* 2008;49:4664–4671) DOI:10.1167/iovs.07-1360

Retinitis pigmentosa (RP) is a heterogenous group of degenerative retinal diseases, which is associated with night-blindness, progressive loss of the peripheral visual field and a slow reduction in central vision and Ganzfeld ERG abnormalities. RP diffusely and primarily affects the photoreceptors, predominantly the rod system, and as the disease progresses, the function of the cone system also declines. The age of onset, rate of progression, and presence or absence of associated ocular features are frequently related to the mode of inheritance, but the clinical appearance may vary, even among family members with the disease.

Characterization and understanding of the visual loss is important for monitoring patients with RP. A detailed differential diagnosis and long-term follow-up are advisable for adequate patient counseling, for predicting visual outcome, and for monitoring the efficacy and safety of new therapeutic options.[1–3]

Clinical psychophysical and electrophysiological measurements have been used to provide objective information regarding changes in retinal function. Whereas examinations, like visual acuity testing and perimetry, rely on subjective responses, electrophysiological methods are used to quantify retinal function in a more objective way. The Ganzfeld ERG allows recording of electrical responses originating from the entire retina when stimulating with a full-field light source.[4–6] In contrast, the multifocal ERG (mfERG) allows assessment of a "map" of electrical activity based on a technique introduced by Sutter and Tran in 1992.[7] It has been applied to various retinal disorders[6] and a standard has become available[8] (see also www.iscev.org). With disease progression, the waveforms may no longer be detected by Ganzfeld ERG, whereas still some residual visual field can be measured. In such cases, localized responses may still be obtained using the mfERG.

The purpose of our study therefore was to investigate the usefulness of the mfERG among other clinical psychophysical and electrophysiological techniques. This article also provides a review of the characteristics and natural course of retinitis pigmentosa. Emphasis is placed on determining the yearly progression of the mfERG responses. We also sought to compare mfERGs and other parameters of disease development.

Methods

Twenty-three patients (9 men and 14 women; median age, 36 years; age at the first presentation, 12–66 years) with different Mendelian inheritance patterns of retinitis pigmentosa were selected from our patient database and included in the study, based on a minimum follow-up time of 3 years and reproducible mfERG responses at the time of the first investigation. The protocol of the study adhered to the provisions of the Declaration of Helsinki. The diagnosis of RP was based on the clinical features, ophthalmoscopic appearance, and the results of perimetry, dark-adapted thresholds, and Ganzfeld-flash ERGs according to the ISCEV (International Society for Clinical Electrophysiology of Vision) Standards.[5] Typical fundus changes and visual field and mfERG findings are presented in Figure 1. Patient characteristics are presented in Table 1. Disease progression in both eyes was followed up over a period of up to 10 years (median, 6 years). At each visit, all patients received standardized examinations including best corrected visual acuity, kinetic perimetry (Goldmann), color vision (Lanthony Panel D-15 test), dark adaptometry, and ISCEV Ganzfeld and multifocal mfERG. At the

From the [1]Centre for Ophthalmology, Institute for Ophthalmic Research, and the [2]Department of Medical Biometry, University of Tübingen, Tübingen, Germany; and the [3]Division of Motility Disorders, Periocular Surgery and Pediatric Ophthalmology, Centre for Ophthalmology, Tübingen, Germany.

Supported by a personal grant from ProRetina Germany (DN) and Grant JA997/8-1 from the German Research Council (HJ, EZ).

Submitted for publication October 22, 2007; revised February 4 and May 14, 2008; accepted August 18, 2008.

Disclosure: **D. Nagy**, None; **B. Schönfisch**, None; **E. Zrenner**, None; **H. Jägle**, None

The publication costs of this article were defrayed in part by page charge payment. This article must therefore be marked "*advertisement*" in accordance with 18 U.S.C. §1734 solely to indicate this fact.

*Each of the following is a corresponding author: Ditta Nagy, Schleichstrasse 12-16, 72076 Tübingen, Germany; ditta_n@hotmail.com. Herbert Jägle, Centre for Ophthalmology, Schleichstrasse 12-16, 72076 Tübingen, Germany; herbert.jaegle@uni-tuebingen.de.

Investigative Ophthalmology & Visual Science, October 2008, Vol. 49, No. 10

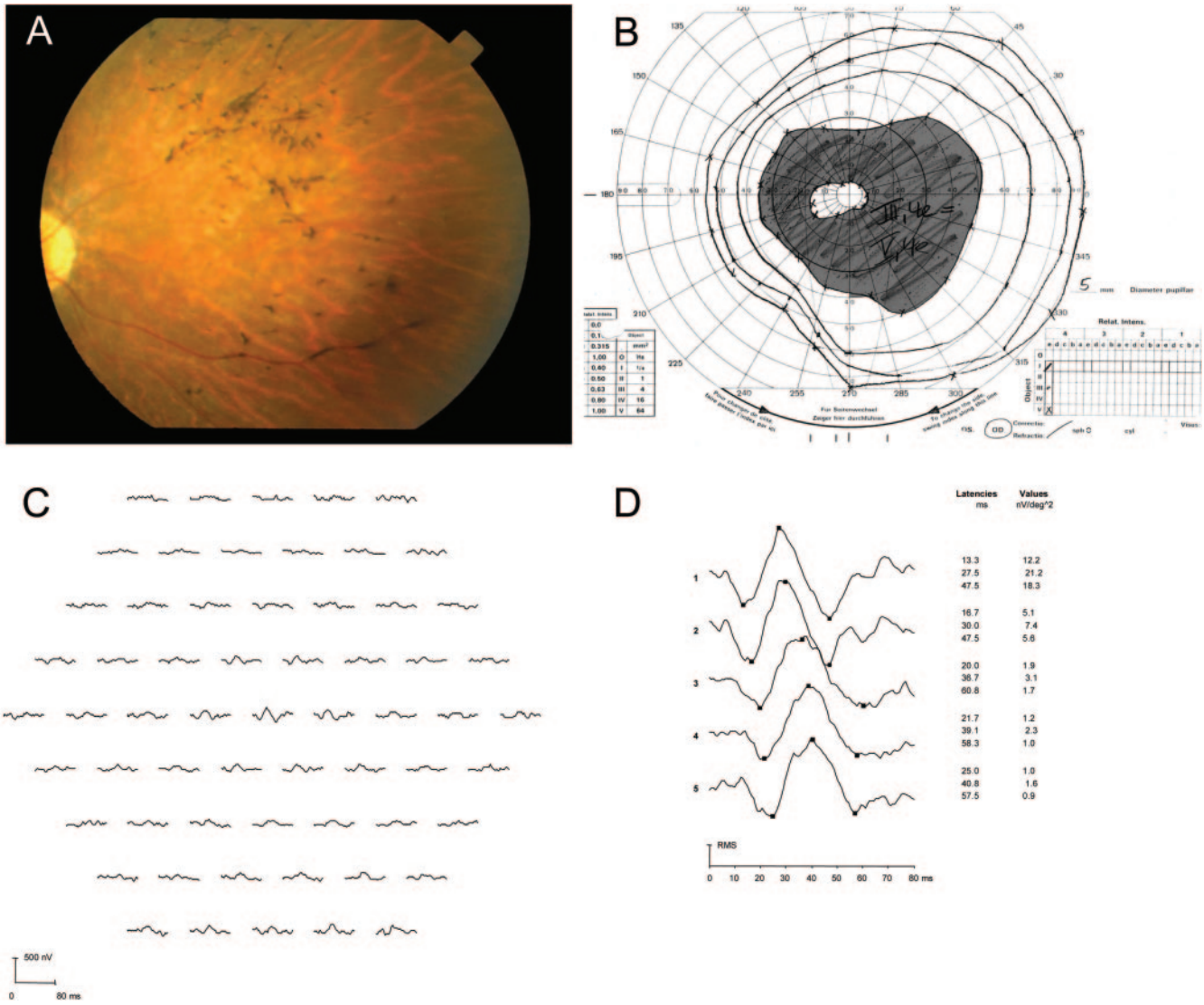

FIGURE 1. A typical fundus photograph of an eye with retinitis pigmentosa with optic disc pallor, bone spicule–like pigment changes, atrophy of the RPE and vessel narrowing (**A**), corresponding visual field defects (**B**), the topography of mfERG responses (**C**), and the ring average analysis used in this study (**D**). Ring average waveforms are shown with normalized root mean square (RMS) amplitude for easier waveform comparison.

patients' request, Ganzfeld ERG was not performed in patient 9 or mfERG in patients 4 and 13 at one visit each.

A series of standardized questions was given to all patients at the first visit, to determine the age of onset (median, 20 years; range, 6–48) based on the appearance of one of the following signs: night blindness, light aversion, loss of peripheral visual field, or reduced visual acuity.

Visual Field

Kinetic perimetry was performed with the Goldmann kinetic perimeter at each visit. To be able to compare the visual field loss to other parameters, fields for target size III4e were taken and computerized and residual field area was measured with a special computer program. The calculated visual field areas were compared with a normal visual field area for target III4e (normal visual field = 1.0). Although the estimated relative field area is subject to distortion and underestimation of the central field area,[9–11] the effect on our exponential model fit is small.

Color Vision

Color vision was tested with the Lanthony panel D-15 desaturated test. The results were quantified according to Bowman's Total Color Difference Score (TCDS), which provides a quantitative index of D-15 performance and color confusions, but does not necessarily differentiate defect type.[12] It is used to follow the progression of an acquired color vision disease process.[12–15] Three subjects (patients 14, 19, and 21) could perform only the Panel D-15 saturated test; their color vision results were excluded from the analysis.

Dark Adaptation

Dark adaptation thresholds were obtained in one eye after 30 minutes of dark adaptation with the Tübingen hand perimeter (THP). A white target with 2° diameter was presented at 20° eccentricity in the nasal visual field for 1 second. Dark adaptation thresholds were ascertained five to six times.

DOI:10.14753/SE.2014.1976 IOVS, October 2008, Vol. 49, No. 10

TABLE 1. Patient Characteristics

Patient	Sex	Inheritance Pattern	Age at Disease Onset	Age at 1st mfERG Recording	Age at Last mfERG Recording	VA at 1st mfERG Recording (OD/OS)	Number of Visits	Years of Follow-up with mfERG
1	Female	Ad	16	18	21	0.8/0.8	2	3
2	Female	Ad	48	56	60	0.8/1.2	2	4
3	Female	Ad	18	37	41	0.7/0.4	2	4
4	Female	Ad	6	41	47	0.6/0.8	4	6
5	Male	Ad	11	27	30	1.0/1.2	2	3
6	Female	Ad	16	40	46	1.2/1.2	2	6
7	Female	Ad	34	34	39	1.6/1.6	3	5
8	Male	Ad	36	36	44	1.2/0.8	2	8
9	Male	Ad	16	16	20	1.5/1.5	3	4
10	Male	Ad	13	47	56	1.5/0.8	2	9
11	Male	Ad	33	54	62	0.8/0.8	3	8
12	Male	Ar	20	37	39	0.8/0.8	3	5
13	Male	Ar	8	12	15	0.8/0.8	3	3
14	Female	Ar	10	26	34	0.3/0.3	3	8
15	Female	Ar	30	53	40	1.5/1.5	4	10
16	Female	Simplex	20	28	35	0.8/0.8	3	7
17	Female	Simplex	34	34	41	1.2/1.5	3	7
18	Male	Simplex	20	42	51	1.0/0.8	4	9
19	Female	Simplex	15	35	41	0.3/0.3	3	6
20	Female	Simplex	10	23	32	0.8/0.5	4	9
21	Male	Simplex	27	66	73	0.5/0.5	2	7
22	Male	Usher II	22	39	48	0.9/0.9	5	9
23	Female	Usher II	14	17	23	1.0/1.2	2	6

VA, visual acuity; Ad, autosomal dominant; Ar, autosomal recessive.

Electrophysiology

Pupils were dilated with tropicamide before the electrophysiological examination. After 30 minutes of dark adaptation, DTL fiber electrodes were positioned according to ISCEV Standards.[5,8] After scotopic measurements, photopic recordings were preceded by a light adaptation of 10 minutes to a background light of 30 cd/m^2. Ganzfeld ERGs were recorded with one of two systems (Spirit; Nicolet Biomedical Instruments, Madison, WI, or UTAS 2000; LKC Technologies, Inc., Gaithersburg, MD). Maximum flash intensity (0 dB) was 2.4 and 2.3 cd · s · m^{-2} for the Nicolet and LKC systems, respectively. Attenuation of the standard rod flash was 24 dB for both systems.

Multifocal ERGs were performed with a VERIS System (ver. 1-4.8; Electro-Diagnostic Imaging, Inc., Redwood City, CA) using the same amplifier (model 12; Grass, Quincy, MA). The stimulus, consisting of 61 scaled hexagonal elements covering a central visual field of 60° × 55°, was presented on a 19-in. monitor at a frame rate of 75 Hz at a distance of 32 cm from the subject's eyes. DTL fiber electrodes were applied to both eyes, waveforms were recorded, amplified (200,000×), and band-pass-filtered (10–100 Hz). Responses were analyzed according to ring averages.[8]

Statistical Methods

Data were analyzed with commercial software (JMP 5.0.1; SAS Institute Inc., Cary, NC) and R 2.2.1 (R Foundation for Statistical Computing, Vienna, Austria).

To describe disease progression, we formulated linear regression models of the response variables visual field and mfERG. The response variables were transformed by taking the logarithm to describe exponential decay of retinal function. In these models, disease duration was included as a fixed factor. Hence, we fit the following equation:

$$response = e^{(\alpha+\beta \cdot \text{disease\_duration})} \quad (1)$$

where *response* is visual field or one of the mfERG values and α and β are intercept and slope.

For modeling repeated measurements, individuals were included as random factors on slope and intercept. The latter was included since disease onset data seemed not to be reliable (some patients could not remember correctly when they first noticed changes in their visual function), so that the slope of the logarithmic decay is estimated from the interval between visits. Including the factor "eye" (left/right) as a random effect nested in the factor "individual" did not increase model fit significantly (ANOVA of the two model versions for all responses with $P > 0.99$). Therefore, we omitted this factor, modeling for every individual the mean value of both eyes. In the plots data of both eyes are shown separately. Residuals' normality and homoscedasticity were assessed by quantile–quantile plots (QQ plot) and residuals by predicted plots, respectively. To identify outliers with high leverage Cook's distance was calculated, and the distribution of random parameters estimates was inspected by histograms. The quality of fits is recorded as adjusted coefficient of determination (adj R^2).

To estimate correlations between the different examination methods describing macular function (mfERG, visual acuity, and color vision) Spearman's r_S was calculated and scatterplots were produced. Correlations and scatterplots were also produced for midperipheral retinal function variables (perimetry, dark adaptation thresholds, Ganzfeld- and mfERG).

RESULTS

The age of the patients at the first mfERG recordings ranged from 12 to 66 years (median, 36 years). Visual acuity at that time varied between 0.3 and 1.6 (median 0.8) consistent with preserved macular function. The change in visual field area for target III4e according to disease duration is presented in Figure 2A. The progression of visual field loss is fairly described by an exponential decay, which is similar to the description by Iannaccone et al.[16] From the estimated slopes (Table 2) we calculated the yearly progression for target III4e: approximately, 14.5% of the visual field area is lost by patients affected with retinitis pigmentosa every year.

DOI:10.14753/SE.2014.1976

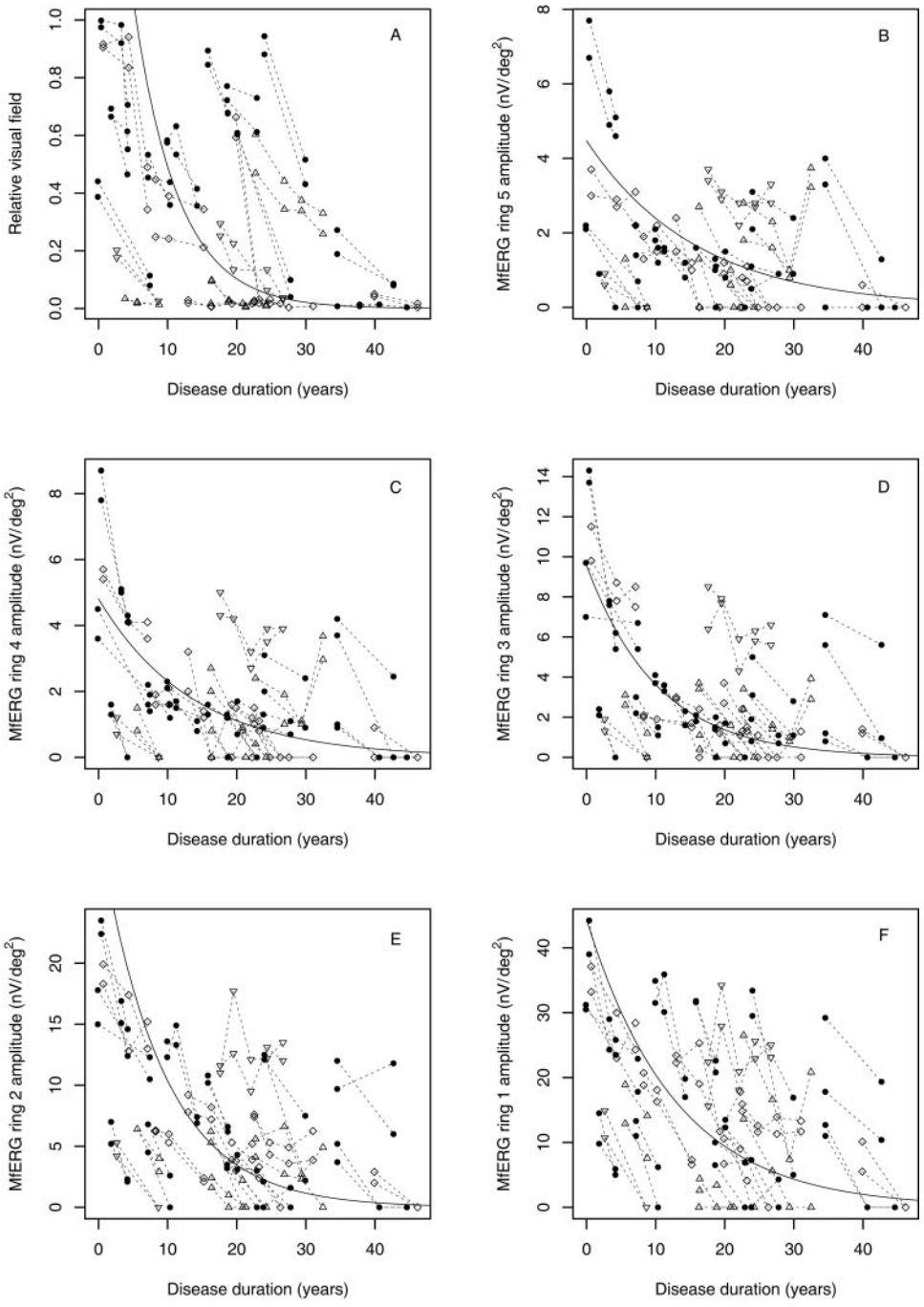

FIGURE 2. Changes of residual visual field (**A**) and mfERG of the outermost ring 5 (**B**), rings 4 to 2 (**C–E**), and the center hexagon (**F**) during disease progression. The progression of visual field loss and changes of the mfERG amplitudes were clearly described by an exponential decay. Symbols indicate heredity of the disease (● autosomal dominant; △ autosomal recessive; ◇ simplex; and ▽ Usher syndrome).

We were using the same type of regression model to define the natural progression of rod and cone functional loss measured by electrophysiological methods. For the Ganzfeld ERG and mfERG amplitudes a well-defined reduction was observed with disease duration. In general, these changes also fit an exponential curve (see Figs. 2B–F and Supplementary Fig. S1, online at http://www.iovs.org/cgi/content/full/49/10/4664/DC1), but for the estimates of the model we found a greater variation between mfERG ring analysis. We calculated the yearly progression according to the mfERG values. Approximately 6% to 10% of the amplitude is lost every year in the outer three rings (Table 3).

We also analyzed the changes in the implicit times of the mfERG, but the trend did not fit an exponential decay well. The implicit times of the central ring responses seemed to remain constant at the normal level. When responses from the outermost rings were measurable, their implicit times were always delayed up to 52 ms, but a clear tendency was not observed during long-term follow-up.

We further compared parameters of disease development with the mfERG values. We categorized the different examination methods according to macular and mid peripheral retinal function. Macular function is usually characterized by means of the visual acuity and color vision test performance. Both involve not only photoreceptor but also postreceptoral retinal and visual pathway function. We found a strong correlation between best corrected visual acuity and mfERG response

DOI:10.14753/SE.2014.1976 IOVS, October 2008, Vol. 49, No. 10

Table 2. Parameter Estimates and Statistics (Fixed Effects) for Disease Duration According to Visual Field Changes from the Literature and in the Present Study*

Study	Target	Adj R^2		Estimate	SE	95% CI Lower	95% CI Upper	P
Iannaccone et al.[16] (n = 19)	I4e		Intercept (α)	7.765	0.508	6.768	8.761	<0.0001
			Slope (β)	−0.172	0.023	−0.216	−0.127	<0.0001
	V4e		Intercept (α)	10.296	0.193	9.917	10.675	<0.0001
			Slope (β)	−0.136	0.010	−0.155	−0.117	<0.0001
Massof et al.[19] (n = 172)	II4e		Slope (β)	−0.170	N/A	N/A	N/A	N/A
	V4e		Slope (β)	−0.145	N/A	N/A	N/A	N/A
Holopigian et al.[20] (n = 23)	V4e		Slope (β)	−0.112	N/A	0.032	−0.192	N/A
Grover et al.[22] (n = 71)	II4e		Slope (β)	−0.102	N/A	−0.078	−0.116	N/A
	V4e		Slope (β)	−0.095	N/A	−0.073	−0.144	N/A
Present study (n = 23)	III4e	0.95	Intercept (α)	10.100	0.679	8.752	11.447	0.214
			Slope (β)	−0.156	0.030	−0.216	−0.096	<0.0001

* For comparison, intercept results of the present study were multiplied ×10,500.

amplitude of the central hexagon (r_S = 0.75; Fig. 3A). In contrast, there was a weak correlation between the mfERG response amplitude of the central hexagon (r_S = −0.40; Fig. 3B) and the TCDS.

Midperipheral retinal function may be characterized by visual field testing, dark adaptation thresholds or Ganzfeld- and mfERG. The mfERG ring 5 amplitude correlated strongly with the mixed cone–rod response amplitude (r_S = 0.87, Fig. 4A; see Table 4 for details) and with the cone (r_S = 0.85, Fig. 4B) and 30-Hz flicker (r_S = 0.85) response amplitude. Similar correlations were also seen between the implicit times of the cone (r_S = 0.77 for ring 5) and 30-Hz flicker (r_S = 0.72 for ring 5) response in the Ganzfeld and mfERG. Of interest, we found no correlation between the mixed cone–rod response and the mfERG response ring averages.

In advanced cases, no reproducible ISCEV Ganzfeld ERG scotopic response was recorded, but with the mfERG, significant responses were still recordable (Fig. 5A) and dark-adaptation thresholds could be measured (Fig. 5B). Interest, mfERG response amplitude of the outermost ring 5, as well as the Ganzfeld ERG mixed cone–rod response b-wave amplitude showed only a mild correlation with visual field area (r_S = 0.61 and 0.58, respectively; Figs. 6A, 6B).

Discussion

In our study, we examined the long-term changes of the mfERG responses in patients with retinitis pigmentosa. We also observed the changes of the visual field parameters and compared them with earlier findings by other authors.[17–30] In our group of patients, the progression of visual field loss followed an exponential decay, which was similar to the change described by Iannaccone et al.[16] (Table 2). Our estimate for the yearly loss of visual field is 14.5%. The slope data (−0.156, respectively) is close to the −0.136 for target V4e and −0.172 for target I4e found by Iannaccone et al.[16] or −0.112 for target V4e found by Holopigian et al.[20] and thus confirm their data. Other studies, in which more patients were included found either somewhat higher[19] or lower slopes[21,22] (for details, see Table 2).

Using a similar regression model, we found a well-defined reduction of Ganzfeld ERG and mfERG amplitudes of 6% to 10% per year of disease duration (see Table 3). To overcome or reduce possible problems arising from changes introduced by the development of the VERIS versions 1 to 4.8, we reanalyzed all data with VERIS version 4.8. Other factors like the onset of disease, which was only determined in case history, still affect our estimates. However, our estimates of amplitude loss per disease year for the mfERG ring averages are similar to those of the visual field with comparable error estimates and confidence limits. Because of averaging, the response waveforms of the hexagons of a given eccentricity the signal-to-noise ratio improves. Other factors like electrode placement or target fixation limit the test–retest reliability and may hide slight disease progression. One should keep in mind that two successive recordings can show 10% to 20% variation in amplitude.[31–34]

Table 3. Parameter Estimates and Statistics (Fixed Effects) for Disease Duration According to Changes in the mfERG Amplitudes

mfERG Ring Amplitudes	Adj R^2		Estimate	SE	95% CI Lower	95% CI Upper	P
Ring 5 (outermost)	0.83	Intercept (α)	1.498	0.235	1.030	1.965	<0.0001
		Slope (β)	−0.062	0.011	−0.085	−0.039	<0.0001
Ring 4	0.71	Intercept (α)	1.570	0.262	1.050	2.090	<0.0001
		Slope (β)	−0.073	0.014	−0.101	−0.045	<0.0001
Ring 3	0.74	Intercept (α)	2.257	0.255	1.751	2.764	<0.0001
		Slope (β)	−0.096	0.014	−0.126	−0.067	<0.0001
Ring 2	0.86	Intercept (α)	3.434	0.241	2.955	3.914	<0.0001
		Slope (β)	−0.109	0.015	−0.141	−0.078	<0.0001
Ring 1 (center)	0.77	Intercept (α)	3.792	0.206	3.382	4.201	<0.0001
		Slope (β)	−0.077	0.011	−0.101	−0.054	<0.0001

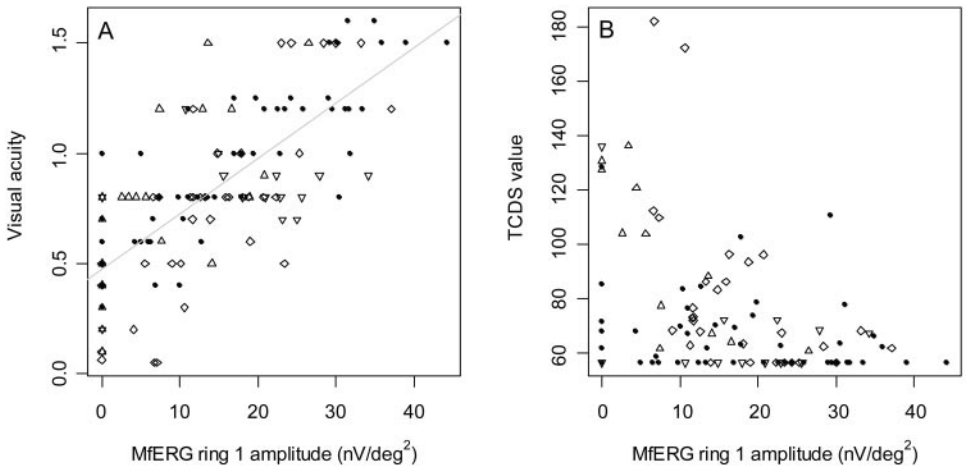

FIGURE 3. Correlations between visual acuity and mfERG amplitude of the central hexagon (**A**, $r_S = 0.75$) and between the mfERG central hexagon amplitude and the TCDS of the Lanthony Panel D-15 desaturated (**B**, $r_S = -0.40$). Of interest, the color vision performance did not correlate with the amplitude of the central hexagon or with visual acuity.

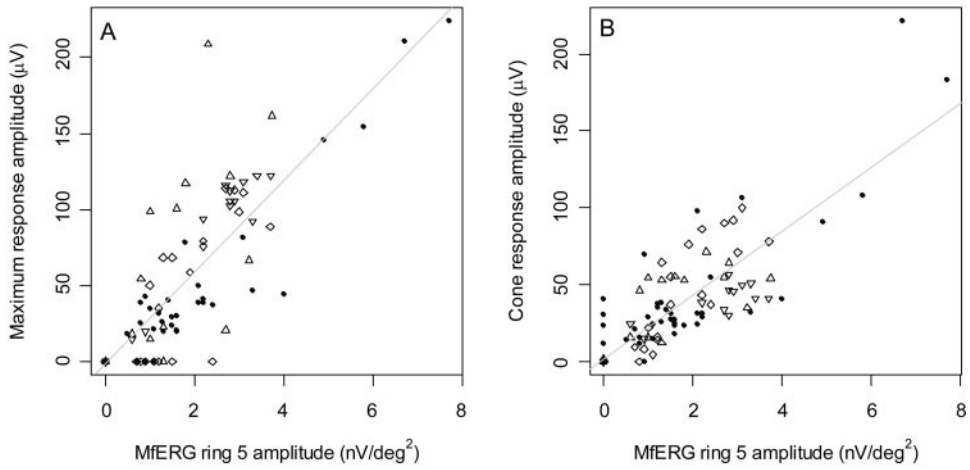

FIGURE 4. Correlations of the mfERG ring 5 amplitudes with the ISCEV Ganzfeld mixed cone–rod response (**A**, $r_S = 0.87$) and with the cone response amplitudes (**B**, $r_S = 0.85$).

TABLE 4. Correlation Coefficients (Spearman's Rho [r_s]) for Electroretinogram Amplitudes (Light Grey Triangle) and Implicit Times (Unfilled Triangle)

	MfERG ring 1	MfERG ring 2	MfERG ring 3	MfERG ring 4	MfERG ring 5	Rod response	Mixed cone-rod response	OP	30 Hz flicker	Cone response
MfERG ring 1		0.66	0.33	0.2	0.15	0.00	0.01	0.38	0.21	0.19
MfERG ring 2	0.95		0.57	0.49	0.42	-0.01	0.29	0.44	0.32	0.2
MfERG ring 3	0.81	0.88		0.89	0.83	-0.16	0.51	0.67	0.7	0.67
MfERG ring 4	0.77	0.83	0.95		0.9	-0.09	0.58	0.69	0.73	0.74
MfERG ring 5	0.73	0.77	0.9	0.95		-0.12	0.4	0.76	0.72	0.77
Rod response	0.46	0.49	0.55	0.58	0.63		-0.05	-0.27	-0.43	-0.42
Mixed cone-rod response	0.54	0.55	0.7	0.77	0.87	0.74		0.11	0.49	0.48
OP	0.55	0.57	0.6	0.65	0.66	0.79	0.7		0.52	0.39
30 Hz flicker	0.57	0.6	0.75	0.81	0.85	0.64	0.85	0.64		0.8
Cone response	0.54	0.58	0.73	0.79	0.85	0.65	0.87	0.63	0.91	

DOI:10.14753/SE.2014.1976

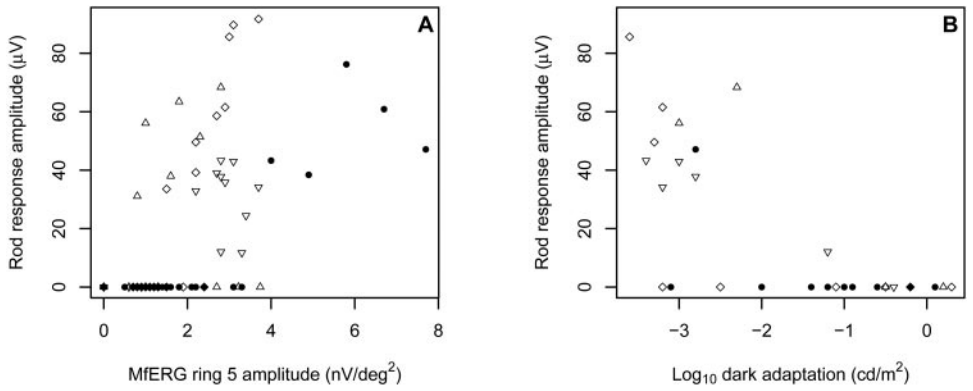

FIGURE 5. Correlations of the ISCEV rod response amplitudes with the mfERG outermost ring 5 average amplitudes (**A**) and with the dark-adaptation thresholds (**B**) indicating that mfERG responses can be recorded and dark-adaptation thresholds can be estimated, even though reproducible Ganzfeld responses are no longer recordable.

We further looked at the relationship between remaining visual field area and mfERG response amplitudes. Even though the loss of mfERG amplitude and the visual field show a similar decay, we found only a weak correlation between both (r_S = 0.61). Similarly, we found a weak (r_S = 0.58) correlation of the scotopic mixed cone–rod response with the visual field loss. Some studies emphasize the existence of a substantial correlation between visual field and Ganzfeld ERG response amplitude.[25–30] Iannaccone et al.[26] found a strong correlation between ERG mixed cone-rod response b-wave amplitude and visual field area determined for Goldmann I4e and III4e isopters (r = 0.89 and r = 0.87, respectively) but similar correlations to ours for the V4e isopter (r = 0.69). Others found only weak correlations between visual field diameter and ERG amplitudes.[28,29] Using a Naka-Rushton equation to estimate maximum amplitude of rod ERG-responses, Birch et al.[30] found a significant correlation of this amplitude to the size of the dark-adapted visual field, whereas Massof et al.[27] did not find a correlation using similar methods but light-adapted visual field testing.

Of note, Sandberg et al.[25] found weak correlations of the 0.5- and 30-Hz ERG amplitudes with visual field area (r_S = 0.54 and 0.60, respectively), but observed higher correlations (r_S up to 0.85) in a subgroup analysis, suggesting that the relationship of visual field size to ERG amplitude depends on genetic type, the altered protein, and/or the specific mutation. Because we found a significant correlation between the outermost ring average amplitude with the Ganzfeld scotopic mixed cone–rod response amplitude (r_S = 0.87) and the cone response amplitude (r_S = 0.85), this may be true of the mfERG results as well.

In conclusion, the mfERG provides a useful measure of the retinal function; it does not replace, but complements psychophysical methods including visual field and color vision testing. The response amplitude follows a similar exponential decay as the visual field and may provide reproducible responses, even if the Ganzfeld ERG is nearly extinguished. This issue is becoming more important, now that essential steps toward possible therapies for retinal degenerations are being made and reliable and objective testing methods are needed. The mfERG is well-suited for observation and long-term follow-up in disease development and—in addition to other psychophysical methods—it could be used as an objective outcome measure in upcoming treatment studies involving patients with advanced retinal diseases.

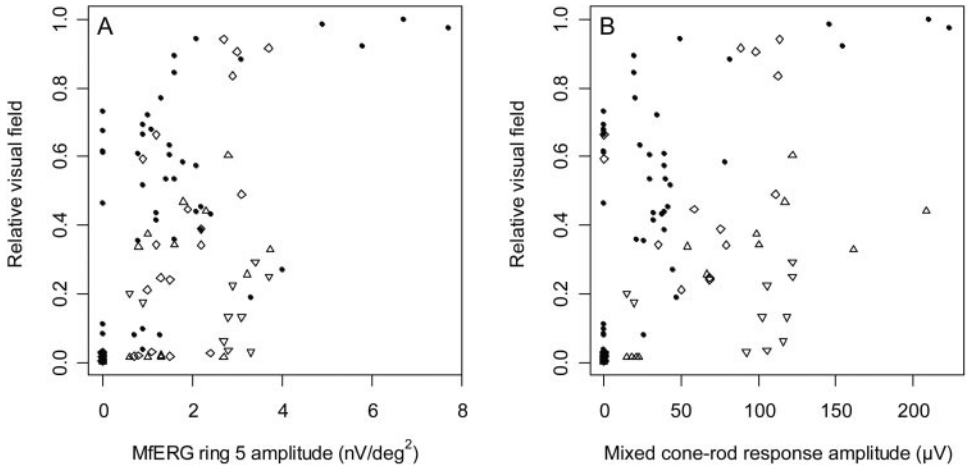

FIGURE 6. Multifocal ERG ring 5 amplitudes (**A**, r_S = 0.61) as well as Ganzfeld mixed cone–rod response amplitudes (**B**, r_S = 0.58) show only a weak correlation to the residual visual field. Thus, psychophysiological and electrophysiological tests are complementary methods.

References

1. Seeliger M, Kretschmann U, Apfelstedt-Sylla E, Ruther K, Zrenner E. Multifocal electroretinography in retinitis pigmentosa (published correction in *Am J Ophthalmol.* 1998 May;125(5):743). *Am J Ophthalmol*. 1998;125(2):214–226.
2. Herse P. Retinitis pigmentosa: visual function and multidisciplinary management. *Clin Exp Optom*. 2005;88(5):335–350.
3. Pagon RA. Retinitis pigmentosa; major review. *Surv Ophthalmol*. 1988;33(3):137–177.
4. Fishman GA, Birch DG, Holder GE, Brigell MG. *Electrophysiologic Testing in Disorders of the Retina, Optic Nerve and Visual Pathway.* 2nd ed. San Francisco: The Foundation of the American Academy of Ophthalmology, 2001:10–11.
5. Marmor MF, Holder GE, Seeliger MW, Yamamoto S. International Society for Clinical Electrophysiology of Vision. Standard for clinical electroretinography (2004 update). *Doc Ophthalmol*. 2004; 108(2):107–114.
6. Hood DC, Odel JG, Chen CS, Winn BJ. The multifocal electroretinogram. *J Neuroophthalmol*. 2003;23(3):225–235.
7. Sutter EE, Tran D. The field topography of ERG components in man. I. The photopic luminance response. *Vision Res*. 1992;32(3):433–446.
8. Hood DC, Bach M, Brigell M, et al. ISCEV guidelines for clinical multifocal electroretinography (2007 edition). *Doc Ophthalmol*. 2008;116(1):1–11.
9. Lindborn B. Cartographic deformations in a parabolic visual field map. *Acta Ophthalmol.* 1988:66:718–720.
10. Weleber RG, Tobler WR. Computerized quantitative analysis of kinetic visual fields. *Am J Ophthalmol*. 1986;101:461–468.
11. Kirkham TH, Meyer E Visual field area on the Goldmann hemispheric perimeter surface Correction of cartographic errors inherent in perimetry. *Curr Eye Res*. 1981;1(2):93–99.
12. Bowman KJ. A method for quantitative scoring of the Farnsworth Panel D-15. *Acta Ophthalmol* (*Copenh*). 1982;60:907–916.
13. Geller AM. A table of color distance scores for quantitative scoring of the Lanthony Desaturate color vision test. *Neurotoxicol Teratol*. 2001;23(3):265–267.
14. Vingrys AJ, King-Smith PE. A quantitative scoring technique for panel tests of color vision. *Invest Ophthalmol Vis Sci*. 1988;29(1): 50–63.
15. Lanthony P. Evaluation of the desaturated Panel D-15. I. Method of quantification and normal scores (in French). *J Fr Ophtalmol*. 1986;9(12):843–847.
16. Iannaccone A, Kritchevsky SB, Ciccarelli ML, et al. Kinetics of visual field loss in Usher Syndrome type II. *Invest Ophthalmol Vis Sci*. 2004;45(3):784–792.
17. Chan HL, Brown B. Investigation of retinitis pigmentosa using the multifocal electroretinogram. *Ophthalmic Physiol Opt*. 1998; 18(4):335–350.
18. Seeliger MW, Zrenner E, Apfelstedt-Sylla E, Jaissle GB. Identification of Usher syndrome subtypes by ERG implicit time. *Invest Ophthalmol Vis Sci*. 2001;42(12):3066–3071.
19. Massof RW, Dagnelie G, Benzschawel T, Palmer RW, Finkelstein D. First-order dynamics of visual field loss in retinitis pigmentosa. *Clin Vis Sci*. 1990;5:1–26.
20. Holopigian K, Greenstein V, Seiple W, Carr R. Rates of change differ among measures of visual function in patients with retinitis pigmentosa. *Ophthalmology*. 1996;103:398–405.
21. Berson EL, Sandberg MA, Rosner B, Birch DG, Hanson AH. Natural course of retinitis pigmentosa over a three-year interval. *Am J Ophthalmol*. 1985;99:240–251.
22. Grover S, Fishman GA, Anderson RJ, Alexander KR, Derlacki DJ. Rate of visual field loss in retinitis pigmentosa. *Ophthalmology*. 1997;104:460–465.
23. Birch DG, Anderson JL, Fish GE. Yearly rates of rod and cone functional loss in retinitis pigmentosa and cone-rod dystrophy. *Ophthalmology*. 1999;106(2):258–268.
24. Granse L, Ponjavic V, Andreasson S. Full-field ERG, multifocal ERG and multifocal VEP in patients with retinitis pigmentosa and residual central visual fields. *Acta Ophthalmol Scand*. 2004;82(6):701–706.
25. Sandberg MA, Weigel-DiFranco C, Rosner B, Berson EL. The relationship between visual field size and electroretinogram amplitude in retinitis pigmentosa. *Invest Ophthalmol Vis Sci*. 1996;37(8): 1693–1698.
26. Iannaccone A, Rispoli E, Vingolo EM, et al. Correlation between Goldmann perimetry and maximal electroretinogram response in retinitis pigmentosa. *Doc Ophthalmol*. 1995;90(2):129–142.
27. Massof RW, Wu L, Finkelstein D, Perry C, Starr SJ, Johnson MA. Properties of electroretinographic intensity-response functions in retinitis pigmentosa. *Doc Ophthalmol*. 1984;57(3):279–296.
28. Fahle M, Steuhl KP, Aulhorn E. Correlations between electroretinography, morphology and function in retinitis pigmentosa. *Graefes Arch Clin Exp Ophthalmol*. 1991;229(1):37–49.
29. Heckenlively JR. RP cone-rod degeneration. *Trans Am Ophthalmol Soc*. 1987;85:438–470.
30. Birch DG, Herman WK, deFaller JM, Disbrow DT, Birch EE. The relationship between rod perimetric thresholds and full-field rod ERGs in retinitis pigmentosa. *Invest Ophthalmol Vis Sci*. 1987;28: 954–965.
31. Seiple W, Clemens CJ, Greenstein VC, Carr RE, Holopigian K. Test-retest reliability of the multifocal electroretinogram and Humphrey visual fields in patients with retinitis pigmentosa. *Doc Ophthalmol*. 2004;109(3):255–272.
32. Bock M, Andrassi M, Belitsky L, Lorenz B. A comparison of two multifocal ERG systems. *Doc Ophthalmol*. 1998–1999;97(2):157–178.
33. Marmor FM. Do you, doctor, take the mfERG. . . for better or for worse (editorial)? *Graefes Arch Clin Exp Ophthalmol.* 2002;240: 241–243.
34. Rudolph G, Kalpadakis P. The role of fixation for reliable mfERG results (letter to the editor). *Graefes Arch Clin Exp Ophthalmol.* 2002;240:874–875.

DOI:10.14753/SE.2014.1976

Der Ophthalmologe

Zeitschrift der Deutschen Ophthalmologischen Gesellschaft

Ophthalmologe 2012 · 109:501–515 · DOI 10.1007/s00347-012-2555-6

D. Zobor · E. Zrenner

Retinitis pigmentosa – eine Übersicht

Pathogenese, Leitfaden für die Diagnostik und Perspektiven

Ophthalmologe 2012 · 109:501–515
DOI 10.1007/s00347-012-2555-6

DOI:10.14753/SE.2014.1976

Punkte sammeln auf...

springermedizin.de/eAkademie

Teilnahmemöglichkeiten
Diese Fortbildungseinheit steht Ihnen als e.CME und e.Tutorial in der Springer Medizin e.Akademie zur Verfügung.
- e.CME: kostenfreie Teilnahme im Rahmen des jeweiligen Zeitschriftenabonnements
- e.Tutorial: Teilnahme im Rahmen des e.Med-Abonnements

Zertifizierung
Diese Fortbildungseinheit ist mit 3 CME-Punkten zertifiziert von der Landesärztekammer Hessen und der Nordrheinischen Akademie für Ärztliche Fort- und Weiterbildung und damit auch für andere Ärztekammern anerkennungsfähig.

Hinweis für Leser aus Österreich und der Schweiz
Gemäß dem Diplom-Fortbildungs-Programm (DFP) der Österreichischen Ärztekammer werden die in der e.Akademie erworbenen CME-Punkte hierfür 1:1 als fachspezifische Fortbildung anerkannt. Der Ophthalmologe ist zudem durch die Schweizerische Gesellschaft für Ophthalmologie mit 1 Credit pro Modul anerkannt.

Kontakt und weitere Informationen
Springer-Verlag GmbH
Springer Medizin Kundenservice
Tel. 0800 77 80 777
E-Mail: kundenservice@springermedizin.de

CME Zertifizierte Fortbildung

D. Zobor · E. Zrenner
Department für Augenheilkunde, Forschungsinstitut für Augenheilkunde, Universitätsklinikum Tübingen, Tübingen

Retinitis pigmentosa – eine Übersicht

Pathogenese, Leitfaden für die Diagnostik und Perspektiven

Zusammenfassung
Retinitis pigmentosa (RP) bezeichnet eine klinisch und genetisch heterogene Gruppe hereditärer Netzhauterkrankungen, die mit einer Prävalenz von 1:4000 die häufigste Form erblicher retinaler Dystrophien darstellt. Über 45 Gene wurden inzwischen identifiziert, in denen Veränderungen zu einem progressiven Verlust der Stäbchen- und anschließend der Zapfenfunktion bis hin zur Erblindung führen. In den letzten Jahren haben die grundlagenwissenschaftlichen und klinischen Forschungen viele neue Erkenntnisse erbracht. Mithilfe der verbesserten molekulargenetischen und funktionellen diagnostischen Methoden ist eine genauere Differenzierung und Früherkennung von Netzhautdystrophien möglich. Auch wenn derzeit mehrere pharmakologische, gentherapeutische und medizintechnische Studien laufen, besteht bei den erblichen Netzhauterkrankungen bisher keine etablierte Behandlungsmöglichkeit, weshalb die sozialen und beruflichen Konsequenzen weiterhin im Vordergrund stehen. Der vorliegende Übersichtsartikel fasst die Grundlagen der retinalen Pathophysiologie, die klinischen Befunde, die Diagnostik und therapeutische Perspektiven zusammen und zeigt die Konsequenzen für die augenärztliche Praxis.

Schlüsselwörter
Retinitis pigmentosa · Klinische Diagnostik · Elektrophysiologie · Molekulargenetik · Therapie

DOI:10.14753/SE.2014.1976

Lernziele

Nach Lektüre dieses Beitrags kennen Sie

- **die Grundlagen der retinalen Pathophysiologie,**
- **die diagnostische Vorgehensweise und**
- **die therapeutischen Möglichkeiten bei Retinitis pigmentosa.**

Alter bei Erkrankungsbeginn, Progressionsrate, Ausmaß des Sehverlustes und assoziierte Augenveränderungen sind vom Vererbungsmodus und genetischen Hintergrund abhängig

Retinitis pigmentosa (RP) ist die Bezeichnung für eine klinisch und genetisch heterogene Gruppe von Netzhauterkrankungen, die vorwiegend zu einem progredienten Verlust der Stäbchenfunktion und anschließend der Zapfenfunktion führt. Das Alter des Beginns der Erkrankung, die Progressionsrate, das Ausmaß des Sehverlustes und assoziierte Augenveränderungen sind häufig vom Vererbungsmodus und genetischen Hintergrund abhängig. Über 45 verschiedene Gene wurden bereits identifiziert, in denen Veränderungen schließlich in gleiche oder ähnliche pathophysiologische Endstrecken diffuser Affektionen der Photorezeptoren und retinalen Pigmentepithelzellen münden [5, 13].

Retinitis pigmentosa ist eine der häufigsten Ursachen des Sehverlustes im mittleren Erwachsenenalter

Schätzungsweise jeder 80. Mensch trägt ein „ungünstig" verändertes Gen in sich, das eine degenerative Netzhauterkrankung verursacht, und die Entwicklung dieser Netzhauterkrankung bei Genträgern oder seinen Nachkommen in Gang setzen kann. Weltweit leiden etwa 3 Mio. Menschen – in Deutschland etwa 30.000 bis 40.000– an einer der verschiedenen Formen der RP. Obwohl sie als seltene Augenerkrankung gekennzeichnet wird, ist sie eine der häufigsten Ursachen des Sehverlustes im mittleren Erwachsenenalter und damit sozioökonomisch hochrelevant. Allerdings existieren bei den erblichen Netzhauterkrankungen bisher keine etablierten Behandlungsmöglichkeiten. Durch interdisziplinäre Forschung und große Studien wurde in den letzten Jahren unser Wissen über Pathophysiologie und genetischen Hintergrund erheblich erweitert, und die Voraussetzungen für zukünftige Therapiemöglichkeiten wurden verbessert. Auch die inzwischen umfassend etablierten diagnostischen Methoden erlauben eine genaue Differenzierung und Früherkennung von Netzhautdystrophien. Die interdisziplinäre Zusammenarbeit und die frühzeitige korrekte Diagnose sind notwendig, um bei diesen Patienten rechtzeitig die Ausbildung und Berufswahl zu fördern und die in Studien bereits in Erprobung befindlichen therapeutischen Maßnahmen rechtzeitig und optimal anwenden zu können. Die humangenetische Beratung kann wichtige Informationen bezüglich Familienplanung liefern.

Interdisziplinäre Zusammenarbeit und frühzeitige korrekte Diagnose sind wichtig

Retinitis pigmentosa – a review · Pathogenesis, guidelines for diagnostics and perspectives

Abstract

Retinitis pigmentosa (RP) is a clinically and genetically heterogeneous group of hereditary retinal disorders, being one of the most common types of retinal degeneration with a prevalence of 1:4,000. More than 45 genes have so far been associated with RP and defects cause a progressive loss of rod photoreceptor function, followed by cone photoreceptor dysfunction often leading to complete blindness. Enormous progress has been made in research in recent years and the new therapeutic approaches are promising. Furthermore, with the help of improved molecular genetic and functional diagnostic tools an early recognition and differentiation has become possible. However, at present no established therapy is available, therefore, social and professional consequences are essential tasks to deal with. This paper summarizes the basic principles of retinal pathophysiology, clinical findings, diagnostics and therapeutic perspectives, furthermore, the implications for general ophthalmologists are provided.

Keywords

Retinitis pigmentosa · Clinical diagnostics · Electrophysiology · Molecular genetics · Therapy

DOI:10.14753/SE.2014.1976

Physiologische Grundlagen und Pathophysiologie

Damit Symptomatik und Verlauf der Retinitis pigmentosa verständlich werden, ist es notwendig, einige grundlegende anatomische und physiologische Kenntnisse zu wiederholen.

Die ins Auge einfallenden Lichtsignale werden in den Photorezeptoren aufgenommen und deren Signale nach einer komplexen Informationsverarbeitung in der Netzhaut dem Gehirn zugeleitet, wo es zur eigentlichen Sehwahrnehmung kommt. Stäbchen und Zapfen übernehmen dabei verschiedene Funktionen: Die **Stäbchen**, die in der mittleren Peripherie der Netzhaut am dichtesten verteilt sind, sind für das Nacht- und Dämmerungssehen („skotopisches Sehen") verantwortlich, während die Zapfen, die hauptsächlich im Zentrum der Netzhaut zu finden sind, ihre Funktion bei Tageslicht aufnehmen („photopisches Sehen"). Die **Zapfen** sind für die Farbwahrnehmung verantwortlich und ermöglichen das Scharfsehen im Gesichtsfeldzentrum. Deshalb ist es leicht zu verstehen, dass eine Funktionsstörung des Stäbchensystems zu Nachtsehstörungen und Einschränkung des mittelperipheren Gesichtsfeldes mit Progression nach innen (konzentrische Einengung) und nach außen (verschwindende periphere Restinseln) führt. Wenn es zu einer Funktionsstörung des Zapfensystems kommt, treten hauptsächlich Visusminderung, Farbsinnstörungen, Blendungsempfindlichkeit und Gesichtsfeldausfälle im Zentrum auf. Da die Photorezeptoren durch das retinale Pigmentepithel (RPE) und die Choriokapillaris versorgt werden, ist es verständlich, dass genetisch bedingte Störungen des RPE ebenfalls zur Schädigung der Photorezeptoren führen können und somit eine wichtige Rolle in dem Pathomechanismus der Netzhautdystrophien spielen [10, 17]. Bei Retinitis pigmentosa handelt es sich um eine hereditäre Netzhautdystrophie, die phänotypisch und genetisch eine sehr heterogene Gruppe darstellt. Sie führt schließlich zu einem progredienten Verlust der Stäbchen und später auch zum Verlust der in Mitleidenschaft gezogenen Zapfen. Die verschiedenen Mutationen können zu herabgesetzter oder fehlender Funktion oder pathologischer Fehlfunktion von Proteinen führen, die für die Funktion oder für die Struktur der Photorezeptoren oder des RPE wichtig sind und für die intrazelluläre Transduktionskaskade, den ziliaren Transport oder für den Ionenaustausch verantwortlich sind. Mittlerweile sind mehr als 45 Gene identifiziert worden, deren Mutationen zu Retinitis pigmentosa führen können. Es ist jedoch davon auszugehen, dass noch längst nicht alle Genorte gefunden wurden. Auch wurden mehrere ursächliche Mutationen eines Gens entdeckt, die zu unterschiedlichen „Untergruppen" des Phänotyps führen können. Das Alter des Beginns der Erkrankung, die Progressionsrate, das Ausmaß des Sehverlustes und assoziierte Augenveränderungen sind häufig vom Vererbungsmodus und vom Genotyp abhängig [10, 17].

Bei Retinitis pigmentosa handelt es sich um eine hereditäre Netzhautdystrophie

Mittlerweile sind mehr als 45 Gene identifiziert worden, deren Mutationen zu Retinitis pigmentosa führen können

Retinitis pigmentosa kann als isolierte, sporadische Erkrankung (ohne weitere Betroffene in der Familie) oder auch autosomal-dominant (AD), autosomal-rezessiv (ar), x-chromosomal (Xr), selten mitochondrial oder mit digenischer Ursache [wobei an zwei verschiedenen Genorten gleichzeitig ein Defekt vorliegt, jedoch nur in jeweils einem Allel (heterozygot)] auftreten. In **Tab. 1** sind die geschätzten Prozentanteile der verschiedenen Vererbungsmodi und die häufigsten Gene je Erbgang dargestellt [5, 17]. Bei **autosomal-dominanter Vererbung** sind mehrere Generationen mit variabler Penetranz betroffen, und die Prognose ist durchschnittlich am günstigsten. Bei **autosomal-rezessivem Erbgang** erkranken nur Angehörige derselben Generation, allerdings können bei Konsanguinität ebenfalls mehrere Generationen betroffen sein. Diese Vererbung ist seltener und hat eine intermediäre Prognose. Bei einer **x-chromosomalen Vererbung** erkranken in der Regel nur Männer, die Frauen (Konduktorinnen) können eine Genmutation über mehrere Generationen weiter vererben. Die Konduktorinnen können klinisch völlig unauffällig sein oder typische Netzhautveränderungen und/oder Funktionsstörungen aufweisen, die allerdings nicht so schwerwiegend sind wie das Krankheitsbild der Männer. Eine x-chromosomal gebundene Vererbung ist zwar am seltensten, hat aber sehr häufig den schwersten Verlauf von allen Erbgängen.

Während die initialen Störungen der Photorezeptoren oder RPE-Zellen je nach genetischem Defekt unterschiedlich sein können, ist die Endphase der Erkrankung ähnlich: Es kommt zu einem Absterben der betroffenen Zellen. Ob hier eine „klassische" Apoptose oder eine besondere Form des Zelltods abläuft, ist nicht ganz geklärt. Letztlich führen aber die Veränderungen zu einer **Netzhautdegeneration** vorwiegend in der stäbchenreichen mittleren Peripherie und in der Mehrzahl der Fälle erst zu einem späteren Zeitpunkt auch in der zentralen Netzhaut [4, 17].

DOI:10.14753/SE.2014.1976

Tab. 1 Liste der verschiedenen RP-Formen, deren Häufigkeit und der bereits identifizierten Gene (ohne Vollständigkeit)

Typ	Häufigkeit (%)	Anzahl der Gene	Häufige, identifizierte Gene (% aller Fälle)
Autosomal-dominante RP	20–25	19	**RHO** (26,5%), *CRX* (1%), *IMPDH1* (2,5%), *PRPF3* (1%), *PRPF8* (3%), *PRPF31* (8%), *PRPH2* (*RDS*, 9,5%), *RP1* (3,5%), *RDH 12*, *GUCA1B*, *BEST1*, *CA4*, *FSCN2*, *KLHL7*, *NR2E3*, *NRL*, *ROM1*, *RP9*, *SEMA4A*, *SNRNP200*, *TOPORS*
Autosomal-rezessive RP	15–20	26	**CRB1** (6,5%), **PDE6A** (4%), **PDE6B** (4%), **ABCA4** (3%), *CNGA1* (2,3%), *RP22*, *RP29*, *RP32*, *BEST1*, *CERKL*, *CNGB1*, *EYS (RP25)*, *RPE65*, *FAM161A*, *IDH3B*, *LRAT*, *MERTK*, *PDE6G*, *RBP3*, *RHO*, *RLBP1*, *RP1*, *RGR*, *PROM1*, *TULP1*
X-rezessive RP	10–15	6	**RPGR** (74,2%), *RP2*, *RP6*, *RP23*, *RP24*, *RP34*
Kongenitale Leber-Amaurose	4	9	**GUCY2D** (*LCA1*, 14%), **RPE65** (*LCA2*, 10%), *CRX* (2%), *AIPL1* (*LCA4*, 7%), *RPGRIP1* (*LCA6*, 5%), *TULP1* (2%), *CRB* (11%), *RDH12* (4%), *LCA3*, *LCA5*, *LCA9*, *LRAT*, *MERTK*
Digenische RP	Sehr selten	k.A.	*PRPH2* (*RDS*) und *ROM1*
Usher-Syndrom	10	11	*MYO7A*, *USH1C*, *CDH23*, *PDCH15*, *USH2A*, *GPR98*, *DNFB3*, *USH3A*
Bardet-Biedl-Syndrom	5	13	*ARL6*, *BBS1*, *BBS2*, *BBS4*, *BBS5*, *BBS7*, *BBS9*, *BBS10*, *BBS12*, *CEP290*, *INPP5E*, *MKKS*, *MKS1*, *TRIM32*, *TTC8*

RP Retinitis pigmentosa, **k.A.** keine Angaben.Die wichtigsten und häufigsten Gene sind fett markiert. Für weitere Informationen s. http://www.sph.uth.tmc.edu/retnet.

Klinisches Bild

Bei Retinitis pigmentosa sterben die Netzhautzellen allmählich ab, in der Regel zunächst die Stäbchen, erst später werden auch die Zapfen in Mitleidenschaft gezogen. Deshalb wird RP oft auch **Stäbchen-Zapfen-Dystrophie** genannt, aber auch andere Terminologien existieren (z. B. tapetoretinale Degeneration). Je nachdem, welcher Bereich der Netzhaut abgestorben ist, sind unterschiedliche Funktionsverluste die Folge. Die gemeinsamen Symptome sind folgende:

- fortschreitende Nachtblindheit (diese ist in der Regel die erste Symptomatik, die sich bereits Jahre vor der Erstdiagnose bemerkbar macht),
- zunehmender Gesichtsfeldverlust zunächst in der mittleren Peripherie (Ringskotom), dann mit weiterer Progression nach außen (und somit Verlust der peripheren Restinseln) und nach innen (konzentrische Einengung),
- erhöhte Blendungsempfindlichkeit,
- reduziertes Farbensehen,
- verlängerte Adaptationszeit und Störung des Kontrastsehens,
- Visusminderung.

Es ist mit einer bilateral symmetrischen Progression zu rechnen

Da es sich um eine genetisch bedingte Erkrankung handelt, ist mit einer bilateral symmetrischen Progression zu rechnen, die insbesondere für die Differenzialdiagnose von großer Bedeutung ist, da Trägerinnen x-chromosomal vererbter Formen als Konduktorinnen nicht selten leichte Symptome zeigen, die in der Regel asymmetrisch verlaufen. Sehr selten kann die Retinitis pigmentosa sektoriell oder unilateral auftreten, in diesen Fällen sind die Symptome weniger oder nur einseitig ausgeprägt. Diese Fälle erfordern den sorgfältigen Ausschluss postentzündlicher oder traumatischer Netzhautdegenerationen.

Die ersten Beschwerden treten häufig bereits in den ersten 2 Lebensdekaden auf

Das Alter bei Erstvorstellung kann abhängig vom Erbgang und Genotyp unterschiedlich sein, jedoch liegt der Beginn der Erkrankung in den meisten Fällen Jahre zurück, da häufig bei Erstvorstellung das Elektroretinogramm bereits massiv verändert ist. Die ersten Beschwerden (Nachtblindheit, Gesichtsfelddefekte) treten häufig bereits in den ersten 2 Lebensdekaden auf, die Diagnosestellung erfolgt meist aber erst später, nämlich in der dritten bis vierten Dekade (im Durchschnitt mit 35,1 Jahren; [1, 2, 9, 12]). Auch hier gibt es deutliche Unterschiede: Bei den x-chromosomalen Fällen, die die schlechteste Prognose haben, kommt es in der Regel zu einer früheren Vorstellung beim Arzt, da diese Fälle häufig bereits im Kindesalter eine deutliche Sehminderung aufweisen können. Bei den autosomal-dominanten Fällen sind zwar die Störungen insgesamt milder und wegen der va-

DOI:10.14753/SE.2014.1976

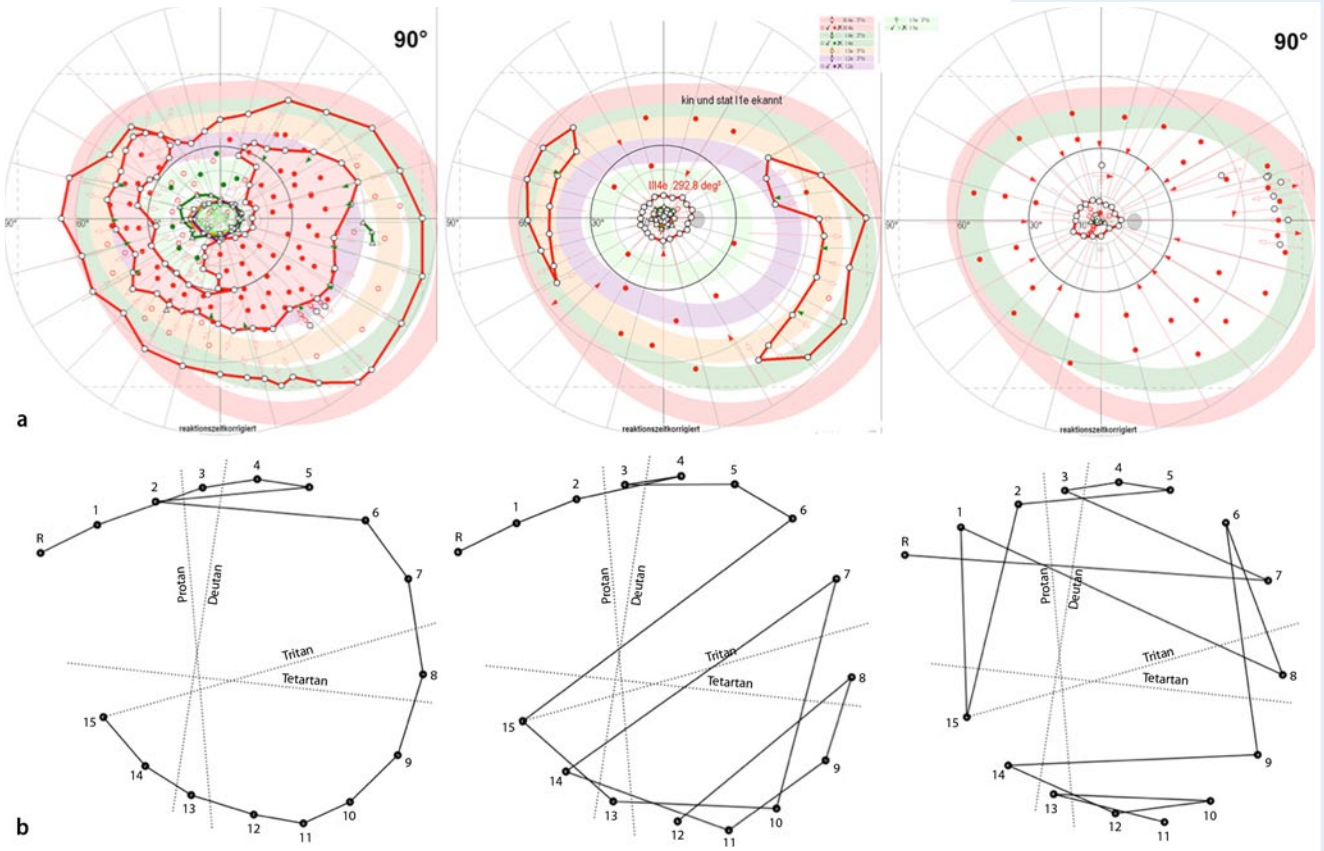

Abb. 1 ▲ **a** Typische Befunde der 90° semiautomatisierten kinetischen Perimetrie bei RP-Patienten mit unterschiedlichem Schweregrad. *Links* ist ein Ringskotom mit der Marke III4e in der mittleren Peripherie zu beobachten, das Zentrum ist noch sehr gut erhalten. Auf dem Befund in der Mitte ist eine konzentrische Einengung des Gesichtsfeldes mit peripheren Restinseln für die Marke III4e zu sehen. Diese Restinseln verschwinden mit dem Fortschreiten der Erkrankung und das Gesichtsfeld engt sich zentral weiter ein (*rechts*). Der Verlust der Restinseln ist ein wesentlicher Verlust, da diese für die Orientierung einen hohen Wert darstellen. Die Farbkodierung der verschiedenen Testmarken ist oben angegeben (rot – III4e, dunkelgrün – I4e, orange – I3e, lila – I2e, hellgrün – I1e). **b** Typische Befunde des Lanthony-Panel-D-15-desaturierten Tests bei RP-Patienten. Der Befund *links* zeigt nur minimale Verwechslungen, im Zuge der Progression werden jedoch die Farbsinnstörungen deutlicher, und es zeigt sich zunächst eine deutliche Blau-Gelb-Sinnstörung (in der *Mitte*) und schließlich eine deutliche, „chaotische" Farbsinnstörung ohne spezifische Achse (*rechts*). Mithilfe dieser Untersuchung können auch bei gutem Visus die ersten Zeichen einer Makulabeteiligung entdeckt werden

riablen Penetranz evtl. auch subjektiv weniger auffallend, jedoch erfolgt wegen der familiären Anhäufung eine Vorstellung beim Augenarzt in der Regel früher. Bei der Erstvorstellung müssen die Art der Beschwerden und der Zeitpunkt des subjektiven Erkrankungsbeginns geklärt werden. Insbesondere bei älteren Patienten sollte die Medikamentenanamnese (zum Ausschluss einer toxischen Netzhauterkrankung) und ein generalisiertes Tumorleiden erfragt werden, da diese differenzialdiagnostisch eine wichtige Rolle spielen [4, 10, 17]. RP kann mit bestimmten systemischen Erkrankungen assoziiert sein, die anamnestisch berücksichtigt werden müssen. Häufig sind Hörstörungen (z. B. Usher-Syndrom), seltener treten neurologische Beschwerden auf (z. B. Refsum-Krankheit, Bassen-Kornzweig-Syndrom) oder komplexe Krankheitsbilder (z. B. Bardet-Biedl-Syndrom, Kearns-Sayre-Syndrom). Die Erstellung eines Stammbaums kann zusätzliche Informationen bieten, insbesondere im Falle betroffener Verwandter in verschiedenen Generationen. Auch Untersuchungen von betroffenen und anamnestisch gesunden Familienangehörigen helfen bei der Diagnosestellung.

Bei der Erstvorstellung müssen die Art der Beschwerden und der Zeitpunkt des subjektiven Erkrankungsbeginns geklärt werden

RP kann mit bestimmten systemischen Erkrankungen assoziiert sein

DOI:10.14753/SE.2014.1976

Diagnostik und Befunde

Funktionsdiagnostik – subjektive Messungen

Die Sehleistungen der zentralen Netzhaut sind am Anfang der Erkrankung nur wenig beeinträchtigt

Häufig ist der erste diagnostische Hinweis auf die Mitbeteiligung der zentralen Netzhaut eine Farbsinnstörung entlang der Blau-Gelb-Achse

Wie von der Pathophysiologie der Erkrankungen zu erwarten, sind die Sehleistungen der zentralen Netzhaut am Anfang der Erkrankung nur wenig beeinträchtigt. Dies bedeutet eine gute, oft volle Sehschärfe und ein unauffälliges Farbensehen. Um diese überprüfen zu können, sind eine detaillierte Refraktion und Visusprüfung sowie ein Farbtest (in der Regel Lanthony-Panel-D-15-desaturierter Test) erforderlich. Häufig ist der erste diagnostische Hinweis auf die Mitbeteiligung der zentralen Netzhaut eine Farbsinnstörung entlang der Blau-Gelb-Achse. Eine Visusminderung bei RP-Patienten kann zusätzlich durch Cataracta complicata (oft in Form einer hinteren Schalentrübung) oder ein zystoides Makulaödem verursacht werden, die bei diesen Patienten durchschnittlich häufiger als in der Normalbevölkerung auftreten können (s. "Morphologie").

Die **Gesichtsfeldprüfung** ist nicht nur für die Diagnosestellung, sondern auch für die Beratung bezüglich Kraftfahrtauglichkeit und Beruf sehr wichtig. Wie bereits ausgeführt, treten zunehmende Gesichtsfeldverluste zunächst in der mittleren Peripherie (Ringskotom) auf, dann folgt die weitere Progression nach außen (und somit Verlust der peripheren Restinseln) und nach innen (konzentrische Einengung). Grundsätzlich kann das Gesichtsfeld am besten mit dem Goldmann-Perimeter oder mit ähnlichen semiautomatischen oder automatischen kinetischen Perimetern getestet werden, die bei fortgeschrittenen Gesichtsfelddefekten für die Patienten weniger belastend sind als statische Verfahren (**Abb. 1**).

Der RP-Betroffene hat häufig Anpassungsschwierigkeiten bei raschem Wechsel von Hell und Dunkel

Bereits vor der Einschränkung des Gesichtsfeldes hat das Absterben der Stäbchen oft den Verlust ausreichender Sehwahrnehmung in Dämmerung und Dunkelheit zur Folge. Bei Tage kann der RP-Betroffene anfangs noch gut sehen, hat allerdings häufig Anpassungsschwierigkeiten bei raschem Wechsel von Hell und Dunkel, z. B. wenn er aus starkem Sonnenlicht in einen schattigen Raum tritt. Diese subjektiven Beschwerden können mit der Messung der Dunkeladaptationsendschwelle oder der Dunkeladaptationskurve bestätigt werden. Je nach Messtechnik ist es möglich, die Zapfen- und Stäbchenfunktion separat zu testen oder eine sog. Absolutschwelle nach 20 min Dunkeladaptation zu messen. Bei den meisten Patienten eignet sich das klassische **Dunkeladaptometer** sehr gut, das die Funktion eines umschriebenen Netzhautareals untersucht. Allerdings ist bei „Low-vision-Patienten" eher eine Bestimmung der Endschwelle nach 20 min Dunkeladaptation mithilfe der FST-Messung (Full-field-Stimulus-Test) zu empfehlen, die eine Ganzfeldstimulation verwendet und von Gesichtsfelddefekten und Nystagmus weniger beeinflusst wird. Generell ist aber bei jeder Messmethode eine deutliche Erhöhung der Endschwelle sowohl für die Stäbchen- als später auch für die Zapfenfunktion zu sehen, die die subjektiven Beschwerden erklärt.

Funktionsdiagnostik – objektive Messungen

Das Ganzfeld Elektroretinogramm ermöglicht eine detaillierte und objektive Untersuchung der verschiedenen Zelltypen der Netzhaut

Es wird zwischen skotopischen und photopischen Bedingungen unterschieden

Um die Netzhautfunktion genauer beurteilen zu können, ist es essenziell, bei jedem Patienten mit Verdacht auf eine Retinitis pigmentosa mindestens einmal eine elektroretinographische Untersuchung durchzuführen. Das Ganzfeld Elektroretinogramm (ERG) ermöglicht eine detaillierte und objektive Untersuchung der verschiedenen Zelltypen der Netzhaut. Dabei werden Lichtreize in einer Halbkugel appliziert und die damit ausgelösten elektrischen Potenziale von der Netzhaut mittels Hornhautelektroden aufgezeichnet. Diese Potenziale spiegeln die elektrische Aktivität, also eine Summenantwort aktivierter Netzhautneurone wider. Es wird zwischen skotopischen (dunkeladaptierten) und photopischen (helladaptierten) Bedingungen unterschieden. Bei skotopischen Bedingungen werden hauptsächlich die Stäbchenfunktionen, bei photopischen Bedingungen die Zapfenfunktionen erfasst (die Photorezeptorantworten spiegeln sich in der a-Welle wider). Zusätzlich können funktionelle Störungen der retinalen Transmission (Bipolarzellen, Müller-Zellen) durch die Analyse der b-Welle beurteilt werden. Eine Ganzfeld-ERG-Untersuchung soll nach internationalen Standards (ISCEV) erfolgen, jedoch ist es möglich und erwünscht, die Netzhautfunktion mit erweiterten Ableitungsprotokollen zu differenzieren. Bei Retinitis pigmentosa ist bereits sehr früh das skotopische ERG als Maß der Stäbchenfunktion subnormal (die Amplituden der Antworten sind reduziert und die Gipfelzeiten verlängert), in fortgeschrittenen Fällen werden die Antworten deutlich reduziert. In Spätstadien sind die Antworten des Standardprotokolls vom Rauschen kaum oder gar nicht mehr zu

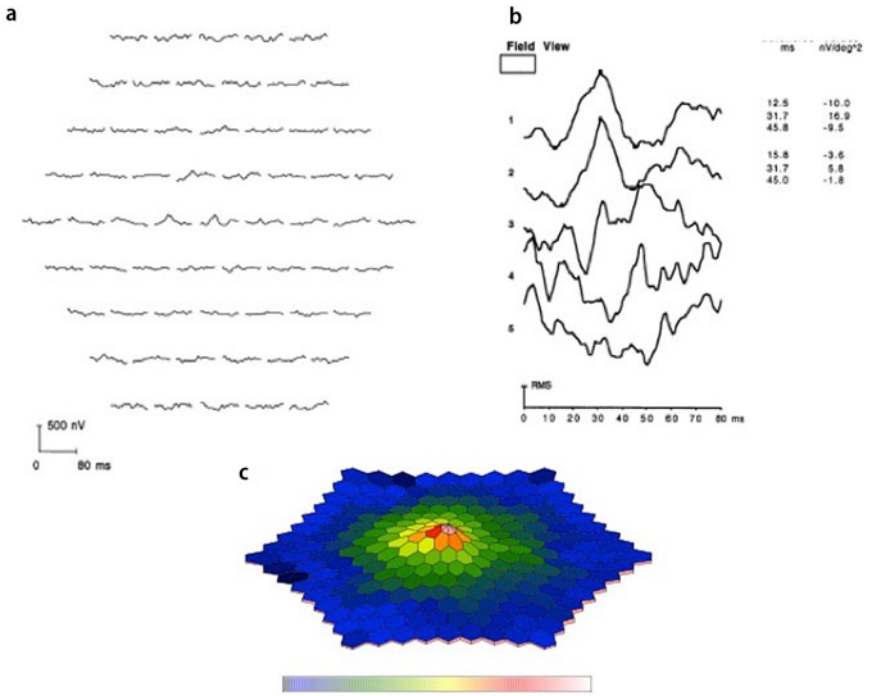

Abb. 2 ▲ Multifokales ERG bei Retinitis pigmentosa. Es zeigen sich **a** in der topographischen Darstellung und **b** in der Ringauswertung zentral nachweisbare Potenziale mit reduzierten Amplituden. Die Antworten in den äußeren Ringen sind nicht mehr vom Rauschen trennbar. **c** Die generalisierte Antwortminderung der Netzhaut ist in der farbkodierten 3D-Darstellung ebenfalls eindeutig zu sehen

trennen. In einigen dieser Fälle kann eine zusätzliche Ableitung eines 9 Hz-Flicker-ERGs, das Restfunktionen sowohl der Zapfen als auch der Stäbchen erfasst und durch Fourier-Analyse eine Trennung von Rauschen erlaubt, immer noch reproduzierbare Antworten zeigen. Im Gegensatz dazu bleibt das zapfendominierte (photopische) ERG bei RP-Patienten zunächst wenig beeinträchtigt, aber mit der Progression der Erkrankung ist auch hier ein objektiver Funktionsverlust zu beobachten, und in fortgeschrittenen Fällen sind keine reproduzierbaren Summenantworten mehr nachweisbar.

Mit Fortschreiten der Degeneration kommt es zu einer deutlichen Funktionsminderung des Stäbchen- und Zapfensystems. Das zentrale Netzhautareal bleibt aber typischerweise lange gut erhalten. Dies beweisen die gute zentrale Sehschärfe und das Farbensehen. Die Makulafunktion kann mithilfe des multifokalen ERGs (mfERG) auch objektiv gemessen werden. Das mfERG erlaubt durch die Verwendung multipler hexagonaler Lichtreize in variabler Kombination eine differenzierte Beurteilung und eine topographische Darstellung der regionalen Netzhautfunktion am hinteren Pol. Die Ableitungen erfolgen am helladaptierten Auge, die damit gewonnenen Antworten sind also zapfendominiert. Für die Durchführung eines mfERGs existieren ebenfalls internationale Standards (ISCEV). Typischerweise lassen sich bei RP-Patienten gut erhaltene Antworten im zentralen Bereich ableiten, die (mittel)peripheren Antworten dagegen sind deutlich reduziert und die Gipfelzeiten verlängert. In fortgeschrittenen Fällen sind die Antworten der mittleren Peripherie – korrespondierend zu den Gesichtsfeldbefunden – nicht mehr vom Rauschen zu trennen, während im Zentrum noch Restfunktionen nachzuweisen sind (◘ **Abb. 2**). Diese Restantworten korrelieren mit der zentralen Sehschärfe gut. Oft kann das mfERG auch dann noch reproduzierbare Antworten der Makula zeigen, wenn im Ganzfeld ERG keine ableitbaren Antworten mehr zu finden sind. Deswegen ist diese Untersuchung für die Erfassung der Restfunktion und für Verlaufskontrollen in fortgeschrittenen Fällen von großer Bedeutung [6, 12].

Die Makulafunktion kann mithilfe des multifokalen ERGs objektiv gemessen werden

Das mfERG ist für die Erfassung der Restfunktion und für Verlaufskontrollen in fortgeschrittenen Fällen von großer Bedeutung

In weit fortgeschrittenen Fällen bzw. im Endstadium der Erkrankung sind elektrophysiologisch keine reproduzierbaren Antworten mehr abzuleiten. Damit ist die objektive Erfassung der Restfunktion schwierig. In solchen Fällen kann eine pupillographische Untersuchung hilfreich sein. Mit **Pupillographie** bezeichnet man die kontinuierliche Messung und Aufzeichnung des Pupillendurchmessers unter verschiedenen Beleuchtungsbedingungen. Die Technik beruht darauf, dass die Pupille mittels

DOI:10.14753/SE.2014.1976

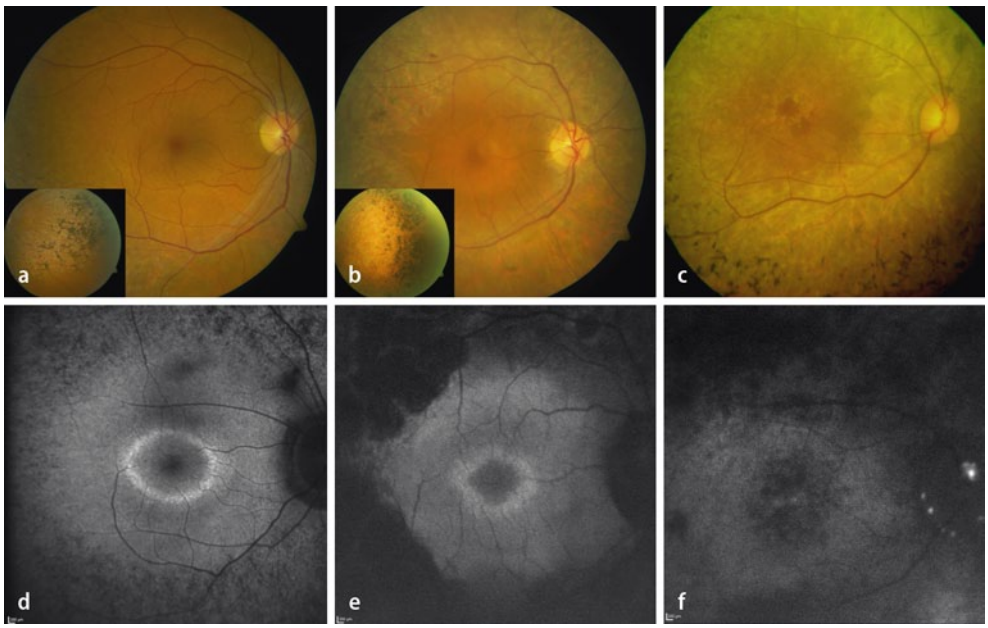

Abb. 3 ▲ Typische Fundusbefunde bei Retinitis pigmentosa. **a–c** Farbfotos, **d–f** Fundusautofluoreszenz (die Fotos in der oberen Reihe korrespondieren nicht unbedingt mit den Autofluoreszenzbildern unten). Bei allen Patienten wurden Mutationen des gleichen Genortes gefunden, jedoch sind die Mutationen und somit der Phänotyp unterschiedlich im Schweregrad. Es zeigen sich typische, aber unterschiedlich ausgeprägte morphologische Veränderungen (RPE-Atrophie und Knochenkörperchen in der mittleren Peripherie, wachsgelbe Papille, Gefäßverengung). Perizentral ist häufig ein Ring vermehrter Autofluoreszenz zu beobachten (**d**, **e**)

einer im nahen infraroten Spektrum empfindlichen Videokamera gefilmt und das Bild computergestützt ausgewertet wird. Sowohl die Latenz als auch die Konstriktionsamplituden der Pupillen (und weitere davon abhängige Parameter), ausgelöst bei verschiedenen Lichtintensitäten, können damit beurteilt werden. Bei RP-Patienten kann mithilfe der Pupillographie die Restfunktion objektiv erfasst werden, sogar wenn dass Licht subjektiv nicht mehr wahrgenommen wird. Diese Untersuchung wird allerdings nur in speziellen Zentren und hauptsächlich im Rahmen verschiedener Studien bei RP-Patienten durchgeführt.

Morphologische Diagnostik

Die typischen **Fundusveränderungen** der Retinitis pigmentosa sind:

- Gefäßverengung,
- wachsgelbe Papillen,
- Makulaveränderungen mit verbreiterten Reflexen durch die irregulären Strukturen der inneren limitierenden Membran (ILM). Gelegentlich kann sich ein zystoides Makulaödem entwickeln,
- Veränderung des retinalen Pigmentepithels (vorwiegend in der mittleren Peripherie), beginnend mit einer Depigmentierung, später übergehend in Hyperpigmentationen mit den typischen Knochenkörperchenstrukturen als Zeichen der intraretinalen Pigmentmigration. Letztere sind in verschiedenen Formen der RP unterschiedlich ausgeprägt, z. B. sind oft bei Usher-Syndrom weniger Knochenkörperchen zu sehen oder fehlen gänzlich.

Diese Veränderungen sind in der Regel beidseits symmetrisch ausgeprägt. Fast immer finden sich auch **Glaskörperveränderungen**, und es können weitere Veränderungen mit RP assoziiert sein:

- Eine posteriore subkapsuläre Linsentrübung ist relativ häufig.
- Eine Drusenpapille wird im Vergleich zu Gesunden öfters beobachtet.
- Eine Myopie ist ebenfalls häufig.
- Ein Keratokonus ist selten.
- Ebenfalls selten kann eine exsudative Vaskulopathie mit Coats-artigem Erscheinungsbild, Lipidablagerungen in der peripheren Netzhaut und einer exsudativen Netzhautablösung beobachtet werden.

DOI:10.14753/SE.2014.1976

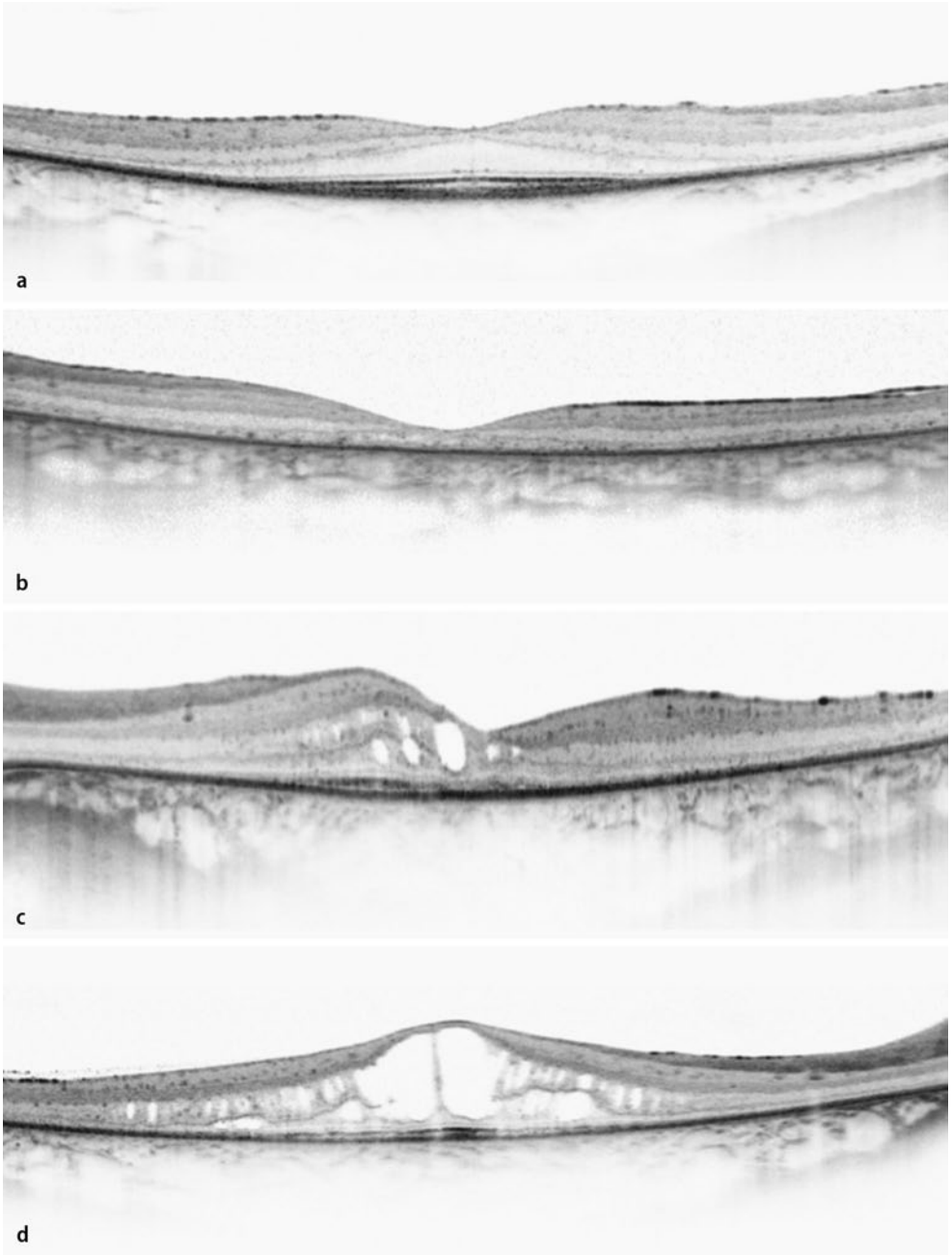

Abb. 4 ▲ Optische Kohärenztomographie (OCT, Spectralis) bei Retinitis pigmentosa. **a** Die gut erhaltenen zentralen Photorezeptoren sprechen für eine erhaltene Makulafunktion, jedoch ist der Verlust der äußeren Schichten nach peripher und eine ausgeprägte RPE-Atrophie mit vermehrter Rückstreuung der Choroidea deutlich zu sehen. **b** In fortgeschrittenen Fällen zeigt sich auch die zentrale Netzhaut deutlich atroph, die inneren Netzhautschichten bleiben aber gut abgrenzbar. **c–d** Zystoides Makulaödem bei Retinitis pigmentosa

Die meisten dieser Veränderungen können biomikroskopisch einfach untersucht werden, eine **Fotodokumentation** für die Verlaufskontrolle ist wichtig (◘ **Abb. 3**). Eine relativ neue Möglichkeit der Diagnostik eröffnet die **optische Kohärenztomographie** (OCT), mit der sich Veränderungen der Netzhautdicke und der Netzhautstruktur an histologieanalogen Schnittbildern beurteilen lassen. Der typische Befund bei Retinitis pigmentosa zeigt den guten Erhalt der inneren Netzhautschichten bei Verlust der äußeren Schichten nach peripher und eine ausgeprägte RPE-Atrophie mit vermehrter Rückstreuung der Choroidea. Der zentrale Bereich mit erhaltenen Photorezeptoren korrespondiert gut mit der Sehschärfe und mit dem zentralen Gesichtsfeldrest. Darüber hinaus kann eine zystoide

DOI:10.14753/SE.2014.1976

Makulaveränderung mittels OCT eindeutig dargestellt werden. Sie ist für die Verlaufskontrolle und Beurteilung des Therapieerfolges ebenfalls ausschlaggebend (**Abb. 4**).

Die Messung der Autofluoreszenz der RPE stellt Veränderungen der Lipofuszinverteilung und anderer Phospholipiden dar

Die Messung der Autofluoreszenz der RPE stellt Veränderungen der Lipofuszinverteilung und anderer Phospholipiden dar. Die Untersuchung ist nicht invasiv und bietet zusätzliche Informationen über die RPE-Schicht. Bei Retinitis pigmentosa wird häufig eine herabgesetzte oder fehlende Autofluoreszenz in der mittleren Peripherie beobachtet, da hier die degenerativen Prozesse zum Verlust von Pigmentepithelzellen führen. Im Zentrum bleibt die Netzhautstruktur länger erhalten, und die Autofluoreszenz ist kaum verändert, perizentral ist aber häufig ein Ring vermehrter Autofluoreszenz zu sehen als Zeichen einer aktiven dystrophischen Prozesses (**Abb. 3**). Studien haben gezeigt, dass die Größe des Ringes mit der zentralen Sehfunktion (Visus, Gesichtsfeld) gut korreliert [15].

Die Kombination der morphologischen und funktionellen Befunde, die sog. **multimodale Diagnostik**, bietet vergleichende Einblicke in Struktur, Funktion und Stoffwechsel der Netzhaut und ist für das Verständnis komplexer Pathologien unerlässlich. Dies erlaubt, krankhafte Veränderungen frühzeitig zu erkennen, zuverlässig zu dokumentieren und optimale und zielgerichtete Therapieentscheidungen zu treffen.

Differenzialdiagnose

Für die tägliche Praxis erscheint auch der Ausschluss von Phänokopien und Syndromen wichtig, um die behandelbaren Formen, die nichtprogressiven Formen und die mit dem Bild einer Retinitis pigmentosa assoziierten Formen mit zusätzlich zu behandelnder Symptomatik zu differenzieren [10, 17]. Im Folgenden möchten wir die wichtigsten Differenzialdiagnosen auflisten.

Postentzündliche Netzhautveränderungen (z. B. nach Lues, Röteln). Chorioretinitiden können RP-ähnliche subjektive Beschwerden (Nachtblindheit, konzentrische Gesichtsfeldeinschränkung) und morphologische Veränderungen (RPE-Atrophie, Hyperpigmentierung) verursachen. Allerdings sind diese in der Regel nicht progressiv, und die ERG-Befunde können intakte oder subnormale Stäbchen- und Zapfenfunktionen zeigen.

Toxische Retinopathien. Eine Chloroquin-Intoxikation oder andere Medikamente (Thioridazin, Chlorpromazin, Tamoxifen) können eine Retinitis pigmentosa vortäuschen. Diese toxischen Retinopathien sind im Endstadium ebenfalls durch den bilateralen diffusen Verlust des RPE, Pigmentveränderungen und Verengung der Arteriolen charakterisiert. Die Nachtblindheit ist jedoch unterschiedlich ausgeprägt, die Veränderungen können asymmetrisch sein, und die Optikusatrophie ist nicht wachsgelb.

Karzinomassoziierte Retinopathien. Die karzinomassoziierten Retinopathien sind ebenfalls durch Nachtblindheit, konzentrische Gesichtsfeldeinschränkung und reduzierte ERG-Antworten gekennzeichnet. Der klinische Verlauf ist jedoch rascher, mit später Erstsymptomatik, und die Pigmentveränderungen sind leicht oder können gänzlich fehlen.

Konduktorinnen. Gelegentlich können auch Konduktorinnen einer x-rezessiven RP das funduskopische Bild eines Betroffenen zeigen. Bei der Beurteilung sind die irregulären Pigmentationen (häufig sektoriell) und die tapetoiden Reflexe am Fundus wichtig. Auch Konduktorinnen können leicht progressive Gesichtsfeldverluste im späteren Lebensalter erleiden. Im ERG finden sich häufig verringerte Amplituden und verlängerte Gipfelzeiten. Die Befunde sind allerdings häufig nicht symmetrisch in beiden Augen.

Stationäre hereditäre Formen. Wichtig ist es, stationäre hereditäre Formen zu differenzieren, wie kongenitale stationäre Nachtblindheit oder Fundus albipunctatus, da die Perspektiven für Patienten dann wesentlich günstiger sind.

Behandelbare Sonderformen. Die behandelbaren Sonderformen der Netzhautdystrophien sollen ebenfalls differenzialdiagnostisch abgeklärt werden. Spezielle Blutwertbestimmungen sind bei Verdacht auf Atrophia gyrata (erhöhter Ornithinspiegel), Refsum-Syndrom (erhöhter Phytansäure-

spiegel) oder Abetalipoproteinämie (Fehlen von Apolipoprotein B) notwendig. Außerdem soll die Bestimmung des Vitamin-A-Spiegels zur Abgrenzung eines Vitamin-A-Mangels indiziert werden.

Genetische Diagnostik

Der Nachweis der spezifischen Genmutation, die für die Erkrankung verantwortlich ist, bietet eine sichere Grundlage für die Patientenberatung, jedoch ist die Identifizierung des betroffenen Genortes nicht immer möglich. Um die „Trefferquote" zu verbessern, ist es notwendig, eine ausführliche Anamnese mit Hinweisen auf den Stammbaum und eine detaillierte funktionelle morphologische Diagnostik durchzuführen. Diese Informationen sind ausschlaggebend für die Molekulargenetiker und helfen bei der Identifizierung der Mutation. Trotz aller Bemühungen kann aber leider nicht garantiert werden, dass die molekulargenetische Untersuchung die verantwortlichen Genveränderungen entdeckt, da zwar die Auswahl an bekannten möglichen Defekten immer größer wird, allerdings immer noch sehr viele auslösende Genveränderungen unbekannt sind [4, 13, 14]. Aus wissenschaftlichen Überlegungen ist die Veranlassung genetischer Untersuchungen bei allen RP-Patienten sinnvoll, da es unser Verständnis der Pathophysiologie der Erkrankung erweitert und somit wertvolle Informationen für die Entwicklung neuer Therapiemöglichkeiten liefert. Auch für die Patienten kann der genetische Befund – vielleicht schon in der näheren Zukunft – bezüglich neuer Therapiemöglichkeiten eine große Bedeutung haben, da es nur bei Patienten mit identifizierten Defekten möglich sein wird, gentherapeutische Behandlungen durchzuführen, die bereits bei der kongenitalen Leber-Amaurose im Rahmen einer Studie eingesetzt wurden.

Es muss eine ausführliche Anamnese mit Hinweisen auf den Stammbaum und eine detaillierte funktionelle morphologische Diagnostik durchgeführt werden

Aus wissenschaftlichen Überlegungen sind genetische Untersuchungen bei allen RP-Patienten sinnvoll

Verlauf und Prognose

Die Langzeitprognose der Retinitis pigmentosa ist in den meisten Fällen schlecht, da es sich um eine progressive Erkrankung handelt und derzeit noch keine etablierten Therapiemöglichkeiten existieren. Es entwickelt sich langfristig ein generalisierter Sehverlust, in vielen Fällen bis hin zur gesetzlichen Blindheit. Typischerweise verläuft der Gesichtsfeldverlust bei RP-Patienten zweistufig [11]. Zunächst kommt es zu einer langsamen Progression, ab einem kritischen Alter beschleunigt sich jedoch der Funktionsverlust fast exponentiell, sodass jährlich etwa 10–20% des Gesichtsfeldes verloren gehen [1, 7, 8]. Das kritische Alter des raschen Verlustes liegt bei der autosomal-dominanten Form bei etwa 32 Jahren, bei der x-rezessiven Form fast 12 Jahre früher und bei den autosomal-rezessiven und Simplex-Fällen dazwischen [17]. Oft ist diese Übergangsphase auch der Zeitpunkt der Erstvorstellung beim Augenarzt. Andere Studien haben auch einen exponentiellen Abfall des Gesichtsfeldes bei RP-Patienten gezeigt, der jährliche Verlust des Restgesichtsfeldes wurde zwischen 11,2 und 17,2% geschätzt, abhängig von der Testmarke in der kinetischen Perimetrie [1, 2, 7, 8, 9, 11, 12]. Dieser exponentielle Trend ist in den elektrophysiologischen Daten ebenfalls zu beobachten: Im Ganzfeld und im multifokalen ERG ist bei RP-Patienten mit etwa 10% Verlust der jeweiligen Restamplitude zu rechnen [1, 2, 6, 12]. Die Progression des Gesichtsfeldes und die Amplitudenreduktion zeigen trotz ähnlicher Tendenz nur eine schwache Korrelation zwischen Gesichtsfeld- und ERG-Parametern in der RP-Gruppe, allerdings wurden in verschiedenen Untergruppen stärkere Korrelationen beobachtet. Dies weist darauf hin, dass abhängig vom genetischen Hintergrund und Erbgang unterschiedliche Verläufe und somit unterschiedliche Prognosen zu beachten sind. Auch können die Verläufe innerhalb einer Familie erheblich variieren.

Langfristig entwickelt sich ein generalisierter Sehverlust, in vielen Fällen bis hin zur gesetzlichen Blindheit

Typischerweise verläuft der Gesichtsfeldverlust bei RP-Patienten zweistufig

Darüber hinaus gibt es RP-Fälle, die sich mit einem relativ frühen Verlust der Stäbchenfunktion, aber lange erhaltener Zapfenfunktion zeigen. In anderen Fällen geschieht der Verlust der Stäbchen- und Zapfenfunktion etwa gleichzeitig, und bei den selteneren Zapfendystrophien beginnt der Verlust im Zentrum. Diese Merkmale sind wichtig bei der Beratung der Patienten hinsichtlich des zu erwartenden Verlaufs. Die zusätzlichen Komplikationen wie eine Kataraktbildung, ein zystoides Makulaödem oder periphere Vaskulopathie können zu weiteren Funktionsminderungen führen. Diese Veränderungen lassen sich aber therapieren, wenn auch mit unterschiedlichem Erfolg. Bei der Behandlung eines zystoiden Makulaödems kommen topische (Dorzolamid 2% 3-mal/Tag) oder systemische (Azetazolamid 500 mg/Tag) Therapien infrage. Diese sollten mindestens über 4 Wochen durchgeführt werden, und die Netzhaut sollte anschließend mittels OCT kontrolliert werden. Auch wurde in einigen Fällen ein positiver Effekt nach intravitrealer Gabe von Bevacizumab beschrieben, jedoch liegen uns hier keine umfangreichen Studienergebnisse vor. Unsere Aufgabe besteht darin, die Ver-

Zusätzliche Komplikationen wie Kataraktbildung, zystoides Makulaödem oder periphere Vaskulopathie können zu weiteren Funktionsminderungen führen

DOI:10.14753/SE.2014.1976

änderungen rechtzeitig zu erkennen und eine optimale Therapie einzuleiten. Da viele Patienten sich oft mit ihren Krankheitsproblemen allein gelassen fühlen, empfiehlt es sich, sie auf **Patientenselbsthilfegruppen** zu verweisen (z. B. Pro Retina Deutschland e.V.)

Neue Perspektiven

Derzeit existieren keine etablierten Therapien

Mit Ausnahme einzelner seltener behandelbarer Netzhautdystrophien bekannte Stoffwechseldefekte (z. B. Atrophia gyrata, Bassen-Kornzweig-Syndrom) existieren derzeit keine etablierten Therapien. Die Behandlungsmöglichkeiten beschränken sich auf den Ausgleich von Refraktionsfehlern, Anpassung von vergrößernden Sehhilfen, UV-Schutz- und Kantenfiltergläsern, sowie den Erhalt klarer optischer Medien und die Behandlung der Komplikationen wie Makulaödem oder chorioidale Neovaskularisation.

Gentherapie. Eine mögliche Hilfe könnte zukünftig jedoch die Gentherapie darstellen. Das Prinzip der Gentherapie besteht darin, dass mithilfe von viralen oder nichtviralen Vektoren die therapeutischen Genabschnitte als Ersatz für nicht funktionierende Genabschnitte in die retinalen Zellen eingebracht werden, um dort die Wiederaufnahme der entsprechenden Zellfunktion zu erreichen. Die möglichen Methoden, ein defektes Gen zu ersetzen oder zu korrigieren, können in 2 Gruppen unterteilt werden:

- Genaugmentation, wobei das eingesetzte Wildtyp-Gen das nicht funktionierende oder erkrankte Gen und dessen Funktion ersetzt,
- Stummschalten von Genen, wobei die Expression des mutierten Gens mittels Ribozyme- oder RNA-Beeinflussung blockiert wird.

Die ersten klinischen Studien laufen bereits bei einer kongenitalen RP-Form (kongenitale Leber-Amaurose (LCA)/aufgrund von RPE65-Mutationen), die Ergebnisse sind vielversprechend. Allerdings sind die genetischen Strategien von der verursachenden Genmutation abhängig, weshalb die Einsetzbarkeit eingeschränkt bleibt [4, 16].

Pharmakologische Substanzen. Sie können einen biochemischen Defekt kompensieren und so eine gute Therapieoption bei Erkrankungen sein, bei denen die zugrunde liegende Pathophysiologie bekannt ist. Bei Retinitis pigmentosa kann diese Strategie insbesondere bei den Formen benutzt werden, bei denen der primäre Defekt in der **Chromophorbiosynthese** liegt und den visuellen Zyklus verändert. Aktuell wird die Wirksamkeit von QLT091001 (QLT Inc., Vancouver, Kanada) bei LCA-Patienten, bei denen eine Mutation in den Genen *RPE65* oder *LRAT* nachweisbar ist, geprüft. QLT091001 ist ein synthetisches Retinoid, das über eine orale Einnahme 11-*cis*-Retinal ersetzen soll. Auch hier zeigen die ersten Studienergebnisse eine positive Tendenz [16].

Ziel ist, einen Schutz der retinalen Zellen zu ermöglichen, um das Überleben der Photorezeptoren zu verlängern

Neuroprotektion. Während die Gentherapie oder pharmakologische Wirkstoffe nur bei bestimmten Formen der RP eingesetzt werden können, ist die Neuroprotektion dagegen von der Ätiologie der Netzhautdegeneration unabhängig. Ziel dabei ist, einen Schutz der retinalen Zellen zu ermöglichen, um das Überleben der Photorezeptoren zu verlängern. Hierbei werden Studien mit Wachstumsfaktoren (z. B. „ciliary neurotrophic factor", CNTF) und Apoptoseinhibitoren [z. B. Docosahexaensäure (DHA), Calpain- oder Ca^{2+}-Inhibitoren] durchgeführt. Die weitere Entwicklung der Anwendung von Neuroprotektiva zur Behandlung von erblichen Netzhautdegenerationen bleibt abzuwarten. Die Gentechnologie, Neuroprotektiva oder Behandlung mit Wachstumsfaktoren können nur bei noch intakten Photorezeptoren eingesetzt werden, was eine weitere Einschränkung der Verwendung in der Therapie bedeutet [16].

Stammzelldifferenzierung. Bei bereits bestehender Blindheit bzw. fortgeschrittener Degeneration der Photorezeptoren werden derzeit als Behandlungsmöglichkeiten mehrere Therapierichtungen entwickelt. Die Stammzelldifferenzierung, mit deren Hilfe versucht wird, die abgestorbenen Netzhautzellen mit sog. Photorezeptorpräkursorzellen zu ersetzen, wird noch nicht ausreichend beherrscht, und eine sichere und wirkungsvolle Anwendung konnte bisher nicht gezeigt werden.

Optogenetische Ansätze. Bei den optogenetischen Ansätzen werden mithilfe der Gentechnologie lichtsensitive/lichtaktivierte Kanäle oder Pumpen in die überlebenden Netzhautzellen hereinge-

bracht, und somit wird versucht, die Lichtaufnahme und die Umwandlung des Lichtes in elektrische Signale in der Netzhaut wiederherzustellen. Die ersten Ergebnisse bei Mäusen wurden bereits publiziert, allerdings ist der Weg zu einer Humantherapie noch lang [3, 16].

Elektronische Netzhautimplantate. In der Entwicklung sind auch sog. elektronische Netzhautimplantate, bei denen die Funktionen der defekten Photorezeptoren durch bildgesteuerte Elektrodenfelder ersetzt werden. Es werden unterschiedliche Implantate entwickelt: kortikale visuelle Prothese, suprachorioidales Implantat, epiretinales Implantat [16], das in einigen Ländern bereits zugelassen ist. Am vielversprechendsten und physiologischsten dürfte jedoch das in Tübingen entwickelte **subretinale Netzhautimplantat** sein, mit dessen Hilfe erblindeten Menschen, die die Photorezeptoren verloren haben, das Sehvermögen wiedergegeben werden kann. Das Implantat wird unter die Netzhaut implantiert. Dadurch ist gewährleistet, dass die vom Implantat abgegebenen elektrischen Ladungen tatsächlich auf diejenigen Nervenzellen der Netzhaut übertragen werden, die physiologischerweise auch von den natürlichen Photorezeptoren angesteuert werden. Somit wird das Informationsverarbeitungsnetzwerk der Netzhaut auf natürliche Weise genutzt. Auf der Basis der technischen Eigenschaften, der durchgeführten Tierexperimente und der ersten klinischen Studienergebnisse bei insgesamt 20 operierten Patienten lässt sich annehmen, dass ein Sehvermögen von 5–10% erzielbar ist. Bisher wurde bei mehreren blinden Patienten eine Sehschärfe von mehr als 1/50, also gerade die gesetzliche Grenze des Sehens erreicht. Damit ist es möglich, sich wieder ohne fremde Hilfen im Raum zu orientieren und sich frei zu bewegen. Auch die Wahrnehmung von Gesichtern ist bei 2 Patienten möglich geworden [18].

Von den verschiedenen Ansätzen sind die Netzhautimplantate am weitesten fortgeschritten und erscheinen auch längerfristig am erfolgversprechendsten für den klinischen Einsatz bei sehr fortgeschrittenen Formen der Retinitis pigmentosa mit dem Ziel, blinden Patienten mit erblichen Netzhautdystrophien wieder Möglichkeiten der visuellen Orientierung und Mobilität geben zu können.

Fazit für die Praxis

- **Retinitis pigmentosa bezeichnet eine klinisch und genetisch heterogene Gruppe von Netzhauterkrankungen, die typischerweise zu einem progredienten Verlust der Stäbchenfunktion und anschließend der Zapfenfunktion führt.**
- **Über 45 verschiedene Gene wurden bereits identifiziert, in denen Defekte schließlich in Degenerationsprozesse der Photorezeptoren und retinalen Pigmentepithelzellen münden.**
- **Die wichtigsten diagnostischen Verfahren sind Anamnese, Visusbestimmung, Perimetrie, Farbtest, Elektroretinographie, Ophthalmoskopie und bildgebende Verfahren (OCT, Autofluoreszenz).**
- **Auch die genetischen Untersuchungen können bei der Abklärung der Diagnose hilfreich sein.**
- **Derzeit existieren keine etablierten Therapien.**
- **Die Behandlungsmöglichkeiten beschränken sich auf optischen Sehhilfen, UV-Schutz und Kantenfiltergläser sowie Behandlung der Komplikationen.**
- **Eine mögliche Hilfe könnten in der Zukunft Gentherapie, Neuroprotektiva oder Behandlung mit Wachstumsfaktoren darstellen.**
- **Bei fortgeschrittener Degeneration der Photorezeptoren stehen derzeit als Behandlungsmöglichkeiten lediglich die elektronischen Netzhautimplantate zur Verfügung.**

Korrespondenzadresse

Dr. D. Zobor
Department für Augenheilkunde, Forschungsinstitut für Augenheilkunde, Universitätsklinikum Tübingen
Schleichstr. 12-16, 72076 Tübingen
ditta.zobor@med.uni-tuebingen.de

Interessenkonflikt. Der korrespondierende Autor gibt für sich und seinen Koautor an, dass kein Interessenkonflikt besteht.

DOI:10.14753/SE.2014.1976

Literatur

1. Berson EL, Sandberg MA, Rosner B et al (1985) Natural course of retinitis pigmentosa over a three-year interval. Am J Ophthalmol 99:240–251
2. Birch DG, Anderson JL, Fish GE (1999). Yearly rates of rod and cone functional loss in retinitis pigmentosa and cone-rod dystrophy. Ophthalmology106(2):258–268
3. Busskamp V, Picaud S, Sahel JA, Roska B (2011) Optogenetic therapy for retinitis pigmentosa. Gene Ther doi:10.1038/gt.2011.155. [Epub ahead of print] PubMed PMID: 21993174
4. Chizzolini M, Galan A, Milan E et al (2011). Good epidemiologic practice in retinitis pigmentosa: from phenotyping to biobanking. Curr Genomics 12(4):260–266
5. Ferrari S, Di Iorio E, Barbaro V et al (2011) Retinitis pigmentosa: genes and disease mechanisms. Curr Genomics 12(4):238–249
6. Granse L, Ponjavic V, Andreasson S (2004) Full-field ERG, multifocal ERG and multifocal VEP in patients with retinitis pigmentosa and residual central visual fields. Acta Ophthalmol Scand 82(6):701–706
7. Grover S, Fishman GA, Anderson RJ et al (1997) Rate of visual field loss in retinitis pigmentosa. Ophthalmology 104:460–465
8. Holopigian K, Greenstein V, Seiple W, Carr R (1996) Rates of change differ among measures of visual function in patients with retinitis pigmentosa. Ophthalmology 103:398–405
9. Iannaccone A, Kritchevsky SB, Ciccarelli ML et al (2004) Kinetics of visual field loss in Usher Syndrome type II. Invest Ophthalmol Vis Sci 45(3):784–792
10. Kellner U, Tillack H, Renner AB (2004) Hereditary retinochoroidal dystrophies. Part 1: Pathogenesis, diagnosis, therapy and patient counselling. Ophthalmologe 101(3):307–319; quiz 320
11. Massof RW, Dagnelie G, Benzschawel T et al (1990) First-order dynamics of visual field loss in retinitis pigmentosa. Clin Vis Sci 5:1–26
12. Nagy D, Schönfisch B, Zrenner E, Jägle H (2008) Long-term follow-up of retinitis pigmentosa patients with multifocal electroretinography. Invest Ophthalmol Vis Sci 49(10):4664–4671
13. Parmeggiani F (2011) Clinics, epidemiology and genetics of retinitis pigmentosa. Curr Genomics 12(4):236–237
14. Parmeggiani F, Sato G, De Nadai K et al (2011) Clinical and rehabilitative management of retinitis pigmentosa: up-to-date. Curr Genomics 12(4):250–259
15. Robson AG, Tufail A, Fitzke F et al (2011) Serial imaging and structure-function correlates of high-density rings of fundus autofluorescence in retinitis pigmentosa. Retina 31(8):1670–1679
16. Sahni JN, Angi M, Irigoyen C et al (2011) Therapeutic challenges to retinitis pigmentosa: from neuroprotection to gene therapy. Curr Genomics 12(4):276–284
17. Zrenner E, Rüther K, Apfelstedt-Sylla E (1992) Retinitis pigmentosa. Clinical findings, results of molecular genetic techniques and research perspectives. Ophthalmologe 89(1):5–21
18. Zrenner E, Bartz-Schmidt KU, Benav H et al (2011) Subretinal electronic chips allow blind patients to read letters and combine them to words. Proc Royal Soc B (278):1489–1497
19. Kanski JJ (2008) Klinische Ophthalmologie: Lehrbuch und Atlas, 6. Auflage. Elsevier, München

DOI:10.14753/SE.2014.1976

CME-Fragebogen

kostenfreie Teilnahme am e.CME für Zeitschriftenabonnenten

Bitte beachten Sie:

- Teilnahme nur online unter: **springermedizin.de/eAkademie**
- Die Frage-Antwort-Kombinationen werden online individuell zusammengestellt.
- Es ist immer nur eine Antwort möglich.

Welche Beschwerden sind bei beginnender Retinitis pigmentosa typisch?

- ☐ Zentralskotom, Farbsinnstörung, Leseschwierigkeit
- ☐ Lichtblitze
- ☐ Metamorphopsien, Visusminderung
- ☐ Nystagmus
- ☐ Nachtblindheit, periphere Gesichtsfeldeinschränkung

Welches sind bei einem RP-Patienten die wichtigsten elektrophysiologischen Untersuchungen?

- ☐ Ganzfeld ERG und mfERG
- ☐ Blitz-VEP
- ☐ Muster-ERG
- ☐ EOG
- ☐ Muster-VEP

Bei welchem Erbgang sind im Durchschnitt die RP-Patienten gleichen Alters am schwersten betroffen?

- ☐ Autosomal-rezessiv
- ☐ Autosomal-dominant
- ☐ x-chromosomal-rezessiv
- ☐ x-chromosomal-dominant
- ☐ Mitochondrial

Welche der hier getroffenen Aussagen über Retinitis pigmentosa ist *falsch*?

- ☐ Die ersten Symptome treten typischerweise im jungen Erwachsenenalter auf.
- ☐ Retinitis pigmentosa kann mit anderen systemischen Veränderungen assoziiert sein.
- ☐ Zystoides Makulaödem ist eine häufige Komplikation bei Retinitis pigmentosa.
- ☐ Eine Kataraktoperation wird bei RP-Patienten nie durchgeführt, da dadurch keine Besserung zu erwarten ist.
- ☐ Im multifokalen ERG bei RP-Patienten können sich zentrale Antworten auch dann noch zeigen wenn das Ganzfeld ERG bereits erloschen ist.

Ein 10-jähriges Kind mit Nachtblindheit stellt sich in der Sprechstunde vor. Anamnestisch ist eine angeborene Taubheit bekannt, das Kind trägt beidseits Cochlearimplantate. Welches ist Ihre Verdachtsdiagnose?

- ☐ Abetalipoproteinämie
- ☐ Usher-Syndrom Typ I
- ☐ Zapfendystrophie
- ☐ Morbus Stargardt
- ☐ Kongenitale stationäre Nachtblindheit

Welche ERG-Befunde sind bei beginnender Retinitis pigmentosa typisch?

- ☐ Normale skotopische und reduzierte photopische Antworten im Ganzfeld ERG
- ☐ Reduzierte bzw. erloschene skotopische und gute photopische Antworten im Ganzfeld ERG
- ☐ Im Ganzfeld ERG sieht man bei RP keine Veränderungen, nur in der VEP-Untersuchung.
- ☐ Negatives ERG
- ☐ Zentral reduzierte Antworten im multifokalen ERG

Welche Erkrankung kommt differenzialdiagnostisch *nicht* infrage bei Retinitis pigmentosa?

- ☐ Postentzündliche Retinopathie
- ☐ Chloroquin-Retinopathie
- ☐ Fundus flavimaculatus
- ☐ Karzinomassoziierte Retinopathie
- ☐ Konduktorinnenstatus bei x-rezessiver Retinitis pigmentosa

Welche Aussage über die Therapiemöglichkeiten der Retinitis pigmentosa ist richtig?

- ☐ Es existieren keine Therapiemöglichkeiten bei Retinitis pigmentosa, und es wird auch nicht danach geforscht.
- ☐ Die Gentherapie ist eine Therapiemöglichkeit, die auch bei weit fortgeschrittenen RP-Fällen eine gute Option sein könnte.
- ☐ Die Gentherapie kann in der Zukunft keine Option für die Patienten sein, da es sich bei Retinitis pigmentosa nicht um eine erbliche, sondern um eine postentzündliche Erkrankung handelt.
- ☐ Gentherapie, Behandlung mit Wachstumsfaktoren und Neuroprotektiva können in der Zukunft eine Therapie für RP-Patienten bedeuten, jedoch fehlen hier noch die ersten klinischen Ergebnisse.
- ☐ In der Entwicklung sind elektronische Netzhautimplantate, bei der die Funktionen der defekten Retina durch bildgesteuerte Elektrodenfelder ersetzt werden.

Welche Aussage ist *falsch*? Retinitis pigmentosa …

- ☐ verursacht in den meisten Fällen asymmetrische Funktionsminderungen.
- ☐ kann unterschiedlich ausgeprägte Pigmentation am Fundus verursachen.
- ☐ kann mit hinterem Polstar der Linse assoziiert sein.
- ☐ verursacht eine Veränderung im ERG.
- ☐ kann mit Schwerhörigkeit oder Ataxie assoziiert sein.

Welche Aussage zur Symptomatik und Diagnostik der Retinitis pigmentosa ist richtig?

- ☐ Autofluoreszenz hat bei Retinitis pigmentosa keinen diagnostischen Wert.
- ☐ Ein perimakulärer Ring vermehrter Autofluoreszenz ist ein häufiges Zeichen bei fortgeschrittener Retinitis pigmentosa.
- ☐ Die korrekte Diagnose einer Retinitis pigmentosa erfordert eine Fluoreszenzangiographie.
- ☐ Die Diagnose einer Retinitis pigmentosa lässt sich allein mit dem OCT stellen.
- ☐ Verdünnung der Nervenfaserschicht im OCT ist ein Frühsymptom bei Retinitis pigmentosa.

Mitmachen, fortbilden und CME-Punkte sichern unter springermedizin.de/eAkademie

DOI:10.14753/SE.2014.1976

GUCY2D- OR *GUCA1A*-RELATED AUTOSOMAL DOMINANT CONE–ROD DYSTROPHY

Is There a Phenotypic Difference?

DITTA ZOBOR, MD,* EBERHART ZRENNER, MD,*¶ BERND WISSINGER, PHD,† SUSANNE KOHL, PHD,† HERBERT JÄGLE, MD*‡

Purpose: To compare the phenotype of patients with heterozygous mutation in *GUCY2D* or *GUCA1A* causing autosomal dominant cone or cone–rod dystrophies.

Methods: Five patients from one family with *GUCA1A* and nine patients from four families with *GUCY2D* mutations were included. Psychophysical and electrophysiological examinations were performed to study retinal function. Fundus autofluorescence imaging and spectral domain optical coherence tomography were performed for morphologic characterization.

Results: Genetic analysis revealed the mutation c.451C>T (p.L151F) in the *GUCA1A* family. In the *GUCY2D* group, c.2512C>T (p.R838C) was the most frequent (2 families), c.2512C>G (p.R838G) and c.2513G>A (p.R838H) were found in one family each. Visual acuity was reduced to 0.04 to 0.7 in *GUCA1A* and to 0.014 to 0.5 in patients with *GUCY2D*. Dark adaptation showed elevated thresholds in the *GUCY2D* group. Scotopic electroretinography revealed a tendency to a more affected rod function in the *GUCY2D* group. Photopic electroretinography showed residual or absent responses in both groups. Fundus alterations were confined to the macula in both groups.

Conclusion: *GUCA1A* and *GUCY2D* mutations are both accompanied by similar pattern of generalized cone dysfunction with a tendency to less involvement of the rod photoreceptors and a less severe phenotype in patients with *GUCA1A*.

RETINA 0:1–12, 2014

Inherited cone and cone–rod dystrophies (CD and CRD) are characterized by progressive loss of photoreceptor function accompanied by retinal degeneration. All modes of inheritance have been observed, and the extensive genetic heterogeneity is typical for these dystrophies. Heterozygous mutations of the *GUCY2D* and *GUCA1A* genes have been shown to cause autosomal dominant CD and CRD.[1–9] Both genes are expressed in cone and rod photoreceptors and are essential for their functional integrity.[10–12] *GUCY2D* encodes the retinal guanylate cyclase (retGC-1), which is responsible for the cyclic guanosine monophosphate synthesis in the recovery of the dark state after light activation within these cells.[13] *GUCA1A* encodes the activating protein guanylyl cyclase activating protein (GCAP1), which regulates GC1 function in a Ca^{2+}–sensitive manner (Figure 1).[10,13,14] Mutations in *GUCA1A* or *GUCY2D*, in conclusion, result in an altered activity of retGC-1 in the dark. The thereby increased cyclic guanosine monophosphate levels keep cyclic nucleotide–gated channels open, allowing an increased Ca^{2+} influx into the photoreceptors causing cell death, which explains the progressive dysfunction in the phenotype. Indeed, this is one of the best-explained disease mechanisms for CRD or CD known in the literature.[3,14]

We conducted this study to investigate whether the 2 different genotypes—mutations either in retGC-1 or

From the *Institute for Ophthalmic Research, University of Tübingen, Tübingen, Germany; †Molecular Genetics Laboratory, Institute for Ophthalmic Research, University of Tübingen, Tübingen, Germany; ‡Department of Ophthalmology, University of Regensburg, Regensburg, Germany; and ¶Werner Reichardt Centre for Integrative Neuroscience (CIN), University of Tübingen, Tübingen, Germany.

Supported by a personal grant of the Kerstan Foundation to D. Zobor and a grant KFO134-Ko2176/1-2 to S. Kohl.

This work was supported by a grant of the BMBF (O1GM1108A) to BW, SK and EZ and of Deutsche Forschungsgemeinschaft (EXC307, CIN) to EZ.

None of the authors have any conflicting interests to disclose.

Reprint requests: Ditta Zobor, MD, Institute for Ophthalmic Research, University of Tübingen, Schleichstrasse 12-16, Tübingen 72076, Germany; e-mail: ditta.zobor@med.uni-tuebingen.de

DOI: 10.14753/SE.2014.1976

COLOR

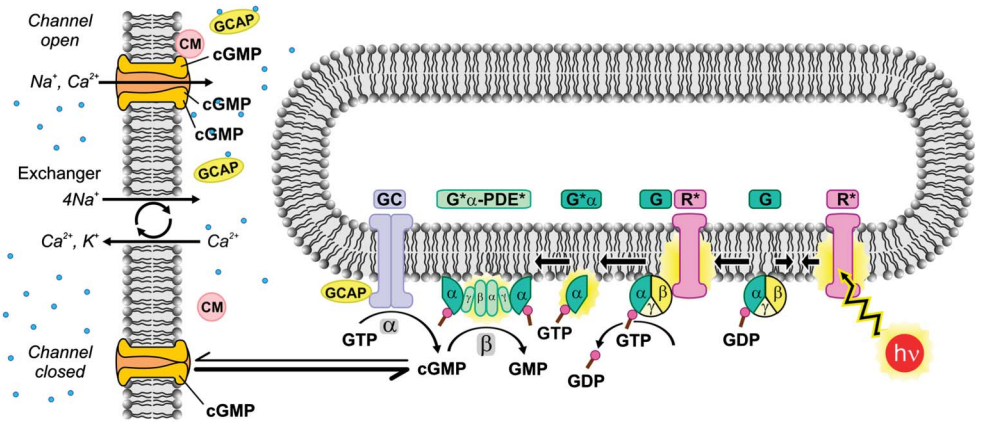

Fig. 1. The phototransduction cascade in photoreceptors. After absorption of a photon (hν), the activated rhodopsin (R^*) repeatedly contacts molecules of the G protein, catalyzing the exchange of GDP for GTP, producing the active form G^* (Gα-GTP). Two G^* subunits bind to the two inhibitory γ subunits of the phosphodiesterase, thereby activating the corresponding α and β catalytic subunits, forming phosphodiesterase*, which then catalyzes the hydrolysis of cyclic guanosine monophosphate. The reduction in cytoplasmic concentration of cyclic guanosine monophosphate leads to the closure of cyclic nucleotide–gated channels and blockage of the inward flux of Na^+ and Ca^{2+}, that is, to a reduction in the circulating electrical current. A Na^+/Ca^{2+}-K^+ exchanger continues to pump Ca^{2+} out, so that the cytoplasmic Ca^{2+} concentration declines, activating "calcium feedback" mechanisms. Release of Ca^{2+} from GCAP allows GCAP to bind to a cytoplasmic domain of the guanylyl cyclase, increasing the cyclase activity, hereby restoring the dark state (after Pugh and Lamb 2000).

its activating protein, GCAP1—make a difference in the phenotype, although they both act at the same step of the visual signal transduction cascade. Our aim was to compare the retinal function and morphology in patients affected by autosomal dominant CD or CRD carrying either a mutation in *GUCY2D* or *GUCA1A* using the same psychophysical, electrophysiological, and morphologic methods.

Patients and Methods

Five patients from a large family with known *GUCA1A* mutation (3 women and 2 men; mean age, 44 years; range, 32–57 years) and 9 patients from 4 families with *GUCY2D* mutation (6 women and 3 men; mean age, 49 years; range, 26–79 years) were included in this study. All examinations were performed after written informed consent and in accordance with the Declaration of Helsinki. The study was approved by the Ethics Committee of the Medical Faculty of University of Tübingen and was performed at the Institute for Ophthalmic Research, University of Tübingen.

A complete ophthalmologic examination was performed including psychophysical tests (visual acuity, saturated Roth 28 hue color test,[15] visual field, and dark adaptation) and extended electrophysiology (Ganzfeld and multifocal electroretinography [ERG]). Visual field tests were performed using an Octopus 900 perimeter (Haag-Streit International, Wedel, Germany). Semiautomated kinetic perimetry using Goldmann stimuli III4e, I4e, and additional dimmer stimuli, if possible, within the 90° visual field and automated static perimetry within the 30° visual field were performed.

Dark adaptation curves were measured with a dark adaptometer (Roland Consult GmbH, Brandenburg, Germany) after pupil dilation with tropicamide. After 3 minutes of bleaching with bright white light (intensity: 5.5 log photopic trolands), a staircase procedure was used to estimate the detection thresholds over a period of 40 minutes. Thresholds were alternately measured for red (635 nm) and green (530 nm) circular targets, presented 20° nasal of the fovea, providing threshold curves with distinct cone–rod system switchovers. Thresholds were then determined by a simultaneous model fit to both curves using the equation:

$$I(t) = \begin{cases} B1 + I1 \times \exp(R1 \times t) - I2 \times \exp(R2 \times t_k) + I2 \times \exp(R2 \times t) & t \geq t_k \\ B1 + I1 \times \exp(R1 \times t) & t < t_k \end{cases},$$

with t_k describing the time to the rod–cone break; $I1$, $R1$ the exponential decay of the cone; and $I2$, $R2$ of the rod thresholds.

Ganzfeld and multifocal ERGs were recorded according to the standards of the International Society for Clinical Electrophysiology of Vision,[16,17] but additional stimuli were included to improve retinal function evaluation. All tests were performed using DTL electrodes with an Espion E^2 (Diagnosys LLC, Lowell, MA) recording device coupled with a ColorDome (Diagnosys LLC) as light source. After 30 minutes of dark adaptation, a series of responses to increasing flash intensities (4 milliseconds: 0.0001–10 cd·s/m^2 in 0.5 log unit steps) were recorded, and the stimulus–response functions were modeled using the equation:

$$V(I) = V_{max} \times I^n / (I^n + K^n),$$

with the saturated b-wave amplitude V_{max}, the flash intensity K required for semisaturation as a measure of retinal sensitivity, and the slope related exponent n.[18,19]

Finally, dark-adapted responses to a series of blue flicker (LED 470 nm) with an intensity of 0.03 cd·s/m^2 and frequencies between 5 Hz and 30 Hz were recorded to isolate temporal retinal characteristics of the rod system.

The light-adapted protocol (10 minutes of light adaptation to a background luminance of 30 cd/m^2) included a single flash cone stimulus and 30 Hz flicker (both: 4 milliseconds, 3.0 cd·s/m^2). In addition, responses to a series of flicker with white stimuli of 3.0 cd·s/m^2 with increasing frequency from 5 Hz to 45 Hz were included to investigate possible alterations in the temporal resolution of the cone retinal pathway.

Multifocal ERG was performed with a VERIS System (version 5.1, Electro-Diagnostic Imaging, Inc., Redwood City, CA) using a Grass amplifier (model 12; Grass Products, Warwick, RI). The stimulus, consisting of 61 scaled hexagonal elements covering a central visual field of 60° × 55°, was presented on a 19′′ monitor at a frame rate of 75 Hz at a distance of 32 cm from the subjects' eyes. Responses were amplified (×200,000), bandpass-filtered (10–100 Hz), and analyzed according to the ring averages.

For detailed morphologic examination, fundus photography, fundus autofluorescence, and spectral domain optical coherence tomography recordings (Heidelberg Engineering GmbH, Germany) were performed in every patient. The statistical analysis of the data was conducted using the JMP 10 statistical software (SAS Institute, Cary, NC), R 2.14.2 (The R Foundation for Statistical Computing), and ggplot 0.9.3.

Results

All of the families showed an autosomal dominant mode of inheritance. Detailed characteristics of the patients are shown in Table 1. Molecular genetic analysis revealed a known mutation c.451C>T (p.L151F) in *GUCA1A* in the large family ZD1, affecting the EF4 hand of GCAP1. All identified mutations in *GUCY2D* were known mutations as well, and clustered to codon 838.[2,8,9] The mutation c.2512C>T (p.R838C) was the most frequent (2 families), c.2513G>A (p.R838H) and c.2512C>G (p.R838G) were found in 1 family each (pedigrees of the families are shown in Figure 2). The genetic results of all patients have been previously published elsewhere.[1,2]

All examined patients reported an onset of visual symptoms in childhood or early teenage years, and progression could be noticed in every case. Further characteristic findings were marked photophobia and color vision disturbances. Interestingly, night blindness was not present in the *GUCA1A* group, but 3 of 9 patients with *GUCY2D* mutation reported difficulties in the dark. Visual acuity was markedly reduced showing a wide range of patients with *GUCA1A* mutations presented with a mean visual acuity of 0.28 ± 0.24 (Snellen; range: 0.04 – 0.7), and the refraction in the family was consistently hyperopia and variable degrees of astigmatism. In contrast, patients with *GUCY2D* mutations had a mean visual acuity of 0.1 ± 0.13 (Snellen; range: counting fingers (CF) – 0.5) with a constant refraction of moderate to high myopia and various astigmatism. The oldest patient (ZD73 I:2) was pseudophakic on both eyes but suffered from high myopia before surgery. Interestingly, in family RCD62, both siblings presented with severely reduced visual acuity, both of them achieving only CF. For statistical analysis, these results were transformed into 0.014 Snellen visual acuity.[20] Furthermore, nystagmus was also obtained in one of the two siblings. Color vision disturbances were similar in both groups; abnormalities varied from blue to yellow defects in the milder cases and to severe color confusions in the more severe phenotypes, and were congruent with visual acuity degrees.

Static perimetry performed in all patients—except ZD131 II.4 and the RCD62 siblings—revealed scattered relative and absolute central scotomas in the 30° visual field. Outer boundaries obtained in the kinetic perimetry were nearly normal in the *GUCA1A* group, a mild to moderate narrowing was observed in the *GUCY2D* group, where also myopia was present. Again, the two siblings of the RCD62 family with *GUCY2D* mutation showed the most severe changes with residual islands in the mid-periphery for the Goldmann target III4e. Perimetry results are presented in Figure 3 and Figure 4 for the *GUCA1A* and *GUCY2D* groups, respectively.

A narrowing of the visual field borders is likely to be accompanied by the elevations of the dark adaptation thresholds. In patients with *GUCA1A* mutations, thresholds for the green stimuli (rod-dominated function) were almost normal (−3.3 log units ± 0.2), thresholds for the red stimuli (cone-dominated part of the function) were slightly elevated (−1.4 log units ± 0.2). In contrast, patients with *GUCY2D* mutations showed larger variability and, on average, a mild elevation of both thresholds (−2.7 log units ± 0.8 and −1.3 log units ± 0.7 for green and red stimuli, respectively). However, some patients retained normal thresholds (Figure 5). Data of the RCD62 siblings were not available.

Scotopic standard Ganzfeld ERG revealed normal or nearly normal amplitudes and slightly prolonged implicit times in the *GUCA1A* family members. Interestingly, scotopic ERGs in patients with *GUCY2D* mutation showed in almost every case a noticeable alteration with subnormal amplitudes and slightly delayed implicit times. Furthermore, in three patients (ZD73 I:2, ZD73 II:2, and ZD131 III:1), a negative

DOI:10.14753/SE.2014.1976

Table 1. Genetic and Clinical Findings of the Patients With Either *GUCA1A* (Gray Background) or *GUCY2D* Mutation

Patient ID	Gender	Age at Examination (years)	Diagnosis	Mutation	VA OD; OS	Refraction OD; OS	Progression	Night Blindness	Color Vision	Other
ZD1 IV:7	F	57	CD	*GUCA1A*: c.451C>T/p.L151F	0.04; 0.04	+2.25 sph –0.5 cyl 160°; +2.75 sph	Yes	No	Severe color confusions	—
ZD1 IV:12	F	51	CD	*GUCA1A*: c.451C>T/p.L151F	0.7; 0.5	+4.0 sph –2.5 cyl 2°; +3.75 sph –2.5 cyl 7°	Yes	No	Tritan defect	—
ZD1 IV:13	F	47	CD	*GUCA1A*: c.451C>T/p.L151F	0.1; 0.08	+3.25 sph –2.5 cyl 2°; +2.5 sph –0.75 cyl 97°	Yes	No	Severe color confusions	—
ZD1 V:5	M	35	CD	*GUCA1A*: c.451C>T/p.L151F	0.3; 0.2	+4.0 sph –0.75 cyl 45°; +3.5 sph –0.5 cyl 127°	Yes	No	Tritan-tetartan defect	Brown syndrome
ZD1 V:6	M	32	CD	*GUCA1A*: c.451C>T/p.L151F	0.4; 0.5	sc; 0.0 sph –0,5 cyl 180°	Yes, mild	No	Tritan defect	Granular corneal dystrophy
ZD111 III:1	F	45	CD	*GUCY2D*: c.2512C>T/p.R838C	0.1; 0.1	–2.25 sph; –1.5 sph –0.75 cyl 77°	Yes	No	Severe color confusions	—
ZD131 II:2	F	59	CRD	*GUCY2D*: c.2512C>T/p.R838C	0.08; 0.08	–12.0 sph; –11.75 sph	Yes	No	Severe color confusions	—
ZD131 II:4	F	66	CRD	*GUCY2D*: c.2512C>T/p.R838C	0.04; 0.06	–7.75 sph –2.25 cyl 22°; –8.0 sph –2.5 cyl 126°	Yes	No	Severe color confusions	—
ZD131 III:1	M	34	CRD (neg. ERG)	*GUCY2D*: c.2512C>T/p.R838C	0.5; 0.4	–2.50 sph –1.25 cyl 10°; –3.0 sph –1.0 cyl 0°	Yes	Yes	Tritan-tetartan defect	Strabismus
ZD73 I:2	F	79	CRD (neg. ERG)	*GUCY2D*: c.2513 G>A/p.R838H	0.1; 0.05	–0.25 sph –1.0 cyl 90°*; –0.25 sph –1.0 cyl 90°*	Yes	No	Severe color confusions	Pseudophakic, high myopia before operation
ZD73 II:2	M	55	CRD (neg. ERG)	*GUCY2D*: c.2513 G>A/p.R838H	0.1; 0.1	–3.0 sph –1.0 cyl 18°; –4.5 sph	Yes	No	Tritan-tetartan defect	—
ZD73 III:2	F	26	CD	*GUCY2D*: c.2513 G>A/p.R838H	0.05; 0.16	–8.0 sph; –7.0 sph –4.0 cyl 160°	Yes	No	Tritan-tetartan defect	Strabismus; Horner syndrome
RCD62 II:1	F	42	CRD	*GUCY2D*: c.2512C>G/p.R838G	CF (0.014); CF (0.014)	–12.0 sph –3.5 cyl 15°; –12.5 sph –2.5 cyl 160°	Yes	Yes	NA	Strabismus
RCD62 II:2	M	39	CRD	*GUCY2D*: c.2512C>G/p.R838G	CF (0.014); CF (0.014)	NA	Yes	Yes	NA	Nystagmus

Both CD and CRD were observed clinically; furthermore, in 3 patients, a negative ERG (neg. ERG) could also be detected. Color vision was tested with the Roth 28 test; in patients from the RCD62 family, the test could not be performed because of severe loss of central vision.

cyl, cylindrical; F, female; M, male; NA, not available; sph, spherical; CF, counting fingers; sc, sine correction, without correction.

ERG was detected. Photopic standard ERG responses were markedly reduced (representative Ganzfeld ERG responses for both groups are shown in Figure 6). The RCD62 siblings with *GUCY2D* mutation showed more severe changes in the ERG as well: scotopic ERG responses were drastically reduced; under photopic conditions, no reproducible responses could be detected. Considerable waveform differences between the *GUCA1A* and *GUCY2D* groups could be observed in the a-wave response to the highest flash intensity (DA 10.0 ERG); whereas patients with *GUCA1A* mutation retained normal a-wave shapes, patients of the *GUCY2D* group (with the exception of patient ZD111 III:1) showed a V-shaped a-wave lacking typical oscillations.

Intensity–response function was measured both under scotopic and photopic conditions (Figures 7 and 8, respectively). The results of the RCD62 family of the *GUCY2D* group were excluded from group comparison because both siblings represented a considerably more severe phenotype. We used a model fit to determine V_{max}, n, and k of the scotopic intensity–response function. Although a clear reduction of the V_{max} was observed in both the groups when compared with normal subjects (V_{max} was 239.54 ± 53.52 μV in *GUCA1A*, 186.56 ± 55.68 μV in *GUCY2D*, and 429.68 ± 132.63 μV in normal subjects, respectively), the parameters n and k did not seem to be notably different or different from normal subjects (n = 0.90 ± 0.17 and k = −2.81 ± 0.34 log cd·s/m^2 in *GUCA1A*, n = 1.19 ± 0.39 and k = −2.72 ± 0.21 log cd·s/m^2 in *GUCY2D*, n = 1.12 ± 0.44 and k = −2.72 ± 0.14 log cd·s/m^2 in normal subjects, respectively). Although the scotopic responses were reduced in both groups ($P < 0.0001$), a significant difference between *GUCA1A* and *GUCY2D* did show up ($P = 0.0022$).

Under photopic conditions, both patient groups showed markedly reduced amplitudes of the cone responses, a clear difference between groups could not be observed. The photopic hill phenomenon could not be seen in these patients (Figure 8).

To study temporal characteristics of rod and cone systems, ERG responses to increasing flicker frequencies were recorded under scotopic and photopic conditions. Interestingly, scotopic ERG flicker responses showed a marked reduction of amplitude for all frequencies and were almost diminished for flicker frequencies above 15 Hz. Photopic Ganzfeld responses were more compromised with little residual or even absent amplitude for increasing flicker frequencies (Figures 9 and 10).

Multifocal ERGs were accomplishable in few patients only and showed diminished central responses, whereas the outer ring averages revealed reduced amplitudes and delayed implicit times. Fundus alterations were typically confined to the macula and presented either with mottling or gross, circumscribed atrophy of the retinal pigment epithelium (RPE) in both groups (Figures 3 and 4). Even among family members, a wide variability was observed. In fundus autofluorescence imaging, mild RPE-alterations presented as slight hypofluorescent areas, in contrast, marked RPE-atrophies were obtained as sharply demarcated hypofluorescent circles surrounded by a ring of increased autofluorescence. The optical coherence tomography images reflected the variety of morphologic findings as well. In the milder cases, optical coherence tomography revealed only a thinner photoreceptor layer in the foveal area, and there was no disruption in the inner segment/outer segment border. In four cases, photoreceptor outer segments were "punched-out," these changes were strictly limited to the foveal area and corresponded with the hypofluorescent area of the fundus autofluorescence images. Two of these patients were members of the same ZD73 family with a *GUCY2D* mutation, the third patient was member of another family carrying a different mutation in the *GUCY2D* gene. The fourth patient was observed in the *GUCA1A* family ZD1. In the more severe cases, the photoreceptor layer was missing, the inner segment/outer segment border was diminished, and an increased backscatter from the choroid was observed because of RPE atrophy. Family RCD62 did not only show more pronounced functional but also morphologic changes: besides marked central RPE-atrophy, attenuation of the vessels, ghost vessels, and even bone spicule-like changes in the periphery were observed.

In one patient (ZD1 V:6) of the *GUCA1A* group, anterior segment examination revealed an additional granular corneal dystrophy. Further investigations of the pedigree elucidated that the retinal dystrophy in this case was inherited maternally and the corneal dystrophy paternally, both in an autosomal dominant manner.

Discussion

The *GUCY2D* gene, located on chromosome 17p13.1, encodes the retGC-1, which is essential for the recovery of the dark state after light excitation of photoreceptors.[12,21–23] Retinal guanylate cyclase is expressed in both photoreceptors, predominantly in cone outer segments, and therefore plays an even more critical role in the function of cones than rods.[10,11] Mutations in *GUCY2D* have been shown to cause various retinal dystrophies[4]; autosomal recessive mutations are a major cause of Leber congenital amaurosis, whereas certain heterozygous mutations result in autosomal

DOI: 10.14753/SE.2014.1976

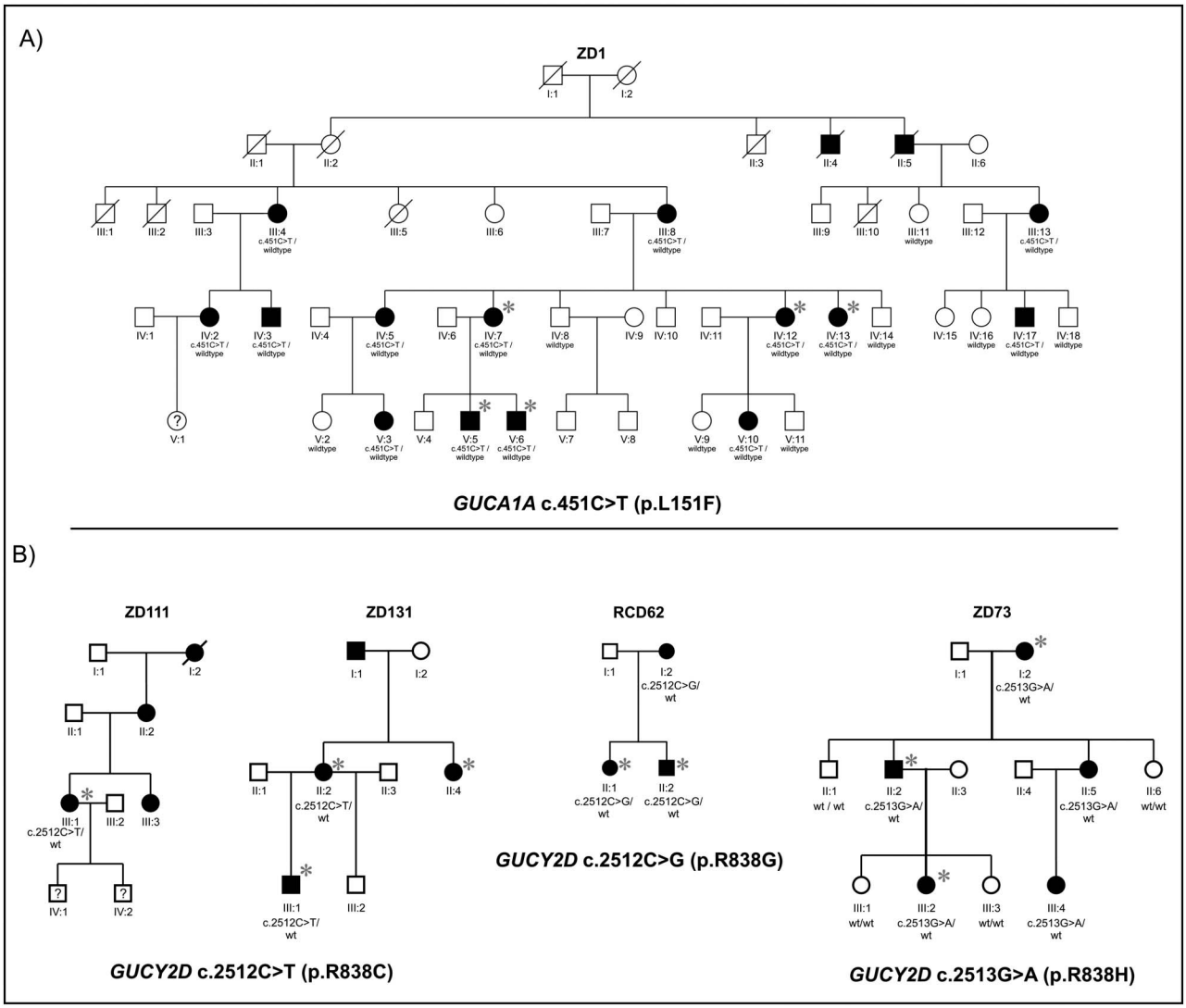

Fig. 2. **A.** Pedigree of family ZD1 with *GUCA1A* mutation c.451C>T p.L151F. **B.** Pedigrees of the families with mutations in the *GUCY2D* gene. The first 2 pedigrees on the left show 2 nonrelated families carrying the same mutation (c.2512C>T p.R838C), whereas the third and fourth families from the left carry the mutations c.2512C>G p.R838G and c.2513 G>A p.R838H, respectively. The stars indicate the investigated patients.

dominantly inherited CD and CRD.[2,8,9,24] Most of the dominant disease-causing sequence variations are located in the putative dimerization domain, which extends from amino acid 817 to 857. Codon 838 is known as a mutational hot spot because replacement of arginine by cysteine, serine, histidine, glycine, or alanine at this position (R838C, R838S, R838H, R838G, and R838A, respectively) is the most common cause of CD or CRD related to *GUCY2D*.[25,26] The mutant retGC-1—in principle—remains functional, but the R838 amino acid substitutions increase the apparent affinity of retGC-1 for GCAP1, thereby allowing GCAP1-mediated activation even at higher Ca^{2+} concentrations. In conclusion, the higher the affinity of retGC-1 to GCAP1 gets, the lower Ca^{2+}-sensitivity of the retGC-1 to GCAP1 unit can be detected.[25,26] However, this effect is caused not in equal measure by the diverse mutations; the mutants show a shift in the Ca^{2+} concentration for half maximal activation to higher Ca^{2+} levels with the effect of R838S > R838H > R838C, with the first (R838S) causing the most severe phenotypic changes.[25] According to further studies, R838H and R838C have relatively similar clinical features of retinal degeneration with less involvement of the rod system,[9,25] whereas R838G seems to cause a more severe phenotype.[1]

The other isoform of guanylate cyclase retGC-2, encoded by *GUCY2F*, also has an important physiologic role in normal phototransduction of human photoreceptors; however, no disease-associated mutations for *GUCY2F* have been reported yet.[4] GCAPs are encoded by the *GUCA* gene family members; three genes have been identified in mammalian genomes so far.

COLOR

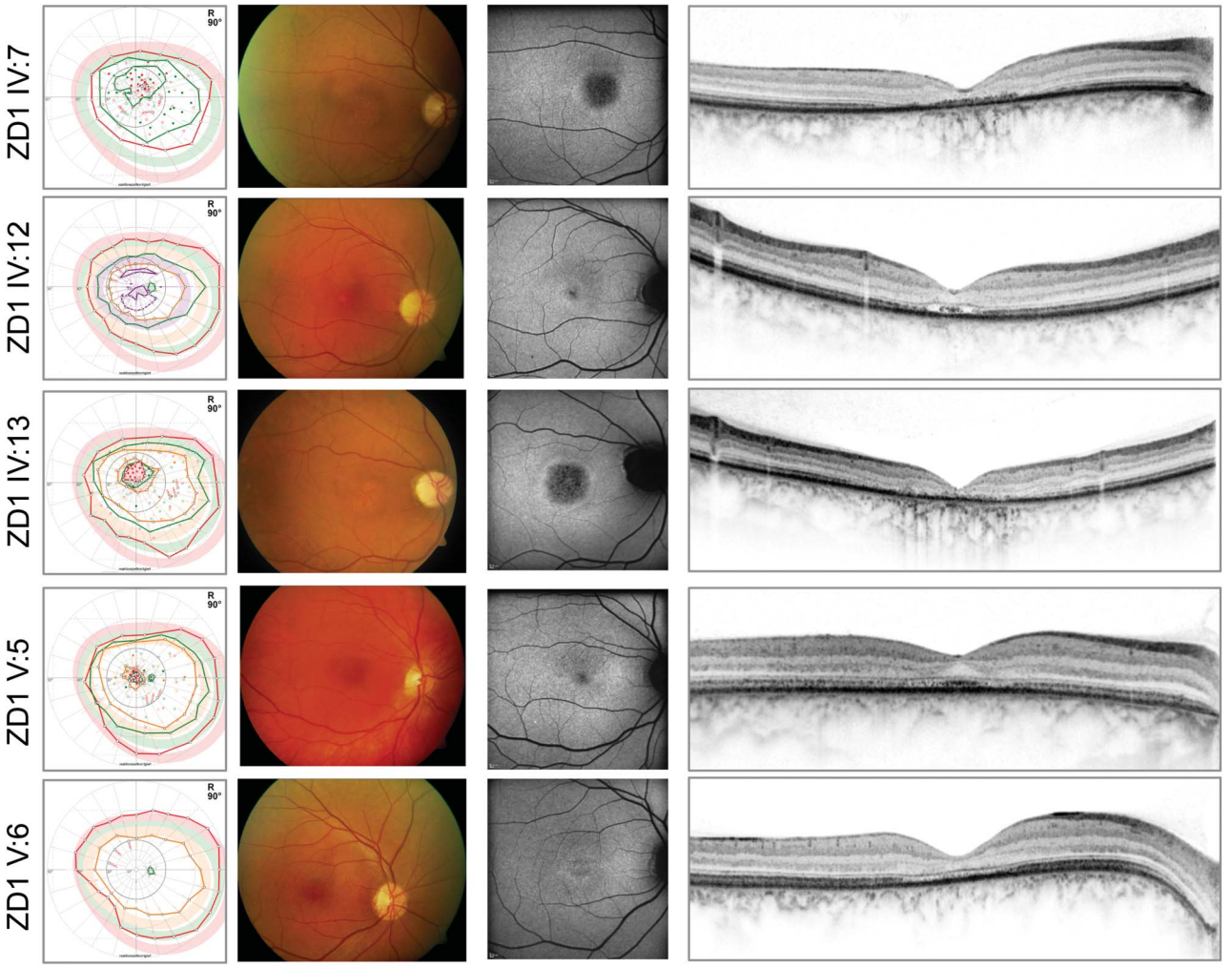

Fig. 3. From left to right: Kinetic perimetry results, fundus photography, fundus autofluorescence, and optical coherence tomography images of the patients of the family with *GUCA1A* mutations. In the perimetric results, central defects were detected, whereas outer boundaries with target III4e (red) were nearly normal.

GUCA1A (GCAP1) and *GUCA1B* (GCAP2), located on chromosome 6p21.1, are both required for normal phototransduction.[10,27–31] They are expressed in both photoreceptor types, but GCAP1 is predominantly present in cones, and GCAP2 is more abundant in rods.[32] *GUCA1C* (GCAP3) was discovered in human retina and is exclusively expressed in cones; however, no mutations in *GUCA1C* have been associated with retinal disease.[4] Furthermore, only one single dominant missense mutation in *GUCA1B* has been linked to macular degeneration.[33] In contrast, heterozygous mutations in *GUCA1A* have been identified in many cases of autosomal dominant CD, CRD, or macular dystrophy.[2,3,6,7] Most of the known dominant mutations, like the L151F mutation in our family, are missense mutations and affect the Ca^{2+}-binding sites on EF3 or EF4 of the GCAP1.[28,34,35] The main functional consequence is a decrease in Ca^{2+}-sensitivity, which leads to a reduced inhibition of retGC-1 at higher intracellular Ca^{2+} concentrations (i.e., in the dark).

Both of the mechanisms affecting retGC-1 or GCAP1 result in reduced sensitivity to intracellular Ca^{2+} concentrations, leading to constitutive activity of retGC-1 in the dark and thereby to higher cyclic guanosine monophosphate levels. This disturbed cyclic guanosine monophosphate, and Ca^{2+} homeostasis of the photoreceptors is thought to be responsible for the progressive dysfunction and for the retinal degeneration.[21–23] Considering all these information, the following question awaits an answer. Is there a difference in the clinical phenotype of *GUCA1A*- or *GUCY2D*-related retinal dystrophies despite the same pathophysiological background?

We presume yes, although only a tendency. The typical phenotype in both of our patient groups was an autosomal dominant cone-dominated retinal dystrophy

DOI: 10.14753/SE.2014.1976

COLOR

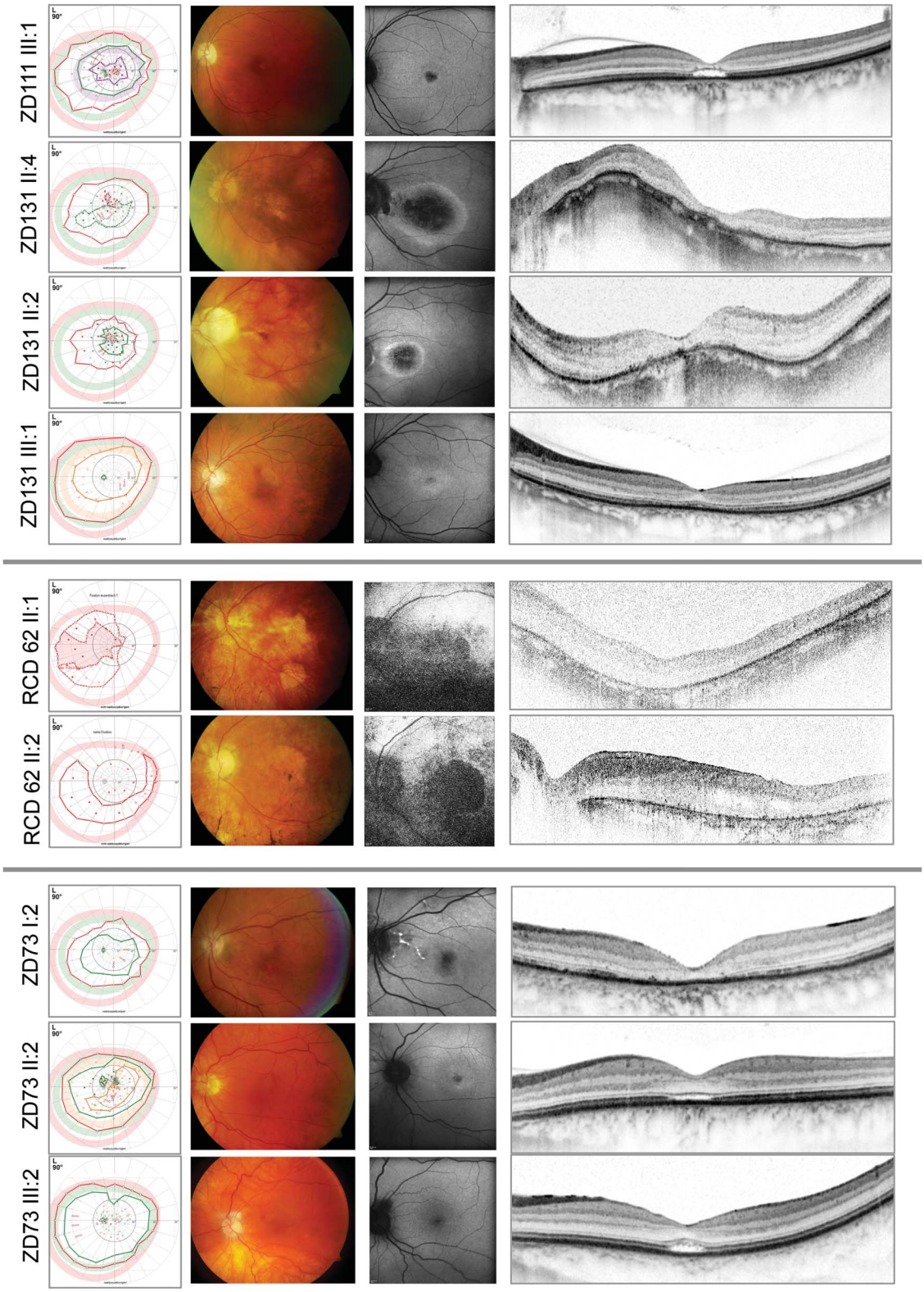

Fig. 4. From left to right: Kinetic perimetry results, fundus photography, fundus autofluorescence, and optical coherence tomography images of the patients of the family with *GUCY2D* mutations. The upper 4 patients are from 2 nonrelated families carrying the same p.R838C mutations in the *GUCY2D* gene. The members of the RCD62 family carrying the p.R838G mutation show a more severe phenotype (fifth and sixth panels). The lower 3 patients are from family ZD73 with p.R838H mutation in the *GUCY2D* gene. The perimetric results show central defects and variable attenuation of the outer boundaries with target III4e (red).

COLOR

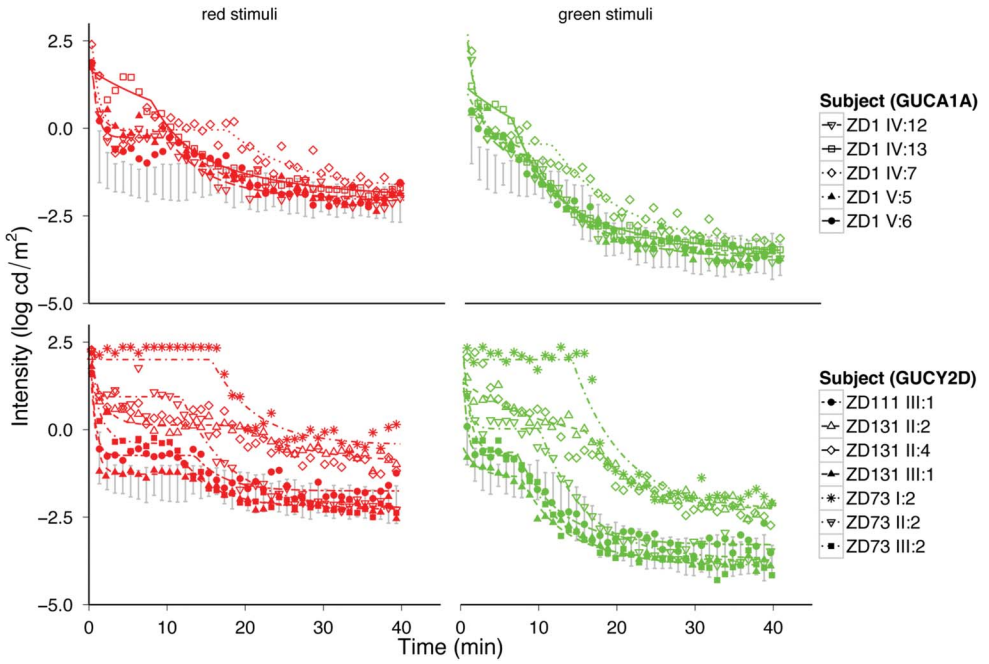

Fig. 5. Dark adaptation thresholds of cone- and rod-dominated function (red and green stimuli, respectively). The upper panels show the results of the patients with *GUCA1A*, whereas the lower panels show the thresholds of the patients with *GUCY2D*. Note that although patients with *GUCA1A* reveal almost normal threshold levels, there is a larger variability in *GUCY2D* patients with more elevated thresholds. The 95% confidence band of normal subjects is marked with gray data of the RCD62 family are not available.

with disease onset in early adolescence, characterized by increased glare sensitivity, severe color vision disturbances, central defects in the visual field, but nearly normal outer boundaries. Retinal morphologic changes were relatively limited to the macular region, however, a great variability-from RPE mottling to large RPE defects-was detected even among families. The fundus autofluorescence and optical coherence tomography images also demonstrated the diversity of macular changes. In comparison, patients with *GUCY2D* mutations seemed to show more severe morphologic changes. These clinical findings are in line with the well-described phenotypes in the literature.[1–4,8,9]

Functional results also suggested a cone-dominated dystrophy in both groups with a rather more severe phenotype in *GUCY2D*. In patients with *GUCA1A* mutation, the diagnosis of CD was more likely, although a slight alteration of rod function in the extended scotopic ERG protocol did show up. Patients with *GUCY2D* mutation revealed even more

COLOR

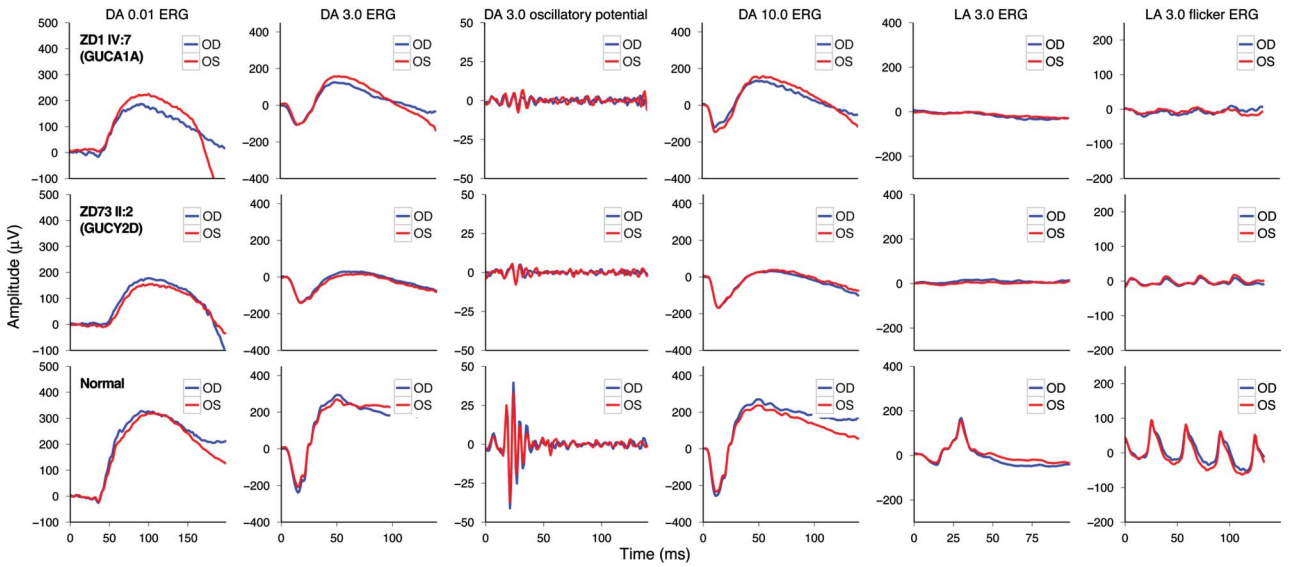

Fig. 6. International Society for Clinical Electrophysiology of Vision standard Ganzfeld ERG responses of a representative patient of each group (upper panel: *GUCA1A*, middle panel: *GUCY2D*) compared with a normal subject (lower panel). Color coding in each panel: blue curves show results of the right eye (OD) and red curves show results of the left eye (OS).

DOI: 10.14753/SE.2014.1976

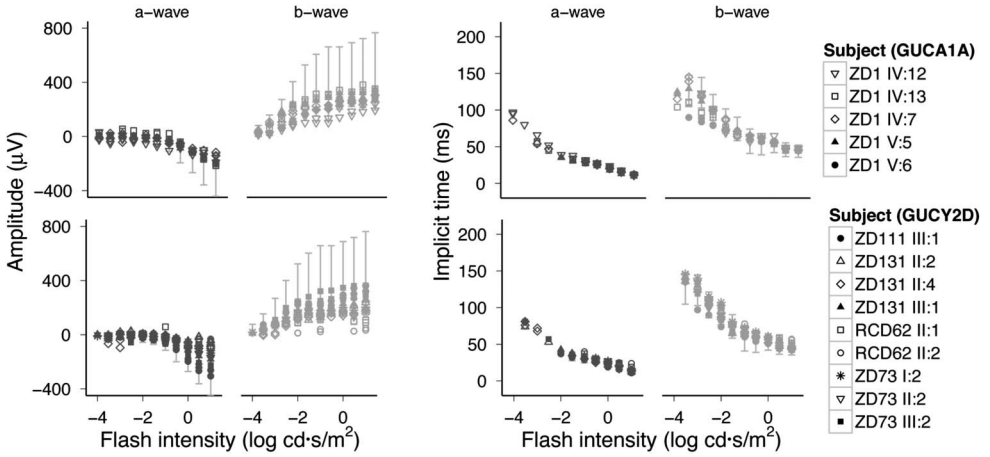

Fig. 7. Intensity–response function kinetics under scotopic conditions. The single flash response a- and b-wave amplitudes (left panel) and implicit times (right panel) to increasing stimulus intensities are presented for both groups (upper subjects: *GUCA1A* group, lower subjects: *GUCY2D* group; the 95% confidence band of normal subjects is marked with gray).

pronounced scotopic changes, so the final diagnosis was mainly CRD—with a negative ERG in three cases, suggesting an early involvement of inner retinal neurons.[4] This difference also showed up in the dark adaptation thresholds. Patients with *GUCA1A* retained more preserved rod function, whereas patients of the *GUCY2D* groups showed elevated dark adaptation thresholds, especially in the elder generation. The more preserved central visual acuity and visual field findings further suggested milder disease characteristics in *GUCA1A* cases. Interestingly, differences in the refractive errors showed up: although patients with *GUCY2D* were rather myopic, patients with GUCA1A revealed hyperopia. However, these characteristics are in line with previous reports known in the literature.[3,4,7–9]

Our results suggest that the defects in GCAP1 (*GUCA1A*) signaling result in a less severe retinal dystrophy. What could be the explanation? GCAP1 and GCAP2 are both essential for normal phototransduction, as discussed before, but their expression in rods and cones shows differences with GCAP1 being predominantly expressed in cones.[23,33] The presence of GCAP1 and GCAP2 in mammalian rods is suggested to be almost equimolar; furthermore, their contribution to the biochemical pathway behind the GC regulation seems to differ. By participating in the activation of retGC-1 even at Ca^{2+} levels at which GCAP1 regulation is expected to predominate, GCAP2 quickens the recovery of the single-photon response and the responses to brighter flashes in rods. This suggests an equally important role for GCAP2 and GCAP1 in rods. Furthermore, GCAP2 has been shown to act with lower activity on retGC-1 (*GUCY2D*), which might explain the more preserved rod function in altered GCAP1 signaling.[32,33]

In contrast, retGC-1 is more predominant in cones but is present in both photoreceptor types, affecting both rod and cone function.[13,25] This clearly matches with the clinical findings, that an autosomal dominant mutation of *GUCY2D* causes CRD, as demonstrated in our cases as well. However, a difference in the severity of phenotype because of various mutation forms could not be further defined. The large variety of functional and morphologic appearance suggests a possible role of other modifying factors. Two siblings of the family RCD62

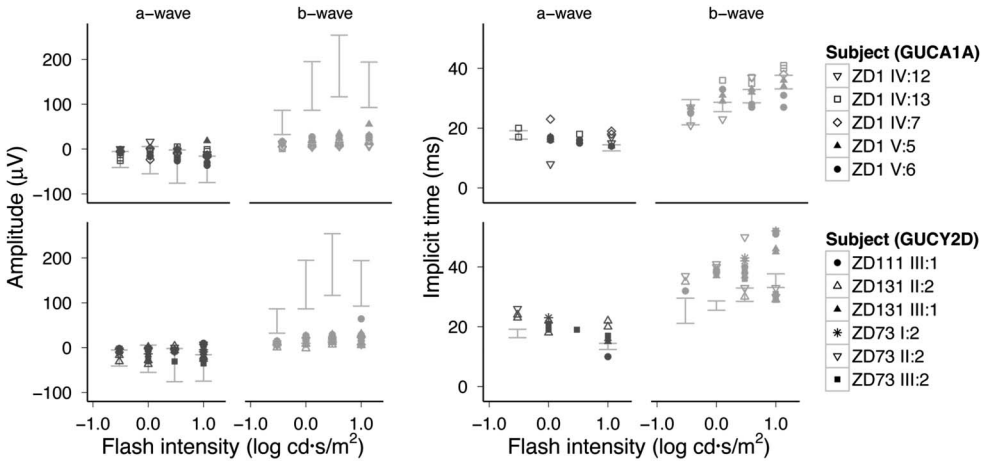

Fig. 8. Intensity–response function kinetics under photopic conditions. The single flash response a- and b-wave amplitudes (left panel) and implicit times (right panel) to increasing stimulus intensities are presented for both groups (upper subjects: *GUCA1A* group, lower subjects: *GUCY2D* group; the 95% confidence band of normal subjects is marked with gray). Note the missing photopic hill phenomenon in patients. Photopic responses were not detectable in the RCD62 family, therefore these data are not shown.

COLOR

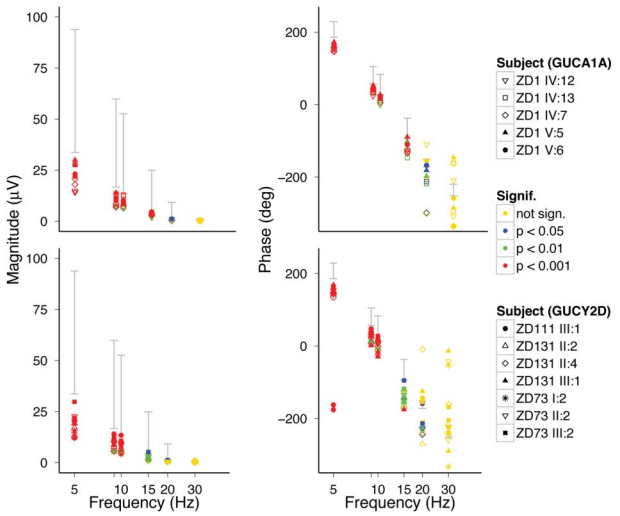

Fig. 9. Scotopic flicker series. Magnitude (left panel) and phase (right panel) of scotopic flicker responses to stimuli of increasing flicker frequency are presented for the *GUCA1A* (upper) and *GUCY2D* (lower) groups. Significance levels are color coded in each figure, the 95% confidence band of normal subjects are marked with gray. The amplitudes of the patients are below normal and not significant for stimuli faster than 15 Hz.

with a heterozygous *GUCY2D* mutation showed a strikingly more severe phenotype with markedly reduced visual acuity, only residual islands in the visual field and markedly reduced scotopic and photopic ERG responses. They were the only patients who showed bone spicule–like pigmentary changes and RPE atrophy in the peripheral retina. The genetic analysis detected an R838G substitution.[1] Whether this mutation or other additional yet unknown modifying factors could be responsible for the more severe phenotype in this family is still unknown.

COLOR

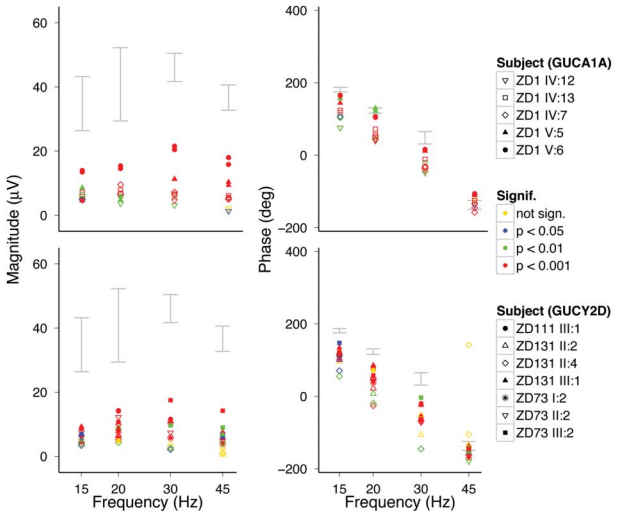

Fig. 10. Photopic flicker series. Magnitude (left panel) and phase (right panel) of photopic flicker responses in a flicker series show similar frequency dependence but lower magnitude in patients with *GUCA1A* (upper) and *GUCY2D* (lower) mutations. Significance levels are color coded in each figure; the 95% confidence band of normal subjects is marked with gray.

Taken together, we suggest that mutations in the *GUCA1A* gene in autosomal dominant retinal dystrophies cause a less severe phenotype and less involvement of rod photoreceptors than *GUCY2D* mutations.

Key words: cone degeneration, cone–rod degeneration, electrophysiology, genetics, genotype–phenotype correlation, retinal degeneration.

Acknowledgment

The authors thank Veronique Kitiratschky for performing the genetic tests; the patients for their participation; the technicians Ulrike Fuchs and Susanne Kramer for performing excellent examinations; and Torsten Strasser for the help with data analysis.

References

1. Kitiratschky VB, Wilke R, Renner AB, et al. Mutation analysis identifies GUCY2D as the major gene responsible for autosomal dominant progressive cone degeneration. Invest Ophthalmol Vis Sci 2008;49:5015–5023.
2. Kitiratschky VB, Behnen P, Kellner U, et al. Mutations in the GUCA1A gene involved in hereditary cone dystrophies impair calcium-mediated regulation of guanylate cyclase. Hum Mutat 2009;30:E782–E796.
3. Hunt DM, Wilkie SE, Newbold R. Dominant cone and cone-rod dystrophies: functional analysis of mutations in retGC1 and GCAP1. Novartis Found Symp 2004;255:37–49; discussion 49–50, 177–178.
4. Hunt DM, Buch P, Michaelides M. Guanylate cyclases and associated activator proteins in retinal disease. Mol Cell Biochem 2010;334:157–168.
5. Small KW, Silva-Garcia R, Udar N, et al. New mutation, P575L, in the GUCY2D gene in a family with autosomal dominant progressive cone degeneration. Arch Ophthalmol 2008; 126:397–403.
6. Sokal I, Dupps WJ, Grassi MA, et al. A novel GCAP1 missense mutation (L151F) in a large family with autosomal dominant cone-rod dystrophy (adCORD). Invest Ophthalmol Vis Sci 2005;46:1124–1132.
7. Jiang L, Katz BJ, Yang Z, et al. Autosomal dominant cone dystrophy caused by a novel mutation in the GCAP1 gene (GUCA1A). Mol Vis 2005;11:143–151.
8. Xiao X, Guo X, Jia X, et al. A recurrent mutation in GUCY2D associated with autosomal dominant cone dystrophy in a Chinese family. Mol Vis 2011;17:3271–3278.
9. Zhao X, Ren Y, Zhang X, et al. A novel GUCY2D mutation in a Chinese family with dominant cone dystrophy. Mol Vis 2013;19:1039–1046.
10. Kachi S, Nishizawa Y, Olshevskaya E, et al. Detailed localization of photoreceptor guanylate cyclase activating protein-1 and -2 in mammalian retinas using light and electron microscopy. Exp Eye Res 1999;68:465–473.
11. Larhammar D, Nordström K, Larsson TA. Evolution of vertebrate rod and cone phototransduction genes. Philos Trans R Soc Lond B Biol Sci 2009;364:2867–2880.
12. Olshevskaya EV, Ermilov AN, Dizhoor AM. Dimerization of guanylyl cyclase-activating protein and a mechanism of pho-

DOI:10.14753/SE.2014.1976

toreceptor guanylyl cyclase activation. J Biol Chem 1999;274: 25583–25587.
13. Olshevskaya EV, Ermilov AN, Dizhoor AM. Factors that affect regulation of cGMP synthesis in vertebrate photoreceptors and their genetic link to human retinal degeneration. Mol Cell Biochem 2002;230:139–147. Review.
14. Duda T, Pertzev A, Sharma RK. Differential Ca(2+) sensor guanylate cyclase activating protein modes of photoreceptor rod outer segment membrane guanylate cyclase signaling. Biochemistry 2012;51:4650–4657. doi: 10.1021/bi300572w.
15. Amos JF, Piantanida TP. The Roth 28-hue test. Am J Optom Physiol Opt 1977;54:171–177.
16. Marmor MF, Fulton AB, Holder GE, et al. ISCEV Standard for full-field clinical electroretinography (2008 update). Doc Ophthalmol 2009;118:69–77.
17. Hood DC, Bach M, Brigell M, et al. ISCEV standard for clinical multifocal electroretinography (mfERG) (2011 edition). Doc Ophthalmol 2012;124:1–13. doi: 10.1007/s10633-011-9296-8.
18. Evans LS, Peachey NS, Marchese AL. Comparison of three methods of estimating the parameters of the Naka-Rushton equation. Documenta Ophthalmol 1993;84:19–30.
19. Robson JG, Frishman LJ. Response linearity and kinetics of the cat retina: the bipolar cell component of the dark-adapted electroretinogram. Vis Neurosci 1995;12:837–850.
20. Schulze-Bonsel K, Feltgen N, Burau H, et al. Visual acuities "hand motion" and "counting fingers" can be quantified with the freiburg visual acuity test. Invest Ophthalmol Vis Sci 2006; 47:1236–1240.
21. Dizhoor AM, Olshevskaya EV, Peshenko IV. Mg2+/Ca2+ cation binding cycle of guanylyl cyclase activating proteins (GCAPs): role in regulation of photoreceptor guanylyl cyclase. Mol Cell Biochem 2010;334:117–124.
22. Peshenko IV, Olshevskaya EV, Dizhoor AM. Ca(2+)-dependent conformational changes in guanylyl cyclase-activating protein 2 (GCAP-2) revealed by site-specific phosphorylation and partial proteolysis. J Biol Chem 2004;279:50342–50349.
23. Peshenko IV, Olshevskaya EV, Dizhoor AM. Binding of guanylyl cyclase activating protein 1 (GCAP1) to retinal guanylyl cyclase (RetGC1). The role of individual EF-hands. J Biol Chem 2008;283:21747–21757.
24. Smith M, Whittock N, Searle A, et al. Phenotype of autosomal dominant cone-rod dystrophy due to the R838C mutation of the GUCY2D gene encoding retinal guanylate cyclase-1. Eye (Lond) 2007;21:1220–1225.
25. Wilkie SE, Newbold RJ, Deery E, et al. Functional characterization of missense mutations at codon 838 in retinal guanylate cyclase correlates with disease severity in patients with autosomal dominant cone-rod dystrophy. Hum Mol Genet 2000;9: 3065–3073.
26. Karan S, Frederick JM, Baehr W. Novel functions of photoreceptor guanylate cyclases revealed by targeted deletion. Mol Cell Biochem 2010;334:141–155.
27. Lim S, Peshenko I, Dizhoor AM, Ames JB. Effects of Ca2+, Mg2+, and myristoylation on guanylyl cyclase activating protein 1 structure and stability. Biochemistry 2009;48:850–862.
28. Wilkie SE, Li Y, Deery EC, et al. Identification and functional consequences of a new mutation (E155G) in the gene for GCAP1 that causes autosomal dominant cone dystrophy. Am J Hum Genet 2001;69:471–480.
29. Jiang L, Wheaton D, Bereta G, et al. A novel GCAP1 (N104K) mutation in EF-hand 3 (EF3) linked to autosomal dominant cone dystrophy. Vis Res 2008;48:2425–2432.
30. Jiang L, Li TZ, Boye SE, et al. RNAi-mediated gene suppression in a GCAP1(L151F) cone-rod dystrophy mouse model. PLoS One 2013;8:e57676. doi: 10.1371/journal.pone. 0057676.
31. Peshenko IV, Moiseyev GP, Olshevskaya EV, Dizhoor AM. Factors that determine Ca2+ sensitivity of photoreceptor guanylyl cyclase. Kinetic analysis of the interaction between the Ca2+-bound and the Ca2+-free guanylyl cyclase activating proteins (GCAPs) and recombinant photoreceptor guanylyl cyclase 1 (RetGC-1). Biochemistry 2004 43:13796–13804.
32. Makino CL, Peshenko IV, Wen XH, et al. A role for GCAP2 in regulating the photoresponse. Guanylyl cyclase activation and rod electrophysiology in GUCA1B knock-out mice. J Biol Chem 2008;283:29135–29143.
33. Kitiratschky VB, Glöckner CJ, Kohl S. Mutation screening of the GUCA1B gene in patients with autosomal dominant cone and cone rod dystrophy. Ophthalmic Genet 2011;32:151–155.
34. Yu H, Olshevskaya E, Duda T, et al. Activation of retinal guanylyl cyclase-1 by Ca2+-binding proteins involves its dimerization. J Biol Chem 1999;274:15547–15555.
35. Buch PK, Mihelec M, Cottrill P, et al. Dominant cone-rod dystrophy: a mouse model generated by gene targeting of the GCAP1/Guca1a gene. PLoS One 2011;6:e18089.

DOI:10.14753/SE.2014.1976

Cone and cone rod dystrophy segregating in the same pedigree due to the same novel CRX gene mutation

V B D Kitiratschky, D Nagy, T Zabel, E Zrenner, B Wissinger, S Kohl and H Jägle

Br. J. Ophthalmol. 2008;92;1086-1091
doi:10.1136/bjo.2007.133231

DOI:10.14753/SE.2014.1976

Cone and cone–rod dystrophy segregating in the same pedigree due to the same novel *CRX* gene mutation

V B D Kitiratschky,[1,2] D Nagy,[3] T Zabel,[3] E Zrenner,[1] B Wissinger,[1] S Kohl,[1] H Jägle[3]

► Four supplementary figures are published online only at http://bjo.bmj.com/content/vol92/issue8

[1] Centre of Ophthalmology, Institute for Ophthalmic Research, Molecular Genetics Laboratory, Tübingen, Germany; [2] Graduate School of Neural & Behavioural Sciences, International Max Planck Research School, University Tübingen, Tübingen, Germany; [3] Centre of Ophthalmology, University Eye Hospital, Tübingen, Germany

Correspondence to: Dr H Jägle, Centre of Ophthalmology, University Eye Hospital, Schleichstr. 12–16, D-72076 Tübingen, Germany; herbert.jaegle@uni-tuebingen.de

Accepted 16 April 2008

ABSTRACT

Aim: To describe the detailed phenotypes of a multigeneration family affected by autosomal dominant cone–rod dystrophy (adCRD) and characterised by marked intrafamilial heterogeneity, due to a novel frameshift mutation in the *CRX* gene.

Methods: Six affected and two unaffected family members underwent detailed ophthalmological examination as well as psychophysical and electrophysiological testing. Mutation screening of the *CRX* gene and segregation analysis were performed in 14 family members from three generations.

Results: Clinical examination of six available mutation carriers showed marked phenotypic heterogeneity, presenting with a reduced cone electroretinogram (ERG) and normal rod ERG in one family branch and a negative ERG in the other as the most striking feature. Genetic screening identified a novel mutation in the *CRX* gene, c.636delC, that independently segregates with the disease in both branches of the family.

Conclusion: The authors identified a novel disease causing mutation in the *CRX* gene associated with adCRD. Furthermore, we show here for the first time the coexistence of a reduced cone and a negative ERG component in different individuals of the same family, all affected by the same mutation.

Inherited progressive cone–rod dystrophies (CRD) are characterised by progressive loss of cone photoreceptor function followed by progressive loss of rod photoreceptor function and often accompanied by retinal degeneration.[1–4] All modes of Mendelian inheritance have been observed, and genetic heterogeneity is a hallmark of CRD.[2] The *cone–rod homeobox* (*CRX*) gene is one of the associated genes which, if mutated, causes non-syndromic autosomal dominant CRD (adCRD), retinitis pigmentosa (adRP) or Leber congenital amaurosis (LCA).[2]

It has not been possible to correlate severity of retinal disease (CRD versus LCA) with particular categories of *CRX* gene mutations (ie, missense versus frameshift mutations).[5] However, in a few cases of adCRD caused by mutations in the *CRX* gene, a so-called negative electroretinogram (ERG) has been recorded.[6–9]

Here, we report the identification of a new *CRX* gene mutation in a family affected by autosomal dominant retinal dystrophy characterised by a highly variable disease expression, including a cone dystrophy in some subjects and a cone–rod dystrophy with a negative ERG in others.

METHODS

Subjects

We screened genomic DNA samples of 14 family members of a large German family (family code ZD58) for mutations in the *CRX* gene. Extensive phenotyping was performed in eight family members. The phenotype was established on the basis of an extensive clinical examination and based on visual acuity, visual field, dark adaptation and electroretinography results.

Clinical examination

The standardised clinical investigations included visual acuity, kinetic (90°) and static (30°) visual field (Octopus 101, Haag Streit, Switzerland), colour vision testing with the Lanthony panel D-15 test, Ganzfeld electroretinography (ERG) according to the ISCEV standard including a series of dark adapted rod responses, maximum responses, oscillatory potentials, cone single flash and flicker responses with the Espion E2 system (Diagnosys, Cambridge, UK) and multifocal electroretinography (mfERG) with the VERIS system (Electrodiagnostic Imaging, San Mateo, CA) and a Grass amplifier (Grass, Quincy, MA).[10 11] All ERG recordings were performed with maximally dilated pupils using a DTL fibre electrode. Interrelation between dark adapted b-wave amplitude and stimulus intensities was modelled using a Naka–Rushton function (equation) with the parameters V_{max} (maximum b-wave amplitude), n (exponential that is related to the slope at the linear phase) and k (semisaturation intensity).[12]

$$V(I) = V_{max} I^n/(I^n+k^n)$$

Increment thresholds were obtained for a white 0.43° diameter target presented on a white background of 10 cd/m^2 central in a Ganzfeld dome. Dark adaptation thresholds were obtained over a period of 30 min by means of a two-colour technique in a Ganzfeld mode. After bleaching with a white light, thresholds for a red (corresponding to cone threshold) and a green (rod threshold) target were repeatedly measured using an adaptive staircase procedure. Finally, fundus photographs were taken with the Zeiss (Bern, Switzerland) fundus camera, and fundus autofluorescence was assessed with the Heidelberg Retina Angiograph 2 (Heidelberg Engineering, Heidelberg, Germany).

DOI:10.14753/SE.2014.1976

Mutation analysis

The three coding exons 2–4 of the *CRX* gene, including approximately 25 bp up- and downstream of the coding regions were amplified by polymerase chain reaction (PCR) using three sets of gene specific primer pairs (exon 2: 5′-CCCATG GTGAGTAACTGGTA-3′, 5′-AGAGGTCCTCCAAGAGATGA-3′; exon 3: 5′-CAACCAGGATGGAATTCTT-3′, 5′-CTGAG ATCACAGGAAGTGTC-3′; exon 4: 5′-TCACCAATAAGTG TCCTCATC-3′, 5′-CTTTCTCAGGAATGCCATC-3′. Annealing temperature for each primer set 55°C). PCR products were purified enzymatically with Exo-SAP-IT (USB, Cleveland, OH) and subjected to cycle sequencing using the same primers as used for PCR (plus a third primer for exon 4, 5′-ATTCCTACAGTCCCCCTCT-3′) and BigDye Terminator v3.1 chemistry (Applied Biosystems, Darmstadt, Germany). The sequencing reaction was then resolved on a 3100 Genetic Analyzer capillary electrophoresis system (Applied Biosystems). Co-segregation analysis for the novel *CRX* mutation c.636delC and the intronic *CRX* sequence variant c.100C>T was done by PCR amplification of exons 4 and 2, respectively, using the respective primer pairs (see above), and subsequent cycle sequencing as described above.

RESULTS

Function and morphology of the central retina

We characterised the phenotypes of six affected and two unaffected family members from two different generations (fig 1). As shown in table 1, visual acuity was similar in the two family branches and depended mainly on age.

Colour vision testing (saturated panel D-15 test, in one patient extra large caps were used) indicated deficiencies along the blue–yellow axis. Increment thresholds for a white central target (26 min diameter) were only slightly decreased in most family members (table 1). The centre of the retina in older patients showed a large pigment epithelial defect corresponding to the hypofluorescent area in the autofluorescence imaging (fig 2C), whereas optic disc appearance was unremarkable, and vessels were normal in the younger family members and slightly narrowed in the older ones (fig 2B). In all patients, multifocal ERG (mfERG) recordings showed a marked reduction in waveform amplitude for the inner two or three ring averages but less profound reduction in the outer rings (fig 2D). These results indicate that even though the density of cones is reduced, those remaining may have an almost normal function.

Peripheral retina

In contrast, peripheral retinal function was clearly different in patients of the two branches of the family. While patient IV:7 showed a marked and IV:11 a slight concentric narrowing in kinetic perimetry (target III/4e), all other patients, including IV:2, showed normal borders (fig 2A).

The Ganzfeld-ERG responses obtained using the ISCEV standard protocol are illustrated in fig 3. The dark-adapted rod response (rows from top to bottom), the maximal response, oscillatory potentials, single flash cone response and the 30 Hz flicker ERG were all recordable in all family members. They were within normal limits in V:2 and V:3. Rod response amplitudes were reduced in all patients of family branch B (IV:7, IV:8, IV:11 and V:4) to values between 70.2 and 125.2 μV (normal 95% CI 130.6 to 420.2 μV). The maximum response a-wave amplitude was normal or at the lower limit of the 95% percentile (109.8 to 388.7 μV) in all patients. However, the a-wave peak amplitude and implicit time may be affected by an early rise of the b-wave. Thus, we additionally analysed the a-wave amplitude at a given implicit time of 11 ms (fig S1). Only for patient IV:2 (amplitude: right eye (OD) 72.5 and left eye (OS) 73.3 μV) of branch A was the amplitude minimally reduced, with results of patients IV:8 (OD 56.0 and OS 74.7 μV) and IV:11 (OD 51.0 and OS 74.0 μV) mildly reduced below the 95% percentile (normal 95% CI 80.0 to 305.2 μV). In contrast, the maximum response b-wave amplitude was not reduced for members of branch A (259.8 to 702.4 μV) so that the b/a ratio was normal (1.65 to 2.4), while family members of branch B showed a reduced maximum response b-wave amplitude between 94.6 and 206.3 μV (normal 95% percentile: 244.6 to 597.3), resulting in a so-called negative ERG due to preservation of the response a-wave (fig 2B).

To further explore rod function, we quantified the interrelation between the response amplitude and the stimulus intensity

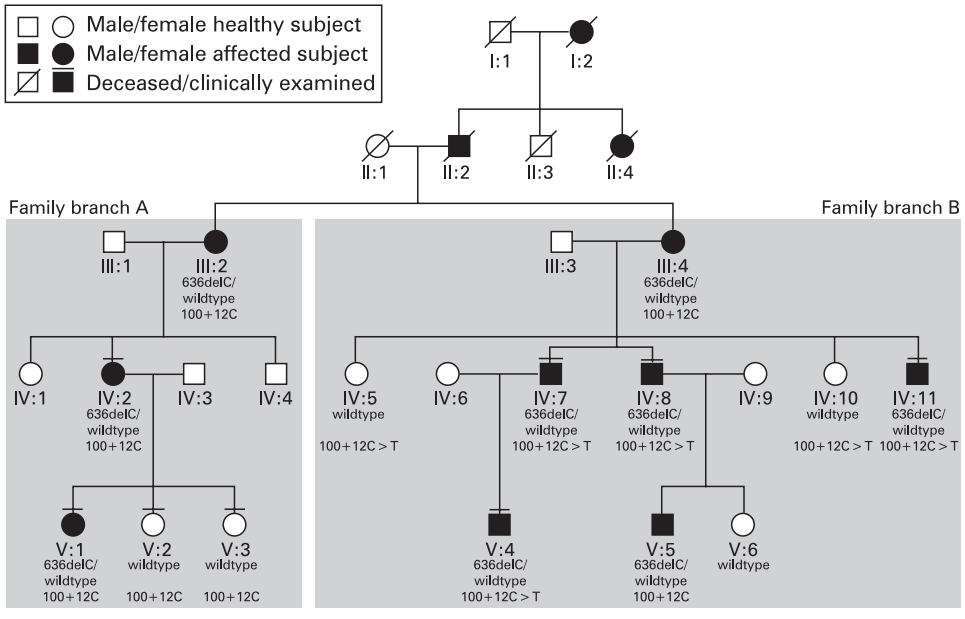

Figure 1 Pedigree of a five-generation family affected by autosomal dominant cone–rod dystrophy. Mutation screening of the *CRX* gene identified a clearly disease-causing mutation in the *CRX* gene, c.636delC, which segregated concordantly with the disease phenotype (the genetic status for the mutation is shown in bold letters). Segregating with the more severe phenotype and an additional rod involvement (family branch B, descendants of patient III:2) we identified the intronic sequence variant of the *CRX* gene c.100+12C>T (the genetic status for the variant is shown in italics under the respective pedigree symbol, c.100+12C for homozygotes, c.100+12C>T for heterozygotes).

DOI:10.14753/SE.2014.1976

Table 1 Basis characteristics of study patients

	Refraction		Visual acuity (Snellen)		Central increment threshold (dB)		Dark adaptation final sensitivity (25 min)	
ID	OD	OS	OD	OS	OD	OS	Cone	Rod
IV:2	−2.25 sph −0.5 cyl 6°	−2.5 sph −0.5 cyl 176°	0.100	0.100	13	8	−2.5	−4.25
V:1	−2.0 sph −0.75 cyl 45°	−2.25 sph −1.0 cyl 151°	0.800	0.800	26	34	−2.25	−4.0
V:2	−2.5 sph	−3.5 sph −0.25 cyl 60°	1.000	1.000	35	33	−2.75	−4.25
V:3	Sc	Sc	1.000	1.000	34	36	−2.75	−4.5
IV:7	*	*	0.029	0.029	17	20	−2.0	−3.0
IV:8	−1.5 sph −0.75 cyl 2°	−1.25 sph −0.5 cyl 180°	0.900	1.000	34	35	−2.5	−3.0
IV:11	−4.5 sph −0.5 cyl 170°	−5.0 sph −1.0 cyl 0°	0.400	0.500	25	29	−1.0	−2.5
V:4	Sc	Sc	1.000	1.000	38	36	−3.0	−4.25

Snellen visual acuity was assessed using refraction. For patient IV.7, visual acuity could not be improved with spectacle correction.
*To be defined.
cyl, cylindrical correction; OD, right eye; OS, left eye; sph, spherical correcton.

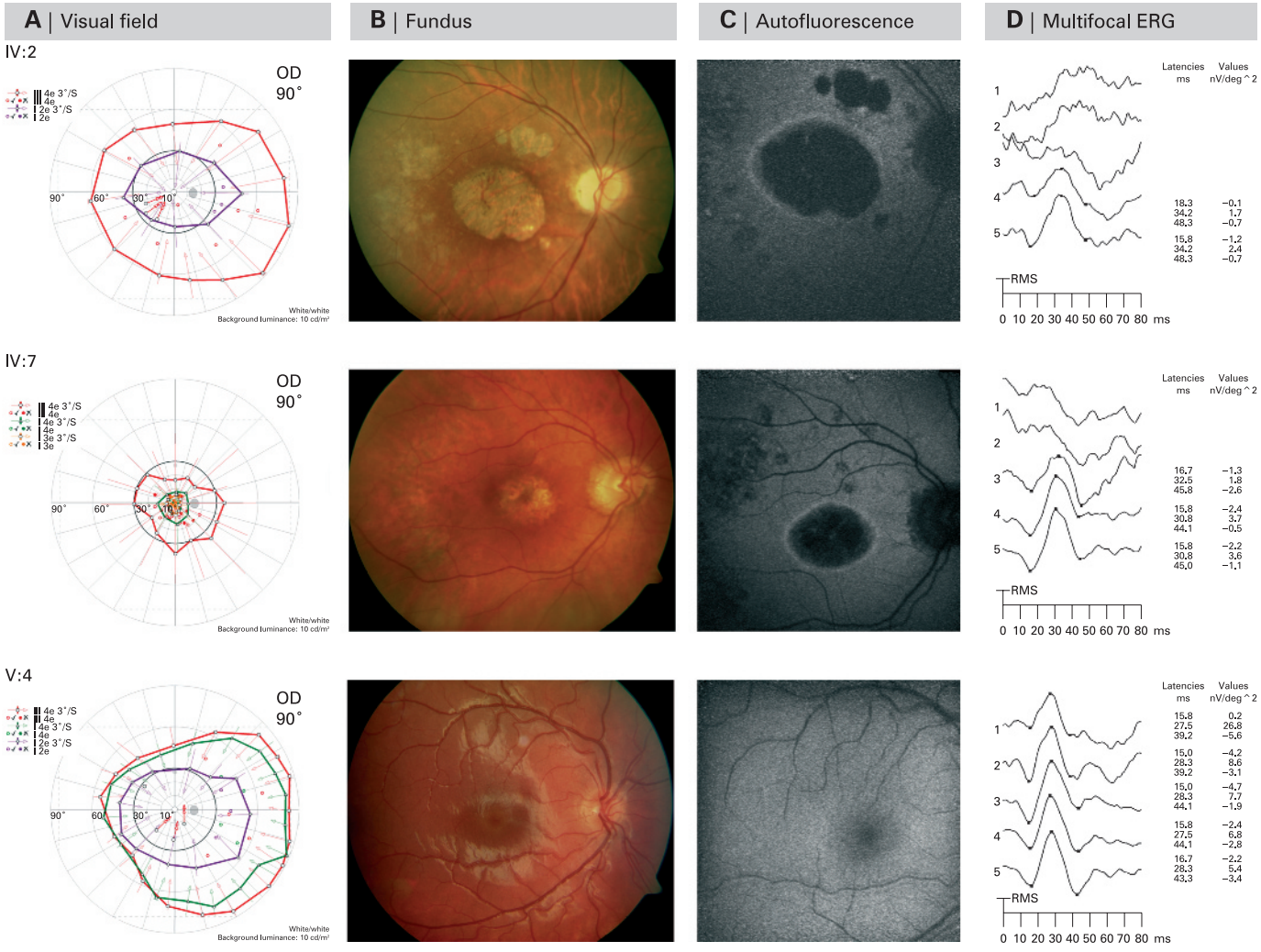

Figure 2 Examples of morphological changes and functional deficits found in three representative patients of two generations. At the age of 45 years, IV:2 had severely reduced visual acuity (0.1/0.1) and severe colour vision defects in the Panel D-15 saturated test. While static perimetry revealed a central scotoma, kinetic perimetry showed normal peripheral fields (A). Patchy atrophy of central RPE was seen in ophthalmoscopy (B) corresponding to the central hypofluorescent areas surrounded by a hyper-fluorescent rim in fundus autofluorescence (FA) (C). Multifocal electroretinogram (mfERG) in IV:2 shows central responses not discernible from noise and preserved peripheral responses with reduced amplitude and prolonged implicit time (D). Her cousin IV:7 also had reduced visual acuity (0.3/0.3), a colour vision disorder, but additionally he suffers from night blindness. Fundus appearance, FA and mfERG are similar in both cousins, but IV:7 had a largely restricted visual field. His son V:4 has normal visual acuity, colour and night vision, a normal fundus and FA appearance, unremarkable visual fields and mfERG (A–D) but a negative electroretinogram (ERG) response in fullfield ERG (see fig 3). Patient consent has been obtained for publication of this figure. OD, right eye.

DOI:10.14753/SE.2014.1976

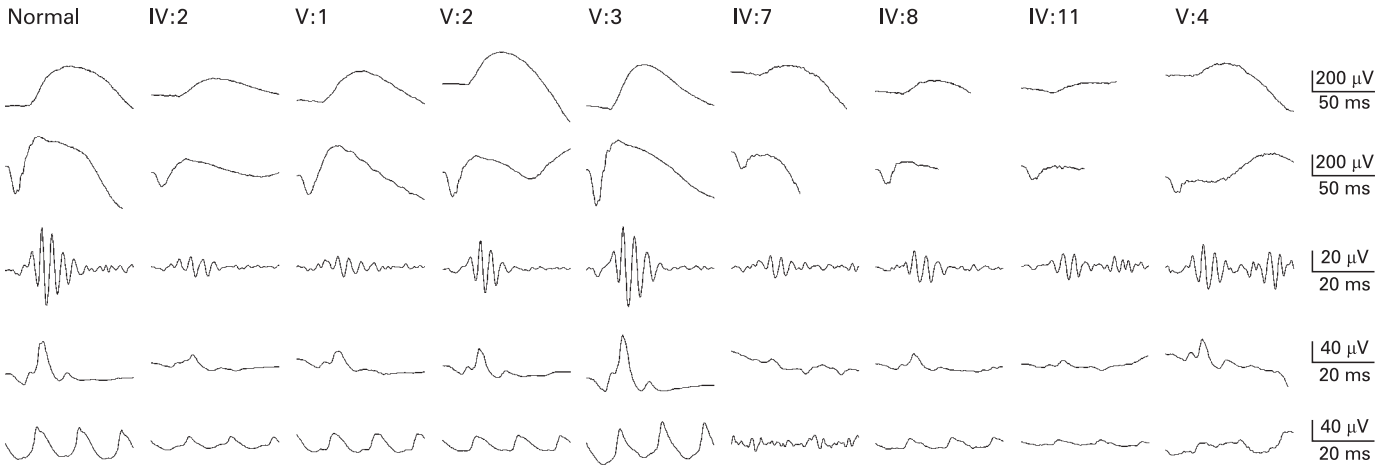

Figure 3 Fullfield ERG according to the ISCEV standard obtained in eight members of the family. From top to bottom, we present rod and maximum responses, oscillatory potentials, cone and flicker responses. Surprisingly, all affected members of the family branch B (IV:7, IV:8, IV:11, V:4) show a negative maximum response waveform, while members of branch A (IV:2, V:1) do not.

by means of a model fit of a Naka–Rushton function (fig 4A). The estimated maximum amplitude (V_{max}) again showed a marked difference between family branch A and B. While V_{max} for all members of branch A was well within normal limits, it was clearly reduced for members of branch B (fig S1). Interestingly, the estimates of n (corresponding to the slope) and the semisaturation intensity K were within normal limits for all patients of both branches.

For the oscillatory potentials and the cone ERG (fig S2), no marked differences were found between the two branches. Apparently, there is an additional functional deficiency in family branch B that affects mainly peripheral retinal function. Cone function in the mid periphery is best characterised by the mfERG responses of ring 5. Interestingly, while, in all patients, the response amplitude was reduced, the implicit time was prolonged, ca. 3 ms for patient IV:2 and less prolonged for V:1 and IV:11. For all others, the implicit time was normal. Taken together, this indicates a disease of the whole posterior pole in family branch B.

Estimates of the cone and rod dark adaptation thresholds after 25 min are provided in table 1. These thresholds are consistent with the visual field findings. While patients from family branch A showed normal rod thresholds, elevated thresholds especially for the rod system were found in all affected members of branch B except patient V:4.

Mutation screening and segregation analysis

Since *CRX* gene mutations have been described in CRD patients with the phenotypic features of intrafamilial variability and a negative ERG,[6–9] we screened the complete coding and flanking intronic sequence of the *CRX* gene in patient IV:7 by direct DNA sequencing. Thus, we identified a hitherto unknown mutation in exon 4 of the *CRX* gene in a heterozygote state (fig S3). The deletion of cytosin at cDNA position 636 (c.636delC) causes a translational frameshift, introducing five out-of-frame amino acid residues followed by a premature termination codon roughly after 2/3 of the normal polypeptide length. As a consequence, the truncated CRX protein lacks its transactivation domain (fig S4).

To verify the segregation of the mutation c.636delC with the disease phenotype, we analysed genomic DNA of all available family members by direct sequencing. Thereby, eight additional heterozygous mutation carriers in three different generations were identified (fig 1). In fact, all heterozygote mutation carriers were clinically affected (see section clinical features), whereas all healthy family members had wildtype *CRX* alleles.

We further identified the sequence variant c.100+12C>T in heterozygote state in patient IV:7, his two brothers and his son, whereas his mother, his nephew, his aunt, her daughter and granddaughter, were all homozygous for the c.100+12C allele (fig 1).

Apart from the mutation c.636delC in exon 4 and the intronic variant c.100+12C>T, no other sequence changes in the coding exons 2–4 of the *CRX* gene and the intronic or non-coding sequences covered by the sequence analysis were identified.

DISCUSSION

The purpose of this study was to identify the causative mutation in a family affected by autosomal dominant cone–rod dystrophy (adCRD), and to precisely describe their clinical features. A negative ERG, which was present in some members of the family and which has been previously described in patients with adCRD due to mutations in the *cone–rod homeobox* gene (*CRX*),[6–9] prompted us to analyse the *CRX* gene. We identified a disease causing 1 bp deletion, c.636delC, that segregated with the disease phenotype in this family.

The transcription factor CRX is important for transactivation of many retina-specific expressed genes, including rhodopsin and recoverin. It is expressed in rod and cone photoreceptors, and cells of the inner nuclear layer[13–15] from 10.5 weeks after conception[15] and maintained throughout life.[13–15] The transactivation domain of CRX has been localised to the C-terminus of the protein.[16–18] Furthermore, CRX has been proposed to form the centre of an interaction network of synergistically working common and retina-specific transcription factors[19 20] which comprises among others the retina-specific transcription factors Nrl and Nr2E3[19 20] and the transcriptional co-activators and histone acetyl transferases p300/CBP.[16] CRX and Nrl interact with each other via their respective DNA binding domains,[20] whereas interaction between CRX and p300/CBP is mediated via their respective C-termini.

Taken together, there are several conclusive reasons which argue in favour of the pathogenicity of the novel 1 bp deletion in the *CRX* gene, c.636delC, present in this family. First, the mutation perfectly segregates with the disease phenotype. All affected family members carry the mutation, whereas all

OPEN ACCESS Freely available online

DOI:10.14753/SE.2014.1976

Rod and Cone Function in Patients with KCNV2 Retinopathy

Ditta Zobor[1]*, Susanne Kohl[2], Bernd Wissinger[2], Eberhart Zrenner[1], Herbert Jägle[1,3]

1 Institute for Ophthalmic Research, University of Tübingen, Tübingen, Germany, **2** Molecular Genetics Laboratory, Institute for Ophthalmic Research, University of Tübingen, Tübingen, Germany, **3** Department of Ophthalmology, University of Regensburg, Regensburg, Germany

Abstract

Background: To investigate rod and cone function and disease mechanisms in patients with KCNV2 retinopathy.

Methodology/Principal Findings: Psychophysical examinations as well as detailed electrophysiological examinations with Ganzfeld and multifocal electroretinogram (ERG) were performed to study response dynamics. Additionally, fundus photography, autofluorescence imaging and spectral domain OCTs were carried out for morphological characterization. Molecular genetic analysis revealed compound heterozygosity in five patients and homozygosity for the *KCNV2* gene in one patient. The mutations resulted in complete absence of Kv8.2 subunits in three patients (no protein group, NOP), while the other three patients expressed mutant Kv8.2 subunits resulting in altered Kv2.1/Kv8.2 heteromeric or residual Kv2.1 homomeric potassium channel function (altered protein group, ALP). Although more advanced morphological changes were visible in the NOP group, a clear functional difference between the two groups could not be observed. All patients showed characteristic dynamics of the b-wave intensity-response function, however, scotopic b-wave response amplitudes were within normal limits. We also observed severely reduced oscillatory potentials.

Conclusions/Significance: A specific genotype-phenotype correlation in retinal function could not be demonstrated. *KCNV2* mutations cause a unique form of retinal disorder illustrating the importance of K^+-channels for the resting potential, activation and deactivation of photoreceptors, while phototransduction remains unchanged. The reduced oscillatory potentials further suggest an altered function of the inner retina. Besides the characteristically steep amplitude-versus-intensity relationship, flicker responses at intermediate frequencies (5–15 Hz) are significantly reduced and shifted in phase.

Citation: Zobor D, Kohl S, Wissinger B, Zrenner E, Jägle H (2012) Rod and Cone Function in Patients with KCNV2 Retinopathy. PLoS ONE 7(10): e46762. doi:10.1371/journal.pone.0046762

Editor: Anneke I. den Hollander, Radboud University Nijmegen Medical Centre, The Netherlands

Received April 24, 2012; **Accepted** September 10, 2012; **Published** October 15, 2012

Funding: This study was supported in part by the German Research Foundation, Pro Retina Society and the Kerstan & Tistou Foundation. The funders had no role in study design, data collection and analysis, decision to publish, or preparation of the manuscript.

Competing Interests: The authors have declared that no competing interests exist.

* E-mail: ditta.zobor@med.uni-tuebingen.de

Introduction

In 1983 Gouras et al. [1] reported an unusual type of retinal dystrophy, which was associated with characteristic alterations in the rod electroretinogram (ERG). This rare, autosomal recessive condition has been reported in several further studies [2,3,4,5,6,7,8,9] and was named "cone dystrophy with supernormal rod responses (CDSRR)". CDSRR is characterized by an early markedly reduced central visual acuity with central scotoma, photophobia, severe color disturbances, and occasionally nystagmus. In contrast to other cone dystrophies, a disease-typical alteration of the rod system could be observed: while rod sensitivity to weak flashes was reduced, an augmented responsiveness to higher levels of flash stimuli could be detected, and implicit times were considerably prolonged [1,2,3,4,5,6,7,8,9]. These characteristics were unique for CDSRR, however, the underlying disease mechanism could not be elucidated at that time.

In 2006 Wu et al [10] successfully linked the disorder to chromosome 9p24 and the *KCNV2* gene, which is predominantly expressed in retinal rod and cone photoreceptors [11]. It encodes a member of voltage gated potassium channels (Kv channels), representing a silent subunit (Kv8.2) that is able to assemble with Kv2.1 to form functional heteromeric channels. This results in a shift in the steady-state activation curve of the Kv2.1 channel towards more negative potentials due to a permanent outward K^+ current, a lower threshold potential for activation, a shortened activation time and slower inactivation kinetics [11,12,13]. A mutation in *KCNV2* may thus alter important characteristics of the I_{kx} current that influences the photoreceptor membrane potential. However, the dysfunction and mechanisms that link *KCNV2* mutations with the clinical picture still remain to be elucidated.

Over 50 different mutations in *KCNV2* have been reported so far, mainly small indel mutations or point mutations that constitute protein truncation mutations and amino acid substitutions [10,14,15,16]. Recently, several large deletions within or of the *KCNV2* gene of up to 237 kb in size have been described [16]. Although the genetically detected patients did show altered rod responsiveness, the term "supernormal rod response" was in many cases deceptive, as previously shown [17]. The term "supernormal rod ERG" is a misnomer and most recently, the disorder has been referred to as "KCNV2 retinopathy" [18].

This study employs detailed psychophysical and electrophysiological testing as well as spectral domain optical coherence

DOI:10.14753/SE.2014.1976

tomography (OCT) and fundus autofluorescence (FAF) to reveal novel insights into disease-specific functional changes in KCNV2 retinopathy. Additionally, we explore differences of disease specific functional aspects in the phenotype that correlate with the underlying *KCNV2* gene alterations. The genotype of three patients has already been published elsewhere [19], the remaining three patients' genetic findings are presented here for the first time.

Methods

Patients

Six otherwise healthy patients of German origin (3 female and 3 male; 2 simplex cases and 2 sibling pairs; mean age: 39 years, range 28–60 years) with previously diagnosed stationary retinal disorder and known mutations in the *KCNV2* gene were examined.

All examinations were carried out after written informed consent and in accordance with the Declaration of Helsinki. The study was approved by the Ethics Committee of the Medical Faculty of University of Tübingen.

Molecular Genetics

Genomic DNA was extracted from venous EDTA-blood samples according to standard procedures. Genetic testing for point mutations was performed by PCR amplification and subsequent Sanger sequencing of both coding exons and flanking intronic sequences of the *KCNV2* gene, as described previously [16].

Analysis for genomic deletion was investigated by quantitative copy number analyses of the *KCNV2* gene, with realtime PCR employing TaqMan technology or SYBR Green detection assays, as reported earlier [16].

Comparative genome hybridizations (CGH) using a prede-signed chromosome 9 specific 385k oligonucleotide array (HG18 CHR9 FT; Roche NimbleGen Inc., Madison, WI) was performed for subject CHRO8.I who had suspected deletions at the *KCNV2* locus (Roche NimbleGen).

The deletion junctions in patients CHRO8.I and RCD307 were determined by long distance PCR amplifications and subsequent Sanger sequencing to define the precise breakpoints.

Independent segregation of the mutations within the families were conducted by Sanger sequencing of PCR amplified genomic DNA for point mutations, and by qPCR in the two families segregating the *KCNV2* gene deletion.

Clinical Examination

A complete ophthalmological examination was performed including psychophysical tests (Snellen visual acuity, Lanthony Panel D-15 and Nagel anomaloscope color vision tests, visual field and dark adaptation) and an extended electrophysiological protocol (Ganzfeld and multifocal ERG).

Psychophysical testing

Kinetic 90° and static 30° visual field tests were carried out with an Octopus 900 perimeter (Haag-Streit International, Germany). Dark adaptation curves were measured with a dark adaptometer (Roland Consult GmbH, Brandenburg, Germany) after pupil dilation with Tropicamid. After 3 minutes of bleaching with bright white light (intensity 5.5 log photopic trolands), a staircase procedure was used to estimate detection thresholds over a period of 40 minutes. Thresholds were alternately measured for red (635 nm) and green (565 nm) circular targets, presented 20° nasal of the fovea. Cone and rod thresholds were then determined by a model fit using the equation:

$$I(t) = \begin{cases} B_1 + I_1 * \exp(R_1 * t) - I_2 * \exp(R_2 * t_k) + I_2 * \exp(R_2 * t) & t \geq t_k \\ B_1 + I_1 * \exp(R_1 * t) & t < t_k \end{cases}$$

with t_k describing the time to the rod-cone break and $I1$, $R1$ the exponential decay of the cone, $I2$, $R2$ of the rod thresholds. Cone and rod parameters are derived from red and green target functions respectively. For group analysis and for comparison to normals the model was fitted to the raw data of each group of subjects.

Electrophysiological testing

Ganzfeld and multifocal electroretinograms ERGs were recorded according to the standards of the International Society for Clinical Electrophysiology of Vision (ISCEV) [20,21]. All tests were performed using DTL electrodes with an Espion E^2 (Diagnosys LLC) recording device coupled with a ColorDome (Diagnosys LLC) as light source. After 30 minutes of dark adaptation a series of responses to increasing flash intensities (4 ms–0.0001 cd.s/m^2 to 10 cd.s/m^2 in 0.5 log unit steps) were recorded and the stimulus-response (S-R) functions modelled using the equation:

$$V(I) = V_{\max} * I_n / (I_n + K_n)$$

with the saturated b-wave amplitude V_{max}, the flash intensity K required for semi-saturation as a measure of retinal sensitivity and the slope related exponent n [22].

Rod response characteristics were estimated from the a-wave by the Hood and Birch (1994) formulation of the Lamb and Pugh model [23] of the biochemical processes involved in the activation of rod phototransduction. The a-wave ensemble was fitted with a computational model describing the response (P_{III}) as a function of time (t) and intensity (I):

$$P_{III}(I,t) = \left[1 - \exp\{-0.5 * I * S * (t - t_d)^2\}\right] * Rm_{P_{III}}$$

where Rm_{pIII} is the maximum amplitude, S is a sensitivity variable and t_d is a brief delay before the response onset.

P_{III} was then subtracted from the original ERG waveform to give the P_{II} response, which is thought to represent mainly the ON-bipolar cell response, but also the postreceptoral activity in other second- and third-order retinal neurons. The relation between flash intensity and the delay between stimulus onset and reaching a given arbitrary criterion voltage of the P_{II} component was then plotted on a log-log coordinate and the slope of this function was calculated. The voltage criterion chosen in this study was 50 μV.

Finally, dark-adapted responses to a series of blue flicker (LED 470 nm) with an intensity of 0.03 cd.s/m^2 and frequencies between 5 and 30 Hz were recorded to isolate temporal retinal characteristics of the rod system [24].

The light-adapted protocol (10 min of light adaptation to a background luminance of 30 cd/m^2) included a single flash cone stimulus and a 30 Hz flicker (both: 4 ms, 3.0 cd.s/m^2). In addition, responses to a series of flicker white stimuli of 3.0 cd.s/m^2 with increasing frequency from 5 to 45 Hz were included to investigate possible alterations in the temporal resolution of the cone retinal pathway.

Multifocal ERG (mfERG) was performed with a VERIS System (Version 5.1) using a Grass amplifier (model 12, Quincy, USA).

DOI:10.14753/SE.2014.1976

The stimulus, consisting of 61 scaled hexagonal elements covering a central visual field of 60×55°, was presented on a 19″ monitor at a frame rate of 75 Hz at a distance of 32 cm from the subject's eyes. The same DTL electrodes as those for the Ganzfeld recordings were used. Responses were amplified (200 000×), bandpass-filtered (10–100 Hz), and analysed according to ring averages.

Morphological testing

Color and infrared fundus photography, autofluorescence (FAF) and spectral domain OCT recordings (Heidelberg Engineering GmbH, Germany) were performed.

Results

Molecular Genetic Findings

Mutation screening and segregation analysis led to the identification of mutations in the *KCNV2* gene in our patients. The genotypes of the six patients are listed in **Table 1**. and the mutation localization is shown in **Figure 1**. We observed compound heterozygous mutations in the two sib pairs (CHRO8.I and CHRO8.II, and BD27.I and BD27.II): both patients from family CHRO8 carried two compound heterozygous nonsense mutations p.Cys113stop and p.Glu148stop, while both patients of family BD27 were compound heterozygous for a complete deletion of the *KCNV2* gene and a missense mutation p.Leu404Pro located in the linker between transmembrane domains S4 and S5. The simplex subject BCM5 harboured two compound heterozygous small deletions: c.8_11del and c.447_449del. The c.8_11del mutation created a frame-shift at the very beginning of the *KCNV2* polypeptide, resulting in a premature stop codon and a severely altered and truncated protein (p.Lys3ArgfsX95). The other deletion only resulted in the loss of a single phenylalanine at position 150 (p.Phe150del) within the NAB domain. The last patient RCD307 was homozygous for another large deletion spanning from exon 1 into the 3′UTR. All mutations, except for the missense mutation p.Leu404Pro and the single amino acid deletion p.Phe150del (see **Table 1**.), are expected to result in the complete loss of Kv8.2. Consequently the siblings BD27.I and BD27.II, and patient RCD307 most likely did not express any KV8.2 gene product, causing an altered subunit composition of the respective Kv-channel and an altered or lost potassium channel function. Previous clinical data have indicated that both the complete absence of Kv8.2 (where Kv2.1 was unaffected) and its altered forms result in CDSRR [10], which suggests that the special constellation of Kv2.1/Kv8.2 heteromeric channels are essential for functionality in the photoreceptor cells. To examine whether these genotype differences are also evident in the phenotype, we divided the six patients into two groups: group 1, NOP (no protein), included the three patients with a complete absence of Kv8.2, and group 2, ALP (altered protein) with three patients with mutant Kv8.2 subunits.

Clinical Findings

Clinical findings are summarized in **Table 1**. All patients reported an early onset of their visual symptoms without any progression or change over the years. Only the oldest patient (RCD307) reported a slight reduction of his visual acuity in the last three years. Marked photophobia and a prolonged light adaptation time were evident in every case. Only the oldest patient complained of nyctalopia, other subjects denied having difficulty with night vision. All patients were myopic with variable degrees of astigmatism; patients of the ALP group showed a slight tendency for higher myopia and astigmatism. Four of six patients had undergone strabological surgery in childhood and two of them had suffered additionally from infantile nystagmus.

Psychophysics

All subjects presented with reduced central visual acuity (mean VA (logMAR): 0.97±0.2 SD). There was a slight tendency to poorer VA in the NOP group (1.06±0.23 SD) compared the ALP group (0.88±0.13 SD). Color vision testing using the Lanthony D-15 Panel desaturated and saturated tests and with fixation with the preferred retinal locus (PRL) showed severe color confusions in all patients predominantly along the scotopic or red-green axis with relative sparing of the tritan axis. The Rayleigh anomaloscope matches, presented eccentrically at the PRL, were consistent with a rather rod dominated function in five of six patients. Only one patient's (RCD307) results suggested protanopia. Perimetric results showed nearly normal outer boundaries of the visual field in all cases. Static perimetry results revealed relative and absolute defects in the central 30° area, being more pronounced in the NOP than the ALP group.

To test cone and rod function loss we measured dark adaptation thresholds for red and green targets. (**Figure 2**). All patients showed significantly elevated thresholds for red and green stimuli, although the elevation was more pronounced in the NOP group with a final rod threshold of −1.9 log cd/m^2 and a cone threshold of 0.4 log cd/m^2 compared to −2.6 log cd/m^2 and −0.3 log cd/m^2 for the rod and cone threshold in the ALP group. Thresholds estimated for normals were −1.5 log cd/m^2 and −3.7 log cd/m^2 for red and green stimuli, respectively. For green stimuli the rod-cone break was normal (11.0 min for the NOP and ALP group, normal: 10.7 min) and for red stimuli the rod-cone break tended to appear earlier (after 15.6 and 15.9 min for NOP and ALP respectively, normal: 16.9 min).

Electrophysiology

Basic clinical investigation included the Ganzfeld ERG according to the ISCEV standard, for which all patients showed the previously described characteristic responses (see **Figure 3** for typical results of a patient from the NOP and ALP group). Most interestingly, oscillatory potentials (OPs) were almost completely absent in the patients' ERG recordings. **Figure 4** shows for each subject the amplitudes and implicit times of the a- and b-waves for the scotopic response series recordings. Typical low or undetectable response amplitudes to weak flashes were evident, with markedly delayed implicit times of the a- and b-wave component. There was also an abrupt increase in amplitude with increasing flash intensity accompanied by a normalization of b-wave implicit times. While mean saturation amplitudes V_{max} of the b-wave model fit were similar for both groups and normals (526 μV for normals, 528 and 493 μV for the NOP and ALP groups, respectively) the intensity K at semi-saturation was significantly shifted to higher intensities (−2.5, −1.7 and −1.7 log cd.s/m^2 for normals, NOP and ALP, respectively). Additionally, the peak a-wave amplitude was normal within the entire stimulus intensity range, but the peak implicit times were prolonged for each stimulus step.

In this study the rod a-wave showed three interesting features (**Figure 5**.): First, in some patients the a-wave of the response to the highest intensity stimulus (4.7 log td*s) was smaller than that to the 4.2 log td*s stimulus. This is depicted for one subject in **Figure 5A**. While R^2 of the fits in normal subjects was above 0.02 in only two eyes, it was higher in seven of the patient eyes (**Figure 5B**). The difference in goodness of the fit is seen in the normal subject in **Figure 5C** and in the representative patient BCM5 in **Figure 5D**.

DOI:10.14753/SE.2014.1976

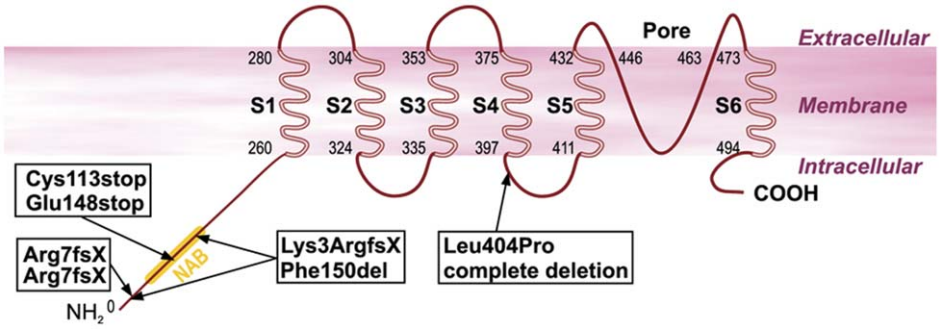

Figure 1. Structure of the Kv8.2 potassium channel and mutation sites detected in our patients. The mutation pairs in each box represent the genetic findings of each patient. The genetic findings of the two sibling pairs are shown once, since the siblings share the same mutation constellation.
doi:10.1371/journal.pone.0046762.g001

Second, the latency of the negative deflection from baseline appeared with normal delay (average of 4.1±0.92 ms and 4.3±0.35 ms for patients and normals respectively).

And third, while the maximum response amplitude Rm_{PIII} estimated from the model fit was not different from that of normals (on average 241±71 μV and 270±83 μV for patients and normals respectively), the sensitivity parameter S was significantly lower in patients (0.73±0.38 SD) than in normals (1.14±0.36 SD).

P_{II} responses were calculated by removal of the fitted P_{III} (**Figure 6**.). The latency at which P_{II} reaches 50 μV is plotted as a function of stimulus intensity on log-log coordinates in **Figure 6C**. In the normal retina we found a slope of −0.18±0.014 SD. In patients with *KCNV2* mutations the mean slopes of regression lines were not significantly different from each other or from the normal mean slope (−0.24±0.065 SD and −0.20±0.038 SD for the NOP and ALP group, respectively), however, a similar and clear shift either representing a response delay or a horizontal shift to higher intensities of approx. 1 log unit was observed in both groups. Latter was consistent with the psychophysically (dark adaptation) estimated rod threshold elevation of approx. 1 log unit.

We additionally recorded responses to various flicker frequencies under scotopic conditions (**Figure 7**). Magnitude (**Figure 7A**) and phase (**Figure 7B**) of the responses to increasing flicker frequencies are demonstrated. The individual data under scotopic conditions showed reduced magnitudes and a phase difference, which was independent from flicker frequency thus suggesting either a rather small constant prolongation of rod photoreceptor recovery or may result from the sensitivity reduction to the flash strength.

Cone responses recorded under photopic conditions showed a marked suppression of response amplitudes, which remained diminished even at the higher flash intensities (**Figure 8**.). Additionally, the amplitudes did not show a photopic hill phenomenon. Implicit times were markedly prolonged for each stimulus step. The photopic negative responses (PhNR) were almost undetectable in patients with *KCNV2* mutations, as depicted in **Figure 9**.

As found for scotopic conditions, the photopic responses to stimuli of increasing frequency (**Figure 10**.) showed a similar dependency but also lower amplitudes and a shift in phase. Interestingly, even at the highest frequency of 45 Hz the response waveform was still significant with an almost normal phase.

Finally, multifocal ERGs showed reduced amplitudes and delayed implicit times in every ring (**Figure 11**.) being more distinct in the central 2 rings. In the outer rings more preserved responses could be obtained. The dysfunction was more sharply limited to the central two rings in the NOP group, which was not observed that clearly in the ALP group. This could be related to the slightly better VA of the ALP group.

Morphology

Fundus photographs, FAF images and OCT scans for each subject can be seen in **Figure 12**. There was a range of macular appearances including discrete disturbances of the retinal pigment epithelium (RPE) and bull's eye maculopathy. Patients with a complete absence of Kv8.2 (NOP group) showed more pronounced changes in the macular area, the mean central retinal thickness was 103.5 μm for the NOP, and 135.1 μm for the ALP group, respectively. In FAF imaging mild RPE-alterations were present as small areas with decreased autofluorescence. In contrast, marked RPE-atrophies were seen as sharply demarcated areas of absent autofluorescence surrounded by a ring of increased signal. The oldest patient (RCD307) revealed additional RPE-defects of the posterior pole and epiretinal gliosis. The OCT images also demonstrated the variety of morphological findings. In the milder cases –mainly in the ALP group- OCT revealed a thinner photoreceptor layer (PRL) in the foveal area, there was no disruption in the inner segment/outer segment (IS/OS) border. In the more severe cases (NOP group) the PRL was missing, the IS/OS border was diminished and an increased backscatter from the choroid was observed due to RPE-atrophy. In one case additional granular echoes were present due to deposits on the fundus of patient BD27.I. Based on the SD-OCT volume scans detected from the central 30°×15° retinal area the peripheral outer retinal structure was well preserved in every patient.

Discussion

This study describes the genotype and phenotype of six patients with a retinal dystrophy due to changes in the *KCNV2* gene. In three patients the mutations resulted in a complete absence of Kv8.2 encoded by the *KCNV2* gene (NOP group). In the other three patients heterozygous mutations of the first allele resulted in a lack of protein product, mutations of the second allele led to mutant subunits with presumably remaining pore function (ALP group).

On the morphological level, macular pathology varied from mild RPE disturbances to large atrophic areas, while the periphery was normal in every case. These findings are consistent with the results described by Robson et al. and Sergouniotis et al. [18], It is interesting to see that the changes are strictly limited to the central macular area in every case, while the specific functional changes of this retinal disorder affect rod-rich mid periphery as well. The

Table 1. Clinical and genetic findings of the six patients.

Patient ID	Gender	Age	VA (RE/LE)	Refraction	Night blindness	Color vision	Nystagmus	Strabismus	Alteration nucleotide sequence	Alteration polypeptide	Allele status
BD27.I	M	36	0.125	−2.0/−1.0×145°	no	achromat	no	no	c.339C>A	p.Cys113X	heterozygous
			0.1	−1.0					c.442G>T	p.Glu148X	
BD27.II	F	40	0.04	−3.5/−2.25×174°	no	achromat	yes	yes	c.339C>A	p.Cys113X	heterozygous
			0.05	n.A.					c.442G>T	p.Glu148X	
RCD307*	M	60	0.16	−3.5/−1.25×0°	yes	protanomalous	no	no	c.19_1356+9571 delinsCATTTG	Arg7fs	homozygous
			0.1	−1.0/−1.0×0°							
CHRO8.I*	M	37	0.1	−8.75/−2.0×18°	no	achromat	yes	yes	g.2657638_2737340del	Deletion	heterozygous
			0.1	−8.25/−2.0×141°					c.1211T>C	p.Leu404Pro	
CHRO8.II*	F	35	0.1	−4.5/−4.0×0°	no	achromat	no	yes	g.2657638_2737340del	Deletion	heterozygous
			0.2	−3.5/−4.0×0°					c.1211T>C	p.Leu404Pro	
BCM5	M	28	0.16	−5.0/−1.5×2°	no	achromat	no	yes	c.8_11del4	p.Lys3ArgfsX29	heterozygous
			0.16	−3.5/−1.0×6°					c.447_449del3	p.Phe150del	

The upper three patients show a complete absence of Kv8.2 due to large deletions or protein truncating mutations of *KCNV2* and so represent the NOP group. The lower three patients represent the ALP group with altered Kv8.2 subunits due to *KCNV2* mutations. The BD27.I and BD27.II are brother and sister of one family, so are CHRO8.I and CHRO.II of another family. Each case shows an autosomal recessive inheritance. A considerable difference between the NOP and ALP group cannot be observed. However, there is a tendency for a slightly better visual acuity (VA) and higher myopia in the ALP group (lower three patients). Interestingly, night blindness, subjective disease progression and a severe protanomaly are present in the only homozygous patient (RCD307), while other patients reveal unchanged visual function over disease duration, no night blindness and color disturbances consistent with a rod dominated function. (Patients marked with * have been published in Wissinger et al. [19]).

doi:10.1371/journal.pone.0046762.t001

DOI:10.14753/SE.2014.1976

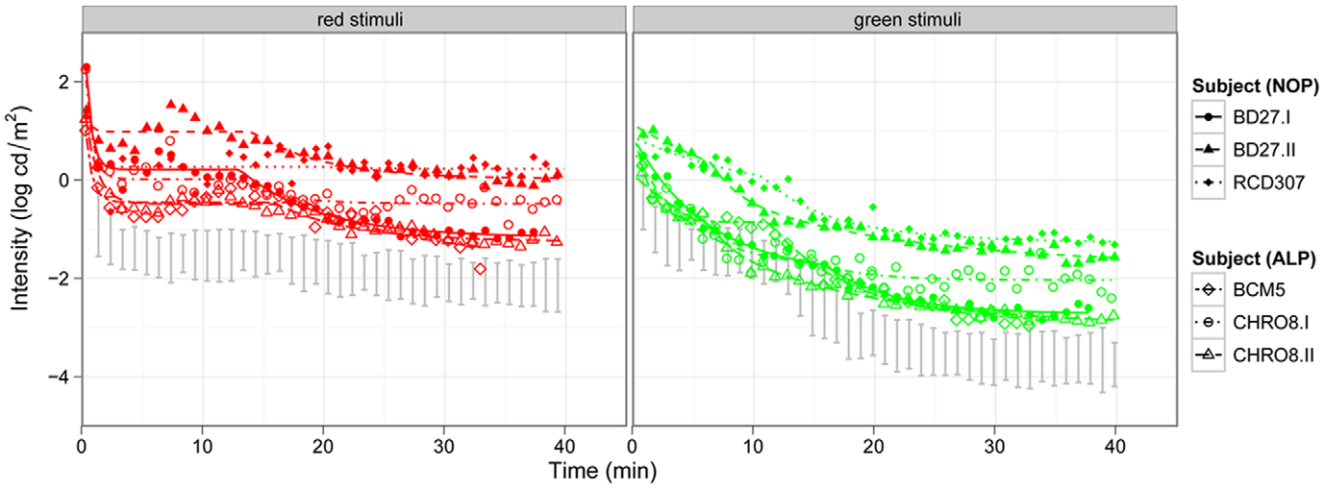

Figure 2. Dark adaptation curves of the patients of both groups compared to normal subjects. The left panel shows the cone (red stimuli), the right panel the rod function (green stimuli) of the NOP and ALP groups (the 95% confidence band of normal subjects is marked with grey). The threshold elevation for both target colors is biggest for two patients of the NOP group.
doi:10.1371/journal.pone.0046762.g002

question of why cones degenerate and rods keep at least their morphological integrity still remains to be unraveled, but the distribution of Müller cells in the retina (i.e. absence in the fovea) could be one important factor, since their regulatory and buffering effect on the extracellular K^+ is missing in the cone-rich area, making cones more vulnerable.

Although there was a tendency for a more pronounced macular lesion (seen in the OCT and FAF imaging), higher myopia and more elevated dark adaptation thresholds in the NOP group, no clear-cut line can be drawn between the two groups. Interestingly, the only homozygous patient (RCD307) seemed to differ in a few aspects from the heterozygous patients: night blindness, protanomaly and reported progression were present only in his case. There was no family history of color disturbances in this subject and the further genetic analysis of the L-M pigment genes showed an intact OPN1MW/OPN1LW gene cluster [25,26], indicating a severe protanomaly rather than protanopia. Furthermore, his morphological results revealed more distinct changes of the fovea resembling a macular hole on the left eye. However, the additional RPE-defects of the posterior pole, the macular hole formation and the accompanying epiretinal gliosis could be due to age related changes, explaining the decreasing visual acuity observed by the

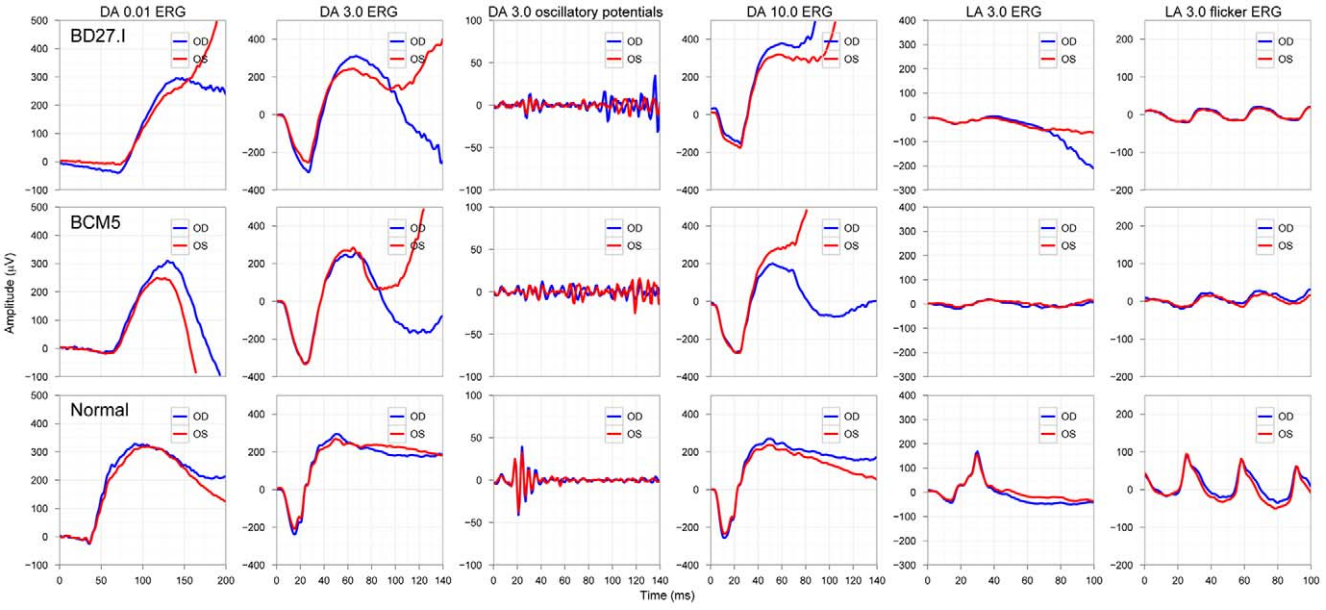

Figure 3. ISCEV standard Ganzfeld ERG responses of a representative patient of each group compared to a normal subject. Patient BD27.I in the upper panels represents the NOP group, while the result of patient BCM5 in the middle panels is an example for the ALP group. The normal subject is represented in the bottom panels. The patients' findings show the characteristic features of the scotopic ERG (dark-adapted (DA)) and the small photopic responses (light adapted (LA). Notice the missing oscillatory potentials on the rising b-wave in patients. (Color coding in each panel: red curves show results of the right eye (OD), blue curves show results of the left eye (OS)).
doi:10.1371/journal.pone.0046762.g003

DOI:10.14753/SE.2014.1976

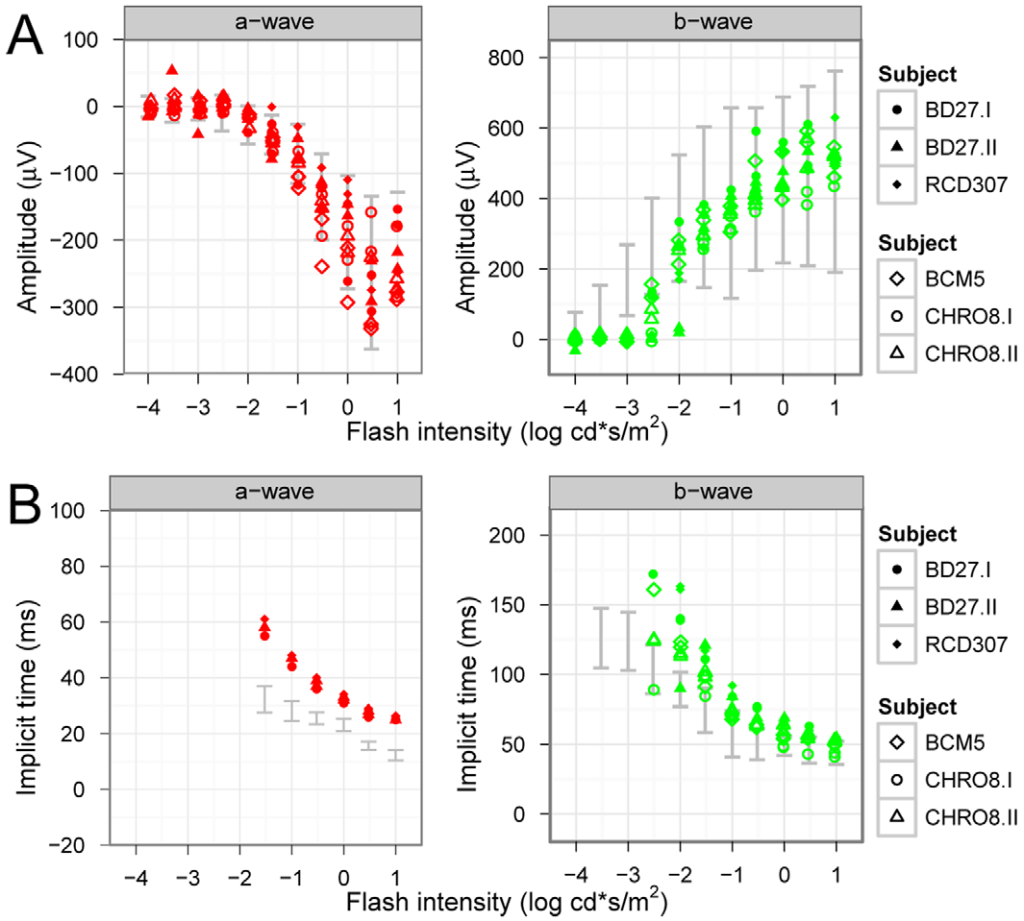

Figure 4. Intensity-response function kinetics under scotopic conditions. The single flash response a- and b-wave amplitudes (A) and implicit times (B) to increasing stimulus intensities are presented for both groups (upper subjects: NOP group, lower subjects: ALP group; the 95% confidence band of normal subjects is marked with grey). While the a-wave amplitude slowly and continuously increases, the b-wave amplitude stays low until the flash intensity reaches −2.5 log cd*s/m^2. While peak implicit times of the a-wave responses are prolonged for all flash intensities, the implicit times of the b-wave approaches the normal range with increasing flash intensity.
doi:10.1371/journal.pone.0046762.g004

60-year-old patient. However, the investigated cohort is small, further large studies are necessary to better highlight the correlations between genotype and phenotype.

Several studies exist on the electrophysiological characteristics of KCNV2 retinopathy. [1,4,6,17,27]. Nevertheless, there are still several aspects of this special retinal disorder, for which an explanation is needed

The lack of Kv8.2 or the presence of mutant subunits eliminates the functional characteristics of Kv2.1/Kv8.2 heteromers leading to a retinal disorder. Only the intact heteromers have the essential specifics to function as a high-pass amplifier and so regulate photoreceptor responses to light flashes. Kv2.1 can form homomeric channels, but without the intact Kv8.2 subunits they activate more slowly and inactivate faster, whereas the voltage dependence of the steady-state inactivation remains unchanged [11,12].

The absence of intact Kv8.2 subunits therefore leads to a positive shift of the steady-state membrane potential, decreasing the dark current and elevating intracellular K^+ level. Kv2.1 channels alone do not produce a permanent outward K^+ current, which also affects the K^+ homeostasis of the photoreceptors. While restoring the integrity of the K^+ levels, secondary mechanisms can also lead to a small drop of intracellular Ca^{2+} levels, probably due to altered/enhanced function of the $Na^+/Ca2^+$-K^+ exchanger. The small drop of cytoplasmic Ca^{2+}, however, can result in increasing cGMP levels due to disinhibiting the activated guanylate-cyclase and finally increases the number of open cyclic nucleotide-gated channels. This shift to a more depolarized state in the dark may also have consequences for recovery: for very brief light flashes the membrane potential may remain below the critical limit of −50 mV before the hyperpolarization-activated cyclic nucleotide-gated channels (HCN channels) become activated [28], thus leading to a prolonged hyperpolarization phase. These mechanisms are well reflected in the electrophysiological findings observed in patients with KCNV2 retinopathy [4,6,17]. The responses are characteristically undetectable or markedly reduced with delayed implicit times for dimmer stimuli and there is an abrupt rise in amplitudes and shortening of implicit time with increasing stimulus intensity. The intensity K at semi-saturation is significantly shifted to higher intensities, the estimated difference in our cohort is around 1 log cd.s/m^2. This shift correlates with the threshold elevation during dark adaptometry (for rod thresholds approximately 1 log unit elevation). However, most of our patients do not suffer from nyctalopia, confirming other reports of this inconsistency between subjective and objective light sensation [4,23].

DOI:10.14753/SE.2014.1976

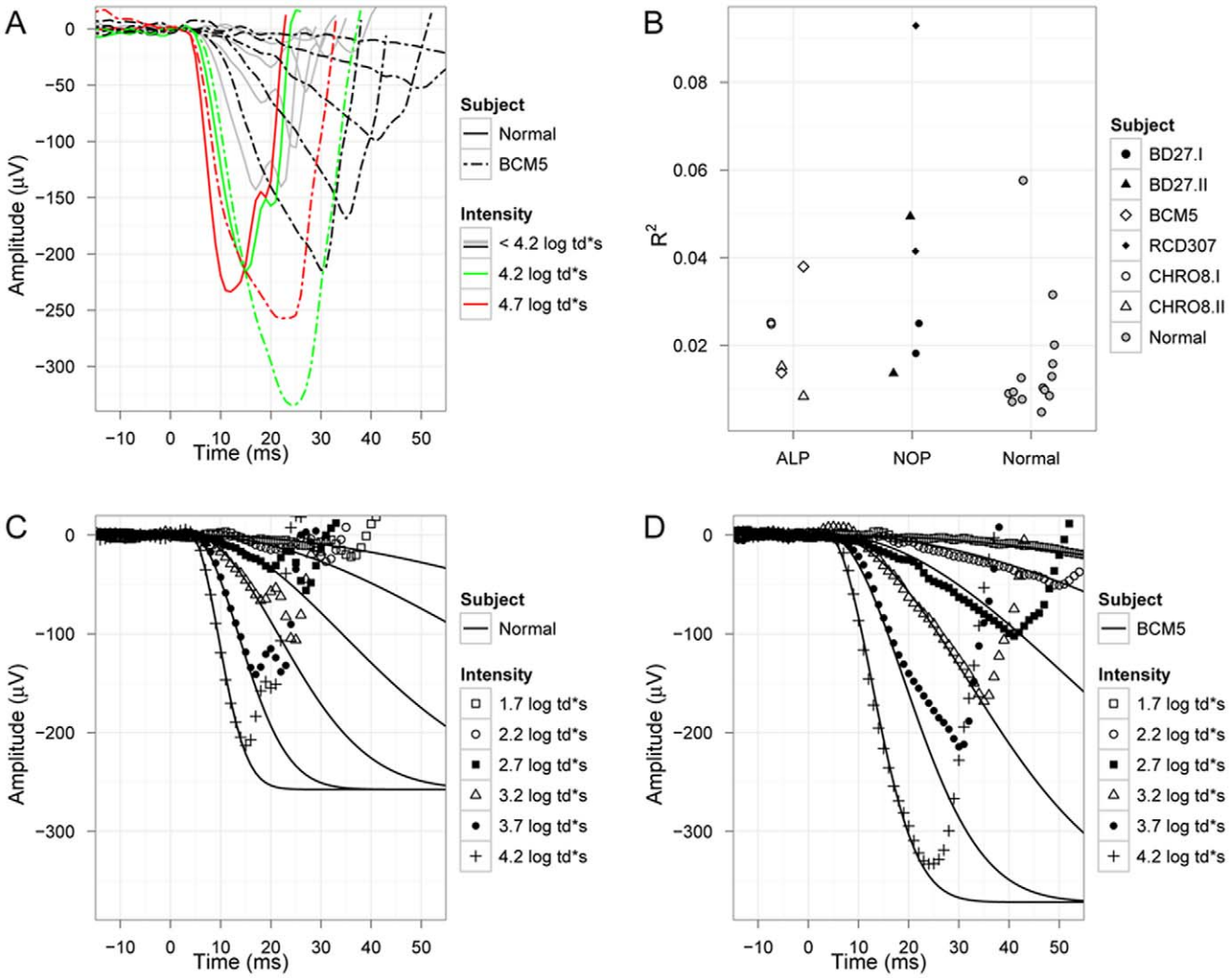

Figure 5. Analysis of the scotopic a-wave (P_{III} response). (A) Scotopic response a-waves to increasing flash intensities show continuous increasing response amplitudes in the normal subject (full lines). The patient's responses (chain lines) also show continuous increasing amplitudes up to a flash intensity of 4.2 log td*s (green color coding), but a lower response amplitude to the flash with highest intensity (red color coding). Therefore responses to highest flash intensity were excluded from a-wave analysis. Interestingly, while R^2 of the fits in normal subjects was above 0.02 in 2 eyes only, it was higher in 7 of the patient eyes (B). The difference in goodness of the fit is seen in the normal subject (C) and in the representative patient BCM5 (D).
doi:10.1371/journal.pone.0046762.g005

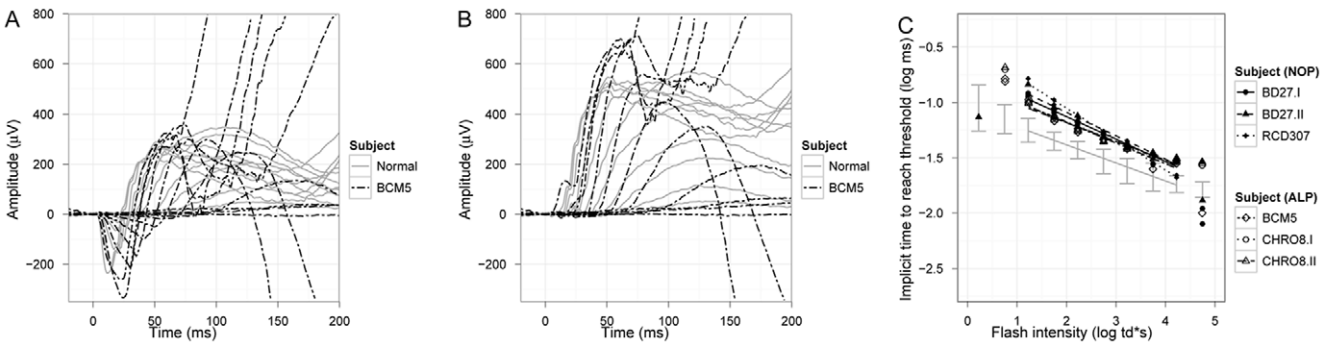

Figure 6. Analysis of the P_{II} response. Overlaid representative scotopic waveforms of a normal subject (grey lines) and patient BCM5 (chain lines) and the extracted P_{II} components (B) are presented. The delay in implicit times to reach a threshold amplitude of 50 μV at each intensity level is plotted in a log-log diagram both for the NOP group and ALP group (C).
doi:10.1371/journal.pone.0046762.g006

DOI:10.14753/SE.2014.1976

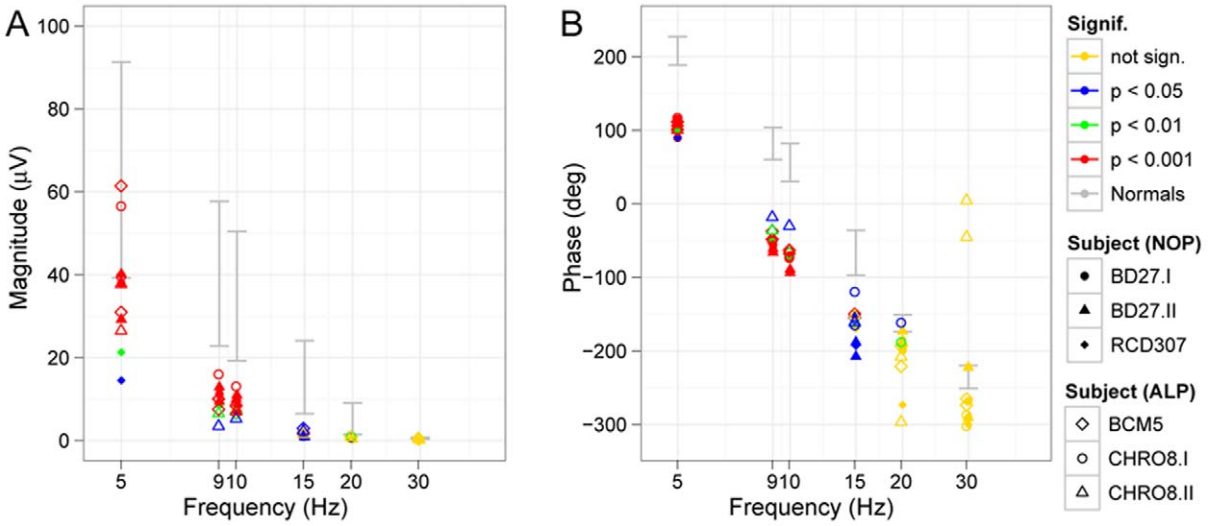

Figure 7. Scotopic flicker series. Magnitude (A) and phase (B) of scotopic flicker responses to stimuli of increasing flicker frequency are presented. Significance levels are color-coded in each figure, the 95% confidence band of normal subjects are marked with grey. The amplitudes of the patients are below normal and not significant for stimuli faster than 15 Hz. The phase shift, however, seems to be independent from flicker frequency.
doi:10.1371/journal.pone.0046762.g007

Our results are in accordance with previous reports and also confirm that "supernormal rod responses" in the ERG - believed to be characteristic for this rare condition - often seem to be missing, as responses, even to high intensity flashes, stay within normal limits in many cases [16,17]. The dynamics of the b-wave intensity-response function is a more constant feature.

In addition, our detailed electrophysiological data show other specific features. The initial phase or leading edge of scotopic response waveforms reflects the activity of photoreceptor cells and arises from light-evoked closure of Na^+ channels along the plasma membrane of the outer segments. Based on the model fits to our electrophysiological data we conclude that phototransduction activation in this retinal dystrophy is normal, since the onset of the deflection from baseline appears with normal delay. While the maximum amplitude Rm_{PIII} was within normal limits, the sensitivity parameter S was significantly lower. Similar results were reported for the patient described by Tanimoto et al. [29]. On the contrary, Hood et al. [4] found essentially normal sensitivity S and a slightly lower Rm_{PIII}, the maximum amplitude, for the rods. However, our patients were included in the study based on confirmed alterations of *KCNV2*, while patients in the study of Hood et al. were chosen on a clinical-electrophysiological basis (i.e. retinal dystrophy with supernormal rod responses). While higher Rm_{PIII} might be explained by an overshoot due to delayed HCN channel activation, lower sensitivity may be related to higher cation channel sensitivity to cGMP due to lower Ca^{2+} levels.

There is also a delayed postreceptoral response, which seems independent from flicker frequency. The delay of the emerging b-wave may have two different origins. Firstly, voltage dependent transmitter release may be delayed due to a small prolongation in reaching hyperpolarization. Secondly, a delayed HCN channel activation and depolarization of the photoreceptor might result in an overshoot of the response of the downstream neuron. Such overshoot would not be associated with changes in the G-protein activation cascade of the bipolar cell, which can be assessed with the P_{II} response analysis. In our *KCNV2* patients the kinetics of the ON-bipolar cell G-protein cascade seems to be normal, however, the cascade is activated with a clear delay. In the study of Robson

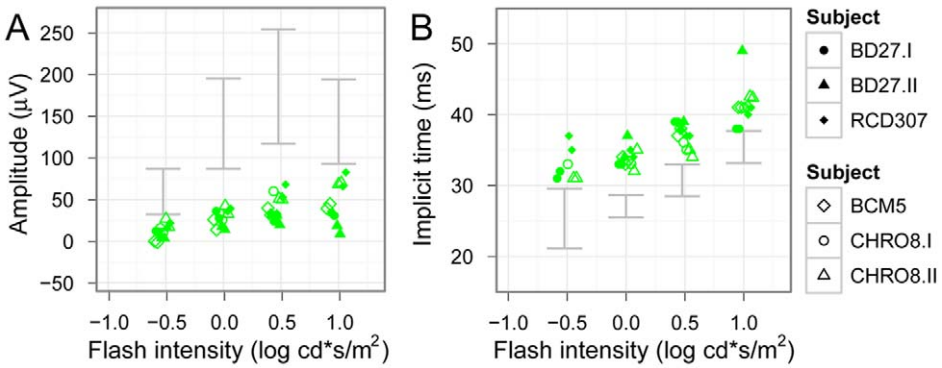

Figure 8. Intensity-response function kinetics under photopic conditions. Photopic response b-wave amplitudes are shown in (A) and implicit times in (B), the 95% confidence band of normal subjects is marked with grey. The photopic hill phenomenon can be observed in normals, however, this phenomenon seems to be missing in patients. Implicit times in both patient groups are moderately delayed (upper subjects: NOP group, lower subjects: ALP group).
doi:10.1371/journal.pone.0046762.g008

DOI:10.14753/SE.2014.1976

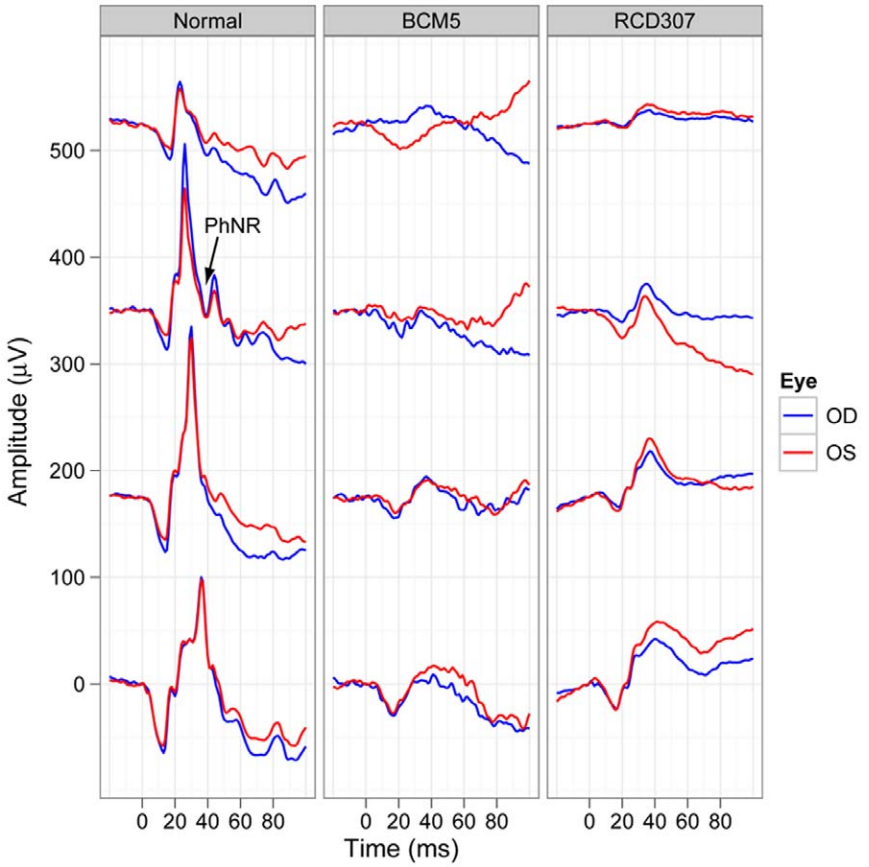

Figure 9. Photopic negative response (PhNR). Photopic single flash response waveforms illustrating the photopic negative response (PhNR) at increasing stimulus intensities (from top to the bottom in each panel) are shown in a normal subject (on the left) and the waveforms of two representative patients of the ALP (patient BCM5 in the middle) and NOP group (patient RCD307 on the right). Notice, that patients lack the PhNR in the given intensity range.
doi:10.1371/journal.pone.0046762.g009

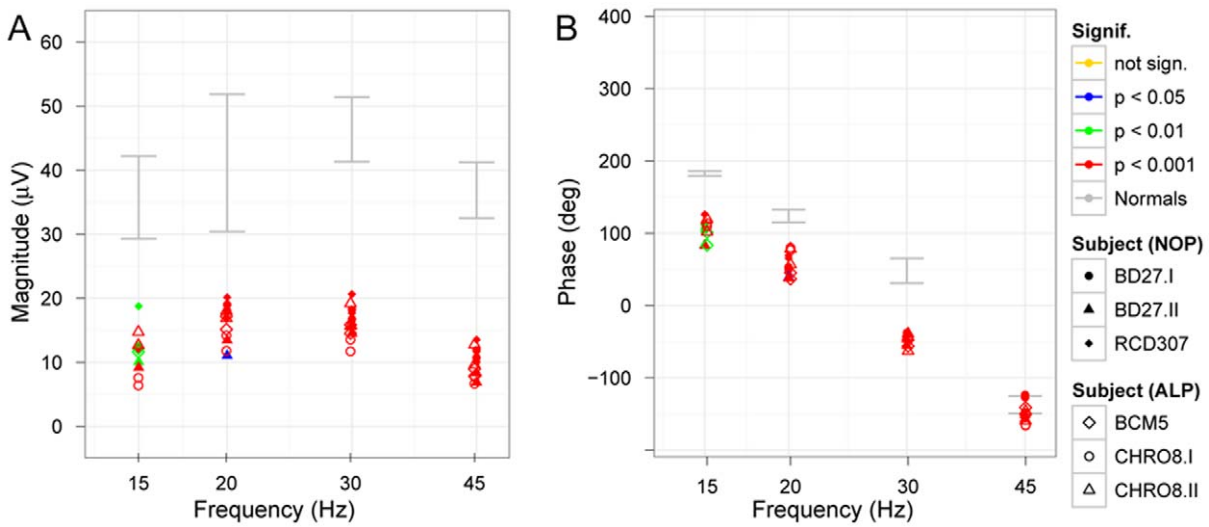

Figure 10. Photopic flicker series. Magnitude (A) and phase (B) of photopic flicker responses in a flicker series show similar frequency dependence but lower magnitude in patients accompanied by a phase shift. Significance levels are color-coded in each figure, the 95% confidence band of normal subjects is marked with grey.
doi:10.1371/journal.pone.0046762.g010

DOI:10.14753/SE.2014.1976

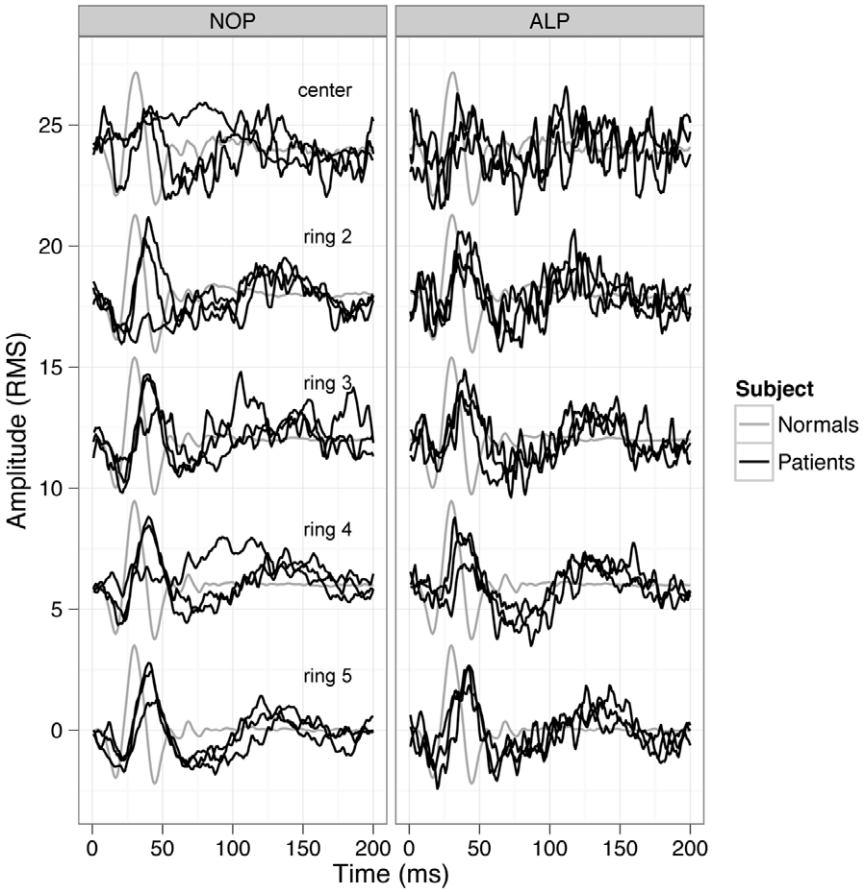

Figure 11. MfERG results. Individual mfERG response waveforms for the subjects of each group (NOP group on the left, ALP group on the right) compared to normal subjects waveforms (black curves represent the responses of the patients, grey curves show normal responses). Responses of patients are reduced and delayed in both groups, more pronounced in the central rings. Interestingly, in the ALP group the central 2 rings tend to show more preserved responses. This could be in relation with the slightly better VA of the ALP group.
doi:10.1371/journal.pone.0046762.g011

et al. [17] including 25 patients with the characteristic scotopic b-wave signs, this delay was seen for the ON-responses and particularly for the OFF-responses as well. A further interesting finding was the marked reduction or even absence of the oscillatory potentials, either suggesting an altered function of the inner retina (i.e. amacrine or interplexiform cells) or more likely a significantly reduced cone function [28].

Moreover, we studied the temporal characteristics of the retina for the first time in this specific retinal disorder. Repetitive stimulation is very demanding for the metabolic process in neurons and changes in the temporal dynamics (e.g. in channelopathies) are evident in flicker ERGs [30]. The impairment of temporal response characteristics can occur due to photoreceptor disturbances as well as postsynaptic mechanisms. Kv2.1/Kv8.2 heteromeric channels contribute to the generation of the K^+ current responsible for the dynamic signal amplification of photoreceptors. The hyperpolarizing overshoot in response to rapid onset illumination has an important role in increasing the sensitivity to fast changes of illumination. Altered Kv2.1/Kv8.2 heteromers lose their ability to function as a high-pass amplifier, which explains the altered temporal characteristics observed in our patients (i.e. there is a constant prolongation of photoreceptor recovery time). Interestingly, even at the highest frequency of 45 Hz the response waveform was still significant with an almost normal phase, which indicates that even though we find clearly reduced amplitudes and a phase shift due to cone dystrophy, the temporal dynamics seem to be almost normal. There is little known about critical flicker fusion in retinal dystrophies in humans, but it has been shown in RCS rats that with progression of the degeneration the amplitude for higher frequency waveforms declines and the critical flicker fusion frequency is shifted to lower frequencies [31]. However, Kv2.1/Kv8.2 heteromeric channels are not the only components of the outward K^+ current in photoreceptors, although they are essential for their functional properties.

These special electrophysiological features are considered to be strictly associated with *KCNV2* mutations, but recently Thompson et al. [32] have shown somewhat similar changes of the dark-adapted electroretinogram in patients with *KCNJ10* mutations. The K^+ channel expressed by the *KCNJ10* gene (Kir4.1) has previously been recognized as pathogenic in man, causing a constellation of symptoms, including epilepsy, ataxia, sensorineural deafness and a renal tubulopathy (EAST syndrome). Kir4.1 constitutes the primary inward rectifying potassium channel of retinal Müller cells [33] and is responsible for the regulation of extracellular K^+. Thompson et al. nicely demonstrated similar dynamics of scotopic intensity-response function in two of four patients. ERGs to dimmer flash stimuli showed a delay of up to 20 ms before the onset of the b-wave, and with increasing intensity a sudden elevation of amplitudes and normal implicit times could be detected. These similarities of the scotopic ERG could be

DOI:10.14753/SE.2014.1976

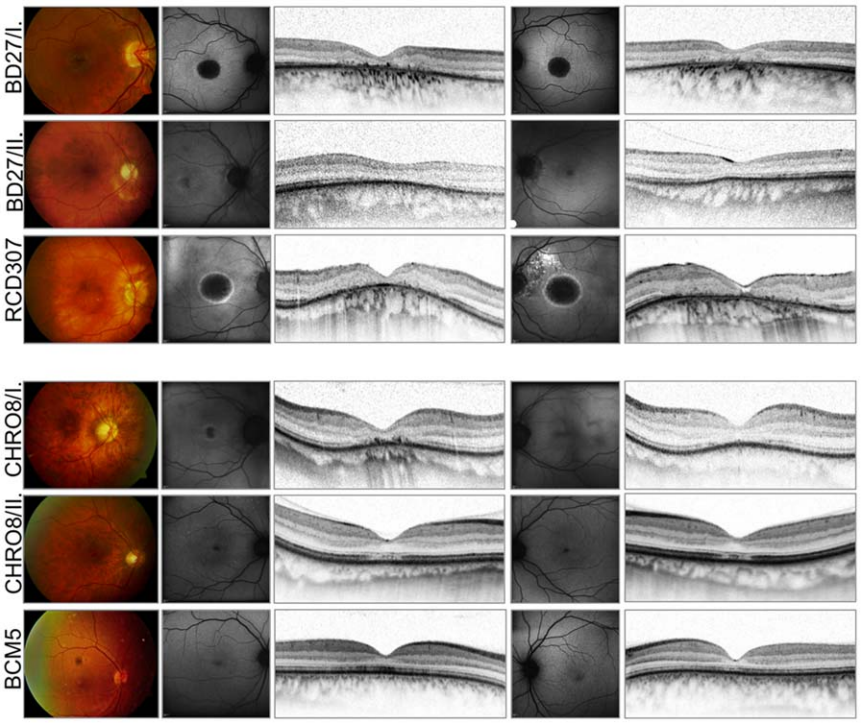

Figure 12. Morphological findings. Fundus photographs of the right eye, FAF and spectral domain OCT images of both eyes of six patients illustrating the variability and extent of foveal changes (NOP group: upper three patients, ALP group: lower three patients). Notice the age-related changes, epiretinal gliosis and macular hole formation on the left eye of the RCD307 patient.
doi:10.1371/journal.pone.0046762.g012

explained with an altered sensitivity at the synapse between rod and ON-bipolar cells due to mutations in *KCNJ10*. Photopic ERGs of all patients showed reduced amplitudes of the photopic negative response (PhNR) and showed a delay in b-wave time to peak, but the photopic hill was preserved. However, these patients did not develop a cone dystrophy, since mutations in *KCNJ10* primarily affect the Müller cell functions, while mutations in *KCNV2* lead to disturbed functional integrity of the photoreceptors and probably impair their postreceptoral signaling.

KCNV2 retinopathy is considered a very rare retinal disorder associated with high but often normal mixed rod-cone response amplitudes, a marked prolongation of b-wave implicit times and a delayed, almost sudden, steep amplitude-versus-intensity relationship under scotopic conditions. Furthermore, while rod phototransduction is intact, there is a constant delay of the responses, which suggests changes in the synapse or in postreceptoral signaling pathway. Inner retinal involvement is also probable, since oscillatory potentials are almost absent. These findings are diagnostic and are exclusively linked to *KCNV2* mutations.

Author Contributions

Performed the experiments: DZ SK BW EZ HJ. Analyzed the data: DZ SK BW EZ HJ. Contributed reagents/materials/analysis tools: DZ SK BW EZ HJ. Wrote the paper: DZ. corrected the manuscript: SK BW EZ HJ.

References

1. Gouras P, Eggers HM, MacKay CJ (1983) Cone dystrophy, nyctalopia, and supernormal rod responses. A new retinal degeneration. Arch Ophthalmol 101: 718–724.
2. Alexander KR, Fishman GA (1984) Supernormal scotopic ERG in cone dystrophy. Br J Ophthalmol 68: 69–78.
3. Foerster MH, Kellner U, Wessing A (1990) Cone dystrophy and supernormal dark-adapted b-waves in the electroretinogram. Graefes Arch Clin Exp Ophthalmol 228: 116–119.
4. Hood DC, Cideciyan AV, Halevy DA, Jacobson SG (1996) Sites of disease action in a retinal dystrophy with supernormal and delayed rod electroretinogram b-waves. Vision Res 36: 889–901.
5. Kato M, Kobayashi R, Watanabe I (1993) Cone dysfunction and supernormal scotopic electroretinogram with a high-intensity stimulus. A report of three cases. Doc Ophthalmol 84: 71–81.
6. Michaelides M, Holder GE, Webster AR, Hunt DM, Bird AC, et al. (2005) A detailed phenotypic study of "cone dystrophy with supernormal rod ERG". Br J Ophthalmol 89: 332–339.
7. Rosenberg T, Simonsen SE (1993) Retinal cone dysfunction of supernormal rod ERG type. Five new cases. Acta Ophthalmol (Copenh) 71: 246–255.
8. Sandberg MA, Miller S, Berson EL (1990) Rod electroretinograms in an elevated cyclic guanosine monophosphate-type human retinal degeneration. Comparison with retinitis pigmentosa. Invest Ophthalmol Vis Sci 31: 2283–2287.
9. Yagasaki K, Miyake Y, Litao RE, Ichikawa K (1986) Two cases of retinal degeneration with an unusual form of electroretinogram. Doc Ophthalmol 63: 73–82.
10. Wu H, Cowing JA, Michaelides M, Wilkie SE, Jeffery G, et al. (2006) Mutations in the gene KCNV2 encoding a voltage-gated potassium channel subunit cause "cone dystrophy with supernormal rod electroretinogram" in humans. Am J Hum Genet 79: 574–579.
11. Czirjak G, Toth ZE, Enyedi P (2007) Characterization of the heteromeric potassium channel formed by kv2.1 and the retinal subunit kv8.2 in Xenopus oocytes. J Neurophysiol 98: 1213–1222.
12. Beech DJ, Barnes S (1989) Characterization of a voltage-gated K+ channel that accelerates the rod response to dim light. Neuron 3: 573–581.
13. Mohapatra DP, Park KS, Trimmer JS (2007) Dynamic regulation of the voltage-gated Kv2.1 potassium channel by multisite phosphorylation. Biochem Soc Trans 35: 1064–1068.
14. Ben Salah S, Kamei S, Senechal A, Lopez S, Bazalgette C, et al. (2008) Novel KCNV2 mutations in cone dystrophy with supernormal rod electroretinogram. Am J Ophthalmol 145: 1099–1106.

DOI:10.14753/SE.2014.1976

15. Thiagalingam S, McGee TL, Weleber RG, Sandberg MA, Trzupek KM, et al. (2007) Novel mutations in the KCNV2 gene in patients with cone dystrophy and a supernormal rod electroretinogram. Ophthalmic Genet 28: 135–142.
16. Wissinger B, Dangel S, Jagle H, Hansen L, Baumann B, et al. (2008) Cone dystrophy with supernormal rod response is strictly associated with mutations in KCNV2. Invest Ophthalmol Vis Sci 49: 751–757.
17. Robson AG, Webster AR, Michaelides M, Downes SM, Cowing JA, et al. (2010) "Cone dystrophy with supernormal rod electroretinogram": a comprehensive genotype/phenotype study including fundus autofluorescence and extensive electrophysiology. Retina 30: 51–62.
18. Sergouniotis PI, Holder GE, Robson AG, Michaelides M, Webster AR, et al. (2012) High-resolution optical coherence tomography imaging in KCNV2 retinopathy. Br J Ophthalmol 96: 213–217.
19. Wissinger B, Schaich S, Baumann B, Bonin M, Jägle H, et al. (2011) Large deletions of the KCNV2 gene are common in patients with cone dystrophy with supernormal rod response. Hum Mutat 32: 1398–1406.
20. Hood DC, Bach M, Brigell M, Keating D, Kondo M, et al. (2008) ISCEV guidelines for clinical multifocal electroretinography (2007 edition). Doc Ophthalmol 116: 1–11.
21. Marmor MF, Fulton AB, Holder GE, Miyake Y, Brigell M, et al. (2009) ISCEV Standard for full-field clinical electroretinography (2008 update). Doc Ophthalmol 118: 69–77.
22. Evans LS, Peachey NS, Marchese AL (1993) Comparison of three methods of estimating the parameters of the Naka-Rushton equation. Doc Ophthalmol 84: 19–30.
23. Hood DC, Birch DG (1994) Rod phototransduction in retinitis pigmentosa: estimation and interpretation of parameters derived from the rod a-wave. Invest Ophthalmol Vis Sci 35: 2948–2961.
24. Schatz A, Wilke R, Strasser T, Gekeler F, Messias A, et al. (2012) Assessment of "non-recordable" electroretinograms by 9 Hz flicker stimulation under scotopic conditions. Doc Ophthalmol 124: 27–39.
25. Sharpe LT, Stockman A, Jägle H, Knau H, Klausen G, et al. (1998) Red, green, and red-green hybrid pigments in the human retina: correlations between deduced protein sequences and psychophysically measured spectral sensitivities. J Neurosci 18: 10053–10069.
26. Nathans J (1989) The genes for color vision. Sci Am 260: 42–49.
27. Friedburg C, Wissinger B, Schambeck M, Bonin M, Kohl S, et al. (2011) Long-term follow-up of the human phenotype in three siblings with cone dystrophy associated with a homozygous p.G461R mutation of KCNV2. Invest Ophthalmol Vis Sci 52: 8621–8629.
28. Barnes S (1994) After Transduction: Response Shaping and Control of Transmission by Ion Channels of the Photoreceptor Inner Segment. Neurosci 58: 447–459.
29. Tanimoto N, Usui T, Ichibe M, Takagi M, Hasegawa S, et al. (2005) PIII and derived PII analysis in a patient with retinal dysfunction with supernormal scotopic ERG. Doc Ophthalmol 110: 219–226.
30. Heckenlively JR, Arden GB (2008) Principle and practice of clinical electrophysiology of vision.: MIT Press Cambridge, Massachusetts, London, England.
31. Pinilla I, Lund RD, Sauve Y (2005) Cone function studied with flicker electroretinogram during progressive retinal degeneration in RCS rats. Exp Eye Res 80: 51–59.
32. Thompson DA, Feather S, Stanescu HC, Freudenthal B, Zdebik AA, et al. (2011) Altered electroretinograms in patients with KCNJ10 mutations and EAST syndrome. J Physiol 589: 1681–1689.
33. Kofuji P, Ceelen P, Zahs KR, Surbeck LW, Lester HA, et al. (2000) Genetic inactivation of an inwardly rectifying potassium channel (Kir4.1 subunit) in mice: phenotypic impact in retina. J Neurosci 20: 5733–5740.

DOI:10.14753/SE.2014.1976

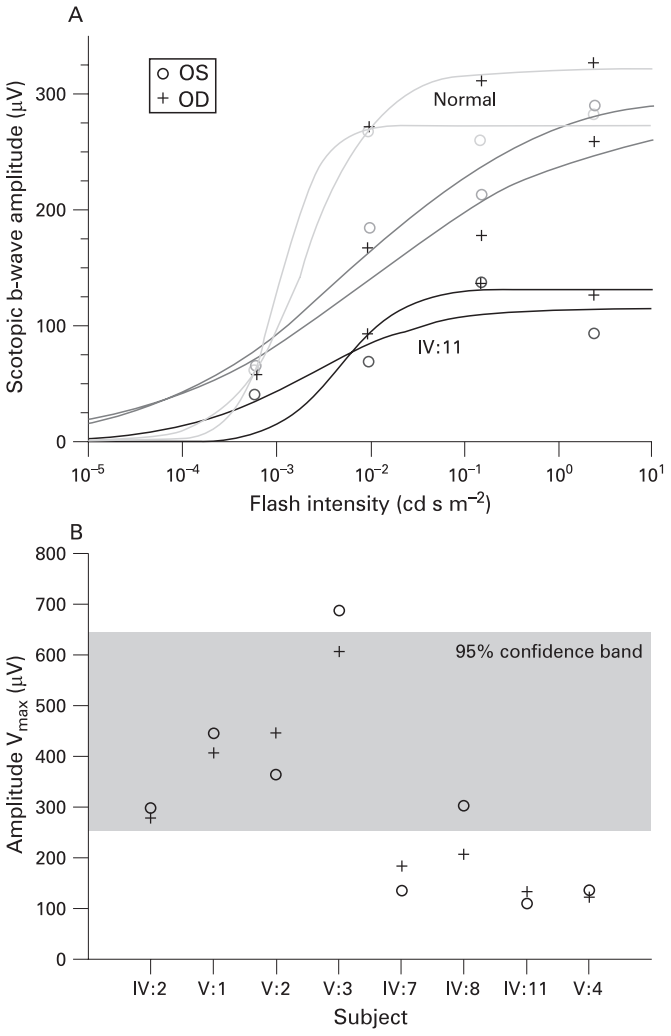

Figure 4 Examples of the response voltage versus log intensity (V-log-I), Naka–Rushton) function of the b-wave from one normal subject, patient IV:2 of family branch A and IV:11 of branch B (A). The estimated maximum response amplitude V_{max} (B) shows a marked difference between patients of family branch A, having a normal amplitude, and those of branch B (IV:7, IV:11, V:4) with a reduced V_{max}. OD, right eye; OS, left eye.

healthy subjects do not. Second, the frameshift mutation introduces a premature termination codon (PTC). Since this PTC is located in the ultimate exon of *CRX*, mutant transcripts may escape nonsense mediated mRNA decay.[21] Then, if translated, the mutation results in a severely truncated protein that is expected to have reduced transactivation activity.[16–18] However, via its intact homeodomain, the mutant protein may still be able to bind to *cis*-regulatory promoter elements or other transcription factors, such as Nrl,[20] thereby blocking binding sites and sequestering normal transcription factors. Thus, as described above the deleterious effects of the CRX mutant c.636delC may be manifold.

Phenotypically, all affected family members show signs of cone dystrophy with severe reduction of macular function in members of the fourth generation. However, in family members of branch B also the rod system is strongly affected. Moreover, patients present with a so-called negative ERG: while the a-wave of the Ganzfeld maximum response waveform, which originates in the photoreceptor outer segments,[22] is well maintained, the b-wave is largely reduced, which originates from retinal cells that are postsynaptic to the photoreceptors.[23] Moreover, maximum b-wave amplitudes and semisaturation intensities estimated from the Naka–Rushton function indicate a reduced number of rods but an almost normal function of the remaining rod photoreceptors.[24]

The observed clinical variability among affected members in this family might have a genetic basis. Potential modifiers might be mutations in the *CRX* gene itself, such as sequence variants in regulatory regions or intronic variants. Noteworthy is that we found that the presence of intronic variant c.100+12T on the wildtype allele was always associated with the rod dysfunction in this family. Yet we cannot rule out mere coincidence without further genetic or functional data. Besides mutation in the *CRX* gene itself, sequence variants in interacting transcription factors, such as Nrl, Nr2E3, p300/CBP,[16 19 20] or genes which are transactivated by CRX, such as rhodopsin[20] might be strong candidates for modulatory effects.

In conclusion, we described the phenotype of a multi-generation family affected by adCRD with marked intrafamilial variability. Whereas all patients presented a reduced cone ERG, those from only one branch also show a reduced rod ERG, with some even displaying a negative combined rod–cone response. We identified a novel disease-associated mutation in the *CRX* gene, c.636delC, which segregates with disease in all affected family members, and a sequence variant, c.100+12 C>T, which is only present in the more severely affected family members. We suggest that this polymorphism might have a modifying effect of the disease phenotype. In addition, we propose that a negative ERG in adCRD might be an indicator of *CRX* gene mutations.

Acknowledgements: We thank B Baumann, E Weber, M Papke, S Kramer and U Kessler for excellent technical assistance.

Funding: German Research Council KFO134—Ko2176/1-1 and JA997/8-1 to SK and BW, and HJ and EZ, respectively, and EU programme Evi-Genoret LSHG-CT-2005-512036.

Competing interests: None.

Ethics approval: This study conformed to the tenet of the Declaration of Helsinki and received approval from the Ethical Committee of the University Tübingen.

Patient consent: Obtained.

REFERENCES

1. **Berson EL,** Gouras P, Gunkel RD. Progressive cone degeneration, dominantly inherited. *Arch Ophthalmol* 1968;**80**:77–83.
2. **Hamel C.** Cone rod dystrophies. *Orphanet J Rare Dis* 2007;**2**:7.
3. **Szlyk JP,** Fishman GA, Alexander KR, *et al*. Clinical subtypes of cone–rod dystrophy. *Arch Ophthalmol* 1993;**111**:781–8.
4. **Yagasaki K,** Jacobson SG. Cone–rod dystrophy. Phenotypic diversity by retinal function testing. *Arch Ophthalmol* 1989;**107**:701–8.
5. **Rivolta C,** Berson EL, Dryja TP. Dominant Leber congenital amaurosis, cone–rod degeneration, and retinitis pigmentosa caused by mutant versions of the transcription factor CRX. *Hum Mutat* 2001;**18**:488–98.
6. **Tzekov R,** Sohocki M, Daiger S, *et al*. Visual phenotype in patients with Arg41Gln and Ala196+1bp mutations in the CRX gene. *Ophthalmic Genet* 2000;**21**:89–99.
7. **Swain PK,** Chen S, Wang QL, *et al*. Mutations in the cone–rod homeobox gene are associated with the cone–rod dystrophy photoreceptor degeneration. *Neuron* 1997;**19**:1329–36.
8. **Lines M,** Hebert M, McTaggart K, *et al*. Electrophysiologic and phenotypic features of an autosomal cone–rod dystrophy caused by a novel CRX mutation. *Ophthalmology* 2002;**109**:1862–70.
9. **Itabashi T,** Wada Y, Sato H, *et al*. Novel 615delC mutation in the CRX gene in a Japanese family with cone–rod dystrophy. *Am J Ophthalmol* 2004;**138**:876–7.
10. **Marmor M,** Hood D, Keating D, *et al*. Guidelines for basic multifocal electroretinography (mfERG). *Doc Ophthalmol. Adv Ophthalmol* 2003;**106**:105–15.
11. **Marmor M,** Holder G, Seeliger M, *et al*. Standard for clinical electroretinography (2004 update). *Doc Ophthalmol. Adv Ophthalmol* 2004;**108**:107–14.
12. **Massof RW,** Wu L, Finkelstein D, *et al*. Properties of electroretinographic intensity-response functions in retinitis pigmentosa. *Doc Ophthalmol* 1984;**57**:279–96.

DOI:10.14753/SE.2014.1976

13. **Furukawa T,** Morrow EM, Cepko CL. Crx, a novel otx-like homeobox gene, shows photoreceptor-specific expression and regulates photoreceptor differentiation. *Cell* 1997;**91**:531–41.
14. **Chen S,** Wang QL, Nie Z, *et al*. Crx, a novel Otx-like paired-homeodomain protein, binds to and transactivates photoreceptor cell-specific genes. *Neuron* 1997; **19**:1017–30.
15. **Bibb LC,** Holt JK, Tarttelin EE, *et al*. Temporal and spatial expression patterns of the CRX transcription factor and its downstream targets. Critical differences during human and mouse eye development. *Hum Mol Genet* 2001;**10**:1571–9.
16. **Yanagi Y,** Masuhiro Y, Mori M, *et al*. p300/CBP acts as a coactivator of the cone–rod homeobox transcription factor. *Biochem Biophys Res Commun* 2000;**269**:410–14.
17. **Chen S,** Wang Q-L, Xu S, *et al*. Functional analysis of cone–rod homeobox (CRX) mutations associated with retinal dystrophy. *Hum Mol Genet* 2002;**11**:873–84.
18. **Chau KY,** Chen S, Zack DJ, *et al*. Functional domains of the cone–rod homeobox (CRX) transcription factor. *J Biol Chem* 2000;**275**:37264–70.
19. **Peng GH,** Chen S. Chromatin immunoprecipitation identifies photoreceptor transcription factor targets in mouse models of retinal degeneration: new findings and challenges. *Vis Neurosci* 2005;**22**:575–86.
20. **Mitton KP,** Swain PK, Chen S, *et al*. The leucine zipper of NRL interacts with the CRX homeodomain. A possible mechanism of transcriptional synergy in rhodopsin regulation. *J Biol Chem* 2000;**275**:29794–9.
21. **Holbrook JA,** Neu-Yilik G, Hentze MW, *et al*. Nonsense-mediated decay approaches the clinic. *Nat Genet* 2004;**36**:801–8.
22. **Brown KT.** The electroretinogram: its components and their origins. *Vision Res* 1968;**8**:633–77.
23. **Miller RF,** Dowling JE. Intracellular responses of the Muller (glial) cells of mudpuppy retina: their relation to b-wave of the electroretinogram. *J Neurophysiol* 1970;**33**:323–41.
24. **Evans LS,** Peachey NS, Marchese AL. Comparison of three methods of estimating the parameters of the Naka–Rushton equation. *Doc Ophthalmol* 1993;**84**:19–30.

RESEARCH ARTICLE DOI:10.14753/SE.2014.1976 Human Mutation

OFFICIAL JOURNAL HGVS HUMAN GENOME VARIATION SOCIETY www.hgvs.org

Large Deletions of the *KCNV2* Gene are Common in Patients with Cone Dystrophy with Supernormal Rod Response

Bernd Wissinger,[1]* Simone Schaich,[1] Britta Baumann,[1] Michael Bonin,[2] Herbert Jägle,[3]† Christoph Friedburg,[4] Balázs Varsányi,[5] Carel B. Hoyng,[6] Hélène Dollfus,[7] John R. Heckenlively,[8] Thomas Rosenberg,[9] Günter Rudolph,[10] Ulrich Kellner,[11] Roberto Salati,[12] Astrid Plomp,[13,14] Elfride De Baere,[15] Monika Andrassi-Darida,[4] Alexandra Sauer,[1] Christiane Wolf,[1] Ditta Zobor,[3] Antje Bernd,[3] Bart P. Leroy,[15,16] Péter Enyedi,[17] Frans P.M. Cremers,[18] Birgit Lorenz,[4] Eberhart Zrenner,[3] and Susanne Kohl[1]

[1]Molecular Genetics Laboratory, Institute for Ophthalmic Research, Centre for Ophthalmology, University Clinics Tübingen, Germany; [2]Department of Medical Genetics, Institute for Human Genetics, University of Tübingen, Germany; [3]University Eye Hospital, Centre for Ophthalmology, University Clinics Tübingen, Germany; [4]Department of Ophthalmology, Justus-Liebig-University Giessen, Giessen, Germany; [5]Department of Ophthalmology, Semmelweis University, Budapest, Hungary; [6]Department of Ophthalmology, Radboud University Nijmegen Medical Centre, Nijmegen, The Netherlands; [7]Centre de Référence pour les Affections Rare en Génétique Ophthalmologique, Hôpitaux Universitaires de Strasbourg, Strasbourg, France; [8]Kellogg Eye Center, University of Michigan, Ann Arbor, MI; [9]Gordon Norrie Centre for Genetic Eye Diseases, National Eye Clinic, Kennedy Center, Hellerup, Denmark; [10]University Eye Hospital, Ludwigs-Maximilians-University, Munich, Germany; [11]Retina Science, Bonn, Germany; [12]IRCCS Eugenio Medea, Bosisio Parini, Italy; [13]Department of Clinical and Molecular Ophthalmogenetics, Netherlands Institute for Neuroscience and Institute of the Royal Netherlands Academy of Arts and Sciences, Amsterdam, The Netherlands; [14]Department of Clinical Genetics, Academic Medical Center, Amsterdam, The Netherlands; [15]Center for Medical Genetics, Ghent University Hospital & Ghent University, Belgium; [16]Department of Ophthalmology, Ghent University Hospital & Ghent University, Belgium; [17]Department of Physiology, Semmelweis University of Medicine, Budapest, Hungary; [18]Department of Human Genetics, Radboud University Nijmegen Medical Centre, The Netherlands

Communicated by Andreas Gal

Received 22 October 2010; accepted revised manuscript 11 July 2011.
Published online 29 August 2011 in Wiley Online Library (www.wiley.com/humanmutation).DOI: 10.1002/humu.21580

ABSTRACT: Cone dystrophy with supernormal rod response (CDSRR) is considered to be a very rare autosomal recessive retinal disorder. CDSRR is associated with mutations in *KCNV2*, a gene that encodes a modulatory subunit (Kv8.2) of a voltage-gated potassium channel. In this study, we found that *KCNV2* mutations are present in a substantial fraction (2.2–4.3%) of a sample of 367 independent patients with a variety of initial clinical diagnoses of cone malfunction, indicating that CDSRR is underdiagnosed and more common than previously thought. In total, we identified 20 different *KCNV2* mutations; 15 of them are novel. A new finding of this study is the substantial proportion of large deletions at the *KCNV2* locus that accounts for 15.5% of the mutant alleles in our sample. We determined the breakpoints and size of all five different deletions, which ranged between 10.9 and 236.8 kb. Two deletions encompass the entire *KCNV2* gene and one also includes the adjacent *VLDLR* gene. Furthermore, we investigated N-terminal amino acid substitution mutations for its effect on interaction with Kv2.1 using yeast two-hybrid technology. We found that these mutations dramatically reduce or abolish this interaction suggesting a lack of assembly of heteromeric Kv channels as one underlying pathomechanism of CDSRR.
Hum Mutat 32:1398–1406, 2011.

KEY WORDS: retinal dystrophy; deletion; Kv channel; *KCNV2*

Introduction

Mutations in the *KCNV2* gene (MIM# 607604) has been recently identified to cause a peculiar form inherited retinopathy known as cone dystrophy associated with supernormal rod response [CDSRR; MIM# 610356; Wu et al., 2006]. This apparently rare form of cone dystrophy is characterized by a congenital or early childhood onset, with poor best-corrected visual acuity (VA), central scotoma, marked photophobia, severe dyschromatopsia, and occasionally nystagmus. Some patients complain of night blindness from childhood onwards or develop night blindness in the later stages of the disease. Fundus findings are highly variable, varying from minute discrete accentuation of the foveal reflexes to unspecific granular changes in the macula; few patients develop foveal or macular retinal pigment epithelium (RPE) atrophy [Michaelides et al., 2005; Wissinger et al., 2008]. A hallmark of CDSRR is the decreased

Additional Supporting Information may be found in the online version of this article.

†Present address: Department for Opthalmology, University Regensburg, Regensburg, Germany.

*Correspondence to: Bernd Wissinger, Molecular Genetics Laboratory, Centre for Ophthalmology, Röntgenweg 11, D-72076 Tübingen, Germany. E-mail: wissinger@uni-tuebingen.de

Contract grant sponsors: Deutsche Forschungsgemeinschaft (KFO 134–KO2176/1-2 (to S.K.), KFO 123–BO2089/1-2 (to M.B.), and LO457/3,1-3 (to B.L.)); Bundesministerium für Bildung und Forschung (HOPE-01GM0850 (to B.W.)); the Foundation Fighting Blindness (to J.H.); The Hungarian National Research Fund (OTKA K75239 (to P.E.)).

and delayed dark-adapted response to dim flashes in electroretinographic (ERG) recordings, which contrasts with the supernormal b-wave response at the highest levels of stimulation. In addition, light-adapted responses to a bright flash and to 30-Hz flickers are delayed and markedly decreased [Gouras et al., 1983; Michaelides et al., 2005]. Several studies have shown that this autosomal recessive inherited phenotype is rather exclusively linked to mutations in *KCNV2* [Ben-Salah et al., 2008; Robson et al., 2010; Sergouniotis et al., 2011; Thiagalingam et al., 2007; Wissinger et al., 2008], and thus strikingly different from the genetic heterogeneity observed for the majority of inherited retinopathies. Up to now 30 different mutations in KCNV2 have been reported. These are almost exclusively small insertion or deletion mutations (so-called indels) and missense or nonsense inducing point mutations. *KCNV2* is predominantly expressed in retinal photoreceptors, most likely in both rods and cones [Czirják et al., 2007; Wu et al., 2006]. It encodes a member of the family of voltage-gated potassium channels (K_v channels), representing a silent subunit (Kv8.2, according to the IUPHAR nomenclature), that does not form functional channels on its own. It has been shown that Kv8.2 is able to assemble with Kv2.1 to form functional heteromeric channels with properties distinct from Kv2.1 homomeric channels, including a shift in the steady-state activation curve toward more negative potentials, a lower threshold potential for activation, a shortened activation time, and slower inactivation kinetics [Czirják et al., 2007]. Heteromeric Kv2.1/Kv8.2 channels show characteristics that resemble the I_{kx} current first observed in amphibian photoreceptors [Beech and Barnes, 1989]. A lack of Kv8.2, as a consequence of a mutation in *KCNV2*, may affect important characteristics of the I_{kx} current, for instance a sustained outward potassium current in the dark, that may influence the photoreceptor membrane potential. However, the mechanisms of dysfunction that link *KCNV2* mutations with the clinical picture of CDSRR still remain to be elucidated.

Subjects, Material and Methods

Patients and family members were recruited over a period of more than 15 years at different clinical centers and venous blood samples were collected after informed consent was obtained.

Ophthalmological Examination

Clinical diagnoses were based on standard ophthalmological examination including evaluation of ocular motility, VA, refraction, color vision and visual field testing, anterior segment pathology using slit lamp examination, fundus examination followed by fundus photography, autofluorescence imaging, and ERG recordings under scotopic and photopic conditions.

Molecular Genetic Analyses

Total genomic DNA was isolated from peripheral blood samples according to standard procedures. Mutation screening of the *KCNV2* gene (cDNA reference sequence NM_133497.3) was carried out by complete sequencing of the coding exons and flanking intronic/untranslated region (UTR) sequences as described previously [Wissinger et al., 2008]. Small heterozygous indel mutations that result in overlaid sequence traces were further confirmed by cloning of PCR products and subsequent sequencing of plasmids from single bacterial colonies.

Deletion breakpoints were bridged by long-distance PCR (LD-PCR) amplifications followed by restriction mapping refinement and finally covered by DNA sequencing applying primer-walking strategy.

Copy number analysis for exon 1 of the *KCNV2* gene was done by quantitative PCR (qPCR) employing TaqMan technology with a custom designed assay as described previously [Wissinger et al., 2008]. Further copy number qPCRs for loci flanking *KCNV2* were performed as follows using SYBR Green for product detection: 20-µl reactions containing 100 ng of genomic DNA, 500 nM of forward and reverse primer, and 10-µl SYBR Green Master Mix (Roche Applied Science, Basel, Switzerland) were subjected to thermal cycling with 5 min at 95°C, followed by 45 cycles of 10 sec at 95°C, 15 sec at 59°C and 30 sec at 72°C on a Lightcycler 480 (Roche Applied Science). An assay that amplifies a fragment at *GAPDH* was used as reference. qPCRs were done in triplicate and mean Ct values were used for calculations. The mean of the ΔCt values ($Ct^{\text{"Target"}} - Ct^{GAPDH}$) of two to four control samples were used as calibrator, and ΔΔCt and $2^{-\Delta\Delta Ct}$ values were calculated for the patient samples to be assessed.

Comparative genome hybridizations (CGH) using a ready-made chromosome 9 specific 385k oligonucleotide array (HG18 CHR9 FT; Roche NimbleGen Inc., Madison, WI) were carried out for two individuals with larger heterozygous deletions at the *KCNV2* locus. Prior to CGH, DNA samples were further purified by phenol/chloroform extraction and checked for DNA integrity by agarose gel electrophoresis. CGH was carried out as a commercial service at Roche NimbleGen, Reykjavik, Iceland.

In order to assess homozygosity regions and potential segments of identity-by-descent, we used restriction-enzyme digested genomic DNA for hybridizations on Affymetrix 250k_NspI single nucleotide polymorphism (SNP) arrays (Affymetrix, Santa Clara, CA). Samples were processed in accordance with the manufacturer's instructions and arrays were scanned with the Affymetrix GeneChip Scanner 3000 7G. Genotypes were called with Affymetrix Genotyping Console Software v2.1 (GTC) using the BRLMM algorithm with default calling threshold of 0.5 and a prior size of 10,000 bases. Samples were required to have a minimum Quality Control SNP call rate of 90%.

Yeast Two-Hybrid Interaction Assays

Yeast two-hybrid bait and prey constructs encoding N-terminal fragments of KCNB1/Kv2.1 (amino acid residues 1–190) and KCNV2/Kv8.2 (amino acid residues 1–257), and cloned into pGBKT7 (as fusion with the Gal4 DNA binding domain) and pGADT7 (as fusion with the Gal4 activation domain) were reported by Ottschytsch et al. [2002] and were kindly provided by Dr. Elke Bocksteins and Dr. Dirk Snyders (Laboratory of Molecular Biophysics, Physiology, and Pharmacology, University of Antwerp, Belgium). Missense mutations were introduced by in vitro mutagenesis using the overlap extension strategy [Ho et al., 1989] and confirmed by DNA sequencing. Purified plasmid DNA was used to transform yeast strains Y2HGold and Y187 (Clontech/Takara Bio Europe, Saint-Germain-en-Laye, France), applying standard protocols. Mated dipoid cells or co-transformed haploid cells were streaked on double dropout (SD-Leu-Trp) and quadruple dropout (SD-Leu-Trp-His-Ade) medium with or without aureobasidin A (125 ng/µl) and X-α-Gal (40 µg/ml), and grown for 72–120 hr at 30°C. β-Galactosidase activity resulting from yeast two-hybrid dependent activation of the LacZ gene expression was determined in lysates of co-transformed Y187 yeast cells using chlorophenyl red b-galactopyranoside (CPRG; Sigma-Aldrich, Taufkirchen, Germany) as substrate according to standard protocols. Mean values and standard deviations of β-Galactosidase activity were calculated from two

replicates of each of three independent yeast colonies using the formula: $1{,}000 \times OD_{570}/(t \times V \times OD_{600})$ with t being the incubation time, V being the dilution factor, and OD_{600} being the cell culture density before harvesting of the cells.

Results

Screening of the *KCNV2* Gene in Patients with an Initial Diagnosis of Cone Dysfunction

Prior studies have shown that the phenotype of CDSRR is exclusively linked to mutations in *KCNV2*. CDSRR was first described in 1983 as a new disease entity [Gouras et al., 1983] and subsequently only few case reports and small patient series have been reported, suggesting that CDSRR is a very rare condition. In order to test whether CDSRR is underdiagnosed or whether *KCNV2* mutations might also be involved in other retinal phenotypes, we applied DNA sequencing to screen for mutations in this gene in a large cohort of 367 independent patients initially referred to us with various diagnoses of cone-related retinal dystrophies including achromatopsia and blue cone monochromacy (n = 167), cone dystrophy (n = 154), and cone-rod dystrophy (n = 43). Patients diagnosed with achromatopsia or blue cone monochromacy were preselected for the absence of mutations in at least *CNGA3* and *CNGB3* [Kohl et al., 1998, 2000; Wissinger et al. 2001], and the cone opsin gene cluster on Xq28, respectively. In addition, we also included three families with CDSRR that were newly diagnosed since our last study. The composition of the patient cohort is listed in Supp. Table S1.

In all three new CDSRR cases, we found *KCNV2* mutations: a homozygous c.1381G>A/p.Gly461Arg mutation in family ZD389 (two affected siblings), compound heterozygous mutations, c.727C>T/p.Arg243Trp and c.794_795dupCC/p.Ser266ProfsX57, in patient RCD425, and compound heterozygous mutations, c.8_11del4/p.Lys3ArgfsX95 and c.775_795dup21/p.Ala259_Ala265dup7, in the index patient of family RCD382 (see Supp. Table S2 for the genotypes of all patients and Table 1 for a list of all mutations and variants identified in this study). This further emphasizes the specificity of the association between CDSRR and *KCNV2* mutation.

In RCD382 (see Fig. 1A for the pedigree), the three sisters of the father had a history of reduced vision with glare, nystagmus, night vision problems since childhood and with maculopathy on external ophthalmological examinations. One affected sister was investigated clinically in detail in comparison with the index patient (Supp. Table S3). At an age of 33 years she demonstrated fine horizontal nystagmus, her VA was 0.03 in both eyes and isopters in Goldmann visual field were constricted for V/4e and III/4e (no smaller/dimmer targets detected). Optic discs appeared normal but her macula had no physiological reflexes. ERGs had signs now known to be typical for mutations in *KCNV2* as summarized in Supp. Table S3 [Friedburg et al., 2007]. The differential diagnosis at the time of investigation was achromatopsia or cone (rod) dystrophy. We found that she and her affected sisters carry the c.775_795dup21 mutation, and in addition a novel heterozygous missense mutation c.989T>C/p.Phe330Ser. The later affects an evolutionary highly conserved phenylalanine residue and was excluded in 75 healthy controls, further supporting that three pathogenic *KCNV2* mutations segregate in this family (Fig. 1A).

Upon screening the sample of patients with an initial diagnosis of other cone-related retinal dystrophies, we found single homozygous or two heterozygous *KCNV2* mutations in a subset of patients: in seven patients with an initial diagnosis of achromatopsia, four patients with cone dystrophy, and one patient with cone-rod dystrophy. Mutations in these patients included two frameshift mutations, two nonsense mutations, one in-frame 9-bp deletion, five missense mutations, and several larger deletions, as described below (Table 1 and Supp. Table S2). None of the point mutations or small indel mutations were observed in healthy controls (n = 59–97). In addition, we found 11 patients (four with a diagnosis of achromatopsia, five with cone dystrophy, and two with cone-rod dystrophy) with single heterozygous mutations. Except for a 9-bp in-frame duplication (c.1133_1141dup/p.Arg386_Ile387dvp), all other single heterozygous mutations represent missense substitutions that have not been observed in other CDSRR patients or controls.

Considering only patients with homozygous or compound heterozygous *KCNV2* mutations, our results indicate that mutations in *KCNV2* account for about 2.2–4.3% of patients with various initial diagnoses of cone dysfunction. Hence, we retrospectively reassessed whether those cases differ from the phenotype of CDSRR. We specifically asked the ophthalmologists in charge, whether—based on the genetic findings—a diagnosis of CDSRR would be more appropriate or specific than the initial diagnosis. Based on follow-up examinations or reevaluation of available clinical data that was done for 10 patients, the answer was positive for nine of these patients (Supp. Table S2). There were different reasons why the patients were initially diagnosed with other retinal dystrophies, for example (1) unawareness of CDSRR, (2) typical features overlooked or not adequately considered, (3) ERG response considered as an artifact, and (4) low-quality ERG data. Only one patient diagnosed with cone dystrophy, who carried two missense mutations (c.491T>C/p.F164S and c.1381G>A/p.G461R), did not fully qualify for a diagnosis of CDSRR, since the bright flash responses in ERG recordings were still in the normal range.

Identification and Characterization of Homozygous Deletions in the *KCNV2* Gene

We repeatedly failed to amplify *KCNV2* exon 1 in two patients (from pedigrees CHRO417 and RCD307 in Fig. 1B), though exon 2 and other genomic loci could be readily amplified. We therefore reasoned that homozygous deletions might be present in those patients. In fact, qPCR-based copy number analysis of *KCNV2* exon 1 in the mother in RCD307 revealed a $2^{-\Delta\Delta Ct}$ value of 0.48, that is, an about 50% reduced copy number. We further pursued with sequence tag site (STS) content mapping and LD-PCR experiments that eventually led to the identification of a deletion of 10,909 bp that encompasses all but the first 18 bp of the coding sequence of exon 1 and most parts of intron 2, and a short 6-bp sequence insertion between the proximal and distal breakpoint (c.19_1356+9571delinsCATTTG; Supp. Fig. S1). Both the mother and the unaffected brother in RCD307 were heterozygous carriers for this mutation (Fig. 1B). Exactly the same mutation was also present in the index patient in CHRO417. There was no evidence of close consanguinity in either family. RCD307 originate from Southern Germany and CHRO417 from Hungary and could not specify any relationship upon personal interview. Still, we suspected a common origin of this very specific deletion + insertion mutation. To evaluate this hypothesis, we performed a comparative high-resolution 250k SNP array analysis with DNA from both patients. We found that both showed significant intervals of homozygosity on chromosome 9p24 (including the *KCNV2* locus) of 8.3 Mb (patient CHRO417) and 1.2 Mb (patient RCD307), respectively (Supp. Fig. S2). Yet, the region of shared SNP genotypes

DOI:10.14753/SE.2014.1976

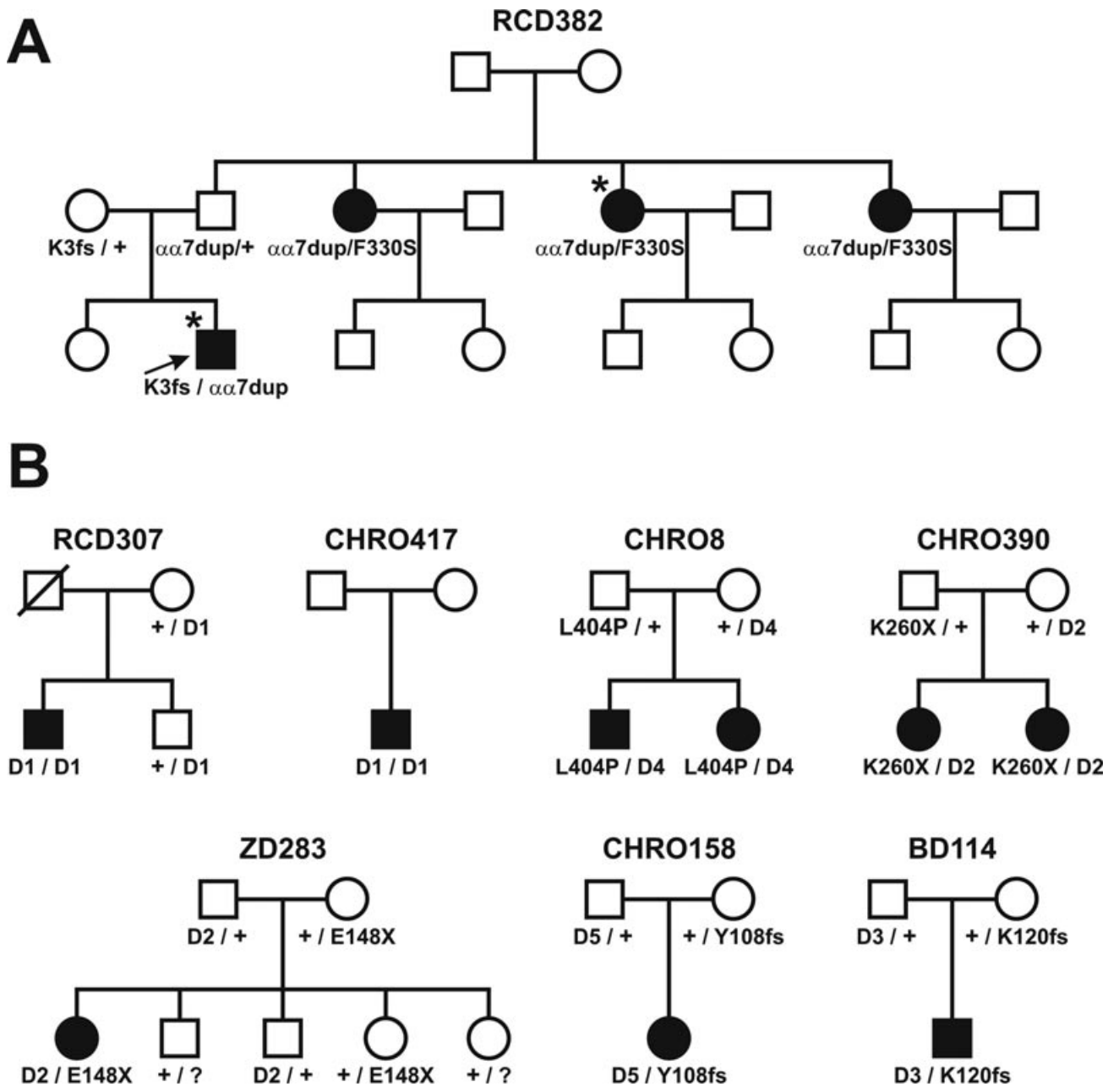

Figure 1. Selected families that segregate *KCNV2* mutations. A: Pedigree of family RCD382, that segregates three *KCNV2* mutations. The arrow marks the index patient and asterisks indicate the patients for which detailed clinical data are provided in Supp. Table S3. B: Pedigrees of the seven families with large deletions at the *KCNV2* locus. Genotypes are given for all probands for which DNA samples were available. Abbreviations of the deletions/mutations are as follows: D1, c.19_1356+9571delinsCATTTG; D2, c.434_*30+154del; D3, g.2696639_2713626del; D4, g.2657638_2737340del; D5, g.2570596_2807413del; αα7dup, c.775_795dup21. "?" in the genotypes for some unaffected members in ZD283 indicates that they have not been tested for the E148X mutation.

between the two patients is rather small with less than 300 kb in size. Nonetheless, a common ancestry of the mutation is very likely, since that interval is covered by 162 SNPs on the high-resolution SNP chip.

Identification and Characterization of Large Heterozygous Deletions at the *KCNV2* Locus

During our initial screening, we found six patients with apparently homozygous point mutations in exon 1 of the *KCNV2* gene, although parental consanguity was not documented in any of these families. Family members for co-segregation analysis were available for five of these six families. Concordant segregation of genotypes was only observed in one family (CHRO246 which segregates the c.1348T>A/p.Trp450Arg mutation), whereas inconsistent segregation was noted in the remaining four families (pedigrees CHRO8, CHRO158, CHRO390, and ZD283, Fig. 1B). In all four families, we observed that the mutation (apparently homozygous in the patient) was only present in heterozygous state in one parent. In order to evaluate the possibility of allelic dropout due to the presence of a heterozygous deletion, we performed qPCR-based copy

DOI:10.14753/SE.2014.1976

Table 1. Mutations and Rare Sequence Variants in the KCNV2 Gene in This Study

Location	Alteration nucleotide sequence[a]	Alteration polypeptide	Total no. of chromosomes[b]	Reference[c]
Mutations				
Exon 1	c.8_11del4	p.Lys3ArgfsX96	3	f
Exon 1	c.323_329del7	p.Tyr108TrpfsX14	1	This article
Exon 1	c.442G>T	p.Glu148X	3	a, b
Exon 1	c.491T>C	p.Phe164Ser	1	This article
Exon 1	c.727C>T	p.Arg243Trp	1	This article
Exon 1	c.778A>T	p.Lys260X	1	a, c
Exon 1	c.782C>A	p.Ala261Asp	2	This article
Exon 1	c.775_795dup21	p.Ala259_Ala265dup7	1	This article
Exon 1	c.794_795dupCC	p.Ser266ProfsX57	1	This article
Exon 1	c.989T>C	p.Phe330Ser	1	This article
Exon 1	c.1016_1024del	p.Asp339_Val341del	1	a, d
Exon 1	c.1211T>C	p.Leu404Pro	1	This article
Exon 1	c.1348T>A	p.Trp450Arg	2	This article
Exon 2	c.1381G>A	p.Gly461Arg	4	a, b, c, f
D1: Exon 1+	c.19_1356+9571 delinsCATTTG	p.Arg7HisfsX57	4	This article
D2: Exon 1+2	c.434_*30+154del	p.Glu145LeufsX4	2	This article
D3: Exon 1+	g.2696639_2713626del	loss	1	a[d]
D4: Complete gene	g.2657638_2737340del	loss	1	This article
D5: Complete gene	g.2570596_2807413del	loss	1	This article
Rare variants				
Exon 1	c.107G>A	p.Arg36His	1	This article
Exon 1	c.190G>A	p.Glu64Lys	1	This article
Exon 1	c.222G>C	p.Glu74Asp	1	This article
Exon 1	c.328C>G	p.Leu110Val	1	This article
Exon 1	c.441C>G	p.Asp147Glu	1	d
Exon 1	c.725A>G	p.Gln242Arg	1	This article
Exon 1	c.853A>T	p.Met285Leu	1	This article
Exon 1	c.874G>A	p.Gly292Ser	1	This article
Exon 1	c.1133_1141dup	p.Leu381_Arg383dup	1	This article
Exon 2	c.1607A>G	p.Asn536Ser	1	This article
Exon 2	c.1616T>C	p.Leu539Pro	1	This article

[a] cDNA Reference Sequence: NM_133497.3 with numbering that denotes the adenosine of the annotated translation start codon as nucleotide position +1. Genomic reference sequence: NT_008413.18.
[b] Chromosomes counted only for the index patients. Homozygous mutations counted as two chromosomes.
[c] References: a, Wissinger et al., 2008; b, Ben-Salah et al., 2008; c, Thiagalingan et al., 2007; d, Wu et al., 2006; e, Robson et al., 2010; f, Sergouniotis et al., 2011.
[d] Described as "gross deletion."

number analysis for *KCNV2* exon 1. This experiment showed a reduced copy number in all tested individuals (affected patients and the transmitting parent) with $2^{-\Delta\Delta Ct}$ values ranging between 0.51 and 0.59 (data not shown), confirming the presence of heterozygous deletions.

For the mapping and characterization of these heterozygous deletions, we performed intrafamilial segregation analysis of polymorphic markers (one STR and 29 SNPs) and qPCR-based copy number analysis (three assays). Based on these approaches, we were able to refine the outermost borders of the deletions in CHRO390, ZD283, and also BD114, a family from our prior study that segregates an as yet uncharacterized heterozygous deletion in *KCNV2* [Wissinger et al., 2008]. Subsequent LD-PCR experiments and primer walking led to the identification of an identical intragenic 11.7-kb deletion (c.434_*30+154del) in both CHRO390 and ZD283, and a 16.9-kb deletion (Chr9:g.2696639_g.2713626del; NCBI Build 36.1 human genome assembly) in BD114 (Supp. Fig. S1 and Fig. 2A). Whereas the first deletion has its junctions within exon 1 and ~150-bp downstream of exon 2, the latter encompasses the complete exon 1 and parts of intron 1.

Deletion mapping by qPCR and segregation analysis in CHRO158 and CHRO8 showed that in both cases the deletions were much larger than in the other families. We therefore performed array CGH experiments employing a chromosome 9 specific 385k NimbleGen oligonucleotide array. In both cases, we observed a clear-cut region of reduced copy number encompassing the *KCNV2* locus (Fig. 2B). We carefully examined the probes at the edges of the deduced deletions in order to design primers for LD-PCR. This approach eventually led to the successful amplification of junction fragments and the subsequent determination of the breakpoint sequences. These experiments revealed a 79.7-kb deletion in CHRO8 (Chr9:g.2657638_g.2737340del) and a 237-kb deletion (Chr9:g.2570596_g.2807413del) in CHRO158 (Fig. 2 and Supp. Fig. S1). In both instances the *KCNV2* gene is completely deleted. In CHRO158 the deletion additionally encompasses the entire *VLDLR* gene, and eliminates the first exon of *LOC401491/FLJ35024*, a transcript cluster annotated as a long noncoding RNA, as well as the five terminal coding exons of *KIAA0020*, a putative protein coding gene of unknown function.

Analysis of Deletion Junctions and Putative Deletion Mechanisms

Analysis of the deletion junctions revealed microhomology of 2 to 6 bp in length and in one case an insertion of 6 bp (Supp. Fig. S1). Five of the 10 breakpoints are located in diverse repetitive DNA sequence elements (LINE, SINE, transposon-derived). When compared with BLAST 2-Sequences, none of the breakpoint junction sequence pairs (±500 bp relative to each breakpoint) showed segments of sequence homology that may be indicative for a homology-based mechanism underlying the deletion. We therefore propose nonhomologous end joining (NHEJ), a mechanism that rather accurately rejoins double-strand breaks (DSBs), as the most likely mechanism. Notably, we have not observed recurrent independent deletions and

DOI:10.14753/SE.2014.1976

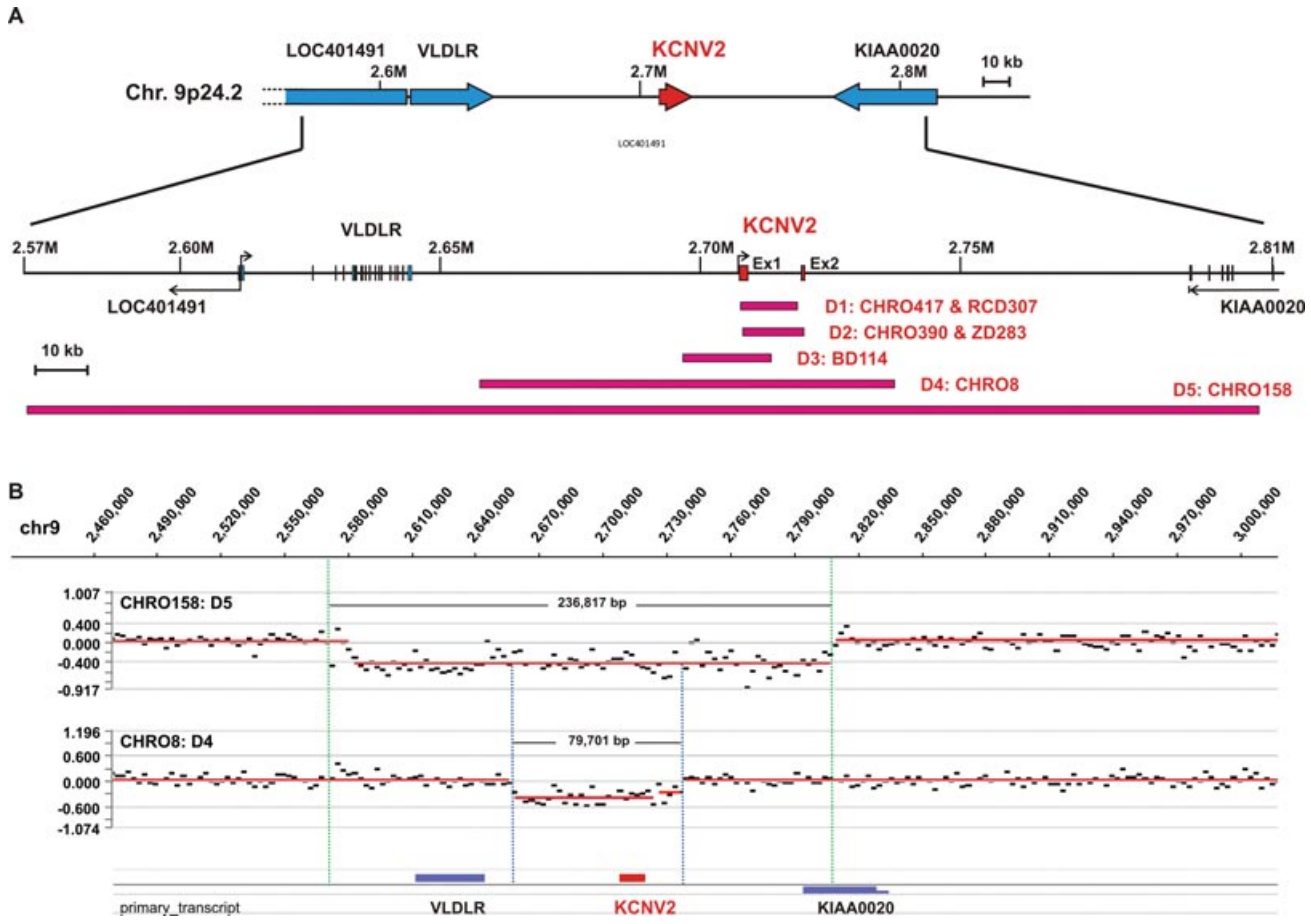

Figure 2. Mapping of deletions at the *KCNV2* locus. A: Overview of the size and coverage of the deletions at the *KCNV2* locus in this study. B: Deletion detection by array-based CGH. Shown are the results of the CGH performed with a 385k chromosome 9 specific Nimblegen oligonucleotide array. The analyzed affected family members of families CHRO8 (top) and CHRO158 (bottom) displayed clear region of reduced copy number (averaged probe intensities) at the *KCNV2* locus.

the deletions breakpoints are rather dispersed except for deletions D1 and D3 in which breakpoints are 415 bp (telomeric side) and 1245 bp (centromeric side) apart. Moreover, there are only few copy number variants (CNVs) from genome-wide studies that map to this region on chromosome 9 (as listed in the UC Santa Cruz Genome browser). These include four copy number losses (size range: 603–20,657 bp) and three copy number gains (size range: 580–1185 bp), all of them localize either upstream or downstream of *KCNV2*.

As a whole, the 237 kb region that encompasses all deletions has a GC content of 40.4% and is enriched for repetitive sequences. A total of 47.2% of the region does represent repetitive sequences compared with an average of 43% for human genome sequences with similar GC content [Smit 1999]. This difference is mainly due to a disproportionately high number of MIR and LTR elements: 4.3% versus 2.3% and 14.4% versus 8.6%, respectively. Yet, the increase in repetitive sequences in the deletion region is not uniform, but mostly restricted to the centromeric half, where its content is as high as 56.8%. The meiotic recombination rate in that region is rather high, on average 2.53 cM/Mb. The region contains four strong recombinational hotspots with a recombination rate >20 cM/Mb (Supp. Fig. S3; hotspots 1–3 and 6) and three weak hotspots with a recombination rate >5 cM/Mb (Supp. Fig. S3; hotspots 4, 5, and 7). Notably three of the five telomeric deletion breakpoints localize to these hotspots including D4-tel that maps to the strong hotspot #2 and one centromeric breakpoint localizes in the close vicinity of a weak hotspot (Supp. Fig. S3). Since NHJE involves rejoining of DSBs one might argue that either the deletions may have occurred during meiotic recombination or that recombinational hotspots per se favor the occurrence of DSBs.

Missense Mutations in the NAB Domain Affect Assembly with Kv2.1

Besides protein truncation mutations and larger deletions described in this article, missense mutations do represent a substantial fraction of all *KCNV2* mutations reported so far with clusters in the pore domain and the N-terminal segment of the protein [Ben-Salah et al., 2008; Thiagalingam et al., 2007; Wissinger et al., 2008; Wu et al., 2006]. The N-terminal segment of voltage-gated potassium (Kv) channels contains conserved sequence motifs (called NAB: N-terminal A and B box domain or T1: N-terminal tetramerization domain, Supp. Fig. S4), which are required for homomeric as well as heteromeric channel recognition and assembly. Kv8.2 (the gene product *of KCNV2*) represents a modulatory channel subunit that is able to form heteroligomeric channels with Kv2.1 in vitro [Czirjak et al., 2007; Ottschytsch et al., 2002]. We therefore wondered whether mutations in the NAB domain of Kv8.2 might affect assembly with Kv2.1 (Supp. Fig. S4). To address this question, we applied yeast two-hybrid technology using the Kv8.2 ($\alpha\alpha$1-250) as prey and Kv2.1 ($\alpha\alpha$1-190) as bait. Wild-type Kv8.2 showed strong

DOI:10.14753/SE.2014.1976

A

	Kv2.1	Kv8.2 -WT	Kv8.2 -L110V	Kv8.2 -D147E	Kv8.2 -F164S	Kv8.2 -E184K	Kv8.2 -E184V	Vector
Kv2.1	+++	++++	+	++	+	-	-	-

B

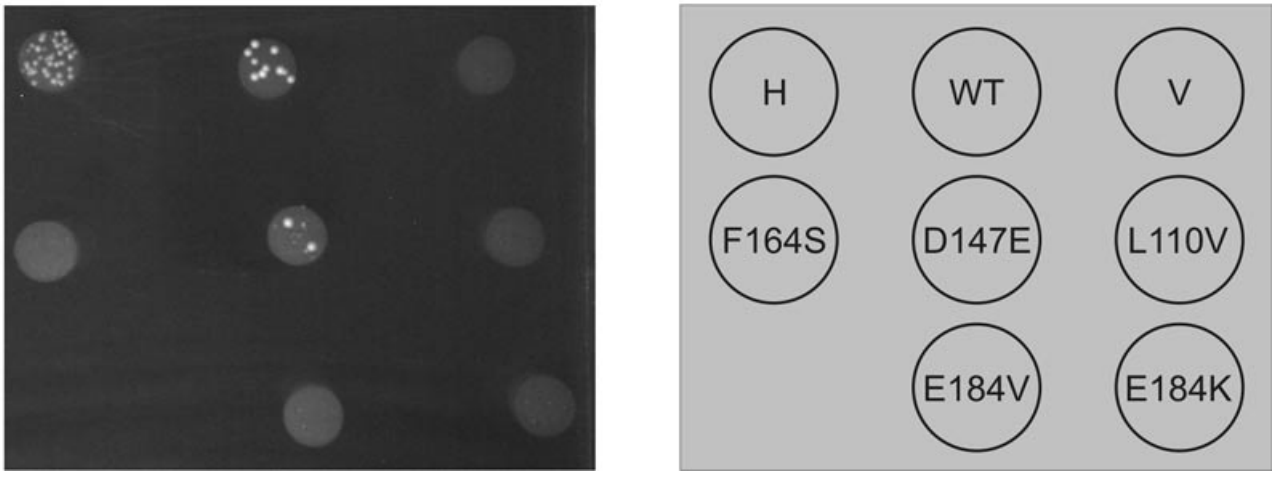

Figure 3. Yeast two-Hybrid phenotype of N-terminal amino acid substitution mutants in KCNV2. Yeast two-hybrid interaction assays were performed using N-terminal fragments of Kv2.1 and Kv8.2 (gene product of *KCNV2*) as bait and prey, respectively. **A:** Qualitative assessment of growth and α-Gal blue coloring of co-transformed yeast colonies on double and quadruple dropout medium with or without aureobasidin. **B:** Growth of co-transformed yeasts on quadruple dropout medium including aureobasidin after 5 days at 30°C. H, homomeric interaction with Kv2.1 as both bait and prey; WT, wild-type Kv8.2; V, co-transformation with empty bait vector.

interaction with Kv2.1 in this assay (as assessed by colony number and size on quadruple dropout medium, and the timing and intensity of α-Galactosidase-based blue staining of colonies). In contrast, we observed that the F164S mutant Kv8.2 fragment (representing a novel mutation described in this article) exhibit reduced interaction, and that E184K as well as E184V mutant Kv8.2 fragments [representing two previously reported *KCNV2* mutations; Wissinger et al. 2008] showed no evidence of interaction with the Kv2.1 fragment (Fig. 3). We also used this assay to analyze the functionality of two other nonsynonymous sequence variants, L110V and D147E, which were found as single heterozygous variants in individual patients. We noted that the D147E variant yielded a growth and color phenotype that outperformed any of the Kv8.2 mutants, whereas the L110V variant exhibit a phenotype of reduced growth comparable with that of the F164S mutant. To quantify these results, we performed interaction-based β-galactosidase activity measurements in lysates of yeasts co-expressing Kv2.1 and wild-type or mutant Kv8.2 fragments, respectively. This assay showed a virtual absence of activity (not significantly different from the negative control) for the E184K and the E184V mutant, respectively, and an about 70-fold reduced activity of both the F164S and the L110V variants compared with the wild-type Kv8.2 protein fragment (Fig. 4). In contrast, we found that the D147E variant exhibited an activity that is still about one-third of the activity of the wild-type.

From these data we conclude that missense mutations that affect the N-terminal portion of Kv8.2 interfere with the interaction between Kv8.2 and Kv2.1, and probably preclude proper assembly of heterooligomeric channels in vivo.

Discussion

Several studies have shown that the phenotype of CDSRR is virtually always associated with mutations in *KCNV2* [Ben-Saleh et al., 2008; Robson et al., 2010; Thiagalingan et al., 2007; Wissinger et al., 2008; Wu et al., 2006]. However, it has not yet been investigated whether mutations in *KCNV2* might also cause other forms of retinopathies, as is the case with several other retinal disease genes (for instance mutations in *ABCA4*, *RDS*, or *NR2E3*). Upon screening of a large cohort of patients with an initial diagnosis of achromatopsia, cone dystrophy, and cone-rod dystrophy, we found a fraction of 2.2–4.3% of patients who carried either homozygous or compound heterozygous mutations in *KCNV2*. Retrospective analysis of the clinical data or clinical reinvestigation of the available patients revealed that their phenotype was indeed fully compatible with a diagnosis of CDSRR, except for one patient in which the bright flash ERG responses were still in the normal range. It has been reported that there is variability in the ERG responses in CDSRR patients and the amplitude of the rod b-wave might not be an unambiguous criterion for CDSRR. Other features such as elevated b-/a-wave ratios in the mixed rod-cone response and the marked prolongation of b-wave implicit times with a steep amplitude versus intensity relationship might be even more helpful in the differential diagnosis [Friedburg et al., 2007; Nagy et al., 2009].

Our study showed that CDSRR is not as rare as previously thought. Therefore, CDSRR should be kept in mind in patients with early onset, slowly progressive cone dystrophy and a thorough electrophysiological examination is warranted, with an ERG which

DOI:10.14753/SE.2014.1976

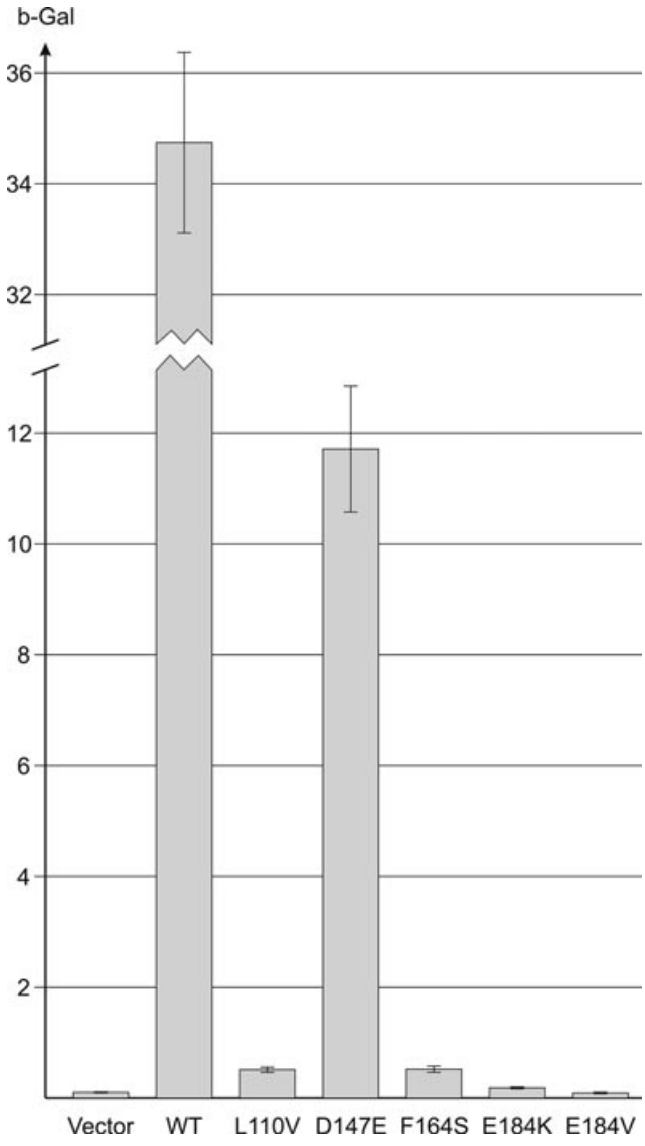

Figure 4. Yeast two-Hybrid based β-Galactosidase activity of KCNV2 wild-type and mutants. Co-transformed Y187 yeast cells were lysed and the β-Galactosidase activity determined by a colorimetric assay using CPRG as substrate. Mean values and standard deviations of the activity were calculated from duplicate measurements of three independent colonies per co-transformation. Note that the Y-axis is interrupted to display the high activity of the wild-type construct.

preferentially is not limited to the standard protocol recommended by the International Society of Clinical Electrophysiology, but also includes an intensity series in the dark-adapted patient.

A main outcome of our study is the identification and characterization of larger deletions encompassing *KCNV2*. Except for a homozygous deletion covering exon 2 [Robson et al., 2010] and an uncharacterized "gross deletion" reported in our previous article [Wissinger et al., 2008], no other larger deletions have as yet been reported for *KCNV2*. Our data show that such deletions do represent a substantial fraction of all mutant *KCNV2* alleles. If we compile the data of this and our previous study, we end up with a prevalance of 15.5% (9/58) of large deletions among all *KCNV2* mutant alleles. The identification of large deletions was largely due to the genotyping of the parents of patients with apparently homozygous mutations. All five different deletions were much larger than the usual amplicon size in PCR-based mutation screenings and would have been missed without segregation analysis. We therefore strongly recommend that parental segregation analysis should be performed in patients with apparently homozygous *KCNV2* point mutations. Alternatively, CNV analysis either by qPCR, multiplex ligation-dependent probe amplification (MLPA), or CGH should be done when samples of the parents are not available.

Two of the large deletions encompass the entire *KCNV2* gene and the remaining alleles are lacking large parts of the gene. We therefore reason that all these deletions represent null alleles for *KCNV2*. Ranging from 10.9 to 236.8 kb, the sizes of the deletions differ considerably. Except for deletion D5, none of the others affect additional genes besides *KCNV2*. D5 additionally encompasses the entire *VLDLR* gene, and parts of two hypothetical genes (LOC401491/*FLJ35024* and *KIAA0020*). Mutations in *VLDLR* have been recently described in autosomal recessive inherited cerebellar hypoplasia and mental retardation [Boycott et al., 2005], which is also associated with quadrupedal locomotion in some pedigrees [Ozcelik et al., 2008; Türkmen et al., 2008]. In addition and interesting for ophthalmologists, *Vldlr* knock-out mice develop intraretinal neovascularization with choroidal anastomosis and has been studied as models for retinal angiomatous proliferation (RAP), a subtype of exudative age-related macular degeneration [Heckenlively et al, 2003; Li et al., 2007]. Not unexpectedly, there was no evidence for either a neurological or a retinal angiogenic proliferation phenotype in the affected patient in family CHRO158, since he is heterozygous for the D5 deletion and carries a small 7-bp deletion in *KCNV2* (c.323_329del7) on the other allele. However, due to the inclusion of both *KCNV2* and *VLDLR* within the deletion, this single mutation gives rise to carriership status for multiple diseases.

We determined the telomeric as well as the centromeric breakpoints of all five different deletions. Two of the deletions (D1 and D5) are accompanied by small insertions (6 bp and 2 bp, respectively) of extra nucleotides at the site of deletion, whereas the remaining three were precise deletions without any additional sequence rearrangement. There were only very short stretches of 2 to 6 bp conserved between telomeric and centromeric junctions of each deletion, which rules out a homology-based mechanism but rather suggests nonhomologous end joining of DSBs as the most likely origin of the deletions.

Besides large deletions and nonsense mutations, a considerable fraction of potentially pathogenic missense mutations in *KCNV2* have been described. Although as a general practice for a recessive condition, the attribute "mutation" is commonly accepted in cases of homozygosity or in compound heterozygous state with another known mutation and its exclusion in a substantial number of controls, the additional validation by functional assays provide a much higher level of confidence. This holds true in particular for so-called private mutations, which have been found in single families or individuals only. In this study and in our previous investigation we have identified several such private missense mutations, three of them affecting amino acid residues at the N-terminus of KCNV2 (p.Phe164Ser, p.Glu184Lys, and p.Glu184Val). All three localize to the NAB domain of the protein that is required for recognition and assembly of homo- and heterotetrameric Kv channels [Wu et al., 1996; Xu et al., 1995; Supp. Fig. S4]. Previous studies have shown that Kv8.2, the gene product of *KCNV2*, assemble with Kv2.1 to form heterooligomeric channels with distinct biophysical properties [Czirjak et al., 2007; Ottschytsch et al., 2002]. Using yeast two-hybrid technology we comparatively assayed the interaction of the NAB domain of Kv2.1 with wild-type and mutant N-terminal fragments of Kv8.2. Our data convincingly demonstrate either a

drastically reduced or even complete lack of interaction of all three tested mutants compared with the wild-type fragment and thus provide further support and evidence for the pathogenicity of these mutations. The sensitivity of the assay prompted us to analyze two further variants p.Leu110Val and p.Asp147Glu, unclassified rare sequence variant observed as single heterozygous substitutions. The strongly reduced interaction that was observed for the p.Leu110Val variant, suggests that this variant most likely represents a pathogenic mutation, although it may not account for the retinal disease in the patient carrying this mutation, since he is lacking a second mutation.

Based on the autosomal recessive inheritance and the large number of presumptive null alleles (e.g., complete gene deletions, early stop or frameshift mutations), one might reason that CDSRR results from the (functional) absence of the gene product. In line with this argumentation, we suggest that Kv8.2 mutants with amino acid substitutions in the NAB domain (as caused by missense mutations) fail to assemble with Kv2.1 that represents the most likely native counterpart. This might either prohibit the formation of any functional Kv channel or result in pure homomeric Kv2.1 channels that lack the functional tuning of the Kv8.2 subunit for proper native function in photoreceptors.

Acknowledgments

We would like to thank the patients and family members for participating in this study. We also thank Elke Bocksteins and Dirk Snyders (Laboratory of Molecular Biophysics, Physiology, and Pharmacology, University of Antwerp, Belgium) for the yeast bait and prey constructs.

References

Beech DJ, Barnes S. 1989. Characterization of a voltage-gated K+ channel that accelerates the rod response to dim light. Neuron 3:573–581.

Ben-Salah S, Kamei S, Sénéchal A, Lopez S, Bazalgette C, Bazalgette C, Eliaou CM, Zanlonghi X, Hamel CP. 2008. Novel KCNV2 mutations in cone dystrophy with supernormal rod electroretinogram. Am J Ophthalmol 145:1099–1106.

Boycott KM, Flavelle S, Bureau A, Glass HC, Fujiwara TM, Wirrell E, Davey K, Chudley AE, Scott JN, McLeod DR, Parboosingh JS. 2005. Homozygous deletion of the very low density lipoprotein receptor gene causes autosomal recessive cerebellar hypoplasia with cerebral gyral simplification. Am J Hum Genet 77:477–483.

Czirják G, Tóth ZE, Enyedi P. 2007. Characterization of the heteromeric potassium channel formed by kv2.1 and the retinal subunit kv8.2 in *Xenopus oocytes*. J Neurophysiol 98:1213–1222.

Friedburg C, Schambeck M, Bonin M, Kohl S, Wissinger B, Lorenz B. 2007. Ocular phenotype in 3 young siblings with a homozygous KCNV2 mutation followed for 14 years. Invest Ophthalmol Vis Sci 48:E3683.

Gouras P, Eggers HM, MacKay CJ. 1983. Cone dystrophy, nyctalopia, and supernormal rod responses. A new retinal degeneration. Arch Ophthalmol 101:718–724.

Heckenlively JR, Hawes NL, Friedlander M, Nusinowitz S, Hurd R, Davisson M, Chang B. 2003. Mouse model of subretinal neovascularization with choroidal anastomosis. Retina 23:518–522.

Ho SN, Hunt HD, Horton RM, Pullen JK, Pease LR. 1989. Site-directed mutagenesis by overlap extension using the polymerase chain reaction. Gene 77:51–59.

Kohl S, Baumann B, Broghammer M, Jägle H, Sieving P, Kellner U, Spegal R, Anastasi M, Zrenner E, Sharpe LT, Wissinger B. 2000. Mutations in the CNGB3 gene encoding the β-subunit of the cone photoreceptor cGMP-gated channel are responsible for Achromatopsia (ACHM3) linked to chromosome 8q21. Hum Mol Genet 9:2107–2116.

Kohl S, Marx T, Giddings I, Jägle H, Jacobson SG, Apfelstedt-Sylla E, Zrenner E, Sharpe LT, Wissinger B. 1998. Total colorblindness is caused by mutations in the gene encoding the α-subunit of the cone photoreceptor cGMP-gated cation channel. Nat Genet 19:257–259.

Li C, Huang Z, Kingsley R, Zhou X, Li F, Parke DW, Cao W. 2007. Biochemical alterations in the retinas of very low-density lipoprotein receptor knockout mice: an animal model of retinal angiomatous proliferation. Arch Ophthalmol 125:795–803.

Michaelides M, Holder GE, Webster AR, Hunt DM, Bird AC, Fitzke FW, Mollon JD, Moore AT. 2005. A detailed phenotypic study of "cone dystrophy with supernormal rod ERG". Br J Ophthalmol 89:332–339.

Nagy D, Kohl S, Zrenner E, Wissinger B, Jägle H. 2009. Detailed functional and morphological analysis in patients with cone dystrophy with supernormal rod response due to mutations in the Kcnv2 gene. Invest Ophthalmol Vis Sci 50:E4757.

Ottschytsch N, Raes A, Van Hoorick D, Snyders DJ. 2002. Obligatory heterotetramerization of three previously uncharacterized Kv channel alpha-subunits identified in the human genome. Proc Natl Acad Sci USA 99:7986–7991.

Ozcelik T, Akarsu N, Uz E, Caglayan S, Gulsuner S, Onat OE, Tan M, Tan U. 2008. Mutations in the very low-density lipoprotein receptor VLDLR cause cerebellar hypoplasia and quadrupedal locomotion in humans. Proc Natl Acad Sci USA 105:4232–4236.

Robson AG, Webster AR, Michaelides M, Downes SM, Cowing JA, Hunt DM, Moore AT, Holder GE. 2010. "Cone dystrophy with supernormal rod electroretinogram": a comprehensive genotype/phenotype study including fundus autofluorescence and extensive electrophysiology. Retina 30:51–62.

Sergouniotis PI, Holder GE, Robson AG, Michaelides M, Webster AR, Moore AT. 2011. High-resolution optical coherence tomography imaging in KCNV2 retinopathy. Br J Ophthalmol:May 10. [Epub ahead of print; PMID-No: 21558291]

Smit AF. 1999. Interspersed repeats and other mementos of transposable elements in mammalian genomes. Curr Opin Genet Dev 9:657–663.

Thiagalingam S, McGee TL, Weleber RG, Sandberg MA, Trzupek KM, Berson EL, Dryja TP. 2007. Novel mutations in the KCNV2 gene in patients with cone dystrophy and a supernormal rod electroretinogram. Ophthalmic Genet 28:135–142.

Türkmen S, Hoffmann K, Demirhan O, Aruoba D, Humphrey N, Mundlos S. 2008. Cerebellar hypoplasia, with quadrupedal locomotion, caused by mutations in the very low-density lipoprotein receptor gene. Eur J Hum Genet 16:1070–1074.

Wissinger B, Dangel S, Jägle H, Hansen L, Baumann B, Rudolph G, Wolf C, Bonin M, Koeppen K, Ladewig T, Kohl S, Zrenner E, Rosenberg T. 2008. Cone dystrophy with supernormal rod response is strictly associated with mutations in KCNV2. Invest Ophthalmol Vis Sci 49:751–757.

Wissinger B, Gamer D, Jägle H, Giorda R, Marx T, Mayer S, Tippmann S, Broghammer M, Jurklies B, Rosenberg T, Jacobson SG, Sener EC, Tatlipinar S, Hoyng CB, Castellan C, Bitoun P, Andreasson S, Rudolph G, Kellner U, Lorenz B, Wolff G, Verellen-Dumoulin C, Schwartz M, Cremers FP, Apfelstedt-Sylla E, Zrenner E, Salati R, Sharpe LT, Kohl S. 2001. CNGA3 mutations in hereditary cone photoreceptor disorders. Am J Hum Genet 69:722–737.

Wu H, Cowing JA, Michaelides M, Wilkie SE, Jeffery G, Jenkins SA, Mester V, Bird AC, Robson AG, Holder GE, Moore AT, Hunt DM, Webster AR. 2006. Mutations in the gene KCNV2 encoding a voltage-gated potassium channel subunit cause "cone dystrophy with supernormal rod electroretinogram" in humans. Am J Hum Genet 79:574–579.

Wu W, Xu J, Li M. 1996. NAB domain is essential for the subunit assembly of both α-α and α-β complexes of shaker-like potassium channels. Neuron 16:441–453.

Xu J, Yu W, Jan YN, Jan LY, Li M. 1995. Assembly of voltage-gated potassium channels. J Biol Chem 270:24761–24768.

Ophthalmic Genetics, 2011, 1–5, Early Online

ISSN: 1381-6810 print/ 1744-5094 online
DOI: 10.3109/13816810.2011.592178

DOI:10.14753/SE.2014.1976

informa
healthcare

CASE REPORT

Cone-rod dystrophy associated with amelogenesis imperfecta in a child with neurofibromatosis type 1

Ditta Zobor[1], Dieter H. Kaufmann[2], Petra Weckerle[1], Bernd Wissinger[3], Helmut Wilhelm[1], and Susanne Kohl[3]

[1]*Centre for Ophthalmology, University of Tübingen, Germany,* [2]*Institute of Human Genetics, University of Ulm, Germany, and* [3]*Molecular Genetics Laboratory, Institute for Ophthalmic Research, University of Tübingen, Germany*

ABSTRACT

Purpose: To report a case of a 9-year-old child with neurofibromatosis type 1 (NF1) and Jalili syndrome, the latter denoting a rare combination of cone-rod dystrophy and amelogenesis imperfecta.

Methods: Detailed ophthalmological and electrophysiological examinations were carried out and blood samples were taken from the patient and her father for molecular genetic analysis by direct DNA sequencing of the NF1 and the ancient conserved domain protein 4 (CNNM4) gene.

Results: The diagnosis of neurofibromatosis type 1 (NF1) could be confirmed clinically and genetically. Furthermore, cone-rod dystrophy and amelogenesis imperfecta could be observed as typical features of a rare condition, acknowledged as Jalili syndrome. The diagnosis was assured on the basis of clinical examinations and molecular genetic analysis of the CNNM4 gene, which was previously shown to cause Jalili syndrome.

Conclusion: Our case shows a unique combination of NF1 and Jalili syndrome. The random association of two diseases is unusual and deserves attention. This case highlights the importance not only of detailed clinical examination, but also of molecular genetic analysis, which together provide a precise diagnosis.

Keywords: Amelogenesis imperfect, cone-rod dystrophy, Jalili syndrome, neurofibromatosis type 1

INTRODUCTION

Neurofibromatosis type 1 is a well-known condition characterized by typical clinical features, such as growth of tumors along nerves in the skin, brain and other parts of the body. The most common neoplasms in young children with neurofibromatosis type 1 (NF1)– among brain tumors– are optic pathway gliomas. These occur in up to 24% of NF1 patients. Optic pathway gliomas (OPG) grow slowly with only a low potential of malignancy, but they are locally invasive and compressive causing loss of visual function.[1–4] Once the diagnosis has been established, children are recommended to undergo ophthalmological examination every 3 months for the first year after diagnosis, and at increasing intervals thereafter, depending on the progression. Magnetic resonance imaging (MRI) may be performed at similar frequency depending on institutional preference and possibilities. According to the evidence-based recommendations from Listernick,[2] longitudinal follow-up of children with known NF1-associated OPG includes the assessment of visual acuity, visual field, color vision and neuroopthalmological examination. Particularly in children, examination results of psychophysical tests are sometimes unreliable due to lack of cooperation, but producibility and reliability become better as young children get older.

If a diagnosis of a "common" disease has been decided, physicians often forget to pay enough attention to further details. Even if an unusual or rare clinical feature is observed, it is in many cases considered as a part of the already known medical condition. Here we report an unusual case of a girl with neurofibromatosis type 1, who unfortunately also suffers from a rare disease, Jalili syndrome, which is a combination of cone-rod dystrophy and amelogenesis imperfect.[5–9]

Received 13 April 2011; revised 00 00 0000; accepted 22 May 2011

Correspondence: D. Zobor, Centre for Ophthalmology, University of Tübingen, Germany, Schleichstrasse 12–16, D-72076 Tübingen, Germany. Tel: +49 7071 29 83736. E-mail: ditta.zobor@med.uni-tuebingen.de

DOI:10.14753/SE.2014.1976

PATIENT AND METHODS

Clinical Assessment

A 9-year-old girl from a Kosovan family was referred to our clinic with reduced visual acuity in both eyes. Previous pediatric examinations suggested the diagnosis of neurofibromatosis type 1 (NF1). Our patient underwent a detailed ophthalmological examination including slitlamp examination, funduscopy, fundus autofluorescence and psychophysical tests (visual acuity, visual field, color vision test). Based on the morphological changes observed on her fundi, Ganzfeld ERG and multifocal ERG (mfERG) were performed according to the standards of the International Society for Electrophysiology of Vision (ISCEV). Furthermore, magnetic resonance imaging (MRI) was carried out to investigate the optic pathway. During our examination, conspicuous dental changes were noticed, which initiated an additional dental consultation.

Genetic Analysis

Blood samples were taken from the child and her father for molecular genetic analysis after informed consent. DNA was isolated from peripheral blood lymphocytes by standard procedures. All coding exons of the NF1 gene and exon 1 of the ancient conserved domain protein 4 (CNNM4) gene were analyzed by PCR amplification and DNA sequencing. Segregation analysis in the father was performed via sequencing of PCR products. No other family members were available for examination.

All examinations were carried out according the tenets of Ethics of the World Medical Association (Declaration of Helsinki).

RESULTS

Clinical Findings

The pediatric examination revealed café-au-lait macule on her chest, freckling in the axillary region, a right anterior chest wall deformity due to protrusion of the costal cartilages adjacent to the sternum (Fig. 1A), and reduced visual acuity on both eyes. From earliest childhood nystagmus, reduced visual acuity and photophobia were reported, whereas night vision was felt normal. The symptoms were experienced as non-progressive.

When examined at the age of 9, her best corrected visual acuity was 0.05 on the right eye (tested with the Snellen chart, RE -0,25/ sph-3,25 cyl 20°) and 0.125 on the left eye (LE−1,5 sph-1,75 cyl 125°). Kinetic perimetry showed a central scotoma and a slight constriction of the visual field for III4e on both eyes. Color vision tested with the Lanthony Panel D-15 saturated test showed severe color confusions most likely along the scotopic axis. Anterior segment examinations revealed Lisch nodules on both eyes and a relative afferent pupillary defect on the right eye. Fundus examination showed bilateral optic disc atrophy, being more pronounced in the right eye. MRI confirmed bilateral optic nerve atrophy and optic pathway gliomas (R>L) on both eyes (Fig. 1B). In addition, lesions with T2 signal intensities of the basal ganglia on T2 were observed, which are typical for NF1.

Interestingly, we noticed retinal pigment epithelium atrophy in the macula on both eyes resembling a bull's eye maculopathy (Fig. 2A–D). For further clarification, Ganzfeld-ERG was carried out, which showed almost normal scotopic responses with slightly delayed implicit times, but no detectable photopic responses. MfERG recording could not show reproducible responses either. These results supported the diagnosis of cone-rod dystrophy.

Additionally, a yellowish-brownish discoloration of the teeth was noticed (Fig. 2E). According to the father`s description, the surface of the teeth was rough and became stained soon after eruption and showed a brownish color somewhat later. The primary teeth were so soft, that one could peel off the enamel with the nails. These features are characteristic for amelogenesis imperfecta and can be confirmed in dental examinations.

Genetics

Our patient was the only affected family member, both for NF1 and for the cone-rod dystrophy associated with amelogenesis imperfecta. There was no evidence for parental consanguinity in this family.

In exon 13 of the NF1 gene a 1bp-insertion at position 2033 (c.2033insC) was detected. This insertion leads to a frame-shift and premature termination codon (stop-codon) after amino acid residue 698 in the NF1 polypeptide (p.Ile679AsnfsX21). This mutation in the NF1 gene is already reported in the literature.[10] Since there is no history of the disorder in the family, the mutation most probably results from a de novo event.

Recently, mutations in the CNNM4 gene have been identified in patients affected by autosomal recessive cone-rod dystrophy and amelogenesis imperfecta, now acknowledged as Jalili syndrome.[11,12] The molecular genetic analysis of exon 1 of the CNNM4 gene revealed a homozygous previously reported mutation c.1312dupC p.Leu438ProfsX9 observed recurrently in patients originating from Kosovo[11,12] (Table 1). Segregation analysis in the father proved him to be heterozygous for this mutation. No further family members were available for testing.

DOI:10.14753/SE.2014.1976

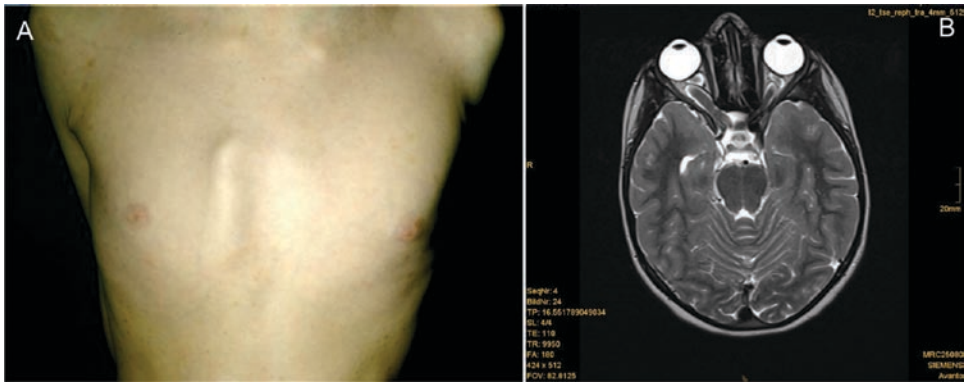

FIGURE 1 Clinical findings of neurofibromatosis type 1. (A) Chest deformity, freckling of the axillary regions and café-au-lait macule. (B) Bilateral optic gliomas were more pronounced on the right eye in magnetic resonance imaging (MRI).

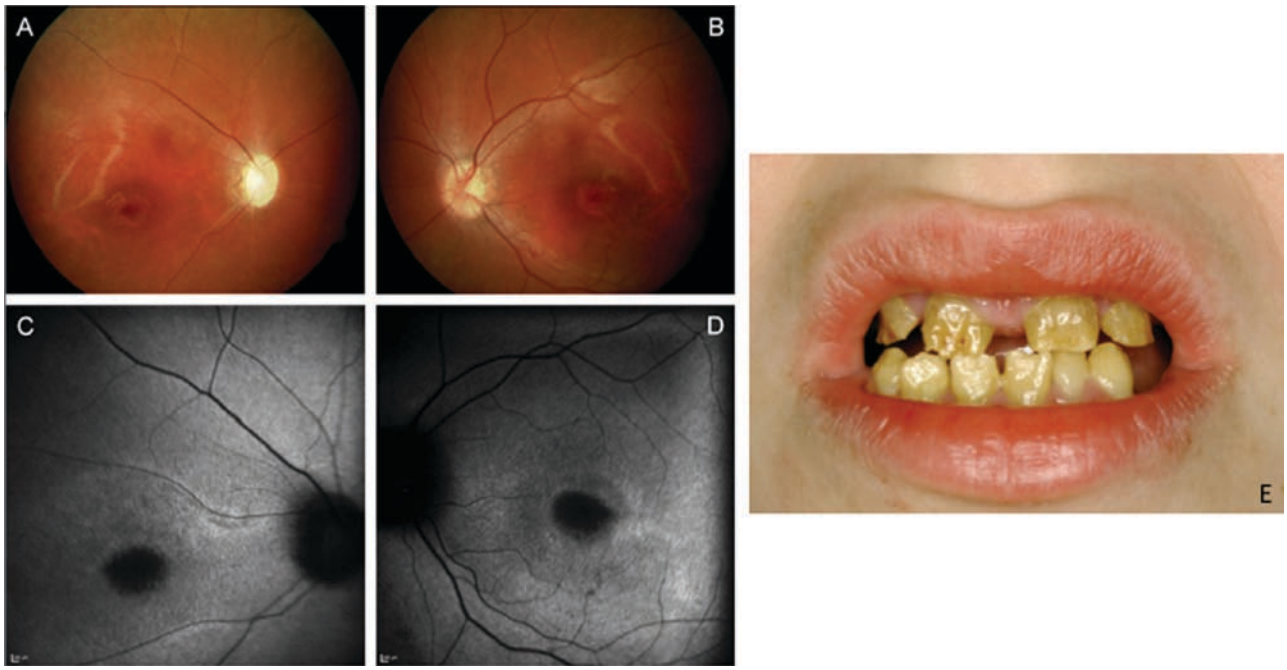

FIGURE 2 Clinical findings of Jalili syndrome. Fundus (A, B) and autofluorescence images (C, D) showing bilateral optic atrophy (R>L), additional macular retinal pigment epithelial mottling and atrophy similar to bull's eye maculopathy. (E) Amelogenesis imperfecta in the mixed dentitial phase observed in our patient.

TABLE 1 Genetic findings in our patient.

Gene	Alteration on the nucleotide level	Alteration on the protein level
NF1	c.2033insC heterozygous	p.Ile679AsnfsX21
CNNM4	c.1312dupC homozygous	p.Leu438ProfsX9

DISCUSSION

Neurofibromatosis type 1 is a condition characterized by growth of tumors along nerves in the skin, brain and other parts of the body, and additional changes in skin coloring. Its prevalence has been estimated as 1 in 2000 to 1 in 5000. This phacomatosis is considered to be inherited as an autosomal dominant trait, however, almost half of the cases result from de novo mutations in the NF1 gene and occur in patients with no family history of the disorder, as is the case in our patient. The product of the NF1 gene, neurofibromin is expressed in many types of cells, including nerve cells, oligodendrocytes and Schwann cells. Neurofibromin acts as a tumor suppressor protein and inhibits cell division. More than 500 NF1 mutations have already been identified, including nonsense mutations, amino acid substitutions, deletions, insertions and splice defects. Most of them are unique to a particular family. Almost 80% of the germline mutations appear to cause severe truncation of the gene product resulting in reduction of neurofibromin (haploinsufficiency) and a second hit in the NF1 gene allows non-cancerous tumors called neurofibromas to form.[1]

Our patient met at least four of the diagnostic criteria for neurofibromatosis type 1 (NF1) according to the

DOI:10.14753/SE.2014.1976

NIH Consensus Conference in 1987. Two of seven are required for positive diagnosis.[1–4]

NF1 with optic pathway glioma (OPG) was not the only disorder found in our patient. The symmetrical macular lesions, revealing a bull's eye pattern, suggested a retinal dystrophy, which could be confirmed by electrophysiological examinations. Scotopic responses were subnormal and no photopic responses could be recorded. This constellation is typical for a cone-rod dystrophy. An association between NF1 and retinal dystrophies has not been reported yet. Furthermore, severe dental anomalies were also noticed, which is not a feature of NF1 either.

The association of cone-rod dystrophy and amelogenesis imperfecta is a known, but very rare autosomal recessive condition, recently acknowledged as Jalili syndrome.[11,12] The first family was described by Jalili and Smith in 1988.[5] Twenty-nine members of a large consanguineous Arabian family were found to be affected with cone-rod dystrophy and amelogenesis imperfecta. All of the affected members suffered from photophobia and nystagmus starting in the first two years of life. Their electrophysiological tests revealed markedly decreased or absent photopic responses and only mildly decreased scotopic ERG responses. Furthermore, older members of the original Arabian family showed loss of the scotopic ERG, reduction of peripheral visual field and pigmentary changes of the retina. Therefore the initial cone dystrophy seems to develop into a cone-rod dystrophy. In 2004, Michaelides[7] described another Kosovan family with two affected siblings showing very similar dental and retinal changes. Since then, only a few additional families of diverse ethnic origin have been reported with Jalili syndrome.[8,9]

A locus for Jalili syndrome was mapped on chromosome 2q11 in the original Arabian family[6] and recently, mutations in the CNNM4 gene were identified in this as well as other Jalili syndrome patients including families from Kosovo.[11,12]

CNNM4 encodes a putative metal transporter, which is implicated in ion transport, possibly of magnesium. Immunohistochemical localization of CNNM4 showed its presence not only in the enamel organ, particularly in the ameloblasts, but also in the eye. In the cornea, CNNM4 localization was mainly observed in the epithelium, keratocytes and in the endoderm. More interestingly, CNNM4 was also detected in the retina, most abundantly in the ganglion cell layers, the IPL (inner plexiform layer) and OPL (outer plexiform layer). The prime physiological function of the CNNM4 metal transporter still remains to be determined. It has been proposed that it may participate in the mineralization of the teeth and may play a supportive role for the transduction processes in the retina, since magnesium ions are an important cofactor of many enzymes involved in phototransduction, adaptation and other vision processes.

Based on these novel findings, we performed molecular genetic testing of the gene CNNM4. In fact, a homozygous mutation c.1312dupC p.Leu438ProfsX9 could be detected in our patient. This mutation had already been described before in two independent families with Jalili syndrome originating from Kosovo and always in homozygous state.[11,12] Consequently it is justified to believe that this mutation is due to a founder mutation within this rather closed community most probably due to a higher allele frequency of this mutation within the Kosovan population.

The various clinical findings in our case are now explained with the coincidence of two independent diseases, neurofibromatosis type 1 and Jalili syndrome. NF1 is a common and well-described genetic disorder with an estimated prevalence of 1 in 2000 to 1 in 5000. Almost half of all affected individuals have a de novo mutation, the cause of the unusually high mutation rate is unknown. In contrast, Jalili syndrome is a very rare condition, only few cases are known worldwide.

The random association of two diseases is unusual and deserves attention. Cone dystrophies in children with NF1 might be overlooked because visual loss is attributed to OPGs. In our case, the additional retinal dystrophy complicates the follow-up of tumor-growth by ophthalmological examinations. In this case, the progression of the OPGs can be determined mainly by MRI examinations. However, retinal dystrophies are usually more or less symmetric and do not show a relative afferent pupillary defect as was the case in our patient. To follow pupillary function is therefore especially helpful, and even the remission of the relative afferent pupillary defect would have to be considered as a sign of tumor progression because it would indicate tumor growth on the other eye.

It is therefore important even in "clinically clear" cases to watch out for unsual additional symptoms not compatible with the initial diagnosis. Our case points to the importance not only of thorough clinical examination, but also of interdisciplinary teamwork.

ACKNOWLEDGMENTS

The molecular genetic analysis was supported by German Research Council (DFG) Grant KFO134 - Ko2176/1-2 to S.K.

***Declaration of interest*:** The authors have no proprietary or commercial interest in any material discussed in this article. The authors alone are responsible for the content and writing of the paper.

REFERENCES

1. Friedman JM. Neurofibromatosis 1. Gene Reviews: www.genetests.org

DOI:10.14753/SE.2014.1976

2. Listernick R, Ferner RE, Liu GT, Gutmann DH. Optic pathway gliomas in neurofibromatosis-1: Controversies and recommendations. Ann Neurol 2007;61:189–198.
3. Chang BC, Mirabella G, Yagev R, et al. Screening and diagnosis of optic pathway gliomas in children with neurofibromatosis type 1 by using sweep visual evoked potentials. IOVS 2007 June;48(6):2895–2902.
4. Opocher E, Kremer LCM, Da Dalt L, et al. Prognostic factors for progression of childhood optic pathway glioma: a systematic review. Eur J Cancer 2006 Aug;42(12):1807–1816.
5. Jalili IK, Smith NJD. A progressive cone-rod dystrophy and amelogenesis imperfecta: a new syndrome. J Med Genet 1988;25:738–740.
6. Downey LM, Keen TJ, Jalili IK, et al. Identification of a locus on chromosome 2q11 at which recessive amelogenesis imperfecta and cone-rod dystrophy cosegregate. Eur J Hum Genet 2002 Dec;10(12):865–869.
7. Michaelides M, Bloch-Zupan A, Holder GE, Hunt DM, Moore AT. An autosomal recessive cone-rod dystrophy associated with amelogenesis imperfecta. J Med Genet 2004;41;468–473
8. Inglehearn CF, El-Sayed W, Shore RC, et al. Jalili syndrome-cone-rod dystrophy (CRD) and amelogenesis imperfecta (AI); six families and consistent linkage to 2q11. ARVO 2008 E-Abstract 457.
9. Mighell AJ, El-Sayed W, Shore RC, et al. Amelogenesis imperfecta and central blindness: an inherited syndrome. IADR 86th General Session & Exhibition, 2008. Abstract 1536.
10. Fahsold R, Hoffmeyer S, Mischung C, et al. Minor lesion mutational spectrum of the entire NF1 gene does not explain its high mutability but points to a functional domain upstream of the GAP-related domain. Am J Hum Genet. 2000 Mar;66(3):790–818.
11. Polok B, Escher P, Ambresin A, et al. Mutations in CNNM4 cause recessive cone-rod dystrophy with amelogenesis imperfecta. Am J Hum Genet 2009;84:259–265
12. Parry DA, Mighell AJ, El-Sayed W, et al. Mutations in CNNM4 cause Jalili syndrome, consisting of autosomal-recessive cone-rod dystrophy and amelogenesis imperfecta. Am J Hum Genet 2009;84:266–273.

DOI:10.14753/SE.2014.1976

11. Acknowledgements

I am grateful to many people who have been supporting my work from the beginning.

First of all, I would like to thank Eberhart Zrenner for inviting me to Tübingen and giving me the chance to work clinically and scientifically in his department. He has introduced me to clinical electrophysiology and with his enthusiasm he could convince me easily to work in this special field of ophthalmology. His huge knowledge, scientific inquisitiveness and continuous energy have always been encouraging and helped me throughout the years.

I am also very grateful to Herbert Jägle, who introduced me to visual science and to clinical work regarding inherited retinal diseases. He has been my scientific tutor for many years and he has contributed extensively to the vast majority of my research. He has been teaching me basically to every aspect of scientific work, from the smallest technical problems of everyday practice to the scientific presentations.

I would also like to thank Susanne Kohl very much for her continuous support both regarding her outstanding scientific skills as a researcher, her “womanpower” and her empathy as a friend.

I would like to thank all the co-authors on the different chapters for their cooperation, especially to: Herbert Jägle, Susanne Kohl, Eberhart Zrenner and Bernd Wissinger. For their scientific and technical support I would like to thank Torsten Strasser, Anne Kurtenbach, Ulrike Fuchs, Susanne Kramer, Gudrun Haerer and Katharina Endress.

Last but not least, I am endlessly grateful to my family, especially to my husband, Gergely Zobor, who always support me in everything I do. It was not always easy regarding the large distance away from home and desired a lot of patience and trust.